Development and characterization of pain-related sodium channel mouse model for Scn10aG1663S

Céleste Chidiac

UNIVERSITY OF STRASBOURG

ECOLE DOCTORALE DES SCIENCES DE LA VIE ET DE LA SANTÉ (ED414)

Institute of Genetics and Molecular and Cellular Biology (IGBMC)

THESIS

Presented by:

Céleste CHIDIAC

Defense date: April 28th 2021

Development and characterization of pain-related sodium channel mouse model for *Scn10a*^{G1663S}

Discipline: Neurosciences

Thesis supervised by:

THESIS DIRECTOR:

M. Yann HERAULT Directeur de Recherche, CNRS, Strasbourg

THESIS CO-DIRECTOR:

Mme. Claire GAVERIAUX-RUFF Professeur, Université de Strasbourg

Rapporteurs:

M. Aziz MOQRICH Directeur de recherche, IBDM, Marseille

M. Eric LINGUEGLIA Directeur de recherche, IPMC, Valbonne

Internal examiner:

Mme. Dominique MASSOTTE Directeur de recherche, INCI, Strasbourg

Other member:

Mme. Angelika LAMPERT PR PUPH, Uniklinik RWTH, Aachen

Table of Contents

Acknowledgments

First, I would like to express my gratitude to my supervisor Dr. Yann HERAULT and my co-supervisor Professor Claire GAVERIAUX-RUFF for giving me the opportunity to work on this challenging and exciting project. I thank you for believing in me and coaching me through this journey. Moreover, I want to thank you for all the advices that you gave to me and for sharing your knowledge and expertise in the domain of pain and genetics. I want to thank you specifically, Dr. Yann HERAULT for sharing your knowledge about genetics, guiding of the genetic model and offering the opportunities to participate in different training courses and congresses. I want to thank you specifically, Professor Claire GAVERIAUX-RUFF for all the discussions and literature review that we did together and for sharing your expertise in the pain domain which was so beneficial for running the behavioral tests and analyzing the results.

I would like also to express my gratitude to the two reporters of my jury members Dr. MOQRICH Aziz and Dr. LINGUEGLIA Eric, my external examiner Pr. LAMPERT Angelika and my internal examiner Dr. MASSOTTE Dominique for agreeing to lend their professionally scientific expertise and their precious time to evaluate my thesis.

I would like to thank Marie-Christine BIRLING for helping to design the different strategies of establishing the mouse model of my PhD project. I want to thank a lot Romain LORENTZ for helping me to validate the protocols of CRISPR-Cas9 system and then to do the cloning step of the homologous recombination. Also, I would like to thank Laurence SCHAEFFER for her help in the confirmation of blastocysts genotype for CRISPR-Cas9 strategies. I also want to acknowledge Marie WATTENHOFER-DONZE for her help in establishing the mouse model using homologous recombination and her follow-up for the injections in blastocysts and the birth of chimeras. I also want to acknowledge Sylvie JACQUOT and Amelie JEANBLANC for designing the protocol for genotyping and genotyping of the first progeny.

I am grateful to the PHENOMIN-ICS animal facility stuff for their services, in particular the animal caretakers Charley PINAULT, Sophie BRIGNON and Dalila ALI-HADJI and the veterinary Isabelle GONCALVES DA CRUZ. I would like to thank Loïc LINDNER and Pauline CAYROU for their help and training for Rt-ddPCR, and Elvire GUIOT for her help and training for confocal microscope.

I would like to thank Maria del Mar MUNIZ MORENO for developing and performing the gdaphen statistical analysis, for all the time and efforts she has put in running the analysis.

I also extend my appreciation to all our collaborators in the ITN-Pain Net, Dr. Stephen Waxman, Dr. Sulayman Dib-Hajj, Dr. Jordi Serra, Pr. Lauria Pinter Giuseppe, Dr. Catharina Faber, Dr. Janneke Hoeijmakers, Dr. Monique Gerrits, Dr. Augusto Caraceni and Dr. Bianca de Greef for all the useful courses and trainings that they gave us during ITN-Pain Net meetings and webinars. I am grateful for Neuroscience Technologies (NT) company in Barcelona for hosting me during my secondement. Specifically, I want to thank Dr. Jordi Serra, Romà Solà, Federico Ponente and Lenin Reyes-Haro for sharing their experience on microneurography. I also want to thank Serena Cogoni and Carla Finocchiaro for organizing all the Pain Net meetings and checking the work packages and deliverables within the project.

I want to highly appreciate the help of my team members. I want to thank Joelle PENSAVALLE for helping me to open a bank account and get my resident permanent. I want to highly thank Yaping XUE for giving me advices for the behavioral tests, mice dissection and RNA extraction. I also want to thank Ameer Abu Baker RASHEED for helping me in mice perfusion and explaining the IHC. A big thank you for Maria del Mar MUNIZ MORENO for her help and advices in the statistical analysis and for her cheerful and positive spirit. Thank you, Arnaud DUCHON for products ordering. Thank you, Monika RATAJ BANIOWSKA, Maria Victoria HINCKELWANIN RIVAS, Claire CHEVALIER and Veronique BRAULT for laboratory organization of equipment, materials and chemicals and their help in the lab daily life. Thank you, Michel Roux for training on Cryostat. At the end, a huge amount of gratitude for our PhD group, Maria del Mar MUNIZ MORENO, Helin ATAS-OZCAN, Marion PELLEN, Ameer Abu Baker RASHEED, Yaping XUE, Alexandra JIMENEZ ARMIJO and Jose Thomas AHUMADA SAAVEDRA for always being there for me, helping me to solve scientific and daily life problems, providing me the support and comfort, and surrounding me as a family.

Most of all, I would like to thank my family members, especially my mother Mona, my brother Anthony and my dad Emile for cheering me up and pushing me to give the best of me. A big part of the person I am today is due to all the efforts my mom did to teach us and blow in us the love for education and the perseverance in life. I am grateful to have her as mom and to have Anthony as brother. I want to thank my best friends Anna-Maria Habib, Maya Machlout and Titsiana Mahayri for keeping our valuable friendshipness across the distances and cheering me up. Finally, I thank all my Lebanese and Arabic friends and all the French people and families that I met here in France, who showed me a lot of love and care. Special thanks to Kamar, Elissa, Naima, Sandra and Ghina for supporting me during the last weeks of preparation for my thesis.

Summary

The sodium channel, encoded by *SCN10A* gene, is a voltage-gated sodium channel that plays an important role in the generation and conduction of action potentials. It is expressed in primary nociceptive neurons and is involved in pain signal transmission. Several *SCN10A* gain-of-function mutations have been found in chronic pain patients with small fiber neuropathy (SFN). Three women bearing the c.4984G>A variant resulting in G1662S mutation in *SCN10A* gene were identified. The G1662 locus in human *SCN10A* corresponds to the G1663 locus in mice *Scn10a*. We have successfully established a mouse model for the G1663S mutation in *Scn10a* gene using homologous recombination in embryonic stem cells and characterized the effect of this mutation on the molecular and cellular levels and on pain sensitivity. The mouse line showed no alteration of growth, survival, and global health state. The G1663S mutation did not alter the *Scn10a* transcript expression in the dorsal root ganglion and spinal cord of the mutant mice. Pain sensitivity of the mutant mice was investigated on both sexes using behavioral tests for thermal and mechanical sensitivity. *Scn10a*^{G1663S} mutant mice were more sensitive to touch than their wildtype littermates in the von Frey test. Female homozygous mutants tended to be more sensitive to cooling stimuli in the acetone test. For heat sensitivity, male homozygous mutants showed shorter latencies to radiant heat in the Hargreaves test while homozygous females had longer latencies in the tail flick test. Also, mutant males displayed a shorter reaction latency on the 54°C hot plate. Collectively, *Scn10a*^{G1663S} mutant mice show a moderate but consistent increased sensitivity in behavioral tests of nociception. This altered nociception found in *Scn10a*^{G1663S} mice demonstrates that the corresponding G1662S mutation of *SCN10A* found in painful SFN patients contributes to their pain symptoms. Extrapolating our findings to patient's symptoms is very essential for a better understanding of pain and opens the door for future pharmacological studies. Our study provides more evidence that *SCN10a* is a key factor for nociception and chronic pain state of SFN patients.

Résumé en Français

Introduction

La douleur agit comme un système physiologique d'alerte et de protection qui permet de ressentir consciemment un dommage dans le corps et de réagir pour éviter ce dommage. L'association internationale pour l'étude de la douleur (International association for the study of pain IASP) a publié en juillet 2020 la définition révisée de la douleur avec ses notes associées:

"Une expérience sensorielle et émotionnelle désagréable associée à, ou ressemblant à celle associée à, des lésions tissulaires réelles et potentielles".

-La douleur est toujours une expérience personnelle qui est influencée à des degrés divers par des facteurs biologiques, psychologiques et sociaux.

-La douleur et la nociception sont des phénomènes différents. La douleur ne peut être déduite uniquement de l'activité des neurones sensoriels.

-Les individus apprennent le concept de la douleur à travers leurs expériences de vie.

-Il convient de respecter le fait qu'une personne qualifie une expérience de douloureuse.

-Bien que la douleur joue généralement un rôle adaptatif, elle peut avoir des effets négatifs sur la fonction et le bien-être social et psychologique.

-La description verbale n'est qu'un comportement parmi d'autres pour exprimer la douleur; l'incapacité de communiquer n'exclut pas la possibilité qu'un humain ou un animal éprouve de la douleur.

La douleur neuropathique est la conséquence directe d'une lésion ou d'une maladie affectant le système somatosensoriel, telle que définie par l'IASP en 2008. Il s'agit d'une douleur pathologique liée à des changements fonctionnels dans les afférences primaires et à une sensibilisation au sein du système nerveux central entraînant à la fois une douleur évoquée et une douleur spontanée, dans laquelle des messages de douleur sont envoyés au système nerveux central indépendamment des stimuli nocifs.

La neuropathie à petites fibres (Small Fiber Neuropathy, SFN) atteint les petites fibres nerveuses sensorielles myélinisées fibres Aδ et non myélinisées fibres C. Elle est généralement caractérisée par des symptômes de douleur neuropathique tels que l'allodynie, la dysesthésie, l'hyperalgésie,

l’hypoesthésie at la paresthésie ainsi que des symptômes autonomes. Des maladies comme le SIDA et le diabète compliquent la SFN. Des mutations gain-de-fonction dans les canaux ioniques voltage-dépendants provoquent aussi une SFN idiopathique. Les canaux sodiques voltage-dépendants sont des protéines transmembranaires dynamiques principalement exprimés sur les membranes des cellules excitables telles que les neurones. Ces canaux passent d'un état fermé à un état ouvert en réponse aux changements du potentiel membranaire, permettant la conduction sélective des ions sodium à travers les membranes cellulaires. Ces modifications des flux de sodium sont vitales pour la génération et la propagation du potentiel d’action dans les cellules excitables, faisant des canaux sodiques les canaux ioniques les plus importants pour l'excitabilité des cellules neuronales et les fonctions physiologiques normales.

Les canaux sodiques à voltage-dépendant sont des complexes d'un pore formé par une sous-unité α de 260 kDa, associée à une ou plusieurs sous-unités β auxiliaires (β1-β4) de 33-36 kDa. Ils se différencient en fonction des isoformes distinctes de la sous-unité α. Toutes les sous-unités α partagent une topologie de structure presque identique, un pli canonique de canal ionique voltage-dépendant constitué de 2000 résidus d'acides aminés organisés en quatre domaines homologues DI-DIV, chacun contenant six segments transmembranaires S1-S6. On pense que des régions spécifiques à l'intérieur de chacun des quatre domaines DI-DIV des canaux ont des rôles distincts, mais intégrés, dans le gating du canal et la stabilité conformationnelle en réponse aux changements du potentiel membranaire. La sous-unité α contient deux entités structurelles fonctionnellement distinctes, à savoir le module de détection de tension (Voltage Sensing Module) VSM) et l'entité de pore (Pore Entity PE). Plus précisément, les segments S5-S6 et la boucle d'interconnexion constituent le PE. La boucle entre S5 et S6 de chaque domaine forme un filtre ionique sélectif étroit du canal qui permet la perméabilité sélective des ions sodium à travers la membrane cellulaire. Les segments S1-S4 constituent le VSM qui détecte les variations du potentiel de la membrane, passant d'une configuration d'arrêt à une configuration activée, ce qui est nécessaire pour l'ouverture du pore. Cette propriété de détection est caractérisée par plusieurs acides aminés (aa) chargés positivement (arginine ou lysine) situés en troisième position du segment S4 dans chaque domaine. Le mouvement vers l'extérieur du segment S4 se traduit directement par des changements de conformation du PE, par l'interaction entre le VSM de chaque domaine avec le PE d'un domaine voisin. Plus précisément, lorsque la cellule est dépolarisée, chaque sous-unité subit seule des transitions voltage-dépendantes, mais le changement final voltage-indépendant menant à l'ouverture du pore se produit de manière coopérative. Par conséquent, lorsque les ions sodium traversent la membrane cellulaire, le courant sodique atteint un maximum puis diminue lorsque le canal sodique cesse de conduire les

ions et commence à se fermer. Ce processus est connu sous le nom d'inactivation. Les canaux inactivés ne peuvent pas rouvrir jusqu'à ce que la membrane soit repolarisée et qu'ils se remettent de l'inactivation. L'activation, l'inactivation et la récupération de l'inactivation se produisent en quelques millisecondes. En plus de ces transitions rapides, les canaux sodiques sont également susceptibles de se fermer par des processus d'inactivation plus lents, qui agissent sur des dizaines de secondes et peuvent se produire en réponse à des dépolarisations prolongées.

Les sous-unités β auxiliaires sont composées d'un repli extracellulaire N-terminal de type immunoglobuline, d'un seul segment transmembranaire et d'un court segment intracellulaire. Les sous-unités β2 et β4 se ressemblent le plus en termes de séquence d'acides aminés et forment des liaisons disulfure avec les sous-unités α, tandis que les sous-unités β1 et β3, qui se ressemblent également, s'associent de manière non covalente aux sous-unités α. Les sous-unités β peuvent agir comme des molécules d'adhésion cellulaire et moduler l'expression de la surface cellulaire du canal sodique dans des endroits spécifiques des cellules excitables, augmentant ainsi la densité des canaux sodiques et l'excitabilité des cellules. Elles peuvent également moduler le trafic membranaire, la dépendance au voltage et la cinétique de gating des canaux. La synergie des sous-unités α et β est spécifiquement particulière au niveau des nœuds de Ranvier des axones myélinisés, où la perte des interactions β1 peut modifier la structure des nœuds de Ranvier et perturber la conduction saltatoire.

A ce jour, 9 isoformes de canaux sodiques voltage-dépendants (nommées avant Nav1.1-Nav1.9) SCN1A-SCN5A et SCN8A-SCN11A ont été identifiées dans différents tissus excitables chez l'homme et les rongeurs. À l'exception de SCN4A, ils sont exprimés dans le système nerveux. Plus précisément, SCN1A, SCN2A, SCN3A et SCN8A sont les principaux canaux sodiques du système nerveux central, tandis que SCN9A, SCN10A et SCN11A sont principalement distribués dans le système nerveux périphérique. SCN5A a été initialement identifié comme un canal sodique cardiaque, mais il a été démontré qu'il était aussi exprimé dans le système nerveux central. SNC4A est principalement exprimé dans les muscles squelettiques. La plupart de ces canaux ont également des niveaux d'expression significatifs en dehors de leurs tissus primaires.

Des mutations dans les canaux sodiques peuvent produire des changements dans les propriétés biophysiques du canal. On sait maintenant que les troubles héréditaires des canaux ioniques sont à l'origine d'un large éventail de maladies humaines, appelées channelopathies. Plus de 1000 mutations liées aux maladies ont été identifiées dans les canaux Nav. En particulier, plusieurs mutations dans le gène *SCN10A* codant pour la sous-unité α du canal sodique ont été identifiées. Le canal SCN10A, codé par le gène *SCN10A*, est principalement exprimé dans le système

nerveux périphérique, en particulier au sein des ganglions sensoriels de la racine dorsale (DRG), où l'on a constaté que l'expression était plus élevée dans les neurones de la fibre C que dans ceux de la fibre A et dans les ganglions trigéminaux. Cependant, le phénotype douloureux des patients SFN est compliqué et jusqu'à présent une compréhension adéquate du rôle que joue le canal SCN10A dans ces neuropathies est encore manquante. SCN10A est un canal sodique voltage- dépendant qui joue un rôle critique dans la génération et la conduction des potentiels d'action. Il est donc important pour la signalisation électrique par la plupart des cellules excitables. En 2012, C.G. Faber et ses collègues ont découvert que deux patientes non apparentées étaient hétérozygotes pour l'une des mutations du gène *SCN10A*, c.4984G>A, p.G1662S. Ces deux patientes se plaignaient de douleurs et ont montré une sensation de douleur anormale au chaud et au froid. L'une des patientes avait 24 ans lors du diagnostic avec 2 ans de douleur. Elle souffrait de picotements continus et des douleurs ressemblant à des crampes dans ses jambes. La température froide et l'exercice ont aggravé ses plaintes. Les couvertures chaudes ont soulagé la douleur. Elle souffrait aussi de l'hyperhidrose occasionnelle et de vertiges orthostatiques. L'examen clinique n'a pas montré d'anormalités. L'étude de la conduction nerveuse et la biopsie de peau étaient normales. Les tests sensoriels quantitatifs ont montré des niveaux anormaux pour les sensations froides et chaudes aux mains. La 2ème patiente avait 62 ans lors du diagnostic avec 16 ans de douleur. Elle souffrait de brûlure continue et douleur poignardante dans les deux pieds. À l'âge de 59 ans, la douleur dans les deux pieds s'est aggravée et les mains ont également été affectées. 6 mois avant l'évaluation elle a développé une peau sensible et une intolérance à porter du tissu au-dessus de ses pieds. Elle souffrait aussi d'épisodes occasionnels de sécheresse oculaire, sécheresse de la bouche, augmentation de la transpiration, diarrhée et constipation, intolérance orthostatique, palpitations et bouffées de chaleur. L'examen clinique a montré une hypoesthésie et une diminution de la sensation de vibration aux pieds. L'étude de la conduction nerveuse et la biopsie de peau étaient normales. Les tests sensoriels quantitatifs ont montré des niveaux anormaux pour les sensations chaudes aux pieds. Quelques années plus tard en 2019, une troisième patiente portant la même mutation a été reportée par I. Eijkenboom et ses collègues. Cette patiente avait 28 ans lors du diagnostic avec 3 ans de douleur. Elle souffrait de douleur de surface et profonde intense, d'intenses netteté, chaleur et matité, désagrément et sensibilité de la peau. L'examen clinique, l'étude de la conduction nerveuse et la biopsie de peau étaient normales. Les tests sensoriels quantitatifs ont montré des niveaux anormaux pour les sensations chaudes.

Il a été montré que la mutation G1662S provoque une hyperexcitabilité des DRG chez les patients SFN et également en culture in vitro des neurones DRG du rat. La mutation G1662S n'affecte

pas l'activation, mais altère plutôt l'inactivation rapide à l'état d'équilibre en déplaçant sa dépendance vis-à-vis du voltage dans une direction dépolarisante, accélère la récupération après l'inactivation, diminue les seuils du courant et multiplie par trois la proportion de cellules qui ont tiré spontanément, ce qui induit à une augmentation de l'excitabilité des neurones du DRG.

Comme les mécanismes sous-tendant les réponses à divers stimuli douloureux sont complexes et impliquant plusieurs types de neurones afférents primaires, nous avons voulu étudier la sensibilité à la douleur d'un modèle de souris porteur de la mutation *Scn10a*^{G1663S}. La mutation G1663S chez la souris correspond à la mutation G1662S chez l'homme.

Projet de thèse

Les douleurs neuropathiques sont la conséquence directe d'une lésion ou de maladies affectant le système somatosensoriel. La SFN est un type de neuropathie où les fibres Aδ- et C sont affectées. Les patients se plaignent de douleurs neuropathiques et de symptômes autonomes. Le canal sodique SCN10A est exprimé préférentiellement dans le système nerveux périphérique au sein des DRG sensoriels et de leurs axones périphériques de petit diamètre, mais aussi dans les ganglions trigéminaux. De manière intéressante, des mutations dans le gène *SCN10A* codant pour la sous-unité α du canal sodique SCN10A ont été trouvées chez des patients atteints de SFN. L'une de ces mutations, c.4984G>A, p.G1662S a été identifiée chez 3 patients non apparentés hétérozygotes pour la mutation. Cette mutation a entraîné une hyperexcitabilité des neurones DRG qui a été démontrée dans des cultures in vitro de neurones DRG de souris. Cependant, le mécanisme détaillé qui sous-tend le lien entre cette mutation, le SFN et la douleur n'est pas très clair jusqu'à présent. Mon projet de doctorat consistait à générer un modèle de souris pour cette mutation et à le caractériser, principalement pour le phénotype de la douleur.

Par suite, dans ce projet de doctorat, nous nous sommes concentrés sur les objectifs suivants:

1. Etablir le modèle de souris portant la mutation G1663S dans le gène *Scn10a* liée à la douleur neuropathique par recombinaison homologue.
2. Procéder à la caractérisation moléculaire et cellulaire de la mutation.
3. Procéder à la caractérisation comportementale du modèle mutant afin d'étudier la sensibilité à la douleur.

Tous les résultats bénéficieront à l'approfondissement de nos connaissances sur l'association génotype-phénotype et également le rôle des mutations *SCN10A* dans la SFN idiopathique.

Méthodes

CRISPR-Cas9 est un outil génétique révolutionnaire. L'enzyme Cas9 est une endonucléase d'ADN présente dans de nombreuses bactéries, où elle fait partie d'un système de défense contre les molécules d'ADN envahissantes, comme les virus. Cas9 possède deux sites actifs qui clivent chacun un brin d'une molécule d'ADN double brin à un locus génomique cible, simulant une cassure double brin. L'enzyme est guidée vers l'ADN cible par une molécule d'ARN, appelée ARN guide simple brin (gRNA), qui contient une séquence de 20 paires de bases (pb) correspondant à la séquence à cliver, laquelle est délimitée par des séquences de motifs adjacents protospacers. On a premièrement construit une stratégie CRISPR utilisant 2 gRNAs, gR93 et gR93b autour de la région cible et on a construit la séquence d'ADN à insérer contenant la mutation. Cette première stratégie n'a pas réussi et on est passé à une 2ème stratégie utilisant 4 gRNAs: gR93, gR93b, gR85 et gR82 avec 2 guides de chaque côté et la même séquence d'ADN à insérer. Cette 2ème stratégie a encore échoué. Ces échecs sont dus à la grande similarité entre le gène *Scn10a* et les autres gènes *Scn*, surtout le *Scn5a* qui est localisé sur le même chromosome que le gène *Scn10a* et au fait que les gRNAs de chaque côté de la région cible ne coupaient pas simultanément permettant la délétion de la région et l'insertion de la nouvelle séquence portant la mutation. On est alors passé à la recombinaison homologue.

La recombinaison homologue est un type de recombinaison génétique dans lequel des séquences d'ADN spécifiques sont échangées entre deux molécules d'ADN similaires ou identiques. En bref, le ciblage génique se fait comme suit : la mutation d'intérêt est introduite dans une copie clonée du gène choisi par la technologie de l'ADN recombinant. La mutation est transférée par recombinaison homologue au locus génomique dans les cellules souches embryonnaires et seules les cellules portant la mutation sont sélectionnées puis injectées dans des blastocystes de souris, qui sont amenés à terme par implantation dans des mères nourricières. Des souris chimériques portant l'allèle recombinant sont générées et sont capables de transmettre efficacement la mutation à leur progéniture.

Un allèle ciblé a été conçu, portant deux bras d'homologie du gène endogène original *Scn10a* et une cassette d'auto-sélection. Le bras 3' d'homologie (1,2 kb) était constitué d'une partie de l'intron 27 qui n'a aucune similarité avec les autres gènes *Scn* et d'une partie de l'exon 28 portant le locus de mutation. Le bras 3' a été cloné dans le vecteur de ciblage C5206 contenant la cassette d'auto-sélection en utilisant les enzymes SbfI et SfI. Le bras 5' d'homologie (1,1 kb) était constitué d'une partie de l'intron 27 et a été cloné dans le vecteur contenant la cassette d'auto-sélection et le bras 3', en utilisant les enzymes AscI et SgrAI.

La cassette d'auto-sélection, positionnée à l'extérieur de la région d'homologie de l'allèle ciblé, était constituée de la séquence codant pour la recombinase d'auto-excision Cre et d'une cassette de gène de résistance à la néomycine flanquée de deux sites LoxP. La cassette d'auto-sélection s'intègre dans le génome par recombinaison homologue, servant à sélectionner les cellules souches embryonnaires hébergeant la mutation. En cas d'intégration aléatoire de l'allèle ciblé, la séquence Cre devrait être incorporée dans le génome. L'expression de la recombinase Cre qui en résulte excise le néo floxé et ces cellules meurent donc en réponse à un traitement antibiotique. Cependant, en cas de recombinaison, la séquence Cre devrait être perdue et la séquence néo incorporée intacte devrait rendre les cellules résistantes aux antibiotiques.

Les cellules souches embryonnaires utilisées dans l'expérience d'injection étaient initialement dérivées d'une souche de souris C57BL/6N, dont le pelage est noir. Les cellules sélectionnées avec la mutation ciblée souhaitée ont été injectées dans des blastocystes isolés de femelles BALB/CN accouplées, qui ont un pelage blanc. Ces blastocystes ont ensuite été implantés dans des mères nourricières CBA C57BL/6 F1 pour permettre aux embryons d'arriver à terme. Pour faciliter l'isolement de la progéniture souhaitée, les cellules et les blastocystes receveurs sont dérivés de souris présentant des allèles de couleur de pelage distincts (comme déjà mentionné, les cellules souches proviennent de souris noires et les blastocystes de souris blanches). Les descendants qui en résultent sont donc des chimères de deux types cellulaires différents : des cellules dérivées de cellules souches et des cellules dérivées de blastocystes de l'hôte. L'importance de la contribution des cellules souches à la formation de la souris chimérique peut être évaluée par une évaluation visuelle du chimérisme de la couleur du pelage. La contribution des cellules souches à la lignée germinale peut être évaluée en observant la couleur du pelage de la progéniture issue de la reproduction de la souris chimérique avec des souris noires. Les clones recombinants #52 et #74 validés dans le processus de criblage ont été injectés dans des blastocystes femelles BALB/CN. Les mâles hautement chimériques qui en résultent avec un score de couleur >85% ont été accouplés avec des femelles C57BL/6NCr sauvages pour étudier si les cellules souches recombinées ont contribué à la couche germinale. La cassette de sélection est supprimée par le moyen de croiser les chimères avec des femelles sauvages détenant une lignée Cre-deleter. Une transmission germinale de 80% de la couleur de la couche germinale des cellules souches a été obtenue et des animaux hétérozygotes portant la mutation *Scn10a*^{G1663S} et un site LoxP ont été générés. Les souris hétérozygotes ont ensuite été croisées pour générer des souris de génotypes homogènes.

Après la génération du modèle de souris porteur de la mutation *Scn10a*^{G1663S}, nous avons procédé à l'évaluation de l'expression du transcrit *Scn10a* dans les ganglions rachidiens dorsaux (DRG), moelle épinière et cerveau des souris sauvages et mutantes, à l'aide de la droplet digital PCR en temps réel (RT-ddPCR). L'ARN a été extrait des ganglions rachidiens dorsaux, moelle épinière et cerveau des souris avec le Trizol. Puis l'ARN est transcrit en ADN complémentaire par transcription reverse et quantifié par RT-ddPCR.

Nous avons aussi déterminé la densité des fibres nerveuses intra-épidermales (IENFD) dans la peau de la patte des souris. Les sections de peau ont été incubées avec un anticorps anti-pgp9.5 pour marquer les terminaisons nerveuses et du DAPI. N= 4 souris par génotype et par sexe ont été utilisées pour la détermination de la densité. La peau des deux pattes postérieures a été prélevée et cinq sections choisies au hasard par patte ont été analysées. Les images ont été visualisées avec le microscope confocal laser UV/Visible Leica SP8 utilisant un objectif sec 20×. Les images ont été acquises avec le logiciel LCS (Leica). La longueur totale des sections de peau a été acquise sous forme de tilescan et une vue d'ensemble de l'épiderme-derme a été reconstruite par l'acquisition de z-stacks d'une profondeur totale de 1 µm en 30 images superposées.

Les fibres nerveuses intra-épidermales sont comptées et la longueur de la surface épidermique est mesurée à l'aide du logiciel ImageJ sur les images confocales numérisées. La densité a été déterminée en divisant le nombre d'afférences traversant la jonction dermo-épidermique, en excluant les ramifications secondaires, par la longueur totale de la section.

Un pipeline pour l'évaluation comportementale a été défini et mené sur les souris pour étudier la nociception et la proprioception. Tous les tests comportementaux ont été réalisés entre 9h00 et 17h00. Les animaux ont été transférés dans la salle d'expérimentation 30 minutes avant chaque test expérimental. Le poids corporel des souris sauvages et mutantes a été mesuré à l'âge de 7-11 semaines. Les tests comportementaux ont été effectués du moins nocif au plus nocif dans l'ordre suivant : test de la ficelle (string test), barre crénelée, von Frey, Hargreaves, test de l'acétone, retrait de la queue (tail flick), pression de la queue (rodent pincher test), plaque froide et plaque chaude. Au moins 2 jours ont été conservés entre deux tests consécutifs. Les femelles et les mâles des différents génotypes ont été testés à l'âge de 2 mois.

Le test de la ficelle (string test) a été utilisé pour mesurer la force musculaire. L'outil consiste en un fil horizontal placé à 40 cm au-dessus d'une table. La souris était suspendue par le membre

antérieur au fil et la latence pour obtenir une traction du membre postérieur était mesurée. Trois essais consécutifs ont été effectués à 5 minutes d'intervalle.

Le test de la barre crénelée a été utilisé pour évaluer la coordination motrice et l'équilibre. En bref, les souris étaient placées sur une barre crénelée surélevée et devaient parcourir la distance entre le début de la barre et l'extrémité où se trouve la cage d'origine. Le temps nécessaire pour parcourir toute la distance de la barre a été enregistré. En outre, le nombre d'erreurs a été défini comme les moments où les souris touchaient les interstices de la barre crénelée avec leurs pattes arrière tout en passant au-dessus de la barre.

Un jour avant le test de Von Frey, les souris ont été placées dans de petites boîtes en plastique transparent sur un sol grillagé pour s'acclimater pendant 45 min. Le jour du test, les souris ont pu s'habituer pendant 30 min avant de commencer le test. La sensibilité mécanique a été déterminée à l'aide de 8 différents filaments de von Frey de forces spécifiques de 0,008g à 2g. Les filaments sont appliqués sur les pattes postérieures en commençant par le filament de 0,4g. La méthode de von Frey "haut-bas" a été utilisée. Chaque essai a été réalisé en appliquant les filaments sur une patte arrière des souris placées consécutivement, puis en les appliquant sur la deuxième patte arrière de chaque souris. Le test a été effectué sur deux jours consécutifs, à raison de deux essais par jour.

Deux jours avant le test de pression de queue (rodent pincher test), les souris ont été habituées à être immobilisées dans un tube de 50 ml, avec toute la queue exposée. Le test a été utilisé pour déterminer la sensibilité aux stimuli mécaniques nocifs, en appliquant une pression progressivement croissante sur la queue des souris. Ce test permet à des pinces calibrées d'induire une stimulation mécanique quantifiable sur une échelle linéaire. Trois mesures ont été effectuées pour chaque souris, en enregistrant sur trois endroits différents de la queue. Le seuil de retrait de la queue a été enregistré, avec un seuil de 500 g.

Le test de l'acétone a été utilisé pour mesurer la sensibilité aux stimuli froids. Les souris ont été placées et habituées de la même manière que pour le test de von Frey. 10 µL d'acétone ont été appliqués au centre de la surface plantaire de chaque patte arrière. L'acétone a été appliquée lors de trois sessions de test successives pour chaque patte. L'intervalle entre chaque application était d'au moins 5 minutes. La durée du retrait de la patte arrière et du battement des doigts a été mesurée pendant 30 secondes après l'application d'acétone. Les valeurs de la durée du retrait de la patte arrière et du flicage dans les six essais ont été additionnées.

Le test de la plaque froide a été utilisé pour évaluer la sensibilité aux températures froides nocives. Un jour avant le test, les souris ont été acclimatées à la plaque à température ambiante, puis le jour du test, les souris ont été testées sur la plaque froide à 5°C. Pour éviter d'endommager les tissus, un seuil de 5 min a été utilisé. Le nombre moyen de soulèvements de la patte arrière et le nombre total de sauts ont été mesurés.

Le test de Hargreaves consistait à appliquer un stimulus thermique infrarouge radiant sur les pattes arrière des souris afin de déterminer les seuils de chaleur. Un jour avant le test, les souris ont été habituées à l'appareil en les plaçant dans de petites boîtes en plastique transparent au-dessus d'une plaque de verre. La latence de retrait a été enregistrée pendant deux jours consécutifs, à raison de deux essais par jour. Un essai était réalisé en appliquant le stimulus thermique sur une patte arrière pour toutes les souris, puis sur la deuxième patte arrière pour toutes les souris, de manière à laisser au moins 5 minutes entre chaque enregistrement de patte arrière des mêmes souris. La moyenne de toutes les mesures des deux pattes arrière a été calculée. La chaleur radiante a été appliquée en utilisant une rampe de température permettant d'obtenir une latence de retrait de la patte de 7s chez les souris sauvages.

Le test de retrait de la queue (tail flick) consistait à appliquer un faisceau lumineux focalisé sur la queue de la souris, afin de déterminer les seuils de chaleur. Deux jours avant le test, les souris sont habituées à être attachées dans un tube de 50 ml, avec toute la queue exposée. Les stimuli thermiques ont été appliqués à trois endroits différents de l'extrémité de la queue et la moyenne des trois latences de retrait a été calculée.

Le test de la plaque chaude a été utilisé comme un test intégré pour déterminer la sensibilité à la chaleur. Un jour avant le test, les souris étaient habituées à la plaque à température ambiante. Dans notre étude, les souris ont été testées à 3 températures différentes sur 3 jours distincts avec des seuils spécifiques pour éviter les dommages tissulaires : 47°C pendant 3 min, 50°C pendant 1 min et 54°C pendant 30s. À chaque température, la latence pour afficher la première réaction des pattes arrières a été enregistrée. En outre, nous avons également mesuré le nombre de réactions d'adaptation comme le soulèvement, la pichenette, le léchage des pattes arrières et le saut. Le nombre total de réactions a été calculé par minute à chaque température.

Résultats

Génération et caractérisation du modèle de souris *Scn10a*^{G1663S}

Dans un premier temps, nous avons essayé de créer le modèle de souris *Scn10a*^{G1663S} grâce à la technologie innovante CRISPR-Cas9. Nous avons essayé deux stratégies différentes qui n'ont

pas abouti en raison de la grande similarité entre *Scn10a* et d'autres gènes *Scn*, en particulier le gène *Scn5a* qui partage le plus de similarité avec *Scn10a* et est exprimé sur le même chromosome. Nous sommes alors passés à la recombinaison homologue dans des cellules souches embryonnaires pour générer la lignée de souris *Scn10a*^{G1663S}. En bref, le vecteur de ciblage G1663S a été électroporé dans des cellules ES C57BL/6N, en même temps que le vecteur plasmidique contenant gR68. L'ARN guide gR68 en association avec la protéine Cas9 génère spécifiquement une cassure double brin dans la région intronique proche de la mutation à introduire. La séquence intronique, contrairement à la séquence exonique, ne présente aucune similarité avec les séquences introniques d'autres gènes *Scn*. La cassure double brin de CRISPR/Cas9 par l'ARN guide gR68 a forcé les cellules souches à réparer et la présence de la construction de ciblage avec la cassette de sélection (NeoR) a augmenté le taux de recombinaison homologue. Parmi les clones positifs, un clone a été sélectionné. L'ADN génomique de l'allèle mutant de ce clone a été amplifié par PCR avec une amorce avant située dans la cassette Cre (Fcre) et une amorce inverse externe 3', puis séquencé. Les résultats du séquençage ont démontré la présence de la mutation dans ce clone ES positif. Les souris *Scn10a*$^{+/G1663S}$ hétérozygotes ont été croisées pour générer les souris *Scn10a*$^{G1663S/G1663S}$ et leurs souris sauvages témoins. Le niveau d'expression de la transcription de *Scn10a* a été évalué dans le DRG des souris G1663S et des souris témoins par RT-ddPCR. L'ANOVA à sens unique a révélé un effet du génotype pour l'expression des transcriptions de chaque allèle (sauvage ou mutant G1663S) dans les sexes groupés ou séparés. Lorsque les ratios des transcrits *Scn10a*$^{+}$ et *Scn10a*^{G1663S} ont été additionnés, aucun effet du génotype ou du sexe n'a été détecté par l'ANOVA à deux voies. Les deux transcrits étaient également exprimés dans le DRG des souris sauvages ou mutantes G1663S/G1663S, respectivement, et dans les deux sexes, ce qui indique que la mutation n'a pas modifié l'expression de *Scn10a*. Les souris hétérozygotes +/G1663S ont exprimé environ 50 % de chaque transcrit allélique dans les DRG.

Réduction de l'IENFD chez les souris *Scn10a*^{G1663S}

Les patients SFN avec la mutation hétérozygote c.4984G>A, p.G1662S ont montré une IENFD normale. Nous avons quantifié l'IENFD chez nos souris mutantes. Aucun effet du génotype ou du sexe n'a été détecté dans le test ANOVA à deux facteurs. L'ANOVA à un facteur a montré un effet du génotype sur les sexes groupés où les souris homozygotes ont montré une IENFD réduite par rapport aux souris sauvages.

Poids corporel et proprioception normaux chez les souris *Scn10a*^{G1663S}

La mutation *Scn10a*^{G1663S} n'a pas affecté le poids corporel des souris mutantes. Les souris hétérozygotes +/G1663S et homozygotes G1663S/G1663S présentaient un poids corporel normal par rapport aux souris sauvages. Pour évaluer si la mutation modifie la proprioception des souris mutantes, les tests de la ficelle et de la barre crénelée ont été réalisés. L'analyse de la latence du test de la ficelle a révélé un effet du sexe (ANOVA à deux facteurs $F_{1, 105}$=10,76, *p*=0,0014) mais aucun effet du génotype. De même, aucun effet du génotype ou du sexe n'a été détecté dans le test de la barre crénelée. Les souris mutantes hétérozygotes et homozygotes se sont comportées de la même manière que les souris témoins dans ces deux tests. Nous avons conclu que la présence d'un ou deux allèles porteurs de la mutation G1663S n'a pas modifié la proprioception chez les souris mutantes.

Sensibilité accrue de la douleur aux stimuli mécaniques chez les souris *Scn10a*^{G1663S}

L'une des patientes SFN porteuse de la mutation hétérozygote c.4984G>A, p.G1662S a développé une sensibilité cutanée et une intolérance aux draps sur ses pieds avec une douleur continue. Nous avons utilisé le test de von Frey pour évaluer l'allodynie tactile et le test de la pression de la queue (rodent pincher test) pour évaluer la sensibilité aux stimuli mécaniques nocifs chez les souris mutantes *Scn10a*^{G1663S}. Dans le test de von Frey, un effet du génotype était présent (ANOVA à deux facteurs $F_{2, 93}$=3,461, *p*=0,0355). L'ANOVA à 1 facteur a montré un effet du génotype sur les sexes groupés où les souris hétérozygotes et homozygotes ont montré une plus grande sensibilité aux stimuli mécaniques par rapport aux souris sauvages. Cette différence n'était pas significative lorsque les mâles et les femelles étaient analysés séparément. Dans le test de la pression de queue, l'analyse bidirectionnelle a révélé un effet du sexe (ANOVA à 2 facteurs $F_{1, 106}$=4,186, *p*=0,043). Il y avait une tendance à une sensibilité plus élevée chez les mutants qui était supérieure au seuil de signification. Par conséquent, les souris mutantes *Scn10a*^{G1663S} ont développé une allodynie mécanique.

Sensibilité aux stimuli froids chez les souris *Scn10a*^{G1663S}

L'une des patientes SFN porteuse de la mutation G1662S a signalé que la température froide aggravait ses troubles et que le QST révélait des seuils anormaux pour la sensation de froid. Nous avons effectué le test de l'acétone pour étudier la sensibilité des souris *Scn10a*^{G1663S} aux stimuli de refroidissement (12°C-15°C) et la plaque de froid à 5°C pour les stimuli de froid. Dans le test à l'acétone, la durée des réactions de retrait et de flicage a révélé une interaction entre le génotype et le sexe (ANOVA à deux facteurs $F_{2, 107}$=4,336, *p*=0,015). L'analyse de Kruskal-Wallis a montré une réponse comportementale nettement plus élevée au stimulus acétone chez les

femelles mutantes, tandis que les mâles ont eu une durée de retrait et des réactions de flicage similaires à celles des mâles sauvages. Dans le test de la plaque froide, le nombre de soulèvements de la patte arrière et de sauts a montré un effet du sexe (ANOVA à deux facteurs $F_{1, 107}$=21,61, p<0,0001) avec moins de réactions chez les mâles. Les souris mutantes et témoins des deux sexes ont eu des réactions comparables sur la plaque froide. Par conséquent, les souris mutantes *Scn10a*^{G1663S} ont montré une plus grande sensibilité aux températures fraîches, mais pas aux températures froides.

La latence de la première réaction de retrait, le nombre moyen de soulèvements de la patte arrière et le nombre total de sauts ont été mesurés à 5°C et 0°C. La latence de la première réaction de retrait dans la plaque froide à 5°C et 0°C a révélé un effet du sexe (ANOVA à deux facteurs $F_{1, 107}$=12.10, p=0.0007 et $F_{1, 88}$=9.019, p=0.0035, respectivement). Un effet du génotype a été détecté pour le nombre de soulèvements de la patte arrière et le total des sauts dans la plaque froide à 0°C, où les mâles +/G1663S faisaient moins de réactions que les mâles sauvages.

Sensibilité accrue à la douleur thermique chez les souris *Scn10a*^{G1663S}

Un seuil anormal de la sensation de chaleur est également une caractéristique clinique importante des patients atteints de SFN présentant la mutation G1662S. La sensibilité des souris mutantes *Scn10a*^{G1663S} aux stimuli thermiques radiants a été testée par le test de Hargreaves et le test de retrait de la queue (tail flick). Les latences dans chacun des tests de Hargreaves et de tail flick ont donné lieu à une interaction entre le sexe et le génotype (ANOVA à deux facteurs $F_{2, 113}$=3,808, p=0,025 et $F_{2, 108}$=3,345, p=0,039 respectivement). Dans le test de Hargreaves, la mutation a réduit de manière significative la latence de la réponse, les mâles homozygotes retirant leur patte arrière plus tôt que les mâles sauvages. Dans le test de tail flick, les souris mutantes femelles ont montré un effet général du génotype.

Le test de la plaque chaude est classiquement utilisé pour déterminer les seuils de chaleur et implique des voies supraspinales. Selon une étude précédente de Huang et ses collègues, la latence de la première réaction de la patte arrière et la latence du premier saut sont des variables importantes dans ce test. Huang et al. ont introduit la notation du nombre et de la durée des léchages et des sauts en tant que comportements d'adaptation. En conséquence, nous avons noté à la fois la latence de la première réaction de la patte arrière à 47°C, 50°C et 54°C, et le nombre de réactions d'adaptation. La latence de la première réaction de la patte arrière dans la plaque chaude a montré un effet du sexe à 54°C (ANOVA à deux facteurs $F_{1, 108}$=5.703,

p=0.0187), et un effet du génotype a été détecté à 54°C pour les mâles homozygotes. Pour les réactions d'adaptation, une tendance à l'effet du génotype a été enregistrée à 47°C, bien qu'elle n'ait pas atteint le seuil de signification.

En plus de ces résultats, nous avons mesuré le nombre de réactions de flicage et de léchage par minute. Un effet du sexe a été révélé pour le nombre de léchages dans la plaque chauffante à 47°C (ANOVA à deux facteurs $F_{1, 101}$=6.032, *p*=0.016). Aucun effet global du génotype n'a été identifié pour le nombre de léchages et le nombre de pichenettes à 47°C, 50°C et 54°C. Aucun phénotype pertinent n'a été identifié dans le nombre de léchages et de flics aux trois températures.

Par conséquent, les souris mâles mutantes *Scn10a*^{G1663S} ont montré une sensibilité accrue à la chaleur.

Analyse de Gdaphen pour l'identification des variables contribuant le plus à la discrimination du génotype ou du sexe

Dans notre étude, nous avons considéré 14 variables au total, le génotype, le sexe ainsi que 12 variables comportementales. Parmi ces 14, 9 variables ont été détectées comme étant les plus pertinentes (>30%) pour discriminer entre les trois génotypes de souris. Ces variables sont le sexe, les réactions d'adaptation dans une plaque chaude à 47°C et 54°C, les réactions d'adaptation et la latence dans la plaque chaude à 50°C, le test à l'acétone, les levées de pattes et les sauts dans la plaque froide à 5°C, la pression de von Frey et la pression de la queue. Nous avons cherché à identifier les variables qui contribuaient le plus à la discrimination du génotype et du sexe, en évaluant la capacité de chaque variable à discriminer entre les trois génotypes et entre les deux sexes. Les classificateurs generalized linear model (GLM) et random forest (RF) ont identifié von Frey comme la variable la plus importante pour la discrimination entre les trois génotypes. Le RF a également été capable d'identifier l'acétone, les réactions d'adaptation et la latence dans la plaque chaude à 50°C et la pression de la queue comme variables majeures. Le GLM et la RF ont identifié la pression de la queue, les levées de pattes et les sauts dans la plaque froide à 5°C et les réactions d'adaptation dans la plaque chaude à 50°C comme les variables les plus importantes pour la discrimination du sexe. Le GLM a également identifié l'acétone comme une variable importante et le RF a également identifié les réactions d'adaptation dans la plaque chaude à 47°C comme une variable importante. D'après la carte à composantes 2D de la discrimination qualitative, le sexe a un effet plus fort que le génotype pour la discrimination entre les groupes. En effet, les animaux hétérozygotes et homozygotes sont plus fortement séparés

des sauvages dans les dimensions 2 et 3, que dans la dimension 1. Les mâles et les femelles sont fortement séparés dans la dimension 1, mais pas dans les autres dimensions. La corrélation entre chaque composante principale des analyses séparées de chaque variable et les composantes principales (dimensions) a révélé que les réactions de von Frey et d'adaptation dans une plaque chaude à 47°C contribuent le plus à la discrimination du génotype dans les dimensions 1 et 2 et les dimensions 2 et 3. La pression de la queue a également été identifiée dans les dimensions 1 et 2 et les soulèvements et sauts de pattes dans une plaque froide à 5°C dans les dimensions 2 et 3. Les réactions d'adaptation dans la plaque chaude à 50°C et 54°C et les soulèvements et sauts de pattes dans la plaque froide à 5°C ont contribué le plus à la discrimination du génotype dans les dimensions 1 et 3, la contribution la plus forte étant dans la dimension 1.

Conclusions et perspectives

Conclusion

La douleur chronique peut être pénible et même torturante pour les patients. Cependant, la sensation de douleur est essentielle pour nous protéger du danger et permettre la réparation des tissus. Les patients atteints d'insensibilité congénitale à la douleur (Congenital insensitivity to pain CIP) ne bénéficient pas de ces particularités, puisqu'ils ne ressentent aucune douleur à la suite de stimuli nocifs, y compris l'inflammation et la chaleur. La SFN comprend un groupe hétérogène de neuropathies affectant de manière sélective ou prédominante les fibres Aδ myélinisées de petit diamètre et les fibres C non myélinisées et épargnant les fibres de grand diamètre. La SFN s'accompagne de symptômes sensoriels positifs, principalement des douleurs spontanées avec des sensations de brûlure, de tir, de type électrique, de picotement ou de démangeaison. Certains patients peuvent développer une peau sensible, une intolérance au port de draps, de chaussettes ou de chaussures sur les pieds et un syndrome des jambes sans repos. Des crampes et des picotements sont également perceptibles dans la partie inférieure des jambes et des pieds. Les symptômes sensoriels négatifs sont également importants, comme la perte des sensations thermiques, des piqûres d'épingle et d'autres sensations nociceptives, ainsi que l'engourdissement ou la sensation d'oppression. Des mutations des gènes *SCN9A* et *SCN10A* ont été trouvées chez une partie des patients atteints de SFN. Des études sur des modèles de rongeurs *Scn10a* ont mis en évidence le rôle important du canal SCN10A dans la nociception. Pour mieux comprendre le mécanisme de la douleur chronique chez les patients et explorer de

nouveaux analgésiques, de nouveaux modèles précliniques pertinents sont nécessaires. Deux équipes ont développé des neurones sensoriels différenciés à partir de cellules souches pluripotentes induites dérivées de patients qui modélisent l'érythromélalgie héréditaire in vitro. Ces cellules peuvent fournir une plateforme permettant d'évaluer les effets des bloqueurs des canaux sodiques in vitro. Il sera ensuite nécessaire d'analyser leurs effets et leur sécurité dans les modèles génétiques *Scn* disponibles et dans d'autres modèles animaux précliniques. La création de modèles animaux porteurs des mutations humaines SCN10A qui ont été identifiées chez des patients atteints de douleur neuropathique est nécessaire et les études pharmacologiques font défaut. La mutation hétérozygote *SCN10A*^{G1662S} a été initialement signalée chez deux patientes atteintes de SFN. Les deux patientes ont signalé des douleurs continues, notamment dans les pieds ou les jambes, ainsi que d'autres symptômes autonomes. L'une d'entre elles présentait des seuils anormaux pour les sensations de chaleur et de froid dans les deux mains. La seconde a développé une peau sensible, une intolérance aux draps sur ses pieds, et a montré une hypoesthésie et une réduction de la sensation de vibration des jambes révélées par l'examen physique et des niveaux anormaux de sensation de chaleur pour les deux pieds. Une troisième patiente présentant la mutation G1662S du gène *SCN10A* a été récemment signalée. Elle présentait des seuils de température anormaux. Le but de notre étude était d'abord de créer le modèle de souris *Scn10a*^{G1663S} et ensuite de procéder à la caractérisation moléculaire, cellulaire et comportementale des souris mutantes. À notre connaissance, nous sommes le premier groupe à avoir créé ce modèle de souris portant une mutation humaine liée à la douleur dans le gène *Scn10a*. Nous avons pu générer cette lignée de souris *Scn10a*^{G1663S} par recombinaison homologue dans des cellules souches embryonnaires. Nous avons augmenté l'efficacité de la recombinaison homologue en utilisant un vecteur contenant le Cas9-gR68. Une transmission germinale de 80% de la couleur du pelage des cellules souches a été obtenue et des animaux hétérozygotes portant la mutation *Scn10a*^{G1663S} ont été générés. Nous avons utilisé la fécondation in vitro pour augmenter le nombre de souris hétérozygotes, puis les souris hétérozygotes ont été croisées pour générer des souris de génotype homogène. La mutation G1663S n'a pas modifié l'expression du transcrit *Scn10a* dans les tissus du DRG et de la moelle épinière des souris mutantes. Les souris mutantes *Scn10a*^{G1663S} ont révélé une sensibilité accrue aux stimuli mécaniques nocifs et non nocifs, comme le montrent respectivement les tests de von Frey et de pression de la queue. Les souris mutantes ont également une réaction accrue aux stimuli froids comme le montre l'application d'acétone et une sensibilité accrue aux stimuli thermiques dans le test de Hargreaves. Par conséquent, nous avons pu prouver l'importance du

canal SCN10A dans la sensibilité aux stimuli mécaniques nocifs et inoffensifs, aux stimuli froids et son implication dans le réflexe spinal.

Densité des IENF chez les souris mutantes

La densité et la morphologie des fibres nerveuses intra-épidermales (IENF) sont en bonne corrélation avec le dysfonctionnement des petites fibres nerveuses et sont des critères importants dans l'évaluation des patients atteints de SFN. La densité des IENF est comparée aux valeurs normatives de référence ajustées en fonction de la décennie de vie et du sexe. Chez trois patients atteints de CIP, il y avait une perte complète des IENF et seules les fibres dermiques étaient présentes. Les trois patientes porteuses de la mutation *SCN10A*^{G1662S} présentaient des valeurs normales d'IENFD par rapport aux valeurs normatives appariées en fonction de l'âge et du sexe. Cependant, les patients porteurs d'autres mutations de *SCN10A* présentaient une perte d'IENF. Chez un couple père-fils, porteur de la mutation L554P du gène *SCN10A*, le père présentait une perte presque complète des IENF et le fils une déplétion complète des IENF et une réduction importante de la densité des faisceaux nerveux dermiques, qui semblaient fragmentés en raison de la dégénérescence axonale. D'autres patients atteints de SFN présentant les mutations I1706V et D1639N du gène *SCN10A* ont également présenté une diminution remarquable des IENFD. Cependant, l'étude de de Greef et al 2018 a indiqué que, sur 921 patients atteints de SFN, 239 + 68 présentaient une IENF anormale alors que 614 avaient une IENFD normale.

Douleur spontanée non évoquée

Les comportements réflexes de la douleur ont été évalués pendant plusieurs années dans des modèles animaux. Néanmoins, la douleur neuropathique est généralement caractérisée par une douleur évoquée, mais aussi par une douleur spontanée non évoquée. Comme les tests comportementaux que nous avons réalisés étaient principalement des tests réflexes, il serait important de réaliser des tests de douleur non-réflexe et non-évoquée sur notre modèle mutant dans de futures études. De nombreux tests et paramètres évaluant la douleur spontanée sont disponibles et ont été utilisés dans des études précédentes. Dans un modèle de cancer osseux induit chez le rat, où les cellules tumorales ont été injectées dans le membre postérieur droit, la douleur spontanée a été évaluée en plaçant l'animal dans un cylindre en plastique transparent et en mesurant la durée de différents comportements spontanés, y compris l'évanouissement spontané ou la garde du membre postérieur affecté et le saut intermittent sans utiliser le membre affecté. Le Catwalk est un système automatisé d'analyse de la démarche basé sur le mouvement volontaire des rongeurs dans une passerelle fermée et utilisé pour évaluer la fonction motrice et la coordination chez les modèles de rongeurs. Cette méthode s'est avérée fiable pour mesurer

les comportements associés à la douleur chez les rongeurs, lorsqu'elle est également évaluée par d'autres tests de douleur évoquée. Le rongeur est d'abord placé à l'extrémité ouverte de la plateforme en verre éclairée et est autorisé à marcher librement dans la passerelle, tandis qu'une caméra à haute vitesse placée sous l'appareil capture des images de la zone éclairée de chaque patte. La garde des membres, qui est une manifestation clinique courante chez les personnes souffrant de douleurs articulaires, neuropathiques et postopératoires, peut être mesurée chez les rongeurs en vérifiant le poids porté sur les membres pendant une courte marche. Dans la même étude sur le modèle de rat du cancer osseux induit, différents paramètres ont été mesurés, la surface maximale de l'empreinte et l'intensité reflétant la pression exercée par le contact maximal d'une patte arrière, la durée du contact au sol d'une patte arrière alors que l'autre patte arrière ne touche pas la plaque et la durée pendant laquelle aucune patte arrière ne touche la plaque de verre. La préférence de place conditionnée peut être utilisée pour inspecter la préférence pour les analgésiques. Au cours d'une phase de préconditionnement, les animaux sont placés dans une boîte composée d'une chambre centrale neutre et de deux chambres différant par des indices visuels, texturaux et olfactifs. Ensuite, des essais de conditionnement sont effectués avec l'administration de l'analgésique dans l'une des deux chambres, associant l'analgésique à une certaine chambre. Le jour du test, le temps passé dans la chambre associée au médicament indique une préférence en l'absence d'analgésique, associant le soulagement de la douleur à un contexte distinct. Le test d'évitement conditionné des lieux reflète les résultats cliniques en ce sens que les patients souffrant de douleurs évitent les stimuli douloureux. Ce test est similaire au test de préférence de place conditionnée, mais lors du conditionnement, les animaux se voient injecter une substance nocive. Le jour du test, en l'absence d'une injection produisant de la douleur, la préférence de place conditionnée est mesurée comme une indication de l'abstention d'une condition nocive.

Tests thermiques additionnels

En plus du test thermique standard des plaques chaudes et froides, d'autres dispositifs peuvent être utilisés pour évaluer les préférences thermiques en tant que tests complémentaires. Le test de choix de deux plaques mesure le temps que l'animal passe sur une plaque à 30°C par rapport à une plaque adjacente à différentes températures. Les souris TRP melastatin 8 KO ont fait des transitions complètes vers le côté le plus froid alors que les souris sauvages préféraient la plaque à 30°C. Néanmoins, les souris KO ont fait des transitions complètes vers le côté le plus froid. Néanmoins, les souris KO ont montré la même préférence pour les plaques à 30°C et les plaques nocives à 49°C, ne montrant pas une déficience générale de la thermosensation. Les souris

mutantes ont montré des latences similaires à celles des souris sauvages pour la première réaction lorsqu'elles étaient placées sur une plaque réglée à 52°C, 10°C, 0°C ou -5°C. Le test du gradient thermique consiste en un gradient de température continu allant du froid aux températures élevées le long d'une plaque métallique sur laquelle l'animal marche librement tout en étant enregistré par vidéo depuis le haut. L'arène est virtuellement divisée en 15 zones de taille égale avec une température spécifique et stable. L'animal montre une préférence pour une plage de température confortable pendant un temps de mesure défini. Les souris mâles KO du membre de la famille Helix-Loop-Helix A9 ont montré une préférence pour les températures plus froides par rapport au sauvage pendant les 30 secondes minutes d'enregistrement. Ce comportement a été fortement accentué au cours des 30 dernières minutes où les souris sauvages préféraient fortement 33°C et les souris KO étaient incapables de distinguer les températures entre 24°C et 37°C. Les souris TRPV1 KO ont montré une légère préférence pour les températures plus chaudes (25°C-36°C) alors que les souris TRPV3 KO ont tendance à préférer les températures plus fraîches (22°C-26°C). Ce phénotype est réduit chez les souris doublement KO TRPV1/ TRPV3. L'essai thermique plantaire opérant est un outil récemment développé qui consiste en deux étages de chambres fixés à une plaque thermorégulatrice. Une bouteille d'eau a été introduite dans chaque chambre. Une bouteille était vide et la seconde contenait une solution de saccharose qui est gratifiante pour les animaux. Les animaux ont été enregistrés sur vidéo et placés du côté neutre au début de chaque session de formation et de test. Le test est basé sur le fait que l'animal apprend et décide d'obtenir une récompense en passant par une température aversive ou en s'en abstenant. Les souris modèles présentant une lésion chronique par constriction et les souris sham ont toutes deux évité les températures élevées et basses, bien que les souris blessées aient passé plus de temps dans la zone de récompense à travers des températures même aversives. Cependant, les souris recevant une administration d'adjuvant complet de Freund ont passé un temps similaire dans la zone de récompense que les souris témoins.

Dans notre étude, en plus de la procédure standard de la plaque chauffante, j'ai mesuré différentes réactions d'adaptation. Cette approche est assez nouvelle dans le domaine de la douleur, et a été introduite pour la première fois par Huang et al. Dans le cadre de notre étude, il serait utile d'effectuer des tests thermiques supplémentaires pour étudier en profondeur la sensibilité et la préférence aux températures chaudes et froides.

Publications and Oral Communication

Publications

1. The human *SCN10A*^{G1662S} point mutation established in mice have a small impact on mechanical, heat and cool sensitivity

   Celeste Chidiac, Yaping Xue, Ameer Abu Bakr Rasheed, Romain Lorentz, Marie-Christine Birling, Claire Gaveriaux-Ruff *and Yann Herault*

   (**Under preparation**)

2. Pain Behavior in SCN9A (NAV1.7) and SCN10A (NAV1.8) mutant mice

   Yaping Xue*, Céleste Chidiac*, Claire Gavériaux-Ruff, Yann Hérault (*equal contribution)

   (**Accepted for publication in Neuroscience Letters**)

Oral Presentations

Date	***Place***	***Meeting***	***Title***
23/04/2018	U Maastricht Netherland	First Annual Meeting PAIN-Net	Development and characterisation of pain-related sodium channel CRISPR-Cas mouse model for Nav1.8
27/11/2018	FINCB, Milan, Italy	PAIN-Net mid-meeting	Development and characterisation of pain-related sodium channel mouse model for Nav1.8
05/04/2019	IGBMC	Second Annual Meeting PAIN-Net	Development and characterisation of pain-related sodium channel mouse model for Nav1.8

Poster Presentations

Date	***Place***	***Meeting***	***Title***
22-23/3/2018	Château du Liebfrauenberg	Translational medicine and neurogenetics Dpt retreat	Development and characterisation of pain-related sodium channel CRISPR-Cas mouse model for Nav1.8-G1662S
12/03/2019	Maison du Kleebach in Munster	Translational medicine and neurogenetics Dpt retreat	Development and characterisation of pain-related sodium channel CRISPR-Cas mouse model for Nav1.8-G1662S

13/09/2019	Strasbourg Doctoral School	“Back to school” of Neuroscience Master students	Development and characterisation of pain-related sodium channel mouse model for Scn10aG1662S
26/09/2019	IGBMC	33rd International Mammalian Genome Conference	Development and characterisation of pain-related sodium channel mouse model for Scn10aG1662S
12/07/2020	Online	FENS 2020	Development and characterisation of pain-related sodium channel mouse model for Scn10aG1662S

Abbreviations

AP: Action Potential
aa: amino acids
bp: base pairs
Cas9: CRISPR associated gene 9
CCM: Corneal Confocal Microscopy
CDT: Cold Detection Threshold
CIP: Congenital Insensitivity to Pain
CNS: Central Nervous System
CRISPR: Clustered Regularly Interspaced Short Palindromic Repeats
crRNA: CRISPR RNA
D: Domain
DRG: Dorsal Root Ganglion
dsDNA: double stranded DNA
DSB: Double Strand Break
EGFP: Enhanced Green Fluorescent Protein
EM: ErythroMelalgia
EMG: ElectroMyoGraphy
ERT2: Estrogen Receptor ligand-binding domain 2
ES: Embryonic Stem
ESC: Electrochemical Skin Conductance
GEFS^{+}: Generalized Epilepsy with Febrile Seizures Plus
GFP: Green Fluorescent Protein
GLM: Generalized Linear Model
GOF: Gain-Of-Function
gR: gRNA: guide RNA
Hprt: Hypoxanthine phosphoribosyl transferase
HR: Homologous Recombination
IASP: International Association for the Study of Pain
ICC: ImmunoCytoChemistry
IEM: Inherited ErythroMelalgia
IENFD: IntraEpidermal Nerve Fiber Density
IHC: ImmunoHistoChemistry
indels: insertions or deletions
iPSCs: Induced Pluripotent Stem Cells
KI: Knock-In

KO: Knockout
LB: Lysogeny Broth
LEPs: Laser Evoked Potentials
LOF: Loss-Of-Function
LQTS: Long QT Syndrome
MFA: Multiple Factor Analysis
MultiGLM: multinomial log-linear Generalized Linear Model
NAV: sodium channel isoforms
NCS: Nerve Conduction Study
NG: Nodose Ganglia
nt: nucleotides
PAM: Protospacer Adjacent Motif
PBS: Phosphate Buffer Saline
PCA: Principal Component Analysis
PCR: Polymerase Chain Reaction
PE: Pore Entity
Penk: Preproenkephalin
PFA: ParaFormAldehyde
PGP: Protein Gene Product
PM: Point Mutation
PNS: Peripheral Nervous System
pre-crRNA: precursor CRISPR RNA
RF: Random Forest
RT: Room Temperature
RT-ddPCR: Real Time droplet digital PCR
QSART: Quantitative Sudomotor Axon Reflex Testing
QST: Quantitative Sensory Testing
S: Segments
SCG: Superior Cervical Ganglion
SFN: Small Fiber Neuropathy
SLIC: Sequence and Ligase Independent Cloning
ssgRNA: single-stranded guide RNA
ssODN: single-stranded Oligo-DeoxyNucleotide
TALEN: Transcription Activator- Like Effector Nuclease
TCA: TriCyclic Antidepressants
TG: Trigeminal Ganglion
TN: Trigeminal Neuralgia

tracrRNA: trans-activating RNA

TRP: Transient Receptor Potential

TRPV: TRP Vanilloid: Transient Receptor Potential Vanilloid

TTX: Tetrodotoxin

TTX-R: Tetrodotoxin-Resistant

TTX-S: Tetrodotoxin-Sensitive

VGLUT3: Vesicular Glutamate Transporter 3

VGSC: Voltage-Gated Sodium Channels

VSM: Voltage-Sensing Module

WDT: Warm Detection Threshold

WT: Wild type

ZFN: Zinc-Finger Nuclease

I Introduction

1. Nociception and Pain

1.1 Definition of Nociception and Pain

The ability of all organisms to detect and respond to various types of external stimuli allows them to remain alive. These stimuli are detected in the sensory nerve endings based on their onset, intensity, duration and location, allowing the conversion of noxious stimuli into electrical signals transmitted to the spinal cord and the brain [1-3]. The physiological term ‘‘nociception” is used to describe these relatively specialized sensory processes. A noxious stimulus is a tissue-damaging event that is detected, transduced and encoded by nociceptors. Some types of tissue damage are not detected by sensory receptors and thus do not cause pain. This phenomenon is well known for solid visceral organs, but also applies to damage to skin and deep somatic tissues, by ultraviolet radiation or X-rays [2]. Nociception is at the core of many painful states; however “Nociception” and “Pain” should not be confused. Nociception can occur without pain sensation and pain can exist regardless of a nociceptive stimulus, such as phantom limb pain which is a pain that feels like it is coming from a body part that is no longer there [2, 4]. R.D. Treede distinguished in 2018 nociception and pain: nociception is a third-person perspective, it is stimulus-related and depends on sensory discrimination, whereas pain is a first-person perspective, it is perception-related and includes suffering [5]. So, what is this thing called pain? What does it mean to be in pain? Pain acts as a warning and protective physiological system that allows to consciously feel a damage in the body and react to avoid such damage [6, 7]. But can pain be exactly defined? In 1942, in his book Pain, a brilliant researcher, T. Lewis, revealed that he was unable to conveniently define pain, and that any attempt to do so “could serve no useful purpose” [8, 9]. In 1960, H. Merskey formulated a definition of pain as “An unpleasant experience that we primarily associate with tissue damage or describe in terms of tissue damage” [10]. This formulation was adapted and revised in 1979 by the International Association for the Study of Pain (IASP) as follow “an unpleasant sensory and emotional experience associated with actual or potential tissue damage, or described in terms of such damage”. This definition added to Merskey’s formulation that pain episodes are sensory and emotional. Since then, huge advances were done in the understanding, assessment and treatment of pain and many studies proved the usefulness of this definition [2, 5, 11, 12]. Other studies criticized this definition and proposed alternative definitions [3, 9, 11-13]. Most sensory experiences are neutral, whereas some are

pleasant and others unpleasant, varying in intensity and duration. Therefore, pain is both an unpleasant sensation in the body and an emotional experience [3, 13]. However, emotion does not have an accepted meaning and so it can be interpreted in many ways [14]. When one is exposed to a nociceptive stimulus such as hitting his elbow on a door, the pain is felt accompanied with irritation, distress and discomfort for just few seconds. These are emotions just lasting few seconds, and are not considered as components of pain, but rather emotional effects of pain [3]. Because of the suggested pain subjectivity, neither an obvious nociception nor clear tissue damage must be evident for the pain to be real [9, 13]. For example, one can express a sensory unpleasant episode, which doesn't reflect pain, when smelling burned food or hearing a noisy sound [3]. Many people report pain sensation due to psychological issues and in the common language usage pain terminology can be a metaphor, when saying "I feel as if there is a knife in my back" or, "my heart is broken" [4, 9, 14]. So, what distinguishes pain as a sensory unpleasant experience is its association with actual or potential tissue damage. Sure there is a complex set of sensory and affective phenomenal qualities distinctive of pain experiences that one is subjectively acquainted with when one is experiencing pain - this is how one generally comes to recognize that one is in pain [3]. Linking the unpleasant sensory and emotional experience with actual or potential tissue damage requires that the experience is associated to the damage by thought [14]. Furthermore, the IASP definition gives power to some patients to bring their pain into existence through self-report. However, newborns, young children, some patients, verbally handicapped individuals, cognitively or developmentally disabled individuals and even primate and non-primate animals can experience pain without being able to clearly think about it and verbalize it [3, 14-16]. It is confusing from whose point of view such an association exists: is it based on the judgment of an outside observer or the experience of the person in pain? [13]. In 2018, M. Cohen et al. added that our own experiences are not simply private events but are linked with other experiences to which publicly shared concepts can be applied. Questions often arise when mentioning pain: "Are you feeling okay? What do you feel? What has caused the pain?" Description of pain sensation is communicated using shared concepts so that others can apprehend what is going on with the person. Although pain is subjective, we cannot deny objective aspects of pain, giving back credits to the observer. In addition, M. Cohen marked that the association of pain to tissue damage puts the focus on a problem of and in the body, and not with the body; suggesting that "Pain is a mutually recognizable somatic experience that reflects a person's apprehension of threat to their bodily or existential integrity" [5, 9, 11]. Williams and Craig defined pain in 2016 as a "distressing experience associated with actual or potential tissue damage with sensory, emotional, cognitive and social components". This suggested definition

considers the cognitive and social components of pain, in addition to sensory and emotional components. It also underlines that pain can be more than an unpleasant experience and can even be a distressing experience [11, 12]. In 2011, A. Wright noted that the term “potential tissue damage” refers to an undamaged tissue state which differs in some objective way from other undamaged tissue or that there is some sort of intermediate tissue state which is neither damaged nor undamaged. The chemical and anatomical profile of the tissue state, defined in terms of the stimuli detected by nociceptors, when a potentially tissue damaging event occurs [2, 14]. A. Wright conceived of “emotion” as the motive that force individuals to change their attitude in order to diminish the unpleasantness or discomfort caused by pain [14, 17]. Based on these points, A. Wright suggested the following definition of pain: “Pain is the unpleasant sensation that has evolved to motivate behaviour which avoids or minimizes tissue damage or promotes recovery” [11, 14].

The task force recommended and published on IASP website the following definition and notes, seeking feedback from the public:

Pain:

An aversive sensory and emotional experience typically caused by, or resembling that caused by, actual or potential tissue injury.

Notes:

-Pain is always a subjective experience that is influenced to varying degrees by biological, psychological, and social factors.

-Pain and nociception are different phenomena: the experience of pain cannot be reduced to activity in sensory pathways.

-Through their life experiences, individuals learn the concept of pain and its applications.

-A person’s report of an experience as pain should be accepted as such and respected.

-Although pain usually serves an adaptive role, it may have adverse effects on function and social and psychological well-being.

-Verbal description is only one of several behaviors to express pain; inability to communicate does not negate the possibility that a human or a nonhuman animal experiences pain [11].

Some criticisms were done on the term “aversive” and the importance of using the simpler term “unpleasant”. Another relevant point was that less emphasis on tissue injury should be made and though reverting “typically caused by” to “associated with” omits the direst cause and effect link between pain experience and tissue injury. Concerning the suggested notes, qualifying pain as “subjective” was not convenient since pain experience remains singular to each individual. The

second note was not precise knowing that some brain regions are expected to be contributors to pain above and beyond nociceptive inputs [11, 18].

Following further discussions based on the feedbacks, the IASP published on July 2020 the revised pain definition with its associated notes [11]:

“An unpleasant sensory and emotional experience associated with, or resembling that associated with, actual and potential tissue damage”.

-Pain is always a personal experience that is influenced to varying degrees by biological, psychological, and social factors.

-Pain and nociception are different phenomena. Pain cannot be inferred solely from activity in sensory neurons.

-Through their life experiences, individuals learn the concept of pain.

-A person’s report of an experience as pain should be respected.

-Although pain usually serves an adaptive role, it may have adverse effects on function and social and psychological well-being.

-Verbal description is only one of several behaviors to express pain; inability to communicate does not negate the possibility that a human or a nonhuman animal experiences pain.

1.2 Nociception and Pain

The somatosensory system allows for the perception of touch, pressure, pain, warm, cold, movement and vibration. The somatosensory nerves arise in the skin, muscles, joints and fascia and include thermoreceptors, mechanoreceptors, chemoreceptors, pruriceptors and nociceptors [19]. Nociceptive fibers can be divided into three different subtypes. **Aβ-fibers** are large myelinated, with a diameter of 6 to 12 µm, a conduction speed of 35 to 90 m/s and function as mechanoreceptors (Figure 1). They carry touch, pressure and vibration information from the skin, conveying innocuous tactile stimuli. Furthermore, they have been shown to generate ectopic action potentials (APs) in some chronic pain models and are known to contribute to the development of tactile allodynia. **Aδ-fibers** are thinly myelinated, with a diameter of 1 to 5 µm, a conduction speed of 5 to 40 m/s and function as nociceptors. They carry thermal and mechanical information from the skin and intervene in pinprick and burning pains (Figure 1). When encountering a noxious stimulus, these fibers are the first to be activated, providing the fast pain.

C-fibers are thin unmyelinated, with a diameter of 0.02 to 1.5 µm, a conduction speed of 0.5 to 2 m/s and function as nociceptors. They carry polymodal information regarding mechanical, thermal, and/or chemical nociception (Figure 1). These fibers provide slow persisting pain, they intervene in deep burning pain and pinprick pain. C-fibers are classified in subpopulations. Type 1A units are mechano-heat-sensitive. Type 1B are mechano-heat-insensitive or silent fibers, they become sensitive to noxious mechanical or heat stimuli after being sensitized by inflammatory mediators (capsaicin, heat sensitization). Type 2 are non-nociceptive fibers, including thermoreceptor fibers and low threshold cutaneous mechanoreceptor fibers as pleasure fibers. Type 3 are cold units and type 4 are sympathetic [20-22]. Following activation of nociceptors, stimuli are transduced into APs that can be directed immediately in a spinal reflex loop, producing a rapid and reflexive withdrawal or transported to the brain for further processing and integrating the information with higher-ordered sensations such as pain [21, 22].

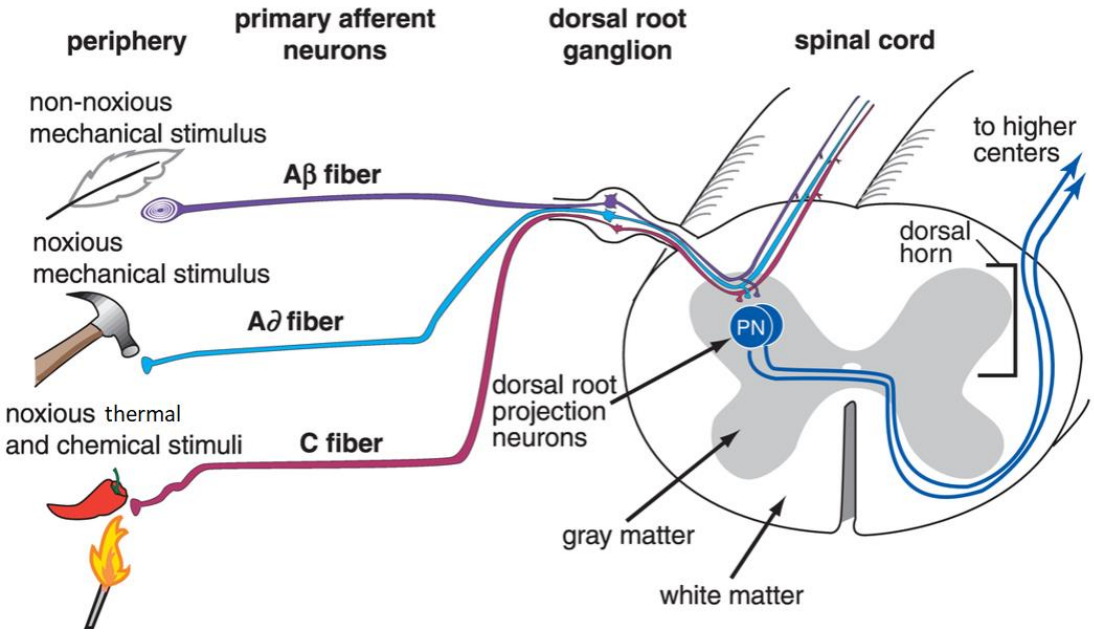

Figure 1: Activation of nociceptive nerve fibers.

Detection of a noxious stimulus occurs at the peripheral terminals of primary afferent neurons and leads to generation of action potentials (AP) that propagate along the axon to the central terminals. Aβ-fibers respond only to non-noxious mechanical stimuli, Aδ-fibers respond to noxious mechanical stimuli and subnoxious thermal stimuli, and C-fibers respond to noxious mechanical, thermal, and chemical stimuli. Primary afferent neurons have their cell bodies in the dorsal root ganglion and send terminals into that spinal cord segment as well as sending less dense collaterals up the spinal cord for a short distance. Primary afferent neurons synapse onto several different classes of dorsal horn projection neurons, which project via different tracts to higher centers. Adapted from Stahl, S. M., 2013 [23].

Pain can range widely in intensity, quality, and duration and has diverse pathophysiologic mechanisms and meanings [4]. It is important to distinguish between acute, persistent and chronic pain. Acute pain is an early-warning protective system, signaling a danger, essential to detect and minimize contact with damaging or noxious stimuli, in order to avoid injuring ourselves. This type of pain is fast, requires direct attention and action, while one needs to rapidly withdraw their hand from sharp, hot or cold stimuli (Figure 2) [1, 7]. Persistent pain is the pain that one feels after an injury, operation or tissue damage, signaling that something is wrong. That pain drives the body to protect the injured site and assists in the healing process until completely recovered. Sometimes, this pain can go on for longer than one has expected and persist even though there is no longer any problem in the body's tissues. Changes occurring in the nervous system can be long-lasting leading to a chronic or pathological pain state. This type of pain, which is different from acute and persistent pain, is regarded as a disease by itself and not a symptom of some disorder. It is not a protective pain, but rather a maladaptive pain serving as a false alarm due to the malfunction of the nervous system [1]. Inflammatory pain can be persistent or chronic. Inflammatory pain is caused by the activation of the immune system in response to tissue injury or damage. Damaged cells release a set of inflammatory mediators such as molecules, peptides, cytokines, prostaglandins and enzymes that directly activate nociceptors (Figure 2). This milieu can enhance the release of more chemicals, sensitizing afferents to a painful response [1, 7]. Neuropathic pain is different than the other pain conditions, and is thus diagnosed and treated differently.

2. Neuropathic pain

2.1 Definition and types

Neuropathic pain "arises as a direct consequence of a lesion or diseases affecting the somatosensory system" as defined by IASP in 2008 [24]. It is a pathological pain related to functional changes in primary afferents, and sensitization within the CNS leading to both evoked pain and spontaneous pain (Figure 2), in which messages of pain are being sent to the CNS regardless of noxious stimuli [6, 24-26]. Neuropathic pain can also be caused by lesions in the CNS, it can occur after stroke [27].

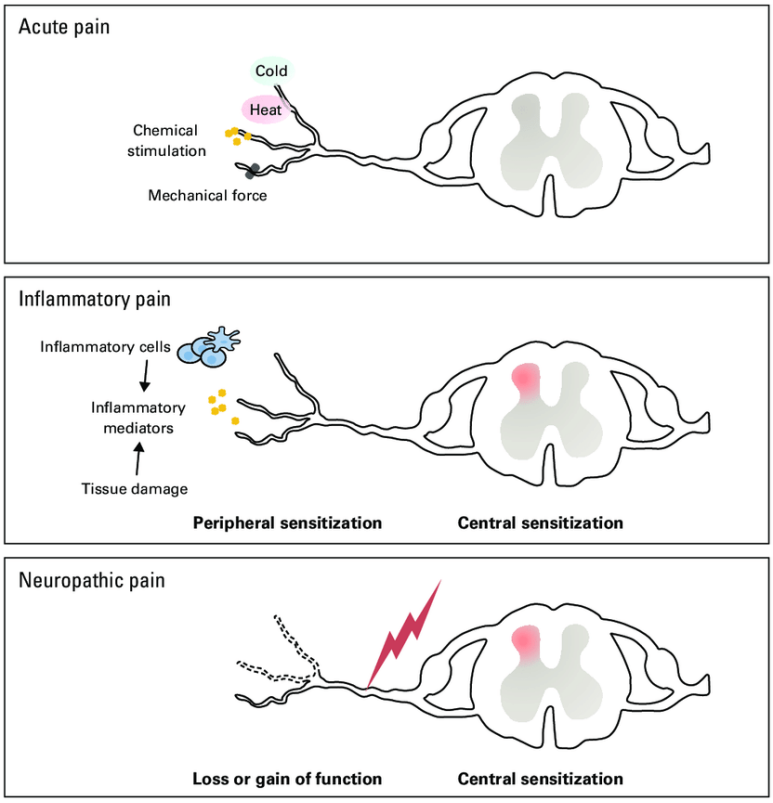

Figure 2: Pain classification.

Pain can be broadly divided into three classes. Acute pain is caused by an activation of nociceptors by noxious stimuli, does not induce long-term tissue or nerve damage, characterized by a normal healing and a normal transmission to spinal cord and brain. Inflammatory pain is caused by chemical activation of nociceptors by mediators produced by damaged tissue and immune cells, induces an ongoing and evoked pain, characterized by a peripheral sensitization, enhanced inputs into spinal cord and transmission to sensory and affective brain areas. Neuropathic pain is caused by a damage or lesion to fibers or neurons, induces an ongoing and evoked pain, characterized by gain and loss of somatosensory function, increased compensatory spinal transmitter release and transmission to sensory and affective brain areas. Adapted from Falk S. and Dickenson A.H., 2014 [28].

Neuropathic pain is characterized by extensive changes in the stimulus-response function leading to allodynia, pain in response to a stimulus that usually does not induce pain, such as touch or brush; dysesthesia, spontaneous unpleasant painful sensations like burning, tingling, or electrical sensations; hyperalgesia, increased response to painful stimuli; hypoesthesia, a numbness or lessening of feeling; paresthesia, spontaneous abnormal nonpainful sensations such as tingling and hyperpathia, exaggerated pain response [1, 25, 26, 29]. Some patients with neuropathic pain experience a constant, relentless and severe sensation of pain, whereas other report paroxysmal intermittent pain, that can be aggravated by stimuli or touch [30]. Some types of neuropathic injury

can produce a distinct set of symptoms, such as burning, tingling and shooting pain traveling along the body [25, 30]. Symptoms can persist and have a tendency to become chronic and respond less to pain medications [19]. Neuropathic pain affects 5% of the general population and 40% of patients with neurological diseases [31].

Neuropathic pain is mechanistically dissimilar to other chronic pain conditions such as inflammatory pain that occurs, for example, in rheumatoid arthritis, in which the primary cause is inflammation with altered chemical events at the site of inflammation [19]. Phantom limb syndrome is one example of neuropathic pain where the patients still feel sensations and pain in an arm or leg that has been removed because of illness or injury, but the brain still gets pain messages from the nerves that originally carried impulses from the missing limb. Patients can percept movement, touch, pressure, vibration, itch and changes in cold and warm sensations of the amputated limb. They also complain about numerous pain sensations such as burning, aching and shooting pain and tingling feelings [32]. Sleep disturbances, anxiety and depression are frequent and severe in patients with neuropathic pain, and quality of life is more impaired in patients with chronic neuropathic pain than in those with chronic non-neuropathic pain that does not come from damaged or irritated nerves [19]. Peripheral neuropathic pain is frequently observed in patients with cancer, AIDS, long standing diabetes, lumbar disc syndrome, herpes infection, traumatic spinal cord injury, multiple sclerosis and stroke [19]. Not all patients with peripheral neuropathy or central nervous injury develop neuropathic pain. Peripheral neuropathy alters the electrical properties of sensory nerves, which then leads to imbalances between central excitatory and inhibitory signaling. At the periphery and in the spinal cord and brain, a gain of excitation and facilitation and a loss of inhibition are apparent. These changes shift the sensory pathways to a state of hyperexcitability. Despite progress in the understanding of this syndrome, the mechanistic details underlying the disease remain elusive [19]. Adequate treatments for painful neuropathies are still not available, there is a lack in drugs acting specifically and selectively on the target site known for its pathogenicity. Less than half of neuropathic patients notice 50% of pain relief, using available analgesics, whereas at least 25% of patients stop taking drugs due to their atypical side effects. In addition, treatments are prescribed to patients suffering from pain without being conveniently selected [33].

As we have already seen, even though chronic pain can be torturing, pain sensation is essential for protecting us from danger and allowing for tissue repair.

Some individuals do not benefit from these particularities, since they are born with the absence of pain perception. Congenital Insensitivity to Pain (CIP) is a hereditary sensory and autonomic neuropathy type 5, where patients do not feel pain from any noxious stimuli, including

inflammation and heat. They can differentiate large temperature changes but not able to detect if something is too hot or too cold [34]. The lack of pain sensation put the individuals in danger because they can hurt themselves without knowing. Infants and young children suffer from self-mutilating injuries of the fingers and oral cavity, burns due to impaired temperature sensation [34, 35]. In 2006, J. J. Cox et al. reported a ten-year-old case child who placed knives through his arms and walked on burning coals but experienced no pain. He died after jumping off a house roof. In the same study, six individuals with CIP coming from three consanguineous families were found to have homozygous nonsense mutations in the *SCN9A* gene coding for SCN9A sodium channel [35].

Erythromelalgia (EM) is an autosomal dominant painful neuropathy characterized by episodes of burning pain, redness, warmth and swelling starting in the feet (patients are unable to wear enclosed shoes), and can also affect hands, ears, and nose. Pain is relieved by cooling and worsen by warming, exercise, prolonged standing, or alcohol [36-38]. EM consists of primary and secondary forms. Primary or inherited EM (IEM) is known to be caused by autosomal dominant mutations in the *SCN9A* gene as firstly described by Y. Yang et al. in 2004 [39]. Twenty mutations in *SCN9A* in IEM patients have been described until now [40]. Secondary EM is a condition with multiple underlying disease associations for which no implicated gene has been identified till now. This form has a later age onset compared to the first form [37].

Paroxysmal extreme pain disorder, also known as familial rectal pain, is an autosomal dominant disorder. It comprises episodic chastening paroxysmal pain attacks in the face, limbs, mandible and orbit, with rectal pain as a recurrent symptom. In addition, autonomic manifestations such as skin flushing and redness, harlequin color changes, pupillary abnormalities and tonic attacks with apnea and bradycardia are common. These episodes occur suddenly and can extend to the entire body [38, 41, 42]. Physical factors like defecating and eating, and strong emotion can be triggers of this pain [38].

Trigeminal neuralgia (TN) is a long-term pain disorder affecting the trigeminal nerve. It is characterized by paroxysmal facial pain along branches of the trigeminal nerve, often triggered by innocuous stimuli, such as eating, shaving, or applying makeup. There are two main types: typical and atypical TN. The typical form consists of episodes of extreme, sudden, shock-like pain in one side of the face that lasts for few minutes. The atypical form results in a continuous burning pain that is less severe. Although neurovascular compression of the trigeminal nerve is common in patients with TN, symptoms can occur in the absence of nerve compression, suggesting contribution of other factors in the disease [43].

Thalamic pain syndrome is another type of neuropathic pain that occurs following a cerebrovascular accident. Following a thalamic stroke, the patient may experience numbness or tingling on the contralateral side of their injury, with burning or freezing sensations occurring over time. The pain is often severe, constant, or intermittent, made worse by touch. Most patients complain about allodynia or diffuse pain to mild palpation following central post-stroke pain. Patients can also suffer from hyperalgesia, unexplained itching and a searing type sensation [27].
Post-herpetic neuralgia is the most common long-term complication of varicella-zoster virus reactivation. The condition affects nerve fibers and skin, causing unilateral neuropathic pain in a dermatomal pattern. Persistent burning pain, allodynia, paresthesias, dysesthesias, and/or hyperalgesia at or near the area of the rash are the hallmark of post-herpetic neuralgia. The pain can last long after the rash and blisters of shingles disappear [44].
Diabetes can produce several types of peripheral nervous system (PNS) damage. The most common type is a bilateral and symmetric damage to nerves of the feet, with a distal-to-proximal gradient of severity. Diabetic peripheral neuropathy is one of the most frequent long-term complications of diabetes associated with significant morbidity. Up to 50% of the patients will develop neuropathic pain with positive sensory symptoms such as allodynia and hyperalgesia, tingling, and prickling sensations in the feet as well as negative symptoms such as numbness [45, 46].
Small fiber painful peripheral neuropathy (SFN) comprises a heterogeneous group of neuropathies selectively or predominantly affecting the small-diameter myelinated Aδ-fibers and unmyelinated C-fibers and sparing the large diameter fibers [47, 48]. The onset of SFN occurs during adulthood and it is accompanied with positive sensory symptoms, mainly spontaneous pain with burning, shooting, electric-like, prickling, or itching sensations. Some patients can develop a sensitive skin, intolerance to wear sheet, socks or shoes over the feet and restless leg syndrome. Cramps and tingling are also noticeable in the lower legs and feet. Negative sensory symptoms are also prominent such as loss of thermal, pinprick and other nociceptive sensations and numbness or tight feeling. SFN sensory symptoms currently manifest in a length-dependent manner, starting at lower limb extremities and ascending more and more to later implicate the upper limbs. Symptoms can also follow a non-length-dependent form with patchy or proximal distribution in the face, scalp, trunk, and upper limbs, before involving the lower limbs. Autonomic symptoms include among others dry eyes or mouth, orthostatic dizziness, bowel and micturition disturbances, changes in sweating, diminished ejaculation or lubrication, hot flushes, or cardiac palpitations [38, 48-50]. These manifestations could be related to the involvement of C-fibers in the exocrine glands or smooth muscle [51]. SFN is different than EM in that symptoms are not

clearly exacerbated by warming and relieved by cooling [38, 48]. So now let’s take a look on the different causes behind SFN.

2.2 Causes of Small Fiber Neuropathy

There are many causes behind SFN, mainly metabolic, inflammatory, toxic, infectious, and genetic and you will find a few examples below. Metabolic causes include glucose intolerance; vitamin B12 or B6 deficiency; chronic kidney failure; and diabetes mellitus. Diabetes counts for the primary metabolic cause of SFN with 4.5% to 31% of all cases of SFN. Glucose intolerance contribute to 15% of SFN cases. Two chronic inflammatory diseases are found to be closely associated with neuropathic pain: Primary Sjögren's Syndrome, a long-term autoimmune disease affecting body's moisture-producing glands and other systems, and sarcoidosis, a disease involving abnormal accumulation of inflammatory cells known as granulomas in lungs, skin and lymph nodes. Primary Sjögren's Syndrome contributes to 3% to 9% of SFN cases. Other autoimmune diseases contributing to a lesser extent to SFN are systemic lupus erythematosus, in which there is inflammation and tissue damage of joints, skin, brain, lungs, kidneys, and blood vessels; celiac disease; rheumatoid and psoriatic arthritis, conditions where joints are damaged, causing swelling and stiffness. Toxic agents such as alcohol and some medications and infectious cases such as HIV infection and hepatitis C can cause SFN [6, 47, 49, 51]. The first genetic cause behind SFN is transthyretin familial amyloid neuropathy, a progressive disease caused by the abnormal deposits of proteins or amyloids around the PNS. Patients have axonal disease of large sensory and motor nerve fibers. The second main genetic cause of SFN is Fabry disease, which is an inherited, X-linked, lysosomal disease [51].

Voltage-gated sodium channels (VGSCs) are required for the firing of APs in Dorsal Root Ganglion (DRG) neurons and are thus implicated in pain signaling in painful conditions. For the first time, Catharina Faber et al. showed the presence of mutations in *SCN9A* and *SCN10A* genes in a proportion of patients with SFN [49, 52]. Gain-of-function (GOF) mutations in *SCN9A* can be found in up to 29% of patients with SFN [49]. In addition, GOF mutations in the transient receptor potential (TRP) ankyrin subtype 1 protein had been linked to pain syndrome [53]. However, in a considerable number of SFN cases, the cause remains unknown [47, 51]. The discovery of mutations in VGSCs led to diagnostic advances, where 29% of idiopathic SFN cases being possibly related to channelopathies [51].

2.3 Diagnosis of SFN

The diagnosis of SFN is based on clinical examination starting with bedside examination, and proceeding with neurophysiological, histological, and morphological investigations to demonstrate neuropathy in the small nerve fibers [48, 51, 54]. Firstly, the clinician investigates visible signs of probable peripheral autonomic manifestations, such as loss of skin color, dryness, and dystrophic changes. Then, the clinician does a comparative evaluation of affected and non-affected skin areas, using different types of stimuli, to define the quality and location of positive and negative sensory signs, based on patients reporting. To evaluate tactile sensation, the clinicians apply several tactile stimuli to the affected region. Patients with tactile hypoesthesia report less sensation in this part compared to the non-affected part. Those with mechanical allodynia feel pain for a soft touch or after von Frey filaments application, defined as static allodynia; and for a slowly brushing with cotton bud at a specific rhythm, defined as dynamic allodynia. The clinician can also look for sensations to punctate stimuli. While prickling with a needle, patients having hyperalgesia will feel an intense pain. After applying a pin or a stick on the concerned region, patients having punctate hypoesthesia report non-punctuate touch-like sensation; whereas those having punctate allodynia will feel a sharp pain. Finger pressure can also be applied on skin to test static allodynia and hyperalgesia. To test thermal sensations, the clinician uses the handle of a tuning fork, normally discerned as cold, and the palm of his hand, normally discerned as warm. In case of thermal hypoesthesia, patients feel reduced cold and/or warm sensations, whereas in case of hyperalgesia, they experience a discomfort or pain [48, 54-56].

Nerve conduction study (NCS) is a diagnostic test commonly used to evaluate the function of large myelinated sensory fibers in terms of conduction velocity, action potential and size of the amplitude, reflecting status of myelination and fiber loss. This technique cannot measure the velocity of small myelinated and unmyelinated nerve fibers. Electromyography (EMG) is a diagnostic procedure that measures amplitude, distal latency, and conduction velocity of motor neurons. It can detect spontaneous activity due to denervation of motor neurons. NCS or EMG should be done at the beginning of the diagnosis to omit the possibility of large fiber neuropathy. Patients with pure SFN will not show abnormalities in NCS and EMG [48, 54, 57, 58].

The measurement of intraepidermal nerve fiber density (IENFD) from skin biopsy is often considered the gold standard technique for the diagnosis of SFN [59]. Punch skin biopsies of 4 to 5 mm in diameter are taken from the thigh and leg. Protein gene product (PGP) 9.5 is used as a marker for peripheral nerve fibers in immunohistochemistry (IHC) (Figure 3) [51]. IENFD is defined by quantifying the number of nerve fibers crossing the dermal-epidermal junction in three different

slices, then dividing by the length of epidermis, resulting in a density value expressed in number of fibers per millimeter (IENF/mm). IENF density and morphology correlate well with small nerve fiber dysfunction (Figure 3) and IENFD is compared to normative reference values adjusted for decade of life and sex [50, 55]. IENFD might be more sensitive, equally or less sensitive than quantitative sensory testing (QST) [59], see below for QST. Skin biopsy is a minimally invasive, safe, largely painless and inexpensive tool, but it should be considered a surgical procedure with rare and mild complications such as bleeding and infection [48, 50].

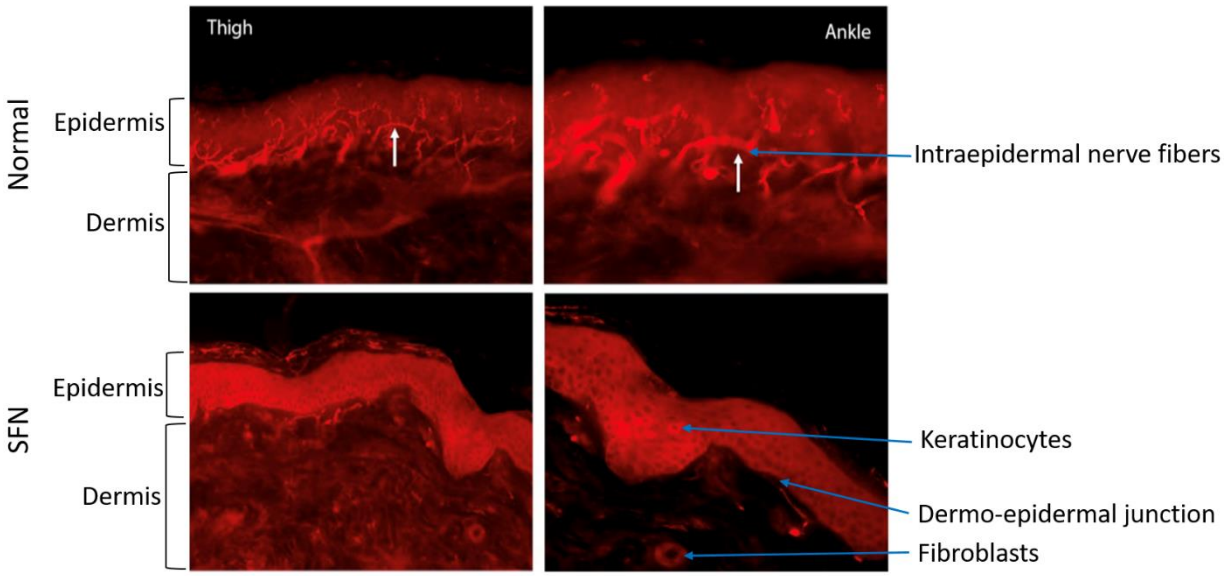

Figure 3: Skin biopsy labeled with anti-PGP9.5 to identify the intraepidermal nerve fibers (in red): The epidermis and dermis layers are identified. Keratinocytes and fibroblasts cells, the dermo-epidermal junction and intraepidermal nerve fibers are indicated with a blue arrow. Note the difference in IENFD at the ankle and thigh between a normal individual and in a patient with SFN. Adapted from Sene, D. et al., 2018 [51].

QST is a non-invasive psychophysical method used to quantify somatosensory function. It is based on two main detection methods: the method of limits used for threshold detection, where the clinician starts with an innocuous stimulus and goes for a noxious stimulus until the patient stops it; the method of levels used for pain rating at threshold and suprathreshold stimulations, including a force choice algorithm after a pre-defined stimulus. It can also evaluate temporal summation and conditioned pain modulation by using dynamic processes. Warm and cold detection thresholds (WDT and CDT) are the most frequent parameters measured in QST. QST is considered as an extension of bedside sensory assessment [48, 56]. QST has been a useful sensitive diagnostic tool [59]. QST can help in describing both single sensory modality threshold and distinct pattern of sensory abnormality related to neuropathy and signs of central

sensitization. Nonetheless, QST cannot distinguish peripheral from central abnormalities [48, 51]. In addition, this technique has other disadvantages: it is time-consuming, it is a semi-objective technique depending on patient's collaboration and requires training of the practitioner [48, 51, 59].

Corneal confocal microscopy (CCM) is an advanced non-invasive, high-resolution, real-time imaging technique aiming to investigate abnormalities of the small corneal fibers. CCM allows in vivo visualization of the unmyelinated C-fibers of trigeminal origin innervating the cornea, using a light beam focused into the examined cornea layer [48, 50, 60]. Corneal nerve fiber density was found to be significantly reduced in patients with SFN [60, 61]. CCM is characterized by its high reproducibility, its easy application for patient follow up, and usefulness for the early detection of nerve pathology [62].

Microneurography is a valued neurophysiological technique allowing single recording of C-nociceptors, thermoreceptors, mechanoreceptors, and sympathetic fibers from peripheral nerves in awake subjects. This technique elucidated the pathophysiological correlates of clinical phenomena in painful syndromes such as spontaneous activity, sensitization and hyperexcitability. The use of microneurography in clinic is still limited because it is a time-consuming and invasive technique; it requires a profound training of the examiner and cooperation from the patient [48, 55].

Laser evoked potentials (LEPs) and contact heat-evoked potentials explore brain responses to fast heating stimuli applied on the skin of the scalp using customized electrodes, which selectively activate Aδ and C fibers [48, 55]. LEPs were found to be strongly correlated to pinprick sensory disturbances, according to age- and gender-corrected normative ranges. In accordance with skin biopsy findings, LEPs showed 78% sensitivity and 81% specificity in SFN diagnosis [63]. The responses to laser stimulation are reproducible, quantifiable, and entirely specific of the small sensory nerve fibers [51]. However, like QST, LEPs and contact heat-evoked potentials do not allow to discriminate between a central and peripheral involvement of the somatosensory system [48]. QST is more widely used and requires less technical experience than LEP [59].

Though SFN is often accompanied with autonomic symptoms, it is important to test sudomotor, and cardiovascular functions. Neurogenic sweating is among the earliest clinical signs of a variety of autonomic neuropathies and neurodegenerative disorders. The quantitative sudomotor axon reflex testing is a sensitive and reproducible technique that can measure the autonomic nerves that control sweating. The test requires a mild electrical stimulation on the skin allowing iontophoresis of acetylcholine that binds to nicotinic and muscarinic receptors, stimulating sweat production. The quantitative sudomotor axon reflex testing measures the volume of sweat

produced by this stimulation to assess sudomotor nerve fiber damage. This technique shows high precision and low variability but is technically demanding [48, 51, 64].

Another interesting test is the sympathetic skin responses measurement at the palms and soles. It requires a multi-synaptic reflex that depends on the integrity of both CNS and PNS. This test has limited sensitivity and poor reproducibility [48, 51]. Recently, electrochemical skin conductance (ESC) was developed as simple, quick and quantitative method that can measure sweat production at the palms and soles to detect sudomotor deregulation. It uses the Sudoscan® device, based on electrochemical reaction between electrodes and chloride ions, after stimulation of sweat glands by a low-voltage current. This technique showed good sensitivity and specificity [65, 66].

Diagnosis of the cardiovascular autonomic functional system could be a part of SFN diagnosis. Several tests are intended to assess the functional integrity of certain autonomic reflex arcs. The afferent pathway must first be activated from the resting state of the patient using a suitable stimulus such as an orthostatic test. Measuring heart rate, blood pressure and noradrenaline concentration can be done while patient change his body position from horizontal to vertical. Blood pressure and heart rate can be simultaneously measured in responses to dynamic maneuvers such as the Valsalva maneuver where the patient exhale through a special mouthpiece. The RR interval is the time elapsed between two successive R-waves of the QRS signal on the electrocardiogram. The RR interval variation can be calculated by the difference of the RR intervals during exhalation minus the RR intervals during inhalation [51, 64].

Diagnosis of the cardiovascular deregulation is an independent measure of SFN given the fact that no correlation was described between autonomic reflexes and IENFD or QST [48].

According to G. Devigili et al. [48, 54], in order to confirm SFN diagnosis, the patient should show at least two clinical signs of SFN; conservation of large fiber functions, such as normal strength, tendon reflexes, and vibration sense; normal NCS of the sural nerves; abnormal psychophysical components in the QST and/or abnormal structural components for the IENFD [48, 54]. In 2015, J.P. Lefaucheur et al. compared the sensitivity of five neurophysiological tests: WDT, CDT, LEP, SSR, and ESC and stressed the importance of combining several tests to optimize SFN diagnostic sensitivity [59]. In 2020, V. Fabry et al. compared a set of 6 diagnostic tests, including skin biopsy, LEP, ESC, QST, quantitative sweat measurement and cardiovascular testing. Their study showed the importance of skin biopsy, LEP, ESC, QST in SFN diagnosis [67].

2.4 Therapeutic strategies for SFN pain

There are two sides for treating SFN patients. The first consists of treating the symptoms and the second consist of treating the underlying causes.

The most efficient and recommended drug classes are represented by antidepressants, anticonvulsants, opioids and localized therapies, with antidepressants and gabapentinoids as the first-line drugs. Antidepressants have both a potential centrally mediated action implying descending controls of nociception, and a potential peripheral mechanism via an activation of β_2-adrenoceptors in DRG. Therefore, noradrenaline is released within supraspinal structures at spinal level by descending noradrenergic inhibitory controls or at peripheral level by sympathetic fibers sprouting in DRG that accompanies peripheral nerve injury. Various studies have shown that long-term antidepressant treatment has an antiallodynic and/or an antihyperalgesic effect in genetically or chemically induced diabetic polyneuropathy and chemotherapy-induced neuropathic models. The tricyclic antidepressant (TCA) amytriptyline have been shown effective in pain improvement. It alleviates constant pain, shooting pain and mechanical allodynia. A local application of amitriptyline induces cutaneous analgesia, accompanied with redness, itching and burning sensations in healthy subjects, while in neuropathic pain patients, it induces redness and isn't more effective than placebo. A large part of amitriptyline action is related to its demethylated active metabolite nortriptyline. The peripheral noradrenergic system is necessary to the antiallodynic property of long-term nortriptyline [68]. However, TCAs are known to be dirty drugs because they can act on several neurotransmitter receptors; they block reuptake of norepinephrine and VGSCs, and are antagonists of H_1-histaminic, muscarinic cholinergic receptors. Some TCAs inhibit serotonin reuptake or are antagonists of serotonin 2A and 2C receptors [6]. Nonetheless, it is still unclear whether the TCAs action on VGSCs could actively contribute to their therapeutic action at clinical doses [68]. The serotonin-norepinephrine reuptake inhibitors duloxetine and venlafaxine emerged as alternatives due to better safety profile and suggested as the first line drug in neuropathic pain, although their analgesic effect may be less marked [48, 51]. Some clinical studies suggested an efficacy of these molecules, while most studies found them not or poorly effective. There are some positive and negative results regarding the involvement of the serotonergic system in antidepressant's role. Thus, chronic inhibition of serotonin uptake alone is not enough to efficiently reduce neuropathic-induced allodynia. Antidepressant's action on the noradrenergic system thus appears more important [68].

Anticonvulsant drugs like gabapentin and pregabalin have been proved to be clinically efficient in a number of neuropathic pain conditions [69]. Gabapentinoids do not primarily target GABA

receptors; but bind to voltage-gated $\alpha_2\delta$-calcium channel suggesting that gabapentinoids' antinociceptive action is mediated through an attenuation of excitatory transmitter release, ectopic discharges and A-fiber hypersensitization. In neuropathic pain conditions, there is an increase in $\alpha_2\delta$-subunit in the spinal cord resulting from an elevation within the presynaptic terminals of damaged primary afferent neurons. Repeated administration of gabapentinoids acts on $\alpha_2\delta$-subunit trafficking from DRG to spinal presynaptic terminals, normalizing $\alpha_2\delta$ increase. Gabapentinoids' role in alleviating pain can be explained by other mechanisms, such as the activation of the descending noradrenergic pain inhibitory system, an indirect inhibitory effect on GABAergic transmission in the locus coeruleus, the decrease of microglial activation and/or proinflammatory cytokines [68]. Some of pregabalin and gabapentin side effects are somnolence, dizziness, ataxia, edema, and tremor. These drugs could have an additional effect when combined with TCAs [69, 70]. Other antiepileptic drugs like carbamazepine and oxcarbazepine have a well-established use in TN. Oxcarbazepine was shown to be effective in a phenotype-stratified study in peripheral neuropathy patients [71].

Opioids refer to all substances that produce morphine-like effects that are blocked by antagonists, such as naloxone, and are produced synthetically or endogenously. They act on opioid receptors in peripheral afferent neurons, dorsal horn of the spinal cord, brainstem, and the brain, leading to analgesia. Opioid agonists can activate receptors located on the presynaptic terminals of C- and A-fibers, which will indirectly inhibit voltage-gated calcium channels, blocking the release of pain neurotransmitters [6]. Long usage of opioid can lead to tolerance and addiction, not to forget the risk of overdose mortality. However, using opioids as an add-on treatment to the first line drugs is convenient for a short period.

Lidocaine and capsaicin application to the localized painful area is considered a second-line treatment. Capsaicin is the principal component in hot peppers and is available at low-concentration in cream. It depolarizes nociceptors and increases their cytosolic free Ca^{2+} concentration. Capsaicinoids exert their effects by activating the TRP vanilloid 1 (TRPV1) receptor. Capsaicin topical application can lead to reversible epidermal nerve fibers degeneration detected by a reduction in the density of epidermal fine nerve endings. However, heat and cold thresholds were unaltered. The underlying mechanisms remain unclear [72]. Application of lidocaine 5% plaster contributes to cooling perception and mechanical protection and acts as inhibitor of the VGSCs, though reducing pain and allodynia [6, 48, 51].

To conveniently treat pain, strategies should focus on the management of the underlying causes. For example, correct vitamin deficiency if present, or metabolic or hormonal unbalance. In diabetic SFN, lifestyle interventions and tight glycemic control resulted in pain relief. Intravenous

immunoglobulin therapy was effective in decreasing pain scores in 76% patients with SFN due to sarcoidosis. To treat SFN associated with sodium channel disorders, selective blocking of the mutated receptors seems appealing. Mexiletine, an antiarrhythmic drug that inhibits VGSCs, has shown successful results in EM patients with or without *SCN9A* mutations [48, 51]. Lacosamide, an anticonvulsant that acts on VGSCs, significantly decreased pain and had a positive effect on sleep quality in SFN patients harboring mutations in *SCN9A*. Lacosamide appears to be as effective as currently available neuropathic pain treatment, with a response rate of 50-60% [73], which is at least comparable to the 50% of patients that have a reduction in pain intensity when treated with currently available therapeutics [69]. However, lacosamide has many side effects including diplopia, vomiting, dizziness, headache, fatigue, tremor and somnolence [73]. Pharmacological treatment of SFN remains ineffective in most cases, and new more efficient drugs need to be developed.

3 Voltage-gated sodium channels

3.1 The VGSCs family

VGSCs are dynamic transmembrane proteins mostly expressed on the membranes of excitable cells such as neurons. These channels switch from a closed to an open state in response to changes in membrane potential, allowing selective conduction of sodium ions through cell membranes. These modifications in sodium fluxes are vital for the generation and propagation of AP in excitable cells, making the VGSCs the most important ion channels for neuronal cells excitability and normal physiological functions [74, 75].

To date, 9 VGSCs isoforms (named before Nav1.1-Nav1.9) SCN1A-SCN5A and SCN8A-SCN11A have been identified in different excitable tissues in human and rodents. Except of SCN4A, they are expressed in the nervous system. Specifically, SCN1A, SCN2A, SCN3A, and SCN8A are the primary VGSCs in the central nervous system (CNS) whereas SCN9A, SCN10A, and SCN11A are mainly distributed in the peripheral nervous system (PNS). SCN5A was originally identified as a cardiac sodium channel but it was shown to be expressed in the CNS. SNC4A is mainly expressed in skeletal muscle. Most of these channels also have significant levels of expression outside of their primary tissues [75, 76].

Whitaker et al. showed that SCN1A, SCN3A, and SCN8A channels were found to be predominant in neuronal cell bodies and processes of neurons, while SCN2A channel was sequestered to axons and nerve fiber bundles. They also confirmed the expression of these four proteins with

different expression levels in cerebral cortex, deep brain nuclei, hippocampal structures, insular cortex and cerebellum [77]. SCN8A was found to be the predominant channel in axon initial segments and mature nodes of Ranvier in myelinated fibers of CNS and PNS, whereas SCN2A was primary localized in unmyelinated or pre-myelinated axons [77, 78]. During nodes of Ranvier initial formation, SCN2A is found at high levels at the nodes, while SCN8A could not be found. While further node growth, there was a developmental switch from SCN2A isoform to SCN8A at initial segments and nodes of Ranvier (Figure 4), so that SCN2A is detected in only small subpopulations of nodes [74, 79]. SCN1A was found to be expressed in nodes of Ranvier throughout the mouse spinal cord and in many brain regions. Three populations of nodes were found to be expressing SCN1A, SCN8A, or both [80]. In human and rodents, SCN3A expression level is high in embryonic and early postnatal brain. During aging, the expression level diminishes, showing a low level in adult brain tissue. SCN5A shows a similar pattern of expression in human's and rodent's brain, to the highest during embryonic and early postnatal period and to the lowest during adulthood. SCN5A was found to be expressed in olfactory tissue [81], limbic system, specifically in hippocampus [74], cerebral cortex, thalamus, hypothalamus, basal ganglia, cerebellum, striatum [82].

SCN1A, SCN8A, SCN9A, SCN10A and SCN11A are expressed in primary sensory neurons (Figure 4). There is maturation to this expression pattern as SCN2A, SCN3A and SCN5A are expressed during the embryonic period and subsequently downregulated. In DRG neurons, the expression of SCN1A and SCN8A was found to be higher in A-fiber than in C-fiber neurons; SCN9A and SCN10A higher in C-fiber than in A-fiber neurons; SCN11A limited to C-fibers (Figure 4) [26, 74]. SCN9A is also expressed in peripheral somatic and visceral sensory neurons, olfactory sensory neurons, and sympathetic ganglion neurons. SCN9A accumulates both at nerve fiber endings in the periphery and presynaptic terminals in the dorsal horn of the spinal cord [43]. SCN11A channel is also expressed in enteric neurons of peripheral nerves [74]. SCN9A and SCN11A are expressed as well in the brain [82]. SCN10A is widely expressed in trigeminal ganglion (TG) neurons and present in intracardiac neurons of the murine heart [83, 84]. Expression and localization of SCN10A will be detailed in section 4.1.

SCN1A, SCN2A, SCN3A, SCN4A, SCN8A and SCN9A are tetrodotoxin (TTX) sensitive (TTX-S) channels; while SCN5A, SCN10A and SCN11A are TTX-resistant (TTX-R) channels.

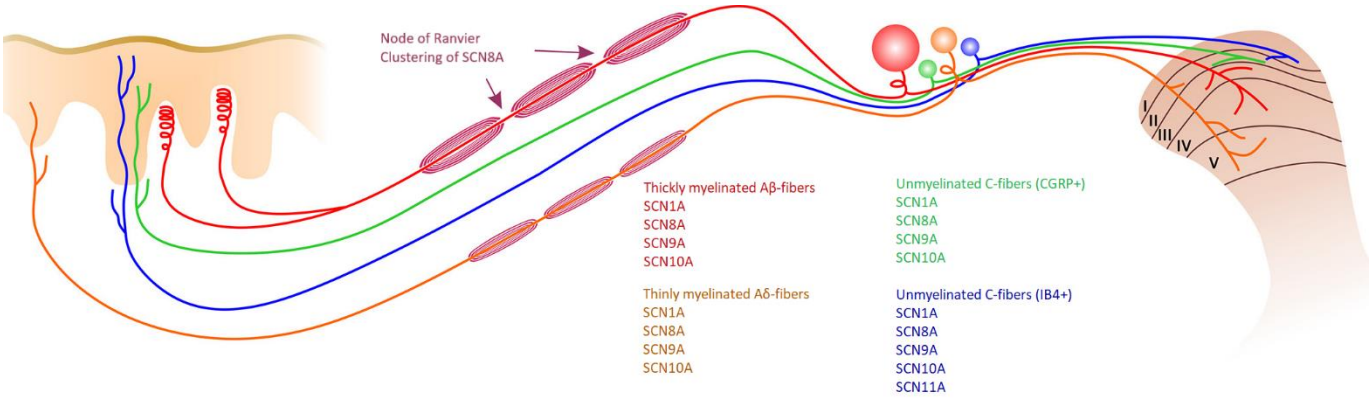

Figure 4: The innervation pattern of mouse DRG sensory neurons.

DRG primary afferent neurons are pseudo-unipolar neurons that innervate peripheral targets, such as the skin and synapse centrally in the dorsal horn of the spinal cord. Each subpopulation of DRG neurons has distinct central termination patterns. Generally, unmyelinated neurons terminate in more superficial laminae compared with the myelinated Aβ- and Aδ-fibers. All neuronal subpopulations express SCN1A, SCN8A, and SCN9A to some extent. Small-diameter nociceptive neurons with unmyelinated C-fibers can be broadly subdivided based on the expression of calcitonin gene-related peptide (peptidergic) or the binding of IB4 (nonpeptidergic). Expression of SCN11A is largely limited to the nonpeptidergic population. SCN8A is clustered at the node of Ranvier in myelinated fibers where it functions in saltatory conduction. Adapted from Bennett, D. L. et al., 2019 [26].

3.2 Structure and Function of the VGSCs

VGSCs are complexes of a pore formed by one α subunit of 260 kDa, associated to one or more auxiliary β subunits (β1-β4) of 33-36 kDa. They are differentiated according to the distinct α subunit isoforms. All α subunits share nearly identical structure topology, a canonical voltage-gated ion channel fold constituted of 2000 amino acid residues organized in four homologous domains DI-DIV, each containing six transmembrane segments S1-S6 (Figure 5) [85]. Specific regions within each of the four domains DI-DIV of VGSCs are thought to have distinct, but integrated, roles in channel gating and conformational stability in response to changes in membrane potential [86]. α subunit contains two functionally distinct structural entities, namely, the voltage-sensing module (VSM) and the pore entity (PE) (Figure 5). Specifically, the segments S5-S6 and the interconnecting loop constitute the PE. The loop between S5 and S6 from each domain form a narrow ion-selective filter of the channel that allows selective permeability of sodium ions across cell membrane [26]. Segments S1-S4 constitute the VSM that senses membrane potential variations, switching from an arresting to an activated configuration, which is necessary for pore opening. This sensing property is featured by several positively charged amino

acids (aa) (arginine or lysine) located at the third position of S4 segment within each domain (Figure 5) [75]. The outward movement of the S4 segment is directly translated into conformational changes of the PE, through interaction between VSM of each domain with the PE of a neighboring domain. More precisely, when cell is depolarized, each subunit alone undergo voltage-dependent transitions, but the final voltage- independent change leading to pore opening occurs in a cooperative way [76]. Therefore, sodium ions cross the cell membrane, sodium current reaches a maximum and then decreases as the sodium channel stops conducting ions and starts closing. This process is known to be inactivation. The inactivated VGSCs cannot reopen until membrane is repolarized and they undergo recovery from inactivation. Activation, inactivation, and recovery from inactivation occur within a few milliseconds (Figure 6). In addition to these rapid gating transitions, sodium channels are also susceptible to closing by slower inactivating processes acting over tens of seconds can occur in response to prolonged depolarizations [26, 87].

The fast kinetics of S4 of DI-DII movement correlate closely with activation of sodium conductance, whereas the relatively slow movement of S4 of DIV aligns with the development of inactivation and with the immobilization of the gating charge. Mutations throughout the channel can affect gating; however, those introduced in DIV tend to most strongly affect inactivation [88]. The cytoplasmic inactivation “gate” is in the loop between DIII and DIV and comprises an IFMT motif formed by four hydrophobic aa isoleucine, phenylalanine, methionine and threonine (Figure 5). During fast inactivation, the flanked residues act as molecular hinges, allowing the IFMT motif to swing and occlude the intracellular mouth of the pore. Inactivation could be achieved by titrating small peptides containing the IFMT motif (Figure 6). Substitution of aa in this region are found to disrupt the inactivation process [75, 87].

Auxiliary β subunits are composed of N-terminal extracellular immunoglobulin-like fold, a single transmembrane segment, and a short intracellular segment (Figure 5). β2 and β4 subunits resemble each other most closely in amino acid sequence and form disulfide bonds with α subunits, whereas β1 and β3 subunits also resembling closely associate non-covalently with α subunits. β subunits can act as cell adhesion molecules and modulate the cell surface expression of the VGSC in specific locations in excitable cells, enhancing sodium channel density and cell excitability. They can also modulate membrane trafficking, voltage dependence, and channel gating kinetics [76, 87]. α and β subunits synergy is specifically particular at the Ranvier nodes of myelinated axons, where the loss of β1 interactions can modify the structure of Ranvier nodes and disrupt saltatory conduction [87].

SCN1A, SCN3A, SCN5A and SCN8A channels seem to be closely related to the generation of neuronal APs, while the SCN2A channel may play an important role in transmission of these APs [74]. SCN11A channel activation and inactivation are slower than the other channels, and this feature is mainly involved in the regulation of the neuronal AP threshold [74].

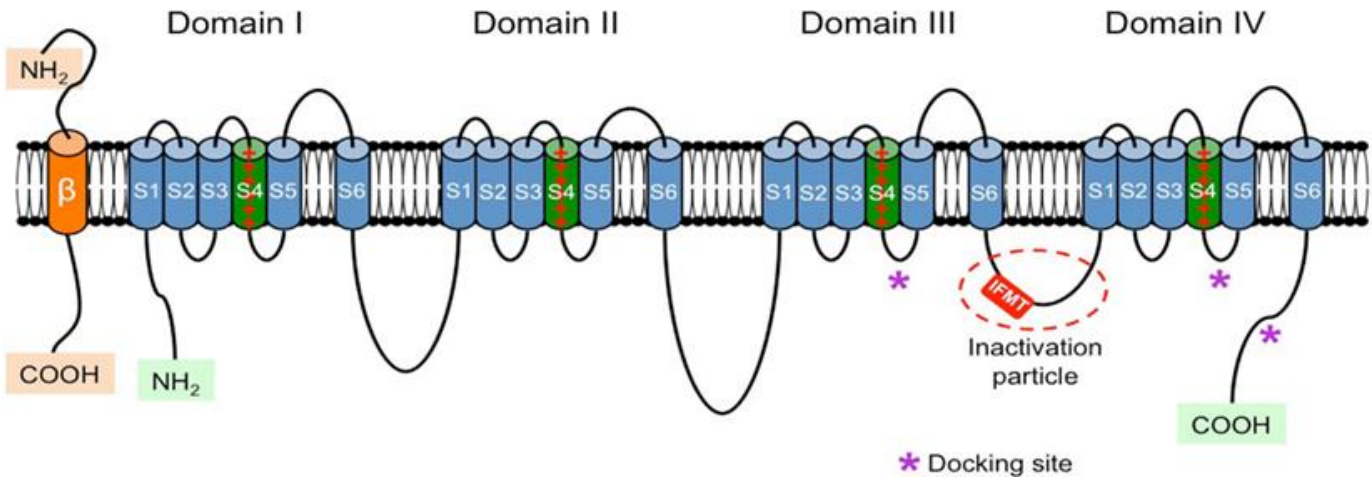

Figure 5: Schematic representation of α and β subunits of the VGSC.

β subunit is represented as constituted of N-terminal extracellular immunoglobulin-like fold, a single transmembrane segment, and a short intracellular segment. The four homologous domains DI-DIV of α subunit are represented; each one containing six transmembrane segments S1-S6. S1-S4 constitute the voltage-sensing module (VSM). Segments S5-S6 and the interconnecting loop constitute the pore entity (PE). In the S4 of each domain positively charged aa (arginine or lysine) are located at the third position. In the cytoplasmic linker between DIII and DIV the IFMT (isoleucine, phenylalanine, methionine, and threonine) region is indicated. This is a critical part of the “inactivation particle” (inactivation gate). The “docking site” consists of multiple regions that include the cytoplasmic linker between S4-S5 in DIII and DIV, and the cytoplasmic end of S6 segment in DIV (*). Depending on the subtype of β-subunit considered they could interact covalently or non-covalently with the α-subunit. Adapted from Savio-Galimberti, E. et al., 2012 [87].

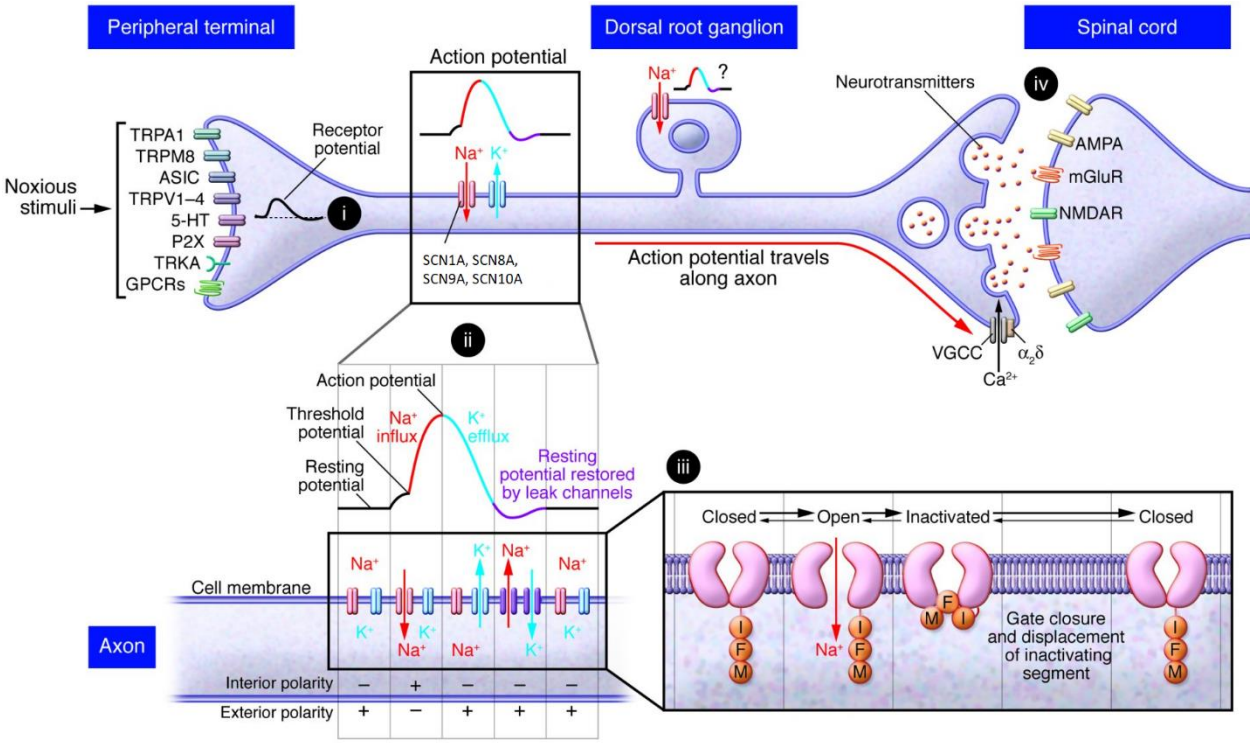

Figure 6: Schematic of ion channels in nociceptor function.

The peripheral terminals respond to noxious stimuli or tissue damage through receptors and ion channels including TRP channels, acid-sensing ion channels (ASIC), serotonin (5-HT) receptors, ATP-gated P2X receptors, tyrosine kinase receptor A (TRKA), and numerous GPCRs that indirectly activate ion channels. Receptors at the terminals respond to noxious stimuli such as heat or pressure (i). When a defined threshold of depolarization is reached, VGSCs are activated and an AP is generated (ii). During an AP, an IFM-inactivating segment moves to block the channel within 0.5-1 ms (iii). In this inactivated state, the channel cannot be opened. Meanwhile, potassium channels open, acting to repolarize the membrane. As the membrane repolarizes, the sodium channel gate is closed and inactivating segment is displaced, returning the sodium channel to a resting closed state (iii). This process is repeated to propagate the AP along the axon (ii). The AP is propagated along the axon to the presynaptic terminal synapses with second-order neurons in the dorsal horn. Calcium influx through voltage-gated calcium channels triggers the release of neurotransmitters such as glutamate from presynaptic terminals (iv). Glutamate activates ionotropic AMPA, NMDA receptor (NDMAR), and metabotropic glutamate receptors (mGluR) on the postsynaptic terminals in the spinal cord, and the signal is transmitted through the ascending pathways to higher centers in the brain. Adapted from Raouf R. et al., 2010 [89].

3.3 VGCSs channelopathies

Mutations in the VGSCs can produce changes in the biophysical properties of the channel. Inherited disorders of ion channels are now known to account for a wide spectrum of human

diseases, called channelopathies. More than 1000 disease-related mutations have been identified in Nav channels [75]. Four groups of these diseases can be distinguished according to the predominant organ involved: brain sodium channelopathies, skeletal muscle sodium channelopathies, cardiac sodium channelopathies, and peripheral nerve sodium channelopathies [87].

Brain sodium channelopathies: epilepsy is one of these diseases. Epilepsy is a brain dysfunction syndrome caused by excessive synchronization of brain neuron discharge. Generalized epilepsy with febrile seizures plus ($GEFS^+$), an autosomal dominant syndrome characterized by febrile and afebrile seizures, can be caused by mutations of the *SCN1A* gene encoding for SCN1A channel. Dravet syndrome or severe myoclonic epilepsy in infancy is the most severe phenotype among $GEFS^+$. It is characterized by several seizure types first occurring during infancy and induced by fever. Dravet syndrome may be typically caused by loss-of-function (LOF) mutations in *SCN1A* that arise de novo. At least 75% of the sodium current in GABAergic interneurons is conducted by SCN1A channels. LOF of SCN1A in a heterozygote mouse model of Dravet syndrome led to 50% loss of sodium current in interneurons, decreasing the GABAergic output, though increasing excitability in GABAergic neurons. In contrast, smaller reduction in sodium current in homozygote mice suggests that SCN3A channel can have a more remarkable compensatory role when SCN1A is completely ablated [90]. Christoph Lossin et al. studied three $GEFS^+$ mutations in *SCN1A* that he found to be GOF mutations, resulting in persistent inward sodium current [91]. These two studies revealed that the phenotypes produced by *SCN1A* mutations can vary widely from LOF to GOF and though be associated with the same disease. This complex phenotype at channel level was also noticed with mutations in *SCN9A* and *SCN10A* [92-95]. For example, the same point mutation (PM) in *SCN9A* produces hyperexcitability in DRG neurons and hypoexcitability in superior cervical ganglion (SCG) neurons due the selective expression of SCN10A channels in DRG and its absence in SCG neurons [96]. Consequently, *SCN1A* mutations effect on brain excitability rely on the type of neuron where the mutant channel is expressed and also on the electrical balance between all the ionic currents [87]. Another distinct disease caused by missense mutations of *SCN1A* is the familial hemiplegic migraine type 3, a rare monogenic autosomal-dominant disease with aura and characterized by focal neurological symptoms such as sensory and motor disturbances. Ten missense mutations of the *SCN1A* gene were reported [97], however GOF and LOF effects were also found to be caused by the same mutation [98]. Mimicking pro-migraine conditions by neuronal firing simulation revealed a GOF effect of the mutation. However, during high-frequency discharges and long depolarizations, the effect turned to be a LOF. Migraine mutations have this singularity of both inducing the cascade

of events that lead to migraine and counteracting the development of extreme hyperexcitability typical of epileptic seizure [98].

Missense mutations of the *SCN2A* gene encoding the SCN2A channel were found in some $GEFS^{+}$ patients with benign familial neonatal-infantile seizures. Some of these mutations were predicted to cause GOF mechanisms and an increase in neuronal firing, while others suggest a LOF by decreased surface expression [99]. SCN3A plays a role in modulation of neuron function in epilepsy and is related to the occurrence and development of epilepsy [100]. GOF mutations in *SCN8A* gene encoding the SCN8A channel were identified in patients affected by infantile epileptic encephalopathy, consisting of early-onset seizures, intellectual disability, ataxia, and sudden unexplained death in epilepsy. These PM resulted in a dramatic increase in persistent sodium current, incomplete channel inactivation, and a depolarizing shift in the voltage dependence of steady-state fast inactivation [101, 102]. Another frame-shift mutation in *SCN8A* was detected in the case of ataxia. This mutation introduced a translation termination codon into the pore loop of DIV, resulting in removal of the C-terminal cytoplasmic domain and predicted a LOF [103]. Due to the expression of SCN5A in the limbic system, a missense mutation in the *SCN5A* gene was detected in the brain of a patient who died of sudden unexpected death in epilepsy [104].

Skeletal muscle sodium channelopathies are caused by mutations in *SCN4A*. Forty missense mutations were described resulting in a GOF [105]. Various mutations in *SCN4A* gene have been related to hypokalemic periodic paralysis, a muscle disease marked by episodes of severe muscle weakness, leading to a transient inability to move muscles of arms and legs. It was reported that mutations in arginine residues in S4 of SCN4A induced a gating pore current during resting membrane potential, which closed during depolarizations [105].

Cardiac sodium channelopathies where mutations in *SCN5A* gene lead to several inherited arrhythmia syndromes, all associated with an increased risk of sudden cardiac death. Long QT syndrome (LQTS) is a condition in which repolarization of the heart after a heartbeat is affected, which can result in fainting, drowning, seizures, or sudden death. About 5-10% of LQTS cases are related to mutations in *SCN5A* (LQTS3). These mutations disrupt fast inactivation, allowing repeated reopening of the channel during sustained depolarization, though delaying the repolarization phase and prolonging AP duration [87]. Brugada Syndrome is associated with ventricular fibrillation, resulting in cardiac arrest with loss of consciousness and no pulse. Near to 20% of patients have mutations in *SCN5A* gene, found to be LOF mutations, at the opposition with LQTS3 mutations. Generation of defective or truncated proteins, faster channel inactivation,

shift of inactivation toward a more depolarized membrane potential, or even slow recovery from inactivation can explain the effect of the mutations [87]. A previously known mutation in *SCN5A* gene was found in a family showing an association between Brugada Syndrome and epilepsy, conferring that this mutation could be responsible for cardiac and brain channelopathies [106].

Peripheral nerve sodium channelopathies are mainly related to mutations in *SCN9A* and *SCN10A* genes. Four human pain disorders were caused by mutations in *SCN9A* gene: dominantly inherited GOF mutations in IEM, PEPD and SFN, and recessively inherited LOF mutations in CIP. As previously mentioned, 20 mutations in the *SCN9A* gene have been described in IEM patients until now [40]. Most of these mutations are located within transmembrane segments and cytoplasmic linkers of DI and DII. IEM mutations lead to a hyperpolarizing shift of activation, depolarizing shift of inactivation and accelerate recovery from inactivation, leading to enhance DRG neuron hyperexcitability. In addition, IEM mutations can reduce firing threshold [43, 107]. However, Anthony M. Rush et al. reported that the same mutation in SCN9A produced hyperexcitability in DRG neurons, but hypoexcitability in SCG neurons [96]. PEPD mutations within the S4-S5 linker of DIII involve destabilization of closed and open fast-inactivated states and this destabilization is due, in part, to the location and orientation of the specific mutations within the DIII/S4-S5 cytosolic linker [86]. This incomplete rapid inactivation leads to a persistent sodium current, also enhancing hyperexcitability [108]. As previously cited, in a study that examined the role of VGSC mutations in 28 patients with pure idiopathic SFN, eight (29%) patients were found to carry eight new missense variants in *SCN9A* [49]. All identified variants were shown to have GOF effect, rendering DRG neurons hyperexcitable [109]. In CIP patients, the mutations identified in *SCN9A* introduce a stop codon leading to the production of truncated proteins that are non-functional or nonsense mediated messenger RNA decay, producing LOF of SCN9A in nociceptive neurons [35]. Other than congenital painlessness, CIP patients suffer from anosmia. IENFD measurements from three CIP patients bearing heterozygous mutations in *SCN9A*, showed markedly reduced IENF [110]. Recent animal studies have shown that the SCN11A channel encoded by *SCN11A* gene mediates neuropathological, inflammatory and visceral pain [74]. Mutations in *SCN8A* were already linked to infantile epileptic encephalopathy [101, 102]. The first PM in *SCN8A* to be related with TN was reported by B. S. Tanaka et al. This mutation was located in S1 of DI; it conferred GOF properties on SCN8A channel and increased the excitability of TG neurons expressing the mutant form. It was thought that this mutation by itself is not enough to cause TN, but it can predispose the carrier to the manifestation of TN. Early-onset seizures and intellectual disabilities associated with *SCN8A* mutations in infantile epileptic encephalopathy

may mask any pain phenotype in these individuals [43, 111]. Mutations in *SCN10A* gene will be reported in section 5.

4 SCN10A Sodium channel

4.1 *Scn10a* expression and distribution

As we have already seen briefly, SCN10A channel, encoded by *SCN10A* gene, is mostly expressed in the PNS, specifically in DRG neurons of the spinal nerve where the expression was found to be higher in C-fiber neurons then in A-fiber neurons [74]. SCN10A is also widely expressed in TG neurons and present in intracardiac neurons of the murine heart [83, 84]. We will look more in details at the expression pattern of SCN10A.

SCN10A was first identified in peripheral sensory neurons of rat DRG [112]. Then it was known for years that SCN10A was widely expressed in small-diameter DRG neurons, mostly nociceptors, but was also reported in some medium- and large-diameter neurons in mice and rats (Table 1) [84, 113-121]. L. Djouhri et al. reported SCN10A positive immunoreactivity in 93% of medium sized Aδ-fiber nociceptive units, 89% of small sized C-fibers and 21% of total medium and large sized Aα/β-fiber units. None of the very largest neurons was positive [114]. However, small and large sensory fibers of human DRG were expressing SCN10A [122].

Scn10a-Cre different mouse lines exhibit slight differences in expression profiles, specifically in the spinal cord, brain, and outside the nervous system, as we will see below.

N. Agarwal et al. generated the Tg(*Scn10a*-cre)1Rkun transgenic line, noted below Tg(*Scn10a*-cre), where the cre cassette was flanked to the 200 bp genomic regions 5' and 3' to the coding ATG of *Scn10a* gene. The Tg(*Scn10a*-cre) mice were crossed with a reporter line Gt(ROSA)26Sor^{tm1sor}, noted ROSA26-LacZ, which carry the gene encoding the β-galactosidase enzyme preceded by a stop codon flanked by LoxP sites (LoxP-stop-LoxP-LacZ fluorescent protein), preventing the expression of LacZ [123]. This cross resulted in offspring in which all cells expressing SCN10A at any time during development undergo cre-mediated recombination to remove the stop codon from the cre-reporter cassette, triggering permanent expression of the fluorescent LacZ protein. Nearly all peptidergic and nonpeptidergic small DRG neurons expressed cre, whereas less than a third of large neurons expressed cre in Tg(*Scn10a*-cre)1Rkun-LacZ mice [113]. M. A. Nassar et al. (2004) generated the KI *Scn10a*$^{tm2(cre)Jwo}$ line in which the exon 1 of *Scn10a* gene was replaced by the Cre recombinase cDNA. *Scn10a*$^{tm2(cre)Jwo}$ mice were crossed with ROSA26-LacZ reporter mice [123]. Functional cre was expressed in a pattern identical to that of SCN10A. Expression was found in small DRG neurons [124]. L. C. Stirling et al. using the

same model found positive LacZ staining in almost all small, some medium and a few large DRG neurons [84]. J. Zhao et al. 2006 generated the *Scn10a*$^{tm3(cre/ERT2)Jwo}$ KI mouse line where the cre recombinase is fused to a mutant estrogen ligand-binding domain (ERT2) that requires the presence of tamoxifen for activity and is knocked-in downstream of the *Scn10a* promoter. *Scn10a*$^{tm3(cre/ERT2)Jwo}$ mice were crossed with ROSA26-LacZ reporter mice [123]. Functional Cre recombinase activity was not found in *Scn10a*$^{tm3(cre/ERT2)Jwo}$-LacZ mice in the absence of tamoxifen, but was present in nociceptive sensory neurons after tamoxifen induction in vivo [125]. However, the percentage of DRG neurons expressing functional Cre activity in *Scn10a*$^{tm3(cre/ERT2)Jwo}$-LacZ mice [125] was less than 10% of the number found in *Scn10a*$^{tm2(cre)Jwo}$-LacZ mice [84]. L. Gautron et al. used *Scn10a*$^{tm2(cre)Jwo}$ mice crossed with a tdTomato reporter line Gt(ROSA)26Sor$^{tm9(CAG-tdTomato)Hze}$ (LoxP-stop-LoxP-tdTomato fluorescent protein). The LoxP-flanked stop cassette prevents the expression of CAG-driven tdTomato expression. In Cre-expressing neurons, the transcriptional termination sequence is excised, allowing tdTomato production [126]. 79.9% of DRG neurons were tdTomato-positive [119]. S. D. Shields et al. (2012) used genetics, IHC, electrophysiology, and calcium imaging to precisely identify SCN10A expression in PNS of the same *Scn10a*$^{tm2(cre)Jwo}$ -tdTomato mice. They were able to show that SCN10A is present in 75% of DRG neurons, specifically in 91% of C-fiber afferents that can be subdivided into distinct populations: 92% of nonpeptidergic C-nociceptors and 93% of peptidergic C-nociceptors expressing SCN10A. C-fibers low-threshold mechanoreceptors have been described to express the vesicular glutamate transporter 3 (VGLUT3). S. D. Shields et al. used transgenic mice in which green fluorescent protein (GFP) labels VGLUT3-expressing cells. VGLUT3-GFP labelled mice were generated by homologous recombination using a shuttle vector flanked by VGLUT3 genomic sequences where GFP cDNA was inserted [127]. VGLUT3-GFP mice were crossed with *Scn10a*$^{tm2(cre)Jwo}$ -tdTomato mice resulting in offspring whose VGLUT3-positive neurons are labeled with GFP and whose SCN10A-positive neurons are labeled with tdTomato fluorescent protein [120]. Using this mouse model, the authors demonstrated that SCN10A expression is not restricted to nociceptors but also prominent in C-fibers low-threshold mechanoreceptors, which are essential for touch sensation. SCN10A was also present in 40% of medium- and large-sized myelinated Aβ/δ-fiber neurons, responsible for detecting and encoding a variety of somatosensory modalities, both noxious and non-noxious. Shields et al. also showed that *Scn10a*$^{tm2(cre)Jwo}$ is only expressed in a subpopulation of sensory neurons that innervate some types of hair follicles (Table 1) [120]. Using the same *Scn10a*$^{tm2(cre)Jwo}$ -tdTomato mice model and IHC, M. S. Minett et al. found that DRG at spinal levels L4, L5 & L6, innervating the hindpaws, express SCN10A (61%) in a lesser proportion than DRG at spinal levels S1 and S2 innervating

the tail (72%) [128]. V. B. Lu et al. (2015) generated a transgenic mouse line in which the enhanced green fluorescent protein (EGFP) labels SCN10A-expressing cells. In this line noted Tg(Scn10a-EGFP)ALmp, the *Scn10a* putative promoter region, a 3.7 kb sequence immediately upstream of a 24 kb intron and transcriptional start site of the *Scn10a* gene, directs the expression of the EGFP. Bright EGFP fluorescence is observed in peripheral sensory neurons, no EGFP expression is shown in sympathetic neurons. The authors recapitulated Tg(Scn10a-EGFP)ALmp distribution in DRG neurons in the majority of small to medium nonpeptidergic neurons and 8%-10% of medium to large A-fiber neurons [121].

SCN10A is also present in all small diameter and some medium and large diameter neurons of TG [84, 129]. Gautron et al. showed that 67% of TG neurons express *Scn10a*$^{tm2(cre)Jwo}$ [119]. In addition, 75% of small and 82% of large diameter neurons in the nodose ganglia (NG) show *Scn10a*$^{tm2(cre)Jwo}$ expression. However, only some neurons of the SCG are expressing *Scn10a*$^{tm2(cre)Jwo}$ [84, 119]. SCN10A is localized at free nerve endings of unmyelinated axons in cornea and epidermis [26]. A recent study, using electrophysiological recordings, described the differential spatial distribution of SCN10A within C-fiber axons, being functionally more prominent in the most distal axons and terminal regions involved in AP initiation as well as conduction [130].

S. D. Shields et al. (2012) identified *Scn10a*$^{tm2(cre)Jwo}$ expression in central terminals of primary afferents in spinal dorsal horn. Peptidergic C fibers terminate in lamina I and outer lamina II whereas nonpeptidergic C fibers terminate in a more ventral distribution, in inner lamina II. Strong labeling in afferent terminals innervating nucleus caudalis, nucleus of the solitary tract, and dorsal column nuclei in the brain stem was detected [120]. Gautron et al. showed *Scn10a*$^{tm2(cre)Jwo}$ expression in central relays within brainstem and spinal cord and no expression in cell bodies within the CNS or peripheral tissues. SCN10A expression was also identified in meninges, gustatory papillae, tongue, lungs, alimentary canal, bladder, skin, liver, gallbladder, duodenum and pancreas [119]. V. B. Lu et al. (2015) recapitulated Tg(*Scn10a*-EGFP)ALmp distribution in Lamina II of the dorsal horn of the spinal cord. Some expression was detected in different regions of the brain, in the basolateral amygdala, globus pallidus, olfactory tubercle, hypothalamus, and brainstem in a cluster of cells close to the spinal nucleus of the trigeminal nerve and sparsely distributed cell bodies in the medulla oblongata [121]. However, S. Udit et al. 2017 found no evidence of any Cre activity in the hypothalamus of *Scn10a*$^{tm2(cre)Jwo}$ -tdTomato mice and only sparse labeled cells in the cortex and basal forebrain (Table 1) [131].

For the first time in any species, in 2011 P. Facer et al. using IHC demonstrated SCN10A-immunoreactive sensory nerve fibers in human atrial myocardium and cardiomyocytes [132],

which was not supported by other studies using IHC in mice, which suggests different expression depending on species [83, 121]. A. O. Verkerk et al. showed that SCN10A is functionally present in mice intracardiac neurons but absent in mice cardiomyocytes [83]. Lu et al. found expression within cardiac ganglion but not in myocardium of EGFP-transgenic mice [121] (Table 1).

Table 1: SCN10A expression in different tissues and/or cells in mice, rats and human.

Publication	Species	Tissue	Tool	SCN10A Expression profile
Sangameswaran L. et al. 1996 [112]	Rats	DRG	IHC	76% of small cell population and 33% of large cell population
Novakovic S.D. et al. 1998 [115]	Rats			93% of small and 31% of medium neurons but not in large neurons
Coward K. et al. 2000 [122]	Human			Small and large neurons
Amaya F. et al. 2000 [116]	Rats			Half of C-fiber neurons, and subset of Aδ- Aβ-fiber neurons
Djouhri L. et al. 2003 [114]	Rats			93% of medium Aδ-fiber neurons, 89% of small C-fiber neurons and 21% of total large Aα/β-fiber neurons. None of the very largest neurons was positive
Hudmon A. et al. 2008 [117]	Rats			Subset of small to medium neurons
Belkouch M. et al. 2011 [118]	Rats			Numerous small to medium neurons
Agarwal N. et al. 2004 [113]	Mice		Tg(*Scn10a*-cre)1Rkun-LacZ mice; IHC	All peptidergic and nonpeptidergic small neurons, less than a third of large neurons
Nassar M. A. et al. 2004 [124]	Mice		*Scn10a*$^{tm2(cre)Jwo}$-LacZ mice IHC	Small neurons
Stirling L.C. et al. 2005 [84]	Mice			All small, some medium and a few large neurons
Zhao J. et al. 2006 [125]	Mice		*Scn10a*$^{tm3(cre/ERT2)Jwo}$-LacZ mice; IHC	Nociceptive sensory neurons
Gautron L. et al. 2011 [119]	Mice		*Scn10a*$^{tm2(cre)Jwo}$-tdTomato mice; IHC	79.9% of DRG neurons
Shields S. D. et al. 2012 [120]	Mice		*Scn10a*$^{tm2(cre)Jwo}$-tdTomato; *Scn10a*$^{tm2(cre)Jwo}$- tdTomato-VGLUT3-GFP mice IHC	Most C-fibers; 90% of nonpeptidergic C-nociceptors; 93% of peptidergic C-nociceptors; 93% of C-low threshold mechanoreceptors; 40% of medium and large Aβ/δ-fiber neurons
Minett M. S. et al. 2014 [128]	Mice		*Scn10a*$^{tm2(cre)Jwo}$-tdTomato mice; IHC	61% in DRG at spinal levels L4, L5 & L6; 72% in DRG at spinal levels S1 and S2
Lu V.B. et al. 2015 [121]	Mice		Tg(*Scn10a*-EGFP)ALmp mice; IHC	Majority of small to medium nonpeptidergic neurons; 8%-10% of medium to large A-fiber neurons
Rush A.M. et al. 2006 [92]	Rats	SCG	IHC	No expression
Facer P. et al. 2011 [132]	Human	Heart		Atria and cardiomyocytes

Verkerk A. O. et al. 2012 [83]	Mice	Heart		Neurons of intracardiac ganglia originating from the pulmonary vein region; absent in cardiomyocytes
Stirling L.C. et al. 2005 [84]	Mice	TG	*Scn10a*$^{tm2(cre)Jwo}$-LacZ mice IHC	All small neurons and some medium to large neurons
		NG, SCG, brain, spinal cord		75% in NG (small neurons); very small number in SCG; no expression in brain and spinal cord
Gautron L. et al. 2011 [119]	Mice	Neuronal cell bodies	*Scn10a*$^{tm2(cre)Jwo}$-tdTomato mice; IHC	82% in NG (large neurons) and the attached jugular/petrosal ganglionic mass; 67% in TG; vestibular/geniculate ganglionic mass; few in SCG
		CNS, peripheral tissues		Central relays within brainstem and spinal cord; no expression in cell bodies within the CNS or peripheral tissues
		Other tissues		Meninges, gustatory papillae, tongue, lungs, alimentary canal, islets of Langerhans in the pancreas, bladder, skin, liver, gallbladder, duodenum, pancreas
Shields S. D. et al. 2012 [120]	Mice	Spinal cord	*Scn10a*$^{tm2(cre)Jwo}$-tdTomato; *Scn10a*$^{tm2(cre)Jwo}$- tdTomato-VGLUT3-GFP mice IHC	Peptidergic C-fibers terminate in lamina I and outer lamina II, nonpeptidergic C-fibers terminate in a ventral distribution, in inner lamina II
		Other CNS areas		Strong labeling in afferent terminals innervating nucleus caudalis, nucleus of the solitary tract, and dorsal column nuclei in brain stem
		Skin		Free nerve endings that cross the dermal-epidermal boundary and penetrate the epidermis; hairy skin from the back of the mouse richly innervated
Lu V.B. et al. 2015 [121]	Mice	Spinal cord; skin	Tg(*Scn10a*-EGFP)ALmp mice; IHC	Lamina II of the dorsal horn; skin samples from the footpads
		Cardiac tissues		Fat pads at the base of the aorta and pulmonary artery, in cardiac ganglion; no expression in myocardium
		CNS		Some expression in basolateral amygdala, globus pallidus, olfactory tubercle, hypothalamus, and brainstem in cells close to the spinal nucleus of the trigeminal nerve and sparsely distributed cell bodies in medulla oblongata
		Other tissues		Weak expression in pancreas and kidney; no expression in spleen, liver, lung, small and large intestine, or stomach
Udit S. et al. 2017 [131]	Mice	Brain	*Scn10a*$^{tm2(cre)Jwo}$-tdTomato mice; IHC	No expression in hypothalamus; sparse labelled cells in cortex and basal forebrain

CNS: Central nervous system; DRG: Dorsal root ganglion; EGFP: Enhanced Green Fluorescent Protein; ERT2: Estrogen Receptor ligand-binding domain 2; GFP: Green Fluorescent Protein; IHC: Immunohistochemistry; ND: Nodose ganglion; SCG: Superior cervical ganglion; TG: Trigeminal ganglion; VGLUT3: Vesicular Glutamate Transporter 3

4.2 SCN10A cellular functioning

SCN10A channel is composed of one α subunit and one or more β subunits. α subunit is formed of four domains DI-DIV, each one containing six transmembrane segments S1-S6. The aromatic residues (Phe/Tyr) in the S5-S6 extracellular linker in DI (Figure 7), which is critical for high-affinity binding of TTX to VGSCs, is substituted by a Ser residue in SCN10A conferring resistance to TTX (Figure 8).

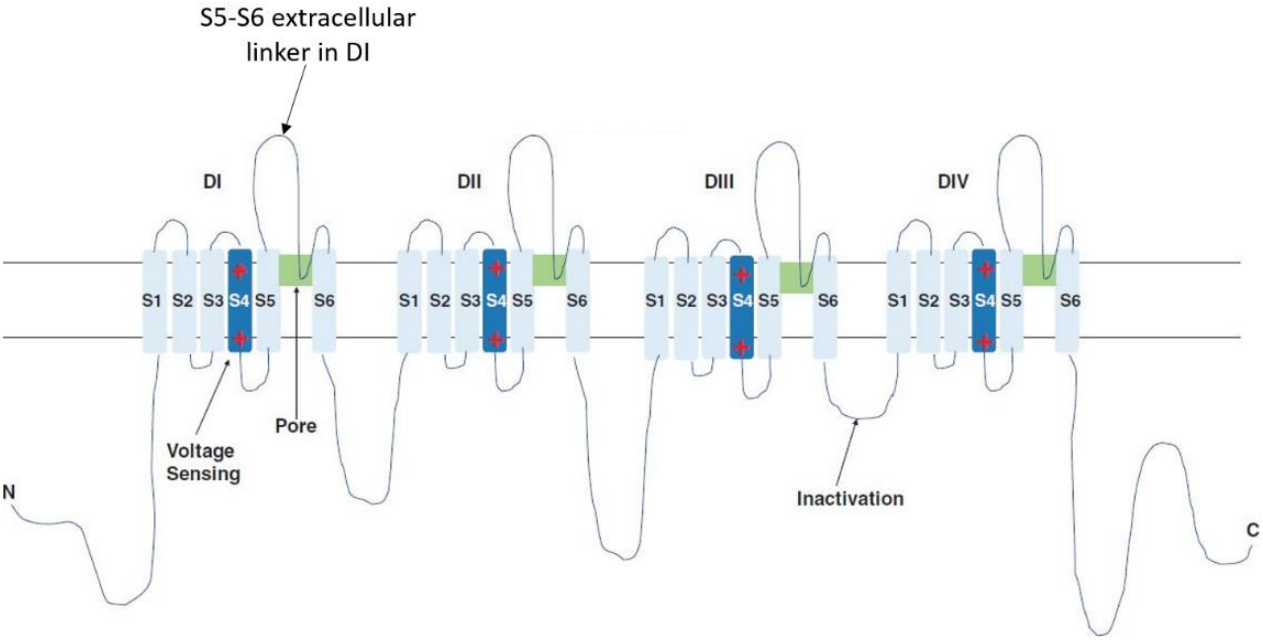

Figure 7: Schematic representation of α subunit of the VGSC showing the S5-S6 extracellular linker in DI.

The S4 segments are voltage sensors containing positively charged ions. The intracellular loop between DIII and DIV form the fast inactivation gate. The S5-S6 extracellular linker in DI is shown by an arrow. At this level the substitution of the aromatic residues (Phe/Tyr) by a Ser residue in SCN10A confers resistance to TTX. Adapted from Hameed, S. et al., 2019 [133].

SCN10A is activated at more depolarized potentials than other isoforms, still it contributes to the majority (58-90%) of the inward current during the rising phase of an all-or-none AP in nociceptive sensory neurons (Figure 8).

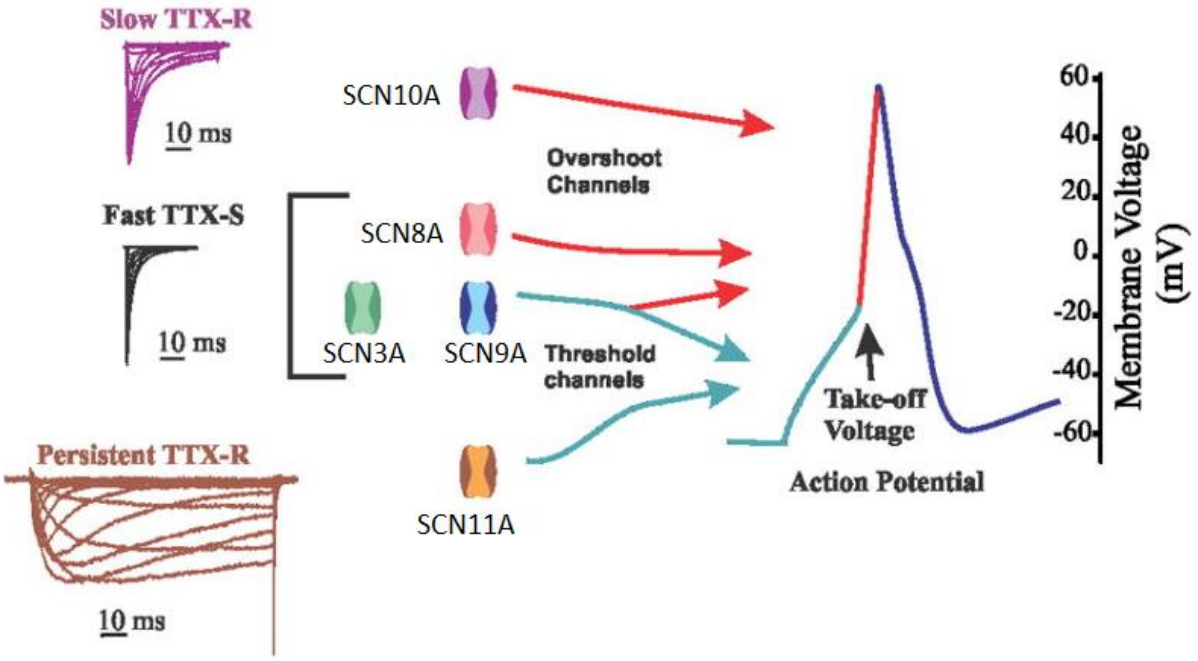

Figure 8: Contribution of sodium channel isoforms to action potential.

Based on their ability to boost subthreshold stimuli, TTX-S channels SCN3A and SCN9A, or hyperpolarized and persistent current, TTX-R channel SCN11A, these channels have been considered threshold channels for action potential firing. TTX-S channels SCN3A, SCN8A (especially at nodes of Ranvier), and TTX-R channel SCN10A (in the neurons in which it is expressed), contribute most of the current for the action potential. Adapted from Dib-Hajj, S.D. et al., 2015 [134].

Voltage-clamp recordings of SCN10A, which was first cloned from rat DRG, revealed a slow-inactivating inward sodium current with depolarized activation and fast inactivation [135]. These physiological properties are similar to those in human DRG neurons [136]. Fast inactivation of SCN10A is incomplete, which results in significant persistent currents. Han et al. 2015 studied the gating properties of human *SCN10A* transfected into *Scn10a*-null mouse DRG neurons as compared with rat *Scn10a* transfected into *Scn10a*-null mouse DRG neurons. DRG neurons were isolated from homozygous *Scn10a*-Cre mice that lack endogenous *Scn10a*. The pcDNA5-*SCN10A* plasmid construct that encodes human SCN10A protein and the plasmid pRK- SCN10A carrying rat *Scn10a* insert, driven by the human cytomegalovirus immediate early enhancer and promoter were transfected into mouse DRG neurons suspension by electroporation. They observed that human SCN10A currents exhibit hyperpolarized activation and depolarized fast inactivation compared with rat SCN10A currents. Moreover, slower kinetics for open-state inactivation enable the human SCN10A channel to remain open longer. Thus, endogenous SCN10A currents in native human DRG neurons produce persistent and ramp currents (respectively 6.1% and 18.6% of peak current) twice as large as that in native rat DRG neurons

(respectively 3.4% and 9.8% of peak current). In addition, these enhanced persistent currents are associated with reduced current threshold and increased firing frequency in transfected DRG neurons. 23% of DRG neurons expressing human SCN10A channel fired prolonged APs with a half-width longer than 10 ms, whereas none of the native rat DRG neurons or *Scn10a*-null mouse DRG neurons expressing rat SCN10A channels did. Human SCN10A increased the average AP half-width by 69% compared with rat SCN10A. The expression of human SCN10A produced a threefold increase in the population of spontaneously firing cells, whereas rat SCN10A did not demonstrate burst-like responses. Given the same external stimuli, DRG neurons expressing human SCN10A fired significantly more AP than those expressing rat SCN10A. Accordingly, DRG neurons display different gating properties, thus different firing patterns after expression of human SCN10A channels compared with rat SCN10A channels. These findings suggest that the unique properties of human SCN10A shape the firing patterns of DRG neurons [137].

When depolarized, SCN10A channel undergoes slow inactivation and then recovers fast from fast inactivation. Therefore, it does not inactivate completely during the falling phase of AP, thus contributing to the AP duration more than other TTX-S VGSCs. Consequently, SCN10A supports high frequency repetitive firing in depolarized neurons and thus may play an important protective role in damaged tissues. This slowly inactivating, rapidly repriming channel also contributes to unique resurgent currents that are enhanced in experimental models of inflammatory pain or when DRG cultures are exposed to inflammatory modulators. These TTX-R resurgent currents are much slower than TTX-S resurgent currents but can contribute to an increased AP firing in sensory neurons [26, 138].

Cooling (from 30°C to 10°C) resulted in marked hyperpolarized shift in inactivation of SCN9A and TTX-S current in DRG neurons. In contrast, the inactivation properties of SCN10A were entirely cold-resistant. Accordingly, the decrease in current amplitudes on cooling was significantly stronger for SCN9A than for SCN10A. This differential sensitivity to cold between TTX-S and TTX-R channels is due to difference in their inherent properties. Thus, in the cold, SCN10A remains available as the sole electrical impulse generator in nociceptors that transmits nociceptive information to the CNS. This cold resistance confers to SCN10A a special role for the perception of noxious cold and mechanical stimulation at low temperatures [139].

4.3 *Scn10a* role *in vivo*

After presenting sodium channels functioning and related channelopathies, especially painful neuropathies, and then introducing SCN10A channel expression and cellular functioning, I will now present the role of SCN10A as investigated *in vivo* in rodent models. Rodent models bearing mutations in *Scn10a* gene or gene inactivation have been previously reported. In the following mini-review, we present the results of pain assessment in *Scn10a* and *Scn9a* mutant models. Beside the other experimental *in vitro* and *in vivo* approaches, the study of pain sensitivity in the mutant animals allows to identify the role of these channels in behaviors elicited by thermal and mechanical challenges, as well as in experimentally-induced chronic pain.

Mini Review Manuscript

Accepted for publication in Neuroscience Letters on the 19th of March 2021

Pain behavior in *SCN9A* (NAV1.7) and *SCN10A* (NAV1.8) mutant rodent models

Yaping Xue*, Céleste Chidiac*, Yann Hérault[$,#] and Claire Gavériaux-Ruff[$]

Institut de Génétique et de Biologie Moléculaire et Cellulaire, Translational Medicine and Neurogenetics Department, 1 rue Laurent Fries, 67400 Illkirch, France

Université de Strasbourg, Illkirch, France

Centre National de la Recherche Scientifique, UMR7104, Illkirch, France

Institut National de la Santé et de la Recherche Médicale, U1258, Illkirch, France

* equal contribution

$ equal last authors

Support and grant information

This work has been funded by the European commission H2020 programme (grant number - 721841 – PAIN-Net)

#Corresponding author:

Name Yann Herault

Mail herault@igbmc.fr

Highlights

Rodent genetic models have highlighted the role of *SCN9A*- and *SCN10A*- encoded NAV1.7 and NAV1.8 voltage-gated sodium channels in pain control.

Global *Scn9a* knockout (KO) animals display pain insensitivity similarly to congenital insensitivity to pain patients.

The conditional KO mouse lines have allowed to assign populations of Scn9a in pain control.

The *Scn10a*-Cre mice allow to conditionally inactivate genes in the primary nociceptive neurons.

Targeting NAV1.7 and NAV1.8 constitute potential therapies for pain.

Abstract

The two voltage gated sodium channels NAV1.7 and NAV1.8 are expressed in the peripheral nervous system and some evidence showed their involvement in various pain conditions including inflammatory and neuropathic pain states. Rodent models bearing deletions or point mutations of the corresponding genes, *Scn9a* and *Scn10a*, were created in order to understand the role of these sodium channels in the pathophysiological mechanism underlying pain symptoms. Complete loss-of-function or knockout (KO) of *Scn9a* or *Scn10a*, conditional KO (cKO) of *Scn9a* in specific cell populations and double knockout (DKO) of both genes were shown to decrease sensitivity to various pain stimuli. The Possum mutant mice bearing a chemically induced dominant hypermorphic mutation in *Scn10a* revealed higher sensitivity to noxious mechanical and cold stimuli. Several gain-of-function mutations were identified in patients with painful small fiber neuropathy. Knowledge from pre-clinical models bearing these mutations will allow to understand how these mutations impact on pain. This review summarizes the pain behavior profiles reported in *Scn9a* and *Scn10a* rodent models. In addition, the review gives suggestions and perspectives for creating models mimicking patients' pain symptoms, and developing highly accurate pain behavioral assessment, in the aim of developing better analgesic strategies.

1. Introduction

Pain is “an unpleasant sensory and emotional experience associated with, or resembling that associated with, actual or potential tissue damage”, as re-defined recently by the International Association for the Study of Pain [1]. Pain is one of leading cause of disability and disease burden, and Mills and colleagues described pain as a common, complex and distressing problem that has a profound impact on individuals and society [2]. Pain is now divided into four major types: nociceptive pain, inflammatory pain, neuropathic pain and dysfunctional pain [3].

As the treatment of pain is still often unsatisfactory for some kinds of pain and for a part of the patients, it is important to identify pain mechanisms for the development of new therapeutic strategies [3, 4]. Generally, injured tissues or nerves release many pro-pain molecules including cytokines, chemokines, prostaglandins, bradykinin, histamine, serotonin and nerve growth factor, which increase sensory neurons excitability, leading to peripheral sensitization. The pain message is transmitted to spinal cord via the central terminal of primary afferents resulting in neuron-neuron and neuron-glial interactions [5]. Then the signals are sent to and integrated in the pain matrix in the brain that also exerts the descending pain control.

Small fiber neuropathies (SFNs), a disorder of Aδ-fibers and C-fibers, is usually characterized by neuropathic pain symptoms and autonomic complaints in the clinics [6]. Interestingly, in idiopathic SFNs, nearly 30% of patients have gain-of-function (GOF) mutations in the *SCN9A* gene encoding for the NAV1.7 channel protein [7]. These mutations were expressed in HEK293 cells or dorsal root ganglia (DRG) and subjected to voltage clamp analysis. They produced impaired inactivation or enhanced resurgent current of voltage-gate properties of NAV1.7 channel. They also induced Increased excitability of transfected DRG neuron [7]. NAV1.7 has been a target for analgesia for decades, but mostly the selective inhibitors could not be developed as therapeutics because they may exert effects on a broader spectrum of sodium channels [8]. Additionally, *SCN9A* loss-of-function (LOF) by bi-allelic inactivating mutations results in the striking clinical phenotype of congenital insensitivity to pain (CIP [9]. Recently, several GOF mutations in the *SCN10A* gene encoding for the NAV1.8 α-subunit of sodium channel have also been reported in SFN patients. Similar to NAV1.7 variants, these NAV1.8 mutations provoke neuronal hyperexcitability after transfection of DRG neurons [7]. However, in contrast to *SCN9A*, there is no report for LOF mutations for *SCN10A* in humans. All of these idiopathic SFN patients display abnormal quantitative sensory testing, but with a complexed response to thermal and mechanical stimuli.

Understanding the pathophysiological mechanism underlying pain symptoms in painful SFN and other pain pathologies is important and requires relevant preclinical models. According to the different and

complex phenotypes in patients, animal models have been generated to model individual cases of idiopathic SFN.

In this review, we provide the profiles of nociceptive behaviors related to NAV1.7 and NAV1.8, by evoking the different preclinical genetic models of NAV1.7 and NAV1.8 used in research until now. It is of high benefit to discuss the advantages and disadvantages of previous studies and provide future suggestions to develop new mouse models for studying heterogeneous pain symptoms in SFN patients and other pain patients. These models may be used to develop novel analgesics targeting these channels.

2. The sodium voltage-gated channels NAV1.7 (SCN9A) and NAV1.8 (SCN10A)

NAV1.7 and NAV1.8 channels are voltage-gated sodium channels that play a critical role in the generation and conduction of action potentials and are important for electrical signaling by most excitable cells. They are composed of one α-subunit associated with one or more β-subunits. The α-subunit consists of four homologous domains (DI-DIV) and each domain consists of six transmembrane segment [10, 11]. NAV1.7 is preferentially expressed in the peripheral nervous system within sensory DRG and sympathetic ganglion neurons and their small diameter peripheral axons [12, 13]. NAV1.7 protein was also detected in lamina I, lamina IIo, and lamina IIi of superficial dorsal horn within primary afferent terminals, but very few transcripts can be detected in dorsal horn cells. Recent study demonstrated that sensory neurons are the source of NAV1.7 in dorsal horn neurons using both immunocytochemistry and immune-electron microscopy [14]. NAV1.7 is tetrodotoxin-sensitive sodium channel, which opens in response to small depolarizations and closes to resting potential [8]. The proteins interacting with NAV1.7 were mapped using epitope-tagged gene-targeted mice, and they included membrane-trafficking proteins [13]. More detailed signal pathway of NAV1.7 involved post-synaptic density scaffolding protein Homer 2, N-acylethanolamines binding protein FABP7, Mitogen-activated protein MAP kinases and Collapsin response mediator protein 2 (CRMP2), described in review by Chew et al [15].

NAV1.8 produces a slow inactivating, tetrodotoxin-resistant current, and is known to recover rapidly from inactivation [8, 16]. NAV1.8 is a major contributor to the uprising phase of the action potential [16]. NAV1.8 is predominately expressed in the peripheral nervous system within small-diameter neurons of trigeminal ganglion and DRG, but also in a small percentage of medium- and large-diameter neurons [8, 17, 18]. The creation of a transgenic mouse line encoding green fluorescent protein under the control of *Scn10a* promoter has allowed to reconsider NAV1.8 expression pattern.

NAV1.8 protein was detected in small and medium diameter DRG neurons as well as lamina I and II of the spinal cord dorsal horn where C-fibers predominantly terminate [19].

The pain behavior analysis of genetic animal models for *Scn9a* and *Scn10a* showed that these sodium channels play important roles for acute pain sensation (nociception) and contribute to the sensitization of pain circuits, leading to hyperalgesia [20]. The present review summarizes the findings on mutant mice and rats for these channels and their behavior in nociception and chronic pain models.

3. Role of SCN9A (NAV1.7) in pain behavior: lessons learnt from rodent models

3.1 Effect on the channel absence as assessed in homozygote global KO mice and rats

Clinical genetic studies have reported that *Scn9a* LOF results in complete inability to experience pain (CIP). Genetic animal models have proved useful tools to study the mechanism of CIP and potentially develop therapies for CIP patients. The absence of NAV1.7 protein has been assessed first by *Scn9a* gene knockout (KO) in the whole body, ie. global KO. Although the global inactivation of *Scn9a* was reported lethal in mice [21], Gingras et al. could overcome the neonatal lethality by changing the original genetic C57BL/6J genetic background to a mixed CD1 and then to BALB/c and obtain a homozygote *Scn9a* knockout mice that were profiled in several behavioral assays as discussed below [22]. While trying to Humanize NAV1.7 in rats Grubinska et al [23] have been generated a partial KO, resulting in NAV1.7 protein loss in DRGs, sciatic nerve, brainstem and gastrointestinal tissues but not in the olfactory tract.

3.1.1 Effect on nociceptive behavior

Measurements of reflexive behaviors to thermal and mechanical stimuli as well as more integrated or spontaneous pain tests were used to examine pain-like responses and pain mechanisms in rodents [24, 25]. Supraspinal responses to a noxious heat stimulus can be assessed by the hot plate test where latency to paw reaction is measured. Interestingly, withdrawal latencies of wild-type (WT) or heterozygous (HET) mice decreased as temperature increased in the hot plate from 48 to 55°C while *Scn9a* KO mice were insensitive to heat [22] (Table 1). The evaluation of sensitivity to mechanical stimuli is done with Von Frey nylon filaments of varying diameters, allowing to assess both mechanical allodynia and hyperalgesia. Other tools include tail clip, Randall-Selitto or pressure analgesimeter for pressure application to paw or tail, that produce results analogous to clinical pressure pain conditions [25, 26]. Global *Scn9a* KOs were insensitive to pressure pain in tail clip assay. However, in Von Frey test, the KOs showed similar touch sensitivity than control mice [22]. The *Scn9a* LOF rats had no or very faint responses to noxious chemical, thermal and prick stimuli [23, 27] (Table 1).

3.1.2 Effect on induced pain

The formalin test is used for testing pain to chemical irritant (phase I, 0-5 min) and subsequent acute inflammatory hyperalgesia (phase II, 10-40 min). It reflects the direct activation of primary nociceptive afferents and inflammation-induced peripheral and central sensitization. The global *Scn9a* KO mice and rat showed a strong decreased or response in phase I and II in the formalin test [23, 27]. The Complete Freund's adjuvant (CFA) model aims at studying chronic inflammatory hyperalgesia in rodents. WT and HET control mice showed expected inflammatory hypersensitivity while whole *Scn9a* KO mice did not display any pain-like behavior [22] (Table 1). The *Scn9a* LOF rats did not experience experimentally-induced neuropathic hypersensitivity [23]. In summary, *Scn9a* LOF induced CIP in rodents wholly analogous to human patients, with insensitivity or reduced sensitivity to noxious heat, cold or pressure. Also, *Scn9a* LOF rodents showed reduced hyperalgesia in inflammatory and a neuropathic model.

3.2 Effect on the *Scn9a* deletion in specific cell population as assessed in conditional KO mice

To study the role of NAV1.7 in precise types of neurons, several mouse lines with conditional deletion of *Scn9a* have been generated. Mice with floxed *Scn9a* gene were crossed with *Scn10a*-Cre, Advillin-Cre, or Wnt-1-Cre mice to obtain *Scn9a* conditional KO (cKO) lines in, respectively, primary nociceptive neurons (small and medium size diameter [21, 28-31], all sensory neurons [28, 30] or sensory and sympathetic neurons [28, 32, 33]. Also, a new mouse line was generated ($Scn9a^{CAGERT}$) where *Scn9a* gene inactivation can be induced at the adult age. Floxed *Scn9a* mice were crossed with mice where the Cre-ERT transgene driven by the CMV early enhancer/chicken beta-actin promoter, allowing Cre recombinase activation upon tamoxifen induction [34]. The induction of *Scn9a* deletion at adulthood may prevent compensatory mechanisms potentially occurring in the other cKO lines. Following tamoxifen induction in the $Scn9a^{CAGERT}$ mouse line, *Scn9a* expression was abolished in the DRG (mRNA, protein), trigeminal ganglia (mRNA) and sympathetic superior cervical ganglia (mRNA) [34].

3.2.1 Effect on nociceptive behavior

The sensitivity to heat noxious stimuli were determined by measuring paw withdrawal latencies in the Hargreaves and hot plate tests. Altogether the different *Scn9a* cKO lines were less sensitive in the Hargreaves test. $Scn9a^{Advillin}$, $Scn9a^{Wnt1}$ and $Scn9a^{CAGERT}$ lines showed behavioral response deficit to heat when applying either fast or slow heat ramps [28, 30, 33, 34] while $Scn9a^{Scn10a}$ lines showed an elevated threshold with the slow ramp only [21, 28, 30, 35]. These data suggest a specific role of NAV1.7 in NAV1.8-positive DRG neurons for mediating response to slowly transduced heat [30]. Furthermore, in the hot plate test that reflects supraspinal response to heat stimuli, only the $Scn9a^{Wnt1}$

and *Scn9a*^{CAGERT} mice showed a pronounced attenuation of response [28, 33, 34] (Table 1). Response to noxious cooling and extreme cold were measured by acetone and cold plate tests [25]. All cKO lines displayed normal response on the cold plate in contrast to LOF rats. Only *Scn9a*^{Advillin} and *Scn9a*^{Wnt1} lines showed deficits in the perception of cooling as assessed in the acetone test (Table 1), indicating that neuronal populations different than the NAV1.8 neurons mediate NAV1.7-dependent perception of moderate cold [28]. This mechanism is corroborated by the attenuated response of *Scn9a*^{Advillin} mice to cooling in the dynamic thermal place preference test [30] (Table 1). Randall-Selitto test and von Frey were employed to assess the responses to touch and pressure in the cKO mice. The different cKO lines displayed a pronounced analgesia to noxious mechanical stimulation in the Randall-Selitto test applied to the tail (Table 1). The cKO lines showed normal response to touch as tested with the von Frey filaments applied to hindpaw glabrous skin, in five articles from two laboratories [21, 28, 30, 32, 34] except when *Scn9a*^{Scn10a} mice were evaluated with the Electronic von Frey Anesthesiometer [14]. This difference may be due to the use of this electronic equipment which applies a maximum force continuously until withdrawal and therefore may lead to a noxious mechanical stimulus rather than a touch stimulus, consolidating the data obtained with the Randall-Selitto test. Interestingly, both *Scn9a*^{Advillin} and *Scn9a*^{Wnt1} mice, but not *Scn9a*^{Scn10a}, mice showed deficits in response when von Frey filaments were applied to the abdomen hairy skin [30] (Table 1). This demonstrated that mechanosensation by hair follicles are dependent on NAV1.7 and mainly in NAV1.8-negative neurons that innervate the hair follicles [30] and is consistent with the results that showed no change in sensitivity to the von Frey filaments in *Scn10a* KO animals (see chapter 4.2 and table 2).

Taken together, these behavioral results indicate that spinal reflex to noxious heat (Hargreaves test) is dependent on NAV1.7 expressed in NAV1.8-positive DRG neurons when using slow temperature ramp only and requires all sensory neurons (Advilin positive neurons) at fast temperature ramp. More integrated response to heat as measured by the hot plate test necessitates in addition the NAV1.7 protein expressed by sympathetic neurons as revealed the Wnt-1-Cre and CAG-ERT mediated cKO mice. Concerning responses to noxious cold, the NAV1.7 expressed by all specific neuron populations tested in the cKO mice, either sensory or sensory plus sympathetic does not appear to be involved. However, the data on *Scn9a* LOF rats implicate the NAV1.7 channel. The results on *Scn10a* global KO and Possum mice lead to the conclusion that NAV1.8 channel is also implicated in noxious cold detection, see in chapter 4. As compared to noxious cold, the behavioral response to cooling (paw acetone test) implicates the NAV1.7 channel and would not require NAV1.7 expressed on NAV1.8 negative cells as found in the in *Scn9a*^{Scn10a}, *Scn9a*^{Advillin} and *Scn9a*^{Wnt1} mice, in agreement with the absence of phenotype in this test in *Scn10a* global KO animals. Lastly, the deletion of NAV1.7 in NAV1.8-positive neuron is sufficient to decrease the NAV1.7-mediated behavioral response to noxious

pressure (Randall-Selitto test), in addition to the role of NAV1.8 shown through the analysis of *Scn10a* KO mice (see chapter 4 and Table 2).

3.2.2 Effect on induced pain

The role of NAV1.7 expressed by NAV1.8-positive neuron in visceral pain was investigated in the *Scn9a*^{Scn10a} mice following capsaicin or mustard oil [29]. *Scn9a*^{Scn10a} animals were equally sensitive than controls, while *Scn9a*^{CAGERT} mice displayed a decreased response in the acetic-acid-induced model (Table 1). Together, this suggests that that NAV1.7 in other neurons than NAV1.8-positive neuron contribute to visceral pain control, although NAV1.8 was shown required for visceral pain control (Table 2).

The different *Scn9a* cKO lines were assessed for their response to inflammatory pain. In addition to the formalin and CFA models described above, the carrageenan model was used which elicits hyperalgesia within hours to days. Both mice with *Scn9a*^{Scn10a} or *Scn9a*^{Advillin} mutations displayed reduced response in the two formalin phases [21, 28], while *Scn9a*^{CAGERT} mice had an attenuation of phase I response only [34]. For carrageenan-induced inflammatory pain, thermal hyperalgesia was absent in *Scn9a*^{Scn10a} mice (Table 1). In the CFA model, hypersensitivity to heat was abolished in both *Scn9a*^{Scn10a} and *Scn9a*^{CAGERT} animals while mechanical allodynia was reduced but still present in *Scn9a*^{CAGERT} mice [34]. Altogether, these results highlighting the major contribution of NAV1.7 protein in peripheral sensory neurons in inflammatory hyperalgesia.

Neuropathic pain is caused by neuron injury in the peripheral or central nervous system. It occurs in many diseases, such as spinal cord injury, peripheral nerve injury, diabetes, postherpetic neuralgia, and cancer. Several successful models have been developed to mimic neuropathic pain evoked by these etiologies [36, 37]. Chronic constriction injury (CCI), spinal nerves transection (SNT) and partial sciatic nerve ligation (pSNL) as nerve injury models were utilized in the *Scn9a* cKO mice [18, 28, 30, 34]. The *Scn9a*^{Scn10a} mice developed mechanical but no or weak cold allodynia following CCI or pSNL while they showed normal allodynia after SNT (Table 1). *Scn9a*^{Advillin} mice showed cold and mechanical allodynia during SNT but developed attenuated allodynia following CCI (Table 1). Deleting *Scn9a* in both sensory and sympathetic neurons (*Scn9a*^{Wnt1}) led to no or low allodynia upon SNT or CCI (Table 1). In *Scn9a*^{CAGERT} cKO mice, SNI induced weak cold allodynia but normal mechanical hypersensitivity [34]. In *Scn9a*^{Wnt1} and *Scn9a*^{Advillin} mice, oxaliplatin-induced neuropathic pain and cancer-induced pain developed as in their control littermates (Table 1). Furthermore, in a burn injury model, NAV1.7 in NAV1.8-positive neurons contribute to induced heat but not mechanical hyperalgesia [31] (Table 1).

Altogether, the behavioral analyses of KO, or cKO, animals show that NAV1.7 is a major contributor to both acute nociception and experimentally-induced chronic hyperalgesia. They suggest that NAV1.7

expressed in *SCN10A* (NAV1.8)-positive nociceptors (*Scn9a*^{Scn10a}) or all sensory neurons (*Scn9a*^{Advillin}) are required for the development of inflammatory pain and neuropathic allodynia in a part of the models tested. Interestingly, constitutive ablation of *Scn9a* in both sensory and sympathetic neurons (*Scn9a*^{Wnt1}) markedly diminished neuropathic pain in both CCI and SNT models while the ablation in these same neurons at adulthood (*Scn9a*^{CAGERT}) attenuated inflammatory pain and SNI-induced neuropathic pain. This suggests that NAV1.7 channels in sympathetic neurons, in addition to sensory neurons, contribute also to neuropathic pain, at least in the SNT model. Additionally, in CIP patients the intra-epidermal nerve fibers are absent [98] whereas these fiber in *Scn9a* KO mice and LOF rats are normal [23, 27]. It means that there are still some different mechanisms between human and rodents.

3.3. Nav1.7 and the opioid receptor pathway

The global *Scn9a* KO in mice or rats and loss-of-function mutations in humans lead to insensitivity to pain. To determine whether these global gene silencing may induce compensations, gene expression was investigated in the DRG of *Scn9a*^{Advillin} mice. *Scn9a* deletion led to changes in transcripts levels in DRG. *Preproenkephalin* (*Penk*) gene encodes for the endogenous opioid peptide enkephalin, and *Penk* mRNA was elevated in *Scn9a*^{Advillin} DRGs. The opioid antagonist naloxone reversed the analgesia in a *SCN9A*-null CIP patient and in *Scn9a*^{Advillin} mice analysed in the Hargreaves and Randall-Selitto tests [38]. This suggested that the endogenous opioid system contributes to the analgesia driven by *Scn9a* gene inactivation. However, naloxone did not reverse analgesia in *Scn9a* LOF rats in the hot plate and formalin tests [27]. The reason for these contrasting findings remains unknown and may be due to the use of different pain behavioral tests. The expression of Penk was also increased in *Scn9a*^{Wnt1} [33]. In order to evaluate whether the activation of mu (MOR) or delta (DOR) opioid receptors was involved in this analgesia, *Scn9a*^{Wnt1} mice were crossed to *Mor* and *Dor* KO mice. Analgesia was abolished in triple *Scn9a*^{Wnt1}/*Mor*/*Dor* KO mice as measured with the Hargreaves test [33]. Altogether, these data showed that the combination of *Scn9a* gene inactivation and opioid system activation are required for analgesia.

4. Role of SCN10A (NAV1.8) in pain behavior: lessons learnt from rodent models

4.1. Pain behavior in the *Scn10a*^{T790A} possum mice.

Following N-ethyl-N-nitrosourea-induced mutation, Blasius et al. 2011 identified a mouse mutant termed Possum which carries a T790A hypermorphic mutation of the *Scn10a* gene. They reported that following scruffing at the back of the neck, the Possum mice became immobile, had apnea, and a rigid posture. When Possum mice were placed at their side or back, they were not able to right themselves, and showed a 'waxy flexibility' where the tail is in a raised position as applied by the experimenter. Heterozygotes showed shorter response (1 min) compared to homozygotes (up to 5 min) [39]. The Possum mice were tested for pain sensitivity. The Possum and WT mice had similar withdrawal responses to Von Frey filaments applied to hind paw [39, 40]. But when a spinal needle prick was applied to the plantar hind paw, Possum mice showed an increased nociceptive response to the stimulus [40]. Concerning thermal stimuli, Possum mice displayed increased sensitivity on cold plate at -1°C, but showed the same sensitivity in the hot plate at 52°C compared to WT controls [39]. Following mustard oil application to hindpaw, Possum mice entered into a Possum-like state, remaining motionless for the 5-minute experimental period while WT mice displayed expected paw lifts and licks. The Possum-like state was reversed by a NAV1.8 antagonist [40]. However, whether this is a pain behavior is not known. Following induction of inflammatory pain by CFA, Possum mice showed a mechanical allodynia similar to WT controls [39] (Table 2). In summary, the Possum mice that have hyperexcitable NAV1.8 channels showed increased sensitivity to extreme noxious mechanical and cold stimuli but no hypersensitivity to other types of pain challenges.

4.2. Effect of NAV1.8 channel absence as assessed in global KO mice

In order to investigate the role of the voltage-gated sodium channel NAV1.8 in pain control, Akopian and colleagues have first generated the *Scn10a* KO mice [41]. The *Scn10a* KO mice were evaluated for basal nociception as well as for experimentally induced chronic hyperalgesia in several studies.

4.2.1. Effect on nociceptive behavior and spontaneous pain

The studies on *Scn10a* KO mice revealed deficits in both mechano- and thermonociception. *Scn10a* KO mice showed analgesia to noxious mechanical pressure assessed in the Randall-Selitto test [18, 30, 41], but no change in mechanical threshold in the Von Frey test [18, 30, 31, 41-43]. Concerning responses to thermal stimuli, *Scn10a* KO animals showed an increased withdrawal latency in a slow but not in a fast heat ramp in the Hargreaves test [30]. The same analgesia was found by Akopian et al. 1999 [41] but not found in other studies [18, 31, 42, 43]. *Scn10a* KO mice were also less sensitive to the tail-flick test [127] but not in the hot plate test [18, 41, 43]. So globally, *Scn10a* KO mice were less or equally sensitive in conditions of spinal reflex to heat, but show no phenotype in the heat supraspinal responses. *Scn10a* deficient mice also revealed a reduced response to cold [44, 45].

Scn10a KO mice were less sensitive than controls to visceral pain elicited by capsaicin or mustard oil [46] (Table 2).

4.2.2. Effect on induced pain

The *Scn10a* KO animals were tested in both inflammatory and neuropathic models. The mutant mice had the same response to formalin as control mice. Following carrageenan challenge, hyperalgesia onset was slightly delayed, from 45 min in the WT to 90 min in *Scn10a* KO mice [41]. In the CFA model, the mutant mice displayed both thermal and mechanical hyperalgesia, but recovered faster from heat pain [43]. Therefore, these results suggest a role of NAV1.8 channel in the kinetics of carrageenan and CFA inflammatory pain, and not in lowering of nociceptive thresholds. The null mutants were comparable to their WT littermates for heat and mechanical hypersensitivity after burn injury [31]. The null mice developed the same allodynia as WT mice following spinal nerve transection [30]. *Scn10a* KO mice showed attenuated cold allodynia in the SNI model [43], while lowered cold allodynia to CCI injury was recorded in one out of two reports [30, 43] (Table 2). Taken globally, NAV1.8 channel plays a role in cold allodynia in some neuropathic pain conditions.

4.3. Effect on the channel as assessed in NAV1.8-Cre mice.

In order to develop conditional KO mice in nociceptive neurons, and as NAV1.8 is specifically expressed in these neurons, *Scn10a-Cre* knock-in mouse lines that express Cre-recombinase driven by the *Scn10a* locus were generated [17, 18, 21]. In these mutant lines, the Cre gene is knocked in the exon-1 of *Scn10a*, 3' UTR was inserted downstream of the Cre gene followed by a polyadenylation signal. *Scn10a -Cre* hemizygous mice were analyzed for nociception and experimentally induced pain. They had a normal phenotype towards mechanical stimulation in the Von Frey and Randall-Selitto assays as well as normal acute thermal responses in the Hargreaves and hot plate tests [17, 18, 21]. Inflammatory pain developed similarly in *Scn10a-Cre* hemizygous mice like in WT mice, in the formalin, carrageenan and CFA models [21]. *Scn10a-Cre*/0 mice were subjected to L5 spinal nerve ligation (SNL) neuropathy model and were then tested for mechanical and heat allodynia. They developed mechanical and thermal pain to the same extent as their littermate controls [18] (Table 2). Therefore, as these *Scn10a-Cre* HET mice behaved as WT mice in nociception and chronic hyperalgesia models, they have been used since then by many teams to conditionally inactivate their genes of interest in nociceptive neurons.

4.4. Role of NAV1.8 channel as assessed by optogenetics

The global knockout approach may lead to compensations at the cellular or circuit levels. As compared to global KO where gene inactivation occurs very early in embryonic stem cells, the optogenetics approach enables a precise spatiotemporal control of the activity of neurons expressing specific pain-

related sodium channels [47]. The activity of NAV1.8-positive neurons could be inhibited or activated by light in the NAV1.8-Arch+ and NAV1.8-ChR2+ genetic mouse models, respectively. Transdermal illumination of NAV1.8-Arch+ mouse hindpaw did not change baseline sensitivity to the von Frey filaments, in agreement with the lack of phenotype of NAV1.8 mice in this test [48]. However, under inflammatory or neuropathic pain conditions, light exposure decreased mechanical allodynia in NAV1.8-Arch+ mice [48]. Light-induced activation of bladder afferent terminals of NAV1.8-ChR2+ mice potentiated the bladder response [49]. These experiments showed that optical silencing or activation of NAV1.8+ afferent neurons in these new optogenetic mouse models modulate the pain behavioral responses. The selective delivery of inhibitory opsins leads to control pain circuits in vivo, with a potential development of clinical trials in patients with chronic irretractable pain

4.5 Role of NAV1.7 and NAV1.8 channels as assessed in double knockout strategies.

4.5.1 Double *Scn10a-Scn9a* knockouts (DKO)

Generating global KOs for both NAV1.7 and NAV1.8 channels and comparing them to single KOs was important to study how the absence of both channels contributes to analgesia. Since *Scn9a* global deletion is lethal at P0 [21], global KO of both *Scn9a* and *Scn10a* could not be obtained from global *Scn9a* KO. Using the *Scn10a-Cre* allele [21], Nassar et al. 2005 could generate double-KO (DKO) mice where the *Scn10a* gene is globally deleted and *Scn9a* is suppressed in NAV1.8-expressing neurons [18]. DKO mice showed similar touch withdrawal thresholds to Von Frey filaments as *Scn10a* KO and WT mice. But when tested for noxious pressure using the Randall-Selitto apparatus, the DKO mice exhibited profound analgesia compared to WT and *Scn10a* KO mice. On the hot plate, DKO mice had same reaction latencies as WT and *Scn10a* KO mice. However, when tested in the Hargreaves plantar test, withdrawal latency was doubled in DKO mice compared to *Scn10a* KO or WT mice [18] (Table 2). Therefore, deleting both *Scn9a* gene from NAV1.8+ neurons and *Scn10a* gene allowed to show that NAV1.7 and NAV1.8 provide additive controls of noxious mechanical and heat pain thresholds.

In the formalin model, DKO, KO and WT groups had similar response during phase 1. However, DKO mice showed a reduced response during phase 2, compared to *Scn10a* KO and WT mice. So, deleting both *Scn10a* and *Scn9a* in nociceptive neurons leads to a higher deficit toward formalin-induced behavior, stressing the additive role of both channels in inflammatory pain [18]. DKO mice developed mechanical allodynia after SNL to the same extent as *Scn10a* KO and WT mice [18] (Table 2). Therefore, the presence of both NAV1.7 and NAV1.8 channels is not essential for mechanical allodynia following SNL [18].

5. Perspectives

The genetic rodent models described here, together with pharmacological approaches that are beyond the scope of this short review, have shown that NAV1.7 and NAV1.8 play important roles in nociception and chronic hyperalgesia. Side-effect of sodium channel blocking analgesics is still a problem for both animals and humans, despite the clear utility of nerve block in pain treatment. To understand the mechanism of chronic pain in patients and explore novel analgesics require novel relevant pre-clinical models. Steve Waxman's team has developed sensory neurons differentiated from patient-derived Induced Pluripotent Stem Cells that model inherited erythromelalgia in vitro [50]. These cells can provide a platform which enables assessment of sodium channel blocker effects in vitro. It will then be necessary to analyze their effects and safety in the genetic models summarized in the review and additional preclinical animal models.

SFNs are a heterogeneous group of disorders affecting thinly myelinated Aδ-fibers and unmyelinated C-fibers with chronic pain symptom. GOF mutants of *SCN9A* and *SCN10A* have been reported in the SFN patients. Patients suffering from SFN usually develop somatic symptoms, which include hyperalgesia as well as reduced pinprick and thermal sensation in the affected areas. It commonly presents with pain, burning, tingling, and numbness. On the contrary, in the CIP patients, LOF of *SCN9A* causes these individuals to not perceive pain in response to noxious stimuli but *SCN10A* LOF mutations were not found yet in these patients. These data suggest that *SCN9A* is mandatory for nociception in human, and elucidating *SCN10A* role would require more clinical investigation. Novel rodent genetic models for these diseases can be generated by using homologous recombination as well as the more recent CRISPR-Cas9 techniques. The CRISPR-Cas9 systems is a research toolbox for genome editing and regulation [51]. Recently, this system has been harnessed to facilitate genetic manipulations in a variety of cell types and organisms [52] and to provide animal models for single base mutation disease [1]. Also, while there are several engineered Adeno-associated viruses successfully delivered to the central and peripheral nervous systems in rodents, the safety and accuracy for gene therapy in human are still challenging [53].

The evaluation of reflexive pain behavior in animal models has been applied in the pain research field since decades. Recently, more clinically relevant approaches to evaluate pain in rodents have been developed. These spontaneous pain behaviors include amongst others preference for the compartment with analgesics as measured by the conditioned place preference test, and avoidance of evoked stimuli recorded by the conditioned place avoidance test [24, 26, 54]. Also, innovative devices have been developed that provide high accuracy assessment of thermal preference through free walking in thermal gradients [55, 56]. Additionally, different parameters have been shown to influence pain sensitivity in behavioral assays including the body location investigated and time of day

[25]. Thus, it is very important and necessary for characterizing the phenotype of novel genetic rodent models to use a range of pain behavioral tests. In addition, the exploration of *Scn* genes roles in pain behavior would necessitate the study of the mutations in different genetic backgrounds, in both sexes, and in different laboratories, to take in account the fact that many laboratory environmental factors can influence pain behavioral results [57].

Although there are differences between rodents and humans, the genetic rodent models are key to understand the mechanism of sodium channels in pain relief and develop novel drugs. Further specific genetic animal models and highly accurate pain behavioral assessment will open a new vision for the role of NAV1.7 and NAV1.8 in pain therapy. Also, the combination of rodent genetic models and other approaches including genetic screening will allow to identify additional components of chronic pain and to design new therapeutic strategies [4].

6. Summary

Recent research has revealed the key role of NAV1.7 and NAV1.8 in pain. In this review, we have summarized published literature on pain behaviors related to *Scn9a* and *Scn10a* in genetics rodent models. Deleting *Scn9a* and *Scn10a* either in the whole body or/and specific neuron populations relieves or attenuates the pain response from thermal, mechanical and chemical stimuli and in inflammatory and neuropathic pain models respectively, which mirrors the clinical features of CIP patients. The genetic rodent models related to *Scn* genes are still needed. Further work could reveal how NAV1.7 and NAV1.8 mediate in the SFN-related pathology (or pain) by establishing animal models for the mutations found in SFN patients and developing novel targeted medicine.

Table 1. Pain Behaviors in *Scn9a* (Nav1.7)-related genetic models

		Rat	Mice				
		Scn9a LOF [23, 27]	*Scn9a* Global KO [22]	*Scn9a*^{Scn10a} cKO [21, 28-32, 35]	*Scn9a*^{Advill} cKO [28, 30, 32]	*Scn9a*^{Wnt1} cKO [28, 30, 32, 33]	*Scn9a*^{CAGERT} KO [34]
Basal nociception							
Mechanical	Von Frey	↘ =	=	Test-site- and condition-dependent deficits			=
	Randall-Selitto or tail clip	NA	↘	↘	↘	↘	↘
	Pin-prick	↘	NA	NA	NA	NA	NA
Heat	Hargreaves	↘	NA	↘ =	↘	↘	↘
	Hot Plate or Tail Immersion	↘	↘	=	=	↘	↘
Cold	Acetone	NA	NA	=	↘	↘	NA
	Cold Plate or Dry ice	↘	NA	=	=	=	NA
Dynamic thermal place preference, cooling		=	NA	NA	↘	NA	NA
Chemically induced visceral pain		NA	NA	=	NA	NA	↘
Inflammatory pain							
Formalin Phase I		↘	↘	=	↘	NA	↘
Formalin Phase II		↘	↘	↘	↘	NA	=
CFA		NA	↘	↘	NA	NA	↘ heat = touch
Carrageenan		NA	NA	↘	NA	NA	NA
Neuropathic pain							
SNT		NA	NA	=	=	↘	NA
CCI		NA	NA	↘ cool = touch	↘	↘	NA
pSNL, SNL or SNI		↘	NA	↘ cool = touch	NA	NA	↘ cool = touch
Oxaliplatin		NA	NA	=	=	=	NA
Other pain models							
Cancer-induced pain		NA	NA	NA	=	=	NA
Burn injury		NA	NA	↘ heat = touch	NA	NA	NA

CCI: Chronic Constriction Injury; CFA: Complete Freund's Adjuvant; KO, knockout; LOF: Loss-of-function; NA: Not Available; SNI: Spared Nerve Injury; pSNL: partial sciatic Nerve Ligation; SNL: Spinal Nerve Ligation; SNT: Spinal Nerve Transection;

=: no change; ↘ : less sensitive compared to control

Table 2. Pain Behaviors in *Scn10a* (Nav1.8)-related genetic models

		Scn10a^{T790A} [39, 40]	*Scn10a* Global KO [18, 30-31,41-46]	*Scn10a*^{Cre} Heterozygotes [17-18, 21]	*Scn10a-Scn9a* Double KO [18]
			Basal nociception		
Mechanical	Von Frey	=	=	=	=
	Randall-Selitto	NA	↘	=	↘
	Needle prick	↗	NA	NA	NA
Heat	Hargreaves	NA	= ↘	=	↘
	Tail Flick or immersion	NA	= ↘	NA	NA
	Hot Plate	=	=	=	=
Cold	Acetone	NA	=	NA	NA
	Cold plantar	NA	=	NA	NA
	Cold plate	↗	↘	NA	NA
Chemically induced Visceral pain		NA	↘	NA	NA
			Inflammatory pain		
Formalin	Phase 1	NA	=	=	=
	Phase 2	NA	=	=	↘
Carrageenan	Hargreaves	NA	=, delayed	=	NA
CFA	Von Frey	=	=	=	NA
	Hargreaves	NA	=, recover faster	=	NA
			Neuropathic pain		
SNT/SNL	Acetone	NA	=	NA	NA
	Von Frey	NA	=	=	=
	Hargreaves	ND	=	=	NA
CCI	Acetone	NA	= ↘	NA	NA
	Von Frey	NA	=	NA	NA
SNI	Acetone	NA	↘	NA	NA
	Von Frey	NA	=	NA	NA
Oxaliplatin	Acetone	NA	=	NA	NA
	Von Frey	NA	=	NA	NA
			Other pain model		
Burn injury		NA	=	NA	NA

CCI: Chronic Constriction Injury; CFA: Complete Freund's Adjuvant; KO: knockout; SNI: Spared Nerve Injury; SNL: Spinal Nerve Ligation; SNT: Spinal Nerve Transection

NA: Not Available; =: no change; ↘ less sensitive compared to control; ↗: More sensitive compared to control

References

1. Raja, S.N., et al., *The revised International Association for the Study of Pain definition of pain: concepts, challenges, and compromises.* Pain, 2020.
2. Mills, S.E.E., K.P. Nicolson, and B.H. Smith, *Chronic pain: a review of its epidemiology and associated factors in population-based studies.* Br J Anaesth, 2019. **123**(2): p. e273-e283.
3. Woolf, C.J., *Capturing Novel Non-opioid Pain Targets.* Biol Psychiatry, 2020. **87**(1): p. 74-81.
4. Calvo, M., et al., *The Genetics of Neuropathic Pain from Model Organisms to Clinical Application.* Neuron, 2019. **104**(4): p. 637-653.
5. Zhang, Z.J., B.C. Jiang, and Y.J. Gao, *Chemokines in neuron-glial cell interaction and pathogenesis of neuropathic pain.* Cell Mol Life Sci, 2017. **74**(18): p. 3275-3291.
6. Cazzato, D. and G. Lauria, *Small fibre neuropathy.* Curr Opin Neurol, 2017. **30**(5): p. 490-499.
7. Faber, C.G., et al., *Gain of function Nanu1.7 mutations in idiopathic small fiber neuropathy.* Ann Neurol, 2012. **71**(1): p. 26-39.
8. Bennett, D.L., et al., *The Role of Voltage-Gated Sodium Channels in Pain Signaling.* Physiol Rev, 2019. **99**(2): p. 1079-1151.
9. McDermott, L.A., et al., *Defining the Functional Role of NaV1.7 in Human Nociception.* Neuron, 2019. **101**(5): p. 905-919 e8.
10. Baker, M.D. and M.A. Nassar, *Painful and painless mutations of SCN9A and SCN11A voltage-gated sodium channels.* Pflugers Arch, 2020. **472**(7): p. 865-880.
11. Shen, H., et al., *Structures of human Nav1.7 channel in complex with auxiliary subunits and animal toxins.* Science, 2019. **363**(6433): p. 1303-1308.
12. Black, J.A., et al., *Expression of Nav1.7 in DRG neurons extends from peripheral terminals in the skin to central preterminal branches and terminals in the dorsal horn.* Mol Pain, 2012. **8**: p. 82.
13. Kanellopoulos, A.H., et al., *Mapping protein interactions of sodium channel NaV1.7 using epitope-tagged gene-targeted mice.* EMBO J, 2018. **37**(3): p. 427-445.
14. Alles, S.R.A., et al., *Sensory neuron-derived NaV1.7 contributes to dorsal horn neuron excitability.* Sci Adv, 2020. **6**(8): p. eaax4568.
15. Chew, L.A., et al., *Mining the Nav1.7 interactome: Opportunities for chronic pain therapeutics.* Biochem Pharmacol, 2019. **163**: p. 9-20.
16. Wood, J.N., et al., *Sodium Channels and Pain*, in *The Oxford Handbook of the Neurobiology of Pain*. 2020. p. 232-262.
17. Agarwal, N., S. Offermanns, and R. Kuner, *Conditional gene deletion in primary nociceptive neurons of trigeminal ganglia and dorsal root ganglia.* Genesis, 2004. **38**(3): p. 122-9.
18. Nassar, M.A., et al., *Neuropathic pain develops normally in mice lacking both Na(v)1.7 and Na(v)1.8.* Mol Pain, 2005. **1**: p. 24.

19. Lu, V.B., S.R. Ikeda, and H.L. Puhl, 3rd, *A 3.7 kb fragment of the mouse Scn10a gene promoter directs neural crest but not placodal lineage EGFP expression in a transgenic animal.* J Neurosci, 2015. **35**(20): p. 8021-34.

20. Hameed, S., *Nav1.7 and Nav1.8: Role in the pathophysiology of pain.* Mol Pain, 2019. **15**: p. 1744806919858801.

21. Nassar, M.A., et al., *Nociceptor-specific gene deletion reveals a major role for Nav1.7 (PN1) in acute and inflammatory pain.* Proc Natl Acad Sci U S A, 2004. **101**(34): p. 12706-11.

22. Gingras, J., et al., *Global Nav1.7 knockout mice recapitulate the phenotype of human congenital indifference to pain.* PLoS One, 2014. **9**(9): p. e105895.

23. Grubinska, B., et al., *Rat NaV1.7 loss-of-function genetic model: Deficient nociceptive and neuropathic pain behavior with retained olfactory function and intra-epidermal nerve fibers.* Mol Pain, 2019. **15**: p. 1744806919881846.

24. Tappe-Theodor, A. and R. Kuner, *A common ground for pain and depression.* Nat Neurosci, 2019. **22**(10): p. 1612-1614.

25. Minett, M.S., K. Quick, and J.N. Wood, *Behavioral Measures of Pain Thresholds.* Curr Protoc Mouse Biol, 2011. **1**(3): p. 383-412.

26. Barrot, M., *Tests and models of nociception and pain in rodents.* Neuroscience, 2012. **211**: p. 39-50.

27. Chen, L., et al., *Pharmacological characterization of a rat Nav1.7 loss-of-function model with insensitivity to pain.* Pain, 2020. **161**(6): p. 1350-1360.

28. Minett, M.S., et al., *Distinct Nav1.7-dependent pain sensations require different sets of sensory and sympathetic neurons.* Nat Commun, 2012. **3**: p. 791.

29. Hockley, J.R., et al., *Visceral and somatic pain modalities reveal NaV 1.7-independent visceral nociceptive pathways.* J Physiol, 2017. **595**(8): p. 2661-2679.

30. Minett, M.S., N. Eijkelkamp, and J.N. Wood, *Significant determinants of mouse pain behaviour.* PLoS One, 2014. **9**(8): p. e104458.

31. Shields, S.D., et al., *Sodium channel Na(v)1.7 is essential for lowering heat pain threshold after burn injury.* J Neurosci, 2012. **32**(32): p. 10819-32.

32. Minett, M.S., et al., *Pain without nociceptors? Nav1.7-independent pain mechanisms.* Cell Rep, 2014. **6**(2): p. 301-12.

33. Pereira, V., et al., *Analgesia linked to Nav1.7 loss of function requires micro- and delta-opioid receptors.* Wellcome Open Res, 2018. **3**: p. 101.

34. Shields, S.D., et al., *Insensitivity to Pain upon Adult-Onset Deletion of Nav1.7 or Its Blockade with Selective Inhibitors.* J Neurosci, 2018. **38**(47): p. 10180-10201.

35. Zhou, X., et al., *Spider venom-derived peptide induces hyperalgesia in Nav1.7 knockout mice by activating Nav1.9 channels.* Nat Commun, 2020. **11**(1): p. 2293.

36. Withey, S.L., D.R. Maguire, and B.D. Kangas, *Developing Improved Translational Models of Pain: A Role for the Behavioral Scientist.* Perspect Behav Sci, 2020. **43**(1): p. 39-55.

37. Gregory, N.S., et al., *An overview of animal models of pain: disease models and outcome measures.* J Pain, 2013. **14**(11): p. 1255-69.

38. Minett, M.S., et al., *Endogenous opioids contribute to insensitivity to pain in humans and mice lacking sodium channel Nav1.7.* Nat Commun, 2015. **6**: p. 8967.

39. Blasius, A.L., et al., *Hypermorphic mutation of the voltage-gated sodium channel encoding gene Scn10a causes a dramatic stimulus-dependent neurobehavioral phenotype.* Proc Natl Acad Sci U S A, 2011. **108**(48): p. 19413-8.

40. Garrison, S.R., et al., *A gain-of-function voltage-gated sodium channel 1.8 mutation drives intense hyperexcitability of A- and C-fiber neurons.* Pain, 2014. **155**(5): p. 896-905.

41. Akopian, A.N., et al., *The tetrodotoxin-resistant sodium channel SNS has a specialized function in pain pathways.* Nat Neurosci, 1999. **2**(6): p. 541-8.

42. Kerr, B.J., et al., *A role for the TTX-resistant sodium channel Nav 1.8 in NGF-induced hyperalgesia, but not neuropathic pain.* Neuroreport, 2001. **12**(14): p. 3077-80.

43. Leo, S., R. D'Hooge, and T. Meert, *Exploring the role of nociceptor-specific sodium channels in pain transmission using Nav1.8 and Nav1.9 knockout mice.* Behav Brain Res, 2010. **208**(1): p. 149-57.

44. Luiz, A.P., et al., *Cold sensing by NaV1.8-positive and NaV1.8-negative sensory neurons.* Proc Natl Acad Sci U S A, 2019. **116**(9): p. 3811-3816.

45. Zimmermann, K., et al., *Sensory neuron sodium channel Nav1.8 is essential for pain at low temperatures.* Nature, 2007. **447**(7146): p. 855-8.

46. Laird, J.M., et al., *Deficits in visceral pain and referred hyperalgesia in Nav1.8 (SNS/PN3)-null mice.* J Neurosci, 2002. **22**(19): p. 8352-6.

47. Mickle, A.D. and R.W.t. Gereau, *A bright future? Optogenetics in the periphery for pain research and therapy.* Pain, 2018. **159 Suppl 1**: p. S65-S73.

48. Daou, I., et al., *Optogenetic Silencing of Nav1.8-Positive Afferents Alleviates Inflammatory and Neuropathic Pain.* eNeuro, 2016. **3**(1).

49. DeBerry, J.J., et al., *Differential Regulation of Bladder Pain and Voiding Function by Sensory Afferent Populations Revealed by Selective Optogenetic Activation.* Front Integr Neurosci, 2018. **12**: p. 5.

50. Wu, W., Y. Yang, and H. Lei, *Progress in the application of CRISPR: From gene to base editing.* Med Res Rev, 2019. **39**(2): p. 665-683.

51. Shah, S.Z., et al., *Advances In Research On Genome Editing Crispr-Cas9 Technology.* J Ayub Med Coll Abbottabad, 2019. **31**(1): p. 108-122.

52. Li, Z.M., L.X. Chen, and H. Li, *Voltage-gated Sodium Channels and Blockers: An Overview and Where Will They Go?* Curr Med Sci, 2019. **39**(6): p. 863-873.

53. Hudry, E. and L.H. Vandenberghe, *Therapeutic AAV Gene Transfer to the Nervous System: A Clinical Reality.* Neuron, 2019. **101**(5): p. 839-862.

54. Turner, P.V., D.S. Pang, and J.L. Lofgren, *A Review of Pain Assessment Methods in Laboratory Rodents.* Comp Med, 2019. **69**(6): p. 451-467.

55. Bohic, M., et al., *Loss of bhlha9 Impairs Thermotaxis and Formalin-Evoked Pain in a Sexually Dimorphic Manner.* Cell Rep, 2020. **30**(3): p. 602-610 e6.

56. Touska, F., et al., *Comprehensive thermal preference phenotyping in mice using a novel automated circular gradient assay.* Temperature (Austin), 2016. **3**(1): p. 77-91.

57. Mogil, J.S., *Laboratory environmental factors and pain behavior: the relevance of unknown unknowns to reproducibility and translation.* Lab Anim (NY), 2017. **46**(4): p. 136-141.

5 Role of *SCN10A* in human neuropathy

5.1 *SCN10A* mutations reported in patients: description, symptoms and molecular analysis

The critical role of SCN10A in repetitive firing and its localization in free nerve endings suggest that this channel play an important role in nociception and chronic pain.

Catharina Faber et al. have reported that 29% of patients with painful SFN carried GOF variants in *SCN9A* gene [49]. In another article, Faber et al. identified GOF mutations in *SCN10A* in patients with painful neuropathy. Among 104 SFN patients, nine, including a father-son pair, carried seven missense variants in the *SCN10A* gene. Two mutations were described, c.1661T > C, L554P and c.3910G > A, A1304T. The PM c.1661T > C found in patients 1 and 2, both in heterozygous state, is located in exon 11 of *SCN10A* gene and substitutes leucine 554, which is highly conserved in loop 1. The PM c.3910G > A found in patient 3 in heterozygous state, substitutes alanine 1304 by threonine, (A1304T), likely resulting in alteration of polarity. The locus A1304 is highly conserved in multiple species and in VGSC family, and is located in S5 of DIII. These mutations have a proexcitatory effect, reduce current threshold and increase firing frequency in response to suprathreshold stimuli (L554P, A1304T), depolarize resting potential (A1304), and induce spontaneous firing of small DRG neurons (L554P) [52].

Another PM c.5116A > G, I1706V was identified in a 61-years-old male patient suffering from burning and tingling sensations in both legs and feet, intolerance to wearing shoes and to sheets over his feet. Cooling tended to relieve the pain. The patient also complained of discoloration, episodic swelling of his feet and other autonomic symptoms. Physical examination showed no clear abnormalities. There were no signs of large nerve fiber involvement on NCV. WDTs in QST were abnormal whereas CDTs were normal. Skin biopsy showed an abnormal IENFD compared with normative values. Based on clinical findings and abnormal IENFD and QST, the patient was diagnosed with SFN. The c.5116A > G variant results in an amino acid substitution from isoleucine to valine at position 1706, located within S6 of DIV. The isoleucine at this position is highly conserved in the VGSC family. Biophysical analysis of I1706V revealed an enhancement of activation to a more hyperpolarized state, which is similar to the effect of A1304T variant and in contrast to the accelerated recovery from inactivation as seen with L554P mutation [52]. In addition, the I1706V mutation also hyperpolarizes the voltage threshold for channel opening, which is not the case of A1304T. In current-clamp recordings, similarly to A1304T and L554P

variants, the I1706V mutation produces hyperexcitability in small DRG neurons, manifested by a reduction in the current threshold, an increase in the population of repetitive firing neurons, and a marked increase in firing frequency in response to graded depolarizing stimuli. However, the I1706V mutation reveals some biophysical changes that don not correlate with hyperexcitability, lesser fractional channels are resistant to fast inactivation in suprathreshold activation range and normalized persistent current is reduced. Nevertheless GOF properties are dominant [52, 94]. Another variant also producing biased functional assessments was reported. c.3218G > A inducing a missense mutation, A1073V was identified in 125 heterozygous and 11 homozygous carriers among 496 individuals. The mutation locus lies in the intracellular loop between DII and DIII of the channel and the major effects of the A1073V substitution are on gating properties of the SCN10A channel. Although the mutant allele has a pro-excitatory effect by shifting channel activation, it also has an anti-excitatory effect by accelerating inactivation, with the net outcome being reduced repetitive firing of DRG neurons, consistent with lower mechanical pain sensitivity [95].

Additional four rare genetic variants were reported within the *SCN10A* gene: E285K, M650K, L741V and V763I [140]. A 53 years old woman with symptoms of EM beginning at the age of 35 carried the heterozygous PM c.1949T > A, M650K. She experienced episodes of redness and painful warm in her feet several times a week, mostly in the evenings and early night; however, skin temperature appears normal upon clinical examination. She described pain sensation as superficial and of a burning and pressing type, only located in the feet, predominantly the soles. Physical activity and exposure to heat aggravated her symptoms. The patient does not receive medication but her pain is relieved by cooling. Clinical and neurological findings, EMG and QST examinations were normal, except for a reduced sensibility for light touch on the feet. There were no signs of large nerve fiber involvement on NCS. A total of 25 C-fibers were examined by microneurography and results correlated to patch clamp findings. A broader AP could lead to more calcium and sodium ion influx, then to facilitated neurotransmitter release in the dorsal horn, thus contributing to increased activity dependent slowing observed in mechano-insensitive C nociceptors and to pain attacks. These changes in SCN10A kinetics could underlie the lower firing rates observed during voltage clamp, parallel the reduced mechanical responses in nociceptors during microneurography and explain the possibility to feel pain despite the ability of the nociceptor to fire only low frequencies [57].

Another study reported a 37-years-old woman with severe progressive gastroparesis and diffuse painful SFN harbored a heterozygous mutation: c.4915G > A, D1639N another missense

mutation in the *SCN10A* gene. This PM is located in the loop of S4 in DIV. Negatively charged aspartic acid is substituted by positively charged asparagine, which could change the channel activity. The locus is highly conserved both in different organisms and in other VGSC. At the age of 32, the patient developed burning pain and tingling in her right leg. Within a year, symptoms gradually spread to involve both legs, thighs, and genital area. At the age of 34, she had severe neuropathic pain of a burning nature, affecting almost her entire body. Simultaneously with pain onset, she had difficulties in swallowing and a heartburn sensation that worsen over time. QST showed normal thresholds to cold, warm, pain and vibratory sensations. However, Skin biopsy showed markedly reduced IENFD. She was also diagnosed with severe gastroparesis, defined as an impaired rate of gastric emptying without evidence of gastric outlet obstruction [47].

Moreover, an individual with painful diabetic peripheral neuropathy was carrying c.724T > A, S242T mutation in *SCN10A* gene. The locus is a conserved position within linker of S4-S5 in DI; S242T substitution is similar to SCN9A-S241T mutation, identified in subjects with IEM. The S4-S5 linker translates movement of the voltage-sensor into a conformational change in the PE during opening of the activation gate, which suggests that this PM alters activation properties of SCN10A. S242T mutation manifests both GOF attributes including a hyperpolarizing shift of activation, and LOF attributes including a hyperpolarizing shift in slow-inactivation, with dominance of the GOF properties rendering DRG hyperexcitable [93].

More mutations in *SCN10A* gene identified in patients with pure SFN are indicated in Table 2 [141].

Table 2: Potentially pathogenic *SCN10A* variants identified in patients with pure SFN at Maastricht UMC+ (n=1139 patients) [141]

c.position	p.position	Number of patients	Classification based on predictive algorithms #	Location	MAF ExAC (%)	Cell electrophysiology	Cosegregation	Classification according to Waxman recommendations
c.41G>T	p.(R14L)	4	3	N-terminus	0.2 (234/121 350)	N/A	1 family tested, segregation inconclusive†	VUS
c.626G>A	p.(R209H)	1	3	Loop DI/S3-DI/S4	0.003 (4/121 360)	N/A	N/A	VUS
c.1141A>G	p.(I381V)	1	4	DI/S6	0.05 (63/121 384)	N/A	N/A	Possibly pathogenic variant
c.1667A>T	p.(Q556L)	1	3	Linker DI/S6-DII/S1	–	N/A	N/A	VUS
c.1879T>C	p.(S627P)	1	3	Linker DI/S6-DII/S1	0.003 (3/120 550)	N/A	N/A	VUS
c.2221C>G	p.(L741V)	1	3	DII/S3	0.01 (18/120 924)	N/A	N/A	VUS
c.2972C>T	p.(P991L)	4	3	Linker DII/S6-DIII/S1	0.09 (108/121082)	N/A	2 family tested, segregation with disease (n=1), segregation Inconclusive (n=1)†	VUS
c.3482T>C	p.(M1161T)	1	4	DIII/S1	0.02 (27/121 036)	N/A	N/A	Possibly pathogenic variant
c.3607C>T‡	p.(L1203F)	1	3	DIII/S2	-	N/A	N/A	VUS
c.3674T>C	p.(I1225T)	1	3	DIII/S3	0.06 (70/121 240)	N/A	1 family tested, segregation with disease	Probably pathogenic variant
c.3766C>T	p.(R1256W)	1	4	DIII/S4	0.003 (3/121 100)	N/A	N/A	Probably pathogenic variant
c.3803G>A	p.(R1268Q)	4	3	Loop DIII/S4-DIII/S5	0.2 (213/120 708)	N/A	N/A	VUS
c.3910G>A	p.(A1304T)	1	4	DIII/S5	0.004 (5/121 410)	Gain-of-function	N/A	Probably pathogenic variant

c.4139G>A	p.(R1380Q)	1	3	Loop DIII/S5-DIII/S6	0.009 (10/110106)	N/A	N/A	VUS
c.4378C>T	p.(R1460W)	1	3	Linker DIII/S6-DIV/S1	0.05 (58/121296)	N/A	N/A	VUS
c.4562G>A	p.(G1521D)	1	3	DIV/S2	-	N/A	N/A	VUS
c.4568G>A‡§	p.(C1523Y)	9	4	DIV/S2	0.1 (135/121358)	DRG neuron hyperexcitability	N/A	Probably pathogenic variant
c.4724T>C	p.(I1575T)	1	4	DIV/S4	-	N/A	N/A	VUS
c.4878G>A	p.(M1626S)	1	3	DIV/S5	0.00008 (1/121408)	N/A	N/A	VUS
c.4984G>A	p.(G1662S)	3	4	Loop DIV/S5-DIV/S6	0.2 (190/121360)	Gain-of-function	N/A	Pathogenic variant
c.5116A>G	p.(I1706V)	1	4	DIV/S6	-	Gain-of-function	N/A	Probably pathogenic variant
c.5200G>A§	p.(E1734K)	1	3	C-terminus	0.02 (20/121400)	N/A	N/A	VUS
c.5474T>C	p.(M1825T)	1	3	C-terminus	-	N/A	N/A	VUS
c.5539C>T	p.(R1847*)	1	3	C-terminus	0.003 (3/121404)	N/A	N/A	VUS
c.5606G>A	p.(R1869H)	1	3	C-terminus	0.004 (5/121402)	N/A	N/A	VUS

c. position, location cDNA; p. position, location in protein.

#2, unlikely to be pathogenic; 3, uncertain clinical significance; 4, likely to be pathogenic.

†Inconclusive, affected family members with minor complaints were negative for the variant (c.41G>T and c.2972C>T).

‡One patient was heterozygous for c.3607C>T and c.4568G>A variant.

§One patient was heterozygous for c.4568G>A and c.5200G>A variant

*Termination codon

MAF ExAC, Minor Allele Frequency Exome Aggregation Consortium; N/A, not available; VUS, variants with uncertain clinical significance. Table copied from Eijkenboom, I. et al., 2019 [141].

5.2 G1662S mutation of *SCN10A* in human

Interestingly, another heterozygous GOF mutation in *SCN10A* gene was initially reported in two female patients with SFN [142]. The c.4984G>A variant in exon 27 results in an amino acid substitution from glycine to serine at position 1662 of the SCN10A (see Table 2). The locus is part of the loop between S5 and S6 of DIV and is invariant in all VGSC [142]. The description of the two patient's, including their symptoms, physical examination, NCS, QST and skin biopsy results are presented in table 3. A third patient with G1662S mutation in *SCN10A* gene was recently reported. She was diagnosed at the age of 28 years-old with pain debuting at the age of 25. IENFD was normal but temperature thresholds were abnormal [141].

Table 3: Description of symptoms, physical examination, NCS, QST and skin biopsy results of two SFN patients with G1662S mutation in *SCN10A* gene.

Patient	Age	Pain-history	Symptoms	Physical examination	NCS	QST	Skin biopsy	Diagnosis
Patient 1 Woman	24y	2y	-Continuous tingling and cramp-like pain in her legs, restless legs. -Cold temperature and exercise aggravated her complaints. Warm blankets gave some pain relief. -Occasional hyperhidrosis and orthostatic dizziness.	No abnormalities	Normal	Abnormal thresholds for warmth and cold sensation in both hands	Normal	Idiopathic-SFN
Patient 2 Woman	62y	16y	-Continuous burning and stabbing pain in both feet. -At age of 59, pain in both feet worsened and hands were also affected. 6 months prior to evaluation she developed sensitive skin, intolerance to sheets over her feet. -Occasional episodes of dry eyes, dry mouth, increased sweating, diarrhea and constipation, orthostatic intolerance, palpitations and hot flashes.	Hypoesthesia and reduced vibration sense of the legs	Normal	Abnormal warmth sensation levels for both feet	Normal	Predominantly painful Idiopathic-SFN

NCS: Nerve conduction studies; QST: Quantitative sensory testing; SFN: Small fiber neuropathy.

G1662S mutation does not affect activation, but rather impairs steady-state fast-inactivation shifting its voltage dependence in a depolarizing direction, accelerates recovery from inactivation,

decreases current thresholds (Figure 9) and increases by threefold the proportion of cells that fired spontaneously inducing an increase in DRG neurons excitability [142].

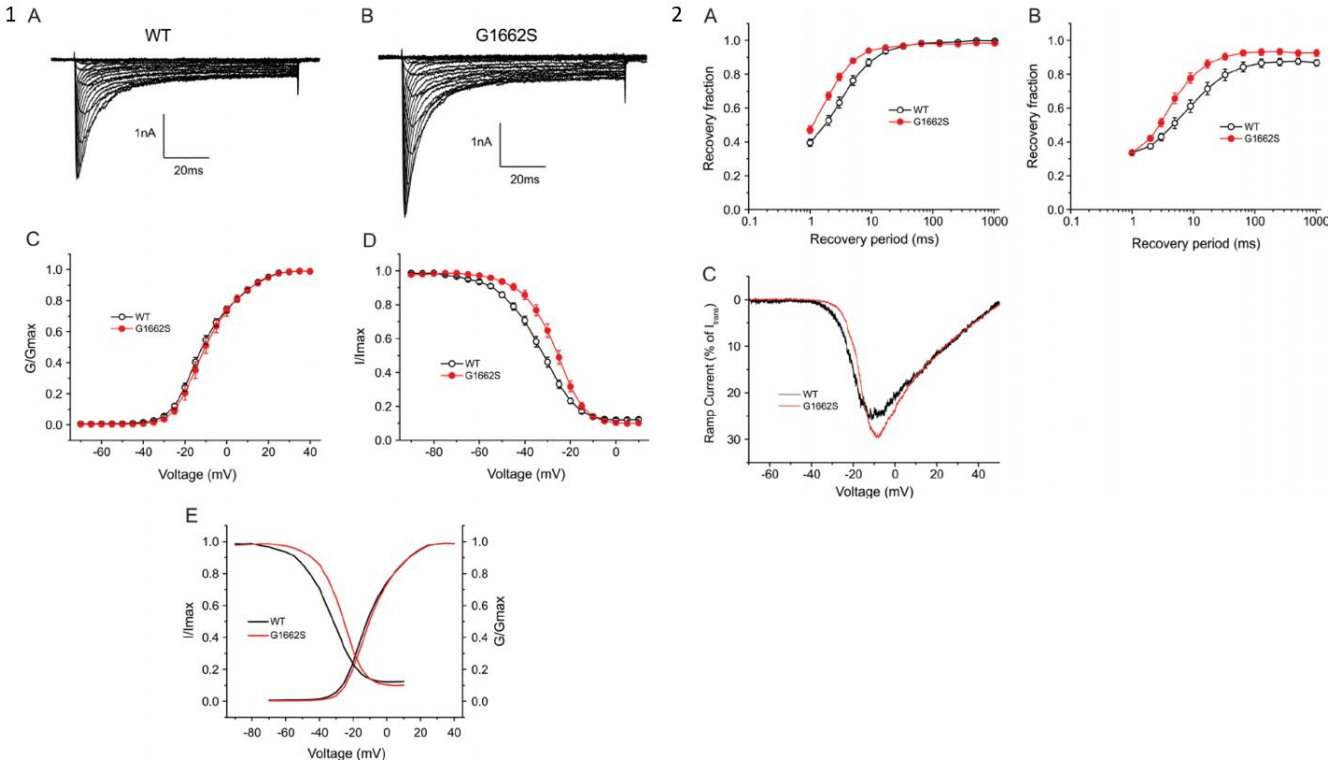

Figure 9: Physiological effects of G1662S mutation

(1) Voltage-clamp analysis of WT and G1662S channels in DRG neurons. Representative current traces recorded from DRG neurons expressing WT (A) or G1662S (B), evoked by voltage steps (100 ms) from -70 mV to 50 mV in 5-mV increments, from a holding potential of −70 mV. (C) Comparison of voltage-dependent activation for WT and G1662S channels. G1662S does not alter activation. (D) Comparison of steady-state fast-inactivation for WT and G1662S channels. G1662S mutation impairs steady-state fast-inactivation by 6.8 mV. (E) Comparison of the overlap of activation and fast-inactivation curves between WT and G1662S.

(2) G1662S displays enhanced recovery from fast-inactivation at -70 mV (A) and -50 mV (B). Note that a logarithmic scale (Log 10) was used for the X-axis. (C) Representative ramp current traces recorded from DRG neurons expressing WT (black) or G1662S (red), evoked by a slow ramp stimulus from –70 mV to 50 mV over 600 ms. Adapted from Han, C. et al., 2014 [142].

6 Gene targeting tools

The use of gene targeting to evaluate the function of genes in living animals has gained large importance over last decades and is more and more used as a routine procedure [143]. It was in the late 1980s that scientists designed a way to modify mammalian genomes in living cells, rendering possible the insertion of a specific DNA sequence at a specific locus in mouse ES cells and then produce mice carrying the genetic modification [143]. The method was originally developed by the three pioneering Nobel Laureates, Capecchi, Smithies and Evans whose important studies are cited here [144-148]. Additionally, Thomas et al. described a protocol to inactivate (knockout) specific genes by HR in mouse [149]. Gene targeting with HR in mouse ES cells has revolutionized the study of gene function in mammals. This method was efficient due to the fact that the selection for the appropriate HR event was done in ES cells instead of whole organisms. The selection consisted of two main steps. First, ES cells whose genome incorporated the targeting vector can be selected by engineering a neomycin resistance conferring cassette into the homology region of the targeting vector [150]. Second, ES cells in which the targeting vector was incorporated by HR and replaced the endogenous gene, without insertion into a random locus, can be selected [150]. This selection was possible by the inclusion of thymidine kinase cassette usually downstream of the homology region of the construct [147]. Due to this double selection strategy, identification of ES cells in which the locus of interest was replaced by the targeting sequence was quicker and more efficient [151]. Later on, the HR methodology was developed at the level of the double selection. For example, an auto-selection targeting vector has been designed in which the Cre encoding sequence controlled by a herpes simplex virus promoter was introduced outside the homology region of the targeting vector, and the neo cassette was flanked with two LoxP sites [152]. Another developing point was to remotely control Cre activity and have cell type conditional KO by combining inducible gene expression systems and cell type restricted conditional KO. Thus, the gene of interest will be deleted only in cells expressing the Cre. Indeed, in transgenic mice where the gene of interest is flanked by LoxP sites and Cre recombinase driven by a tissue-specific promoter, gene deletion occurs in the tissue where Cre is expressed. For example, in 1996 Feil et al. and Zhang et al. reported conditional site-specific recombination achievable through a Cre/LoxP system in which Cre expression is rendered inducible, temporally controllable. They fused Cre to a mutated ligand-binding domain of the oestrogen receptor. The mutant protein lost its binding property to 17 β-estradiol but can still binds to anti-oestrogen drug, tamoxifen. This Cre system is a functional tamoxifen-induced recombinase in cultured cells and transgenic mice [153, 154]. Further advances in the manner to

generate genetically and/or epigenetically reprogrammed pluripotent cells functioning as ES cells are much promising to adapt HR in various species [155]. Although, HR in ES cells was ground-breaking, the process is time consuming, labor intensive and expensive. Newly innovative techniques gained popularity at the expense of the classical gene targeting methodology. In mid 1990s, efficient genome editing was reported by introducing a DSB at a specific genomic locus using a highly specific endonuclease. In 1996, the zinc-finger nuclease (ZFN) was introduced to address the need for more specific restriction endonucleases [156]. ZFNs-fusion proteins composed of a zinc-finger DNA-binding domain and a FokI endonuclease catalytic domain, were used to induce a DSB at a specific genomic locus. In late 2009, another tool emerged: the Transcription Activator- Like Effector Nuclease (TALEN) which uses a precise code of modular domains to target specific DNA sequences [157, 158]. TALEN can be used to correct a mutant gene, insert a sequence mimicking a specific human mutation, and/or to insert reporter sequences [159]. More information about ZFN and TALEN techniques, their advantages and disadvantages can be found in [158-164].

CRISPR sequence was first described in 1987 when Ishino et al. discovered series of short noncontiguous palindromic repeats separated by short variable sequences called spacers and adjacent to Cas genes, on the genome of *Escherichia coli*. [165]. The function of CRISPR and CRISPR-Cas genes was confirmed in 2007, by Barrangou et al. who proved that *Streptococcus thermophilus* can gain an adaptive defense mechanism against phages by incorporating a virus genome fragment into its CRISPR locus [166]. After this integration, the loci are transcribed into precursor CRISPR RNA (pre-crRNA) molecules followed by enzymatic cleavage, generating small CRISPR RNA (crRNA). crRNA can pair with target invading DNA based on complementarity of protospacer sequences and though act as a guide for the Cas endonuclease to cleave the invading DNA [167]. CRISPR-Cas systems are classified into three types (I, II and III), several sub-types (I-A to I-F, II-A and II-B, III-A and III-B) and characterized by Cas protein signatures (Cas3, Cas9, Cas10 for types I, II and III). The three systems use various molecular mechanisms for crRNA biogenesis and interference. In the bacterial and archaeal type I and III systems, specific Cas endonuclease process the pre-crRNAs, and once mature, crRNAs assemble into a large multi-Cas protein complex able to recognize and cleave the matching DNA sequence [167, 168]. However, the bacterial type II system processes the pre-crRNAs by a different mechanism. Cas9 endonuclease complexed with trans-activating RNA and crRNA cleaves the DNA, without the need for a complex of Cas proteins [167]. The crRNA and trans-activating RNA in the original system were simplified into sgRNA of 100 nt [167]. Cas9 programmed with sgRNA was proved to be effective in guiding targeted gene alterations allowing site-specific gene editing in many

species. It is more and more used as a tool to recapitulate models of human diseases. Its popularity is due to the fact that sgRNA is easily prepared with one cloning process, Cas9 can be re-used without any change, and multiplexing is obtained using several sgRNAs [162].
KI and KO models can be created simultaneously using CRISPR-Cas9 system.

7 Thesis project

Neuropathic pain arises as a direct consequence of a lesion or diseases affecting the somatosensory system. SFN is a type of neuropathy where Aδ- and C-fibers are affected. Patients complain about neuropathic pain and autonomic symptoms. SCN10A sodium channel is preferentially expressed in the PNS within sensory DRG and their small diameter peripheral axons, but also in TG and NG. Interestingly, mutations in *SCN10A* gene encoding for the SCN10A α-subunit of sodium channel were found in patients with SFN. One of these mutations, c.4984G>A, p.G1662S was identified in 3 unrelated patients heterozygous for the PM. This mutation resulted in DRG neurons hyperexcitability that was shown in in vitro culture of mouse DRG neurons. However, the detailed mechanism underlying the link between this mutation, SFN and pain is not very clear until now. My PhD project was on generating a mouse model for this mutation and characterized it, mainly for pain phenotype.

Therefore, in the project, we focus on following objectives:

1. To establish the mouse model bearing the G1663S mutation in *Scn10a*.
2. To characterize the effects of this mutation at the cellular and molecular levels.
3. To characterize the mutant mouse model for pain sensitivity using behavioral testing.

These investigations aim to better understand the genotype-phenotype association and the role of SCN10A mutations in SFN.

II Materials and Methods

This Material and Methods section contains the methods that are not described in the manuscript for publication (Section III).

The first aim of this project was to create the Knock-in (KI) mouse model that recapitulates the gain-of-function mutation in *Scn10a* gene (*Scn10a*^{G1663S}). The creation of the mutant mice was performed with the help of Romain Lorentz at Institut Clinique de la Souris (ICS) under the supervision of Marie-Christine Birling. Some protocols and figures of strategies shown below have been provided by Romain Lorentz and Marie-Christine Birling.

Initially, we used the Clustered Regularly Interspaced Short Palindromic Repeats (CRISPR)-and CRISPR associated gene 9 (Cas9) technology. We defined two strategies that were unsuccessful as we couldn't obtain the mutant sample carrying the targeted PM. We have some elements suggesting that the failure of these strategies was indeed due to the high degree of conservation among the *Scn* genes of the region encompassing the G1663 amino-acid coding sequence. Details about these two strategies will be detailed below. We then defined a more classical strategy to engineer the mutation using homologous recombination (HR) in embryonic stem (ES) cells.

Following the generation of the *Scn10a*^{G1663S} mutant mice by HR, I proceeded to the cellular and molecular characterization of the mutation. Then I conducted a detailed behavioral phenotyping analysis of the mutant mice for pain sensitivity using specific nociceptive tests.

1. Creation of the Knock-in mouse model that recapitulates gain-of-function mutation in *Scn10a* gene (*Scn10a*^{G1663S})

1.1 1st and 2nd targeting strategies using CRISPR-Cas9 technology

The enzyme Cas9 is a DNA endonuclease found in many bacteria, in which it functions as part of a defense system against invading DNA molecules, such as viruses. Cas9 has two active sites that each cleave one strand of a double-stranded DNA molecule (dsDNA) at a target genomic locus, simulating a double strand break (DSB). The enzyme is guided to the target DNA by a RNA

molecule, called single-stranded guide RNA (sgRNA), that contains a 20 base pairs (bp) sequence that matches the sequence to be cleaved, which is demarcated by protospacer adjacent motif (PAM) sequences (short conserved sequence NGG) [169]. Cas9 nuclease will form a complex with the sgRNA and site specifically cleaves dsDNA at 3 nucleotides (nt) from the 5' side of the PAM, leading to a DSB. Then the cell will repair this DSB by two major systems: the error prone non-homologous end joining resulting in random insertion or deletions (indels) disrupting the target sequence or the homologous directed repair pathway where PM and KI can be made by providing a homologous DNA repair template as a single-stranded DNA oligo-deoxynucleotides (ssODN) identical to the broken region and containing the PM to be introduced (Figure 10).

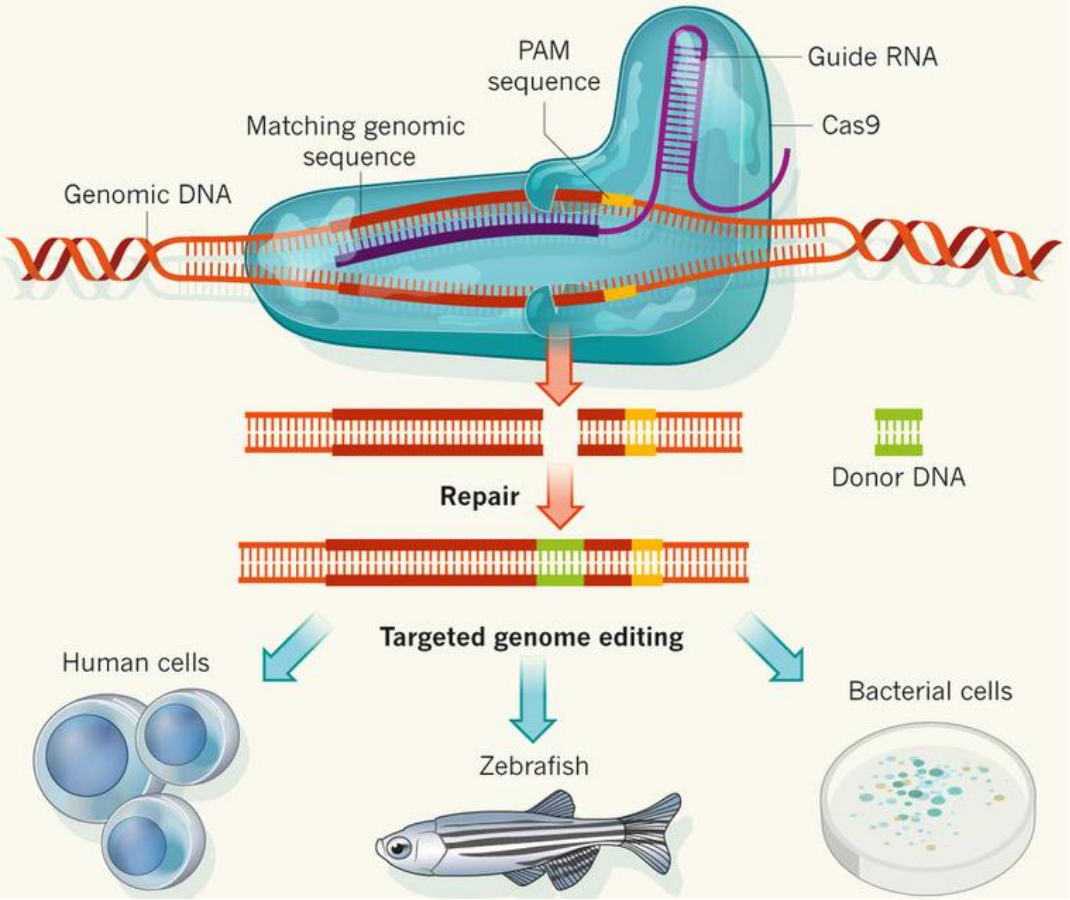

Figure 10: The principle of CRISPR-Cas9 editing genome technique. The Cas9 enzyme has two active sites that each cleave one strand of a double-stranded DNA molecule (dsDNA). Cas9 is guided to the target DNA by an RNA molecule, called single-stranded guide RNA (sgRNA) that contains a sequence that matches the sequence to be cleaved, which is demarcated by protospacer adjacent motif (PAM) sequences. RNA-guided Cas9 activity creates site-specific double-stranded DNA breaks (DSB), which are then repaired by either non-homologous end joining or homologous directed repair. During homologous directed repair, the addition of donor DNA template as a single-stranded DNA oligo-deoxynucleotides (ssODN) enables new sequence information to be inserted at the break site. CRISPR-Cas9 technique can be used to engineer the genomes of human and mouse cell lines, bacteria and, by modifying one-cell-stage embryos, zebrafish. Adapted from Charpentier E. and Doudna J. A. et al. 2013 [169].

1.1.1 Primers validation test

First, we selected several forward and reverse primers to amplify the targeted DNA sequence. Primer sequences were selected using Vector NTI 5.0 software. Optimal primers anneal at least 200 bp away from the intended sgRNAs cutting sites to ensure them not to be included within large deletion events and to allow for the full characterization of nucleotide changes induced by the CRISPR/Cas9 system. Care was taken to avoid amplicons containing repeat sequence wherever possible as these would potentially affect subsequent sequence analysis.

DNA amplification with these specific primers (Supplementary Table S1) was done using Phusion Hot Start II High-Fidelity DNA polymerase kit and Red Hot Taq DNA Polymerase kit (Thermo Scientific™) to check which primers give the best products on gel (Supplementary Figure 1). Oligos and gDNAs sequences were purchased from Sigma-Aldrich.

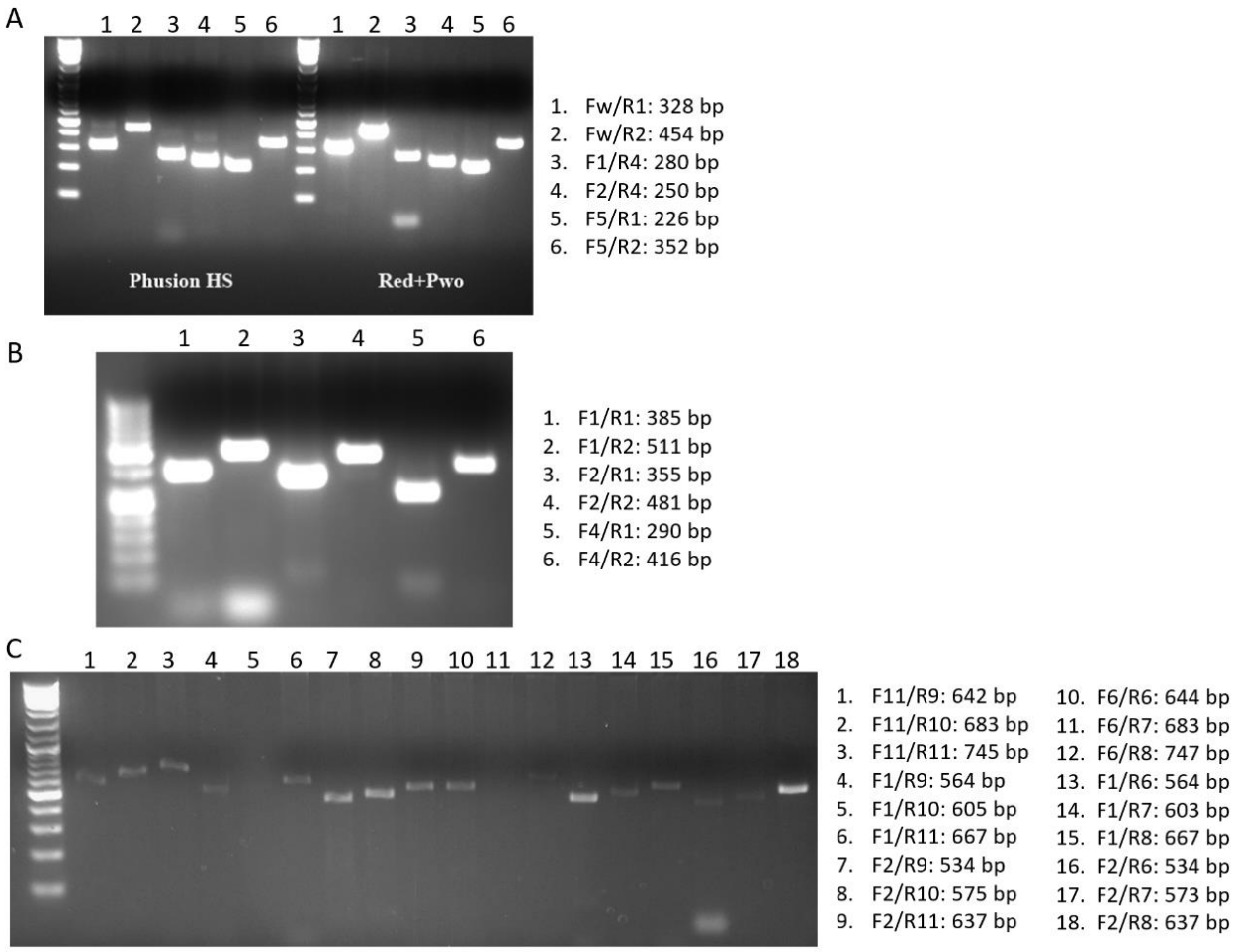

Supplementary Figure 1: Gel electrophoresis results of PCR amplification of wt DNA with specific oligonucleotides. The oligonucleotide sequences are indicated in Supplementary Table S1.

A. B. DNA Amplification of *Scn10a* gene using Phusion and/or RED PCR and several primarily designed oligonucleotides. After noticing the high similarity between *Scn10a* and *Scn5a* genes at the level of these designed oligonucleotides, new oligonucleotides specific for each gene were designed. DNA amplification of *Scn10a* and *Scn5a* genes with the newly designed oligonucleotides using RED PCR is shown in **C.**

Supplementary Table S1: Oligos and gRNAs used for strategies 1 and 2

Oligos/gRNAs position	Oligos/gRNAs sequence
crF1	CATCCTCAGGCTGATTCGAGCAGCC
crR1	GAAGGAGATGATGATGTAGGTGGTG
crF2	GATTCGCACGCTGCTCTTCGCCCTC
crR2	GTCAAACTTCTCCCAGGTCTCATAG
crF4	TCTTCCTCGTCATGTTCATCTACTC
crR4	TGGTCCTGTGTTGAGGATGGGGCTG
crF5	GGCTGGCATCGACGACATGTTCAAC
crF6	TTTTCTGCGATCCTTAGCTCACTAG
crR6	GTGTCTGCAAAGTCTGAGAGGGCAG
crR7	TTCTGATTAGGTTTTGGGATTCTAA
crR8	GAGGATGTCCAAACAGTGGATCTTA
crF11	TGTCCTCTCCGACATCATCCAGAAG
crR9	GCATCGGCAAAGTCGGACAGGGCCA
crR10	TTATCTGGTTGGGCTTGGCGATGCG
crR11	CAGGATGTCCATACAGTGGATGCGG
gR93	ATCTATGACATTAGCGAAGC
gR93b	GCCGGTTGGGGTCGCAGTAG
gR82	GAAGCTGGCCATGCCGAAGA
gR85	CCCCCTACTGCGACCCCAAC

1.1.2 gRNAs and donor oligonucleotides design

We used the CRISPOR software (http://tefor.net/crispor/crispor.cgi), developed by the French TEFOR infrastructure, to select gRNAs. Simply, we downloaded the C57BL/6NCr mouse *Scn10a* sequence from Ensembl database (http://www.ensembl.org/index.html) and put the targeted exon (*Scn10a* exon28) sequence into CRISPOR software. Then we choose the species genome and PAM to submit. Finally, we got all of possible gRNA with specificity score and off targets. We choose high specificity score gRNAs with low number of off targets to use (Supplementary Figure 2). Each gRNA name refers to the specificity score given by the software. gR93 and gR93b were used for strategy 1 (Figure 11A); gR93, gR93b, gR82 and gR85 were used for strategy 2 (Figure 11B).

We designed sequences for donor templates with homology arms (ssODN) at least 60nt in size flanking the intended G1663S PM. To prevent re-cutting of the modified allele by Cas9, we introduced in the ssODN two silent mutations C>A at the level of PAM loci of gR93 and gR93b for strategy 1 (Figure 11A); and four silent mutations for strategy 2, three C>A at the level of PAM loci of gR93, gR82 and gR93b and one G>T at the level of PAM locus of gR85 (Figure 11B). We didn't need to introduce another silent mutation in the ssODN to generate the enzymatic restriction site that was used for subsequent animal genotyping. The introduction of GGC>AGC mutation generated NheI restriction site. ssODN donor sequence was ordered using GATC-Biotech services.

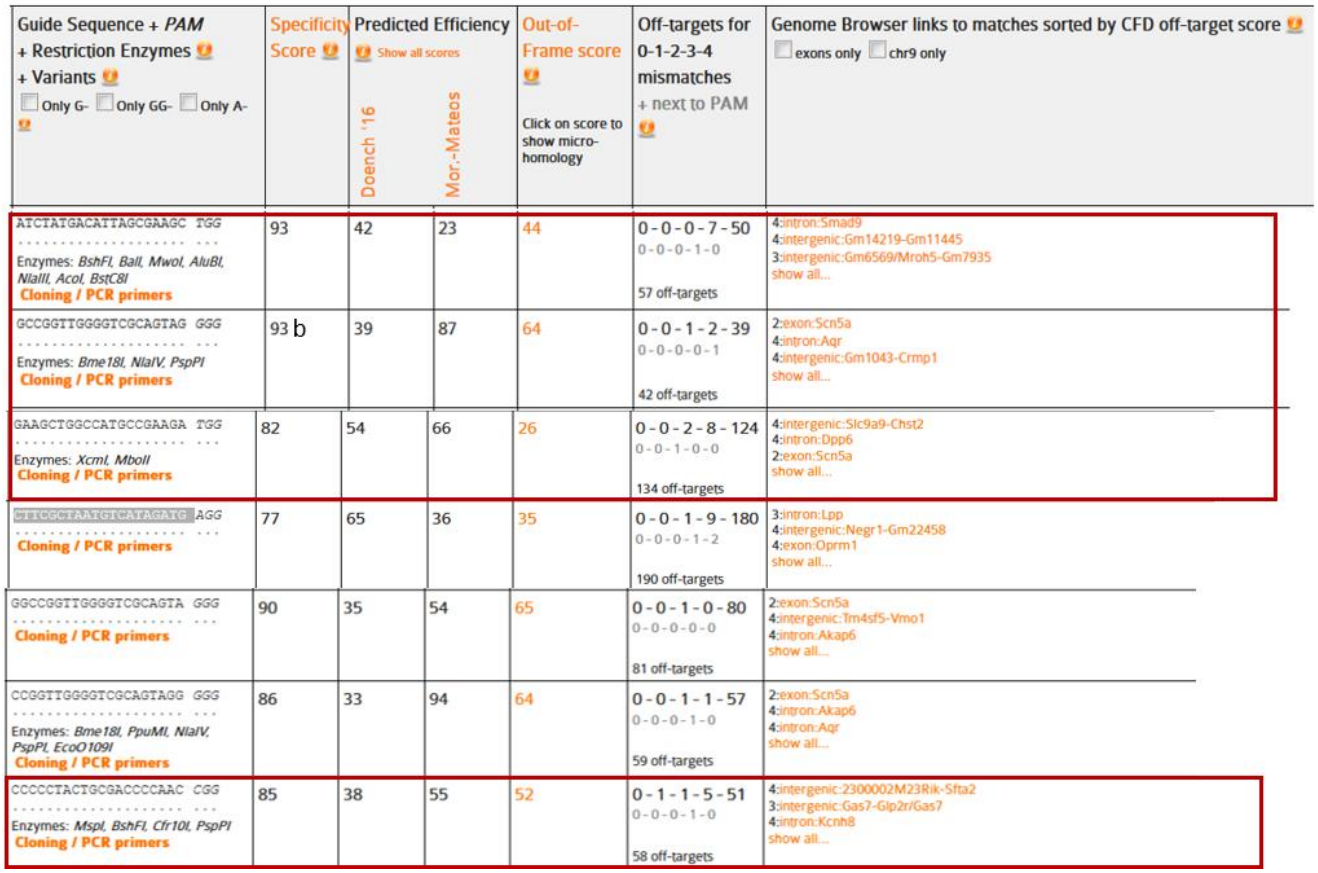

Guide Sequence + *PAM* + Restriction Enzymes + Variants (Only G- / Only GG- / Only A-)	Specificity Score	Predicted Efficiency (Show all scores) Doench '16	Mor.-Mateos	Out-of-Frame score (Click on score to show micro-homology)	Off-targets for 0-1-2-3-4 mismatches + next to PAM	Genome Browser links to matches sorted by CFD off-target score (exons only / chr9 only)
ATCTATGACATTAGCGAAGC *TGG* Enzymes: *BshFI, BalI, MwoI, AluBI, NlaIII, AcoI, BstC8I* **Cloning / PCR primers**	93	42	23	44	0 - 0 - 0 - 7 - 50 0 - 0 - 0 - 1 - 0 57 off-targets	4:intron:Smad9 4:intergenic:Gm14219-Gm11445 3:intergenic:Gm6569/Mroh5-Gm7935 show all...
GCCGGTTGGGGTCGCAGTAG *GGG* Enzymes: *Bme18I, NlaIV, PspPI* **Cloning / PCR primers**	93 b	39	87	64	0 - 0 - 1 - 2 - 39 0 - 0 - 0 - 0 - 1 42 off-targets	2:exon:Scn5a 4:intron:Aqr 4:intergenic:Gm1043-Crmp1 show all...
GAAGCTGGCCATGCCGAAGA *TGG* Enzymes: *XcmI, MboII* **Cloning / PCR primers**	82	54	66	26	0 - 0 - 2 - 8 - 124 0 - 0 - 1 - 0 - 0 134 off-targets	4:intergenic:Slc9a9-Chst2 4:intron:Dpp6 2:exon:Scn5a show all...
CTTCGCTAATGTCATAGAIG *AGG* **Cloning / PCR primers**	77	65	36	35	0 - 0 - 1 - 9 - 180 0 - 0 - 0 - 1 - 2 190 off-targets	3:intron:Lpp 4:intergenic:Negr1-Gm22458 4:exon:Oprm1 show all...
GGCCGGTTGGGGTCGCAGTA *GGG* **Cloning / PCR primers**	90	35	54	65	0 - 0 - 1 - 0 - 80 0 - 0 - 0 - 0 - 0 81 off-targets	2:exon:Scn5a 4:intergenic:Tm4sf5-Vmo1 4:intron:Akap6 show all...
CCGGTTGGGGTCGCAGTAGG *GGG* Enzymes: *Bme18I, PpuMI, NlaIV, PspPI, EcoO109I* **Cloning / PCR primers**	86	33	94	64	0 - 0 - 1 - 1 - 57 0 - 0 - 0 - 1 - 0 59 off-targets	2:exon:Scn5a 4:intron:Akap6 4:intron:Aqr show all...
CCCCCTACTGCGACCCCAAC *CGG* Enzymes: *MspI, BshFI, Cfr10I, PspPI* **Cloning / PCR primers**	85	38	55	52	0 - 1 - 1 - 5 - 51 0 - 0 - 0 - 1 - 0 58 off-targets	4:intergenic:2300002M23Rik-Sfta2 3:intergenic:Gas7-Glp2r/Gas7 4:intron:Kcnh8 show all...

Supplementary Figure 2: gRNA design protocol.

Using the CRISPOR software, we identified gRNAs with high specificity score and low number of off-targets. gR93 and gR93b were used for strategy 1; gR93, gR93b, gR82 and gR85 were used for strategy 2.

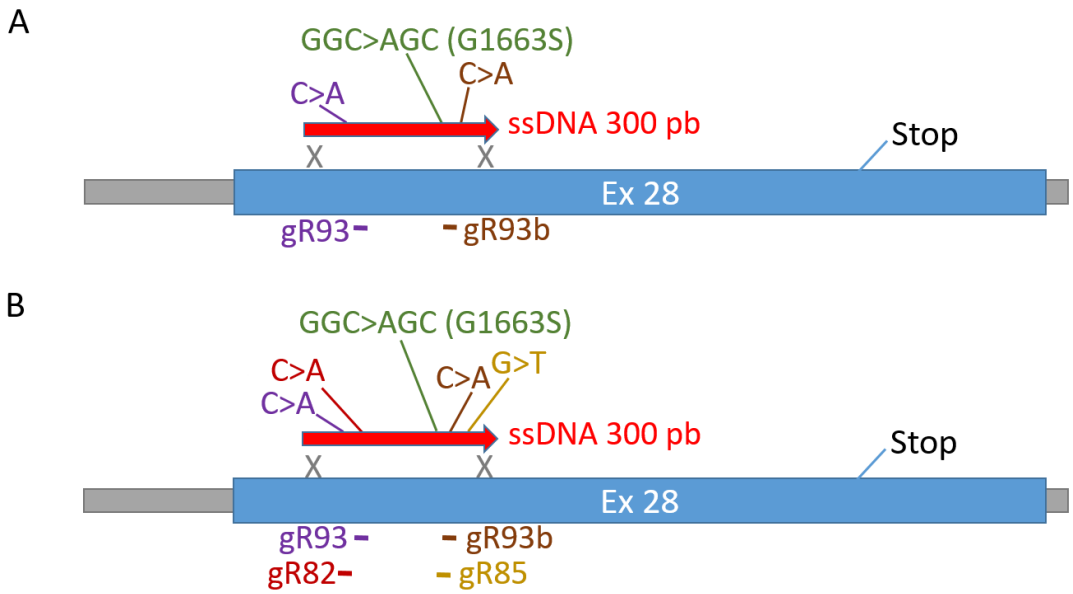

Figure 11: Targeting *Scn10a* gene using CRISPR-Cas9 1st (A) and 2nd (B) strategies.

A. In strategy 1, 2 gRNAs were used gR93 and gR93b. ssODN was designed with GGC>AGC PM and two silent mutations C>A at the level of PAM loci of gR93 and gR93b.

B. In strategy 2, 4 gRNAs were used gR93, gR93b, gR82 and gR85. ssODN was designed with GGC>AGC PM and four silent mutations: three C>A at the level of PAM loci of gR93, gR93b and gR82 and one G>T at the level of PAM locus of gR85. The silent mutations in the PAM sequences were designed to avoid Cas9 recut.

1.1.3 In vitro transcription of Cas9 mRNA and gRNAs

The Cas9 vector (T7-Cas9 wt cloned in pUC57) with T7 promoter was first linearized with AccI for use as a template for in vitro transcription with T7 polymerase. Cas9 mRNA was transcribed using mMESSAGEmMACHINE T7 Ultra Kit (Life Technologies). 1 µg plasmid containing gRNA scaffold (C5648) was linearized with BgII restriction enzyme. The linearized plasmid was purified with the Nucleospin Gel and PCR Clean up (Macherey Nagel) following the kit instructions

gDNAs were synthesized using Phusion HS PCR with forward oligo containing T7 promoter + gRNA and CRISPR reverse primer (scaffold). The gDNAs were purified with the Nucleospin Gel and PCR Clean up (Macherey Nagel). Then the size of PCR band was checked on 2.5% agarose gel. Then transcription of gRNAs templates was performed with the MEGAshort script Kit (Life Technologies). Samples were incubated 4h in water bath at 37°C; then 1µl of Turbo DNase was added; then incubated for 15min at 37°C.

Cas9 mRNA and sgRNAs were purified with the MEGAclear Kit (Life Technologies) and eluted in TE buffer (10 mM Tris-HCl, 0.1 mM EDTA, InVitrogen) for microinjections.

1.1.4 In vitro cleavage assay to validate gRNA's functionality

Before injecting gRNAs in eggs, all the gRNAs were tested *in vitro* on the targeted DNA PCR product in order to validate their efficiency. PCR surrounding the targets were performed using Red Hot Taq. PCR amplification was performed using F1/R1 primers pair to test gR93 validity, F5/R2 to test gR93b and F1/R2 for gR82 and gR85 used in strategy 2. Target PCR product was mixed with Cas9 protein (PNA Bio Inc), and gRNAs. Concentration of target PCR product was adjusted to 50 ng/µl and gRNA concentration at 100 ng/µl (Supplementary table S2).

As a negative control the Cas9 protein was omitted. Two additional reactions can be done: one with PCR product, water and buffer only; the second one with the gRNA, water and buffer only (Supplementary Figure 3). The reactions were incubated at 30°C for 30 min, then at 65°C for 15 min. Then the reactions were loaded on a 2.5% agarose gel. The correct sizes after Cas9 cleavage allow to validate the functionality of the tested guide (Supplementary Figure 3). Only sgRNAs showing a cut (even partial) were injected in eggs.

Supplementary Table S2: PCR reactions for checking in vitro gRNA validity

Reagent	Positive control	Negative control	PCR product	gRNA
Cas9	1µl	-	-	-
Target DNA at 50 ng/µl	2µl	2µl	2µl	-
gRNA at 100 ng/µl	1µl	1µl	-	1µl
Buffer 2.1 NEB	2µl	2µl	2µl	2µl
H2O up to 20 µl	14µl	15µl	16µl	17µl

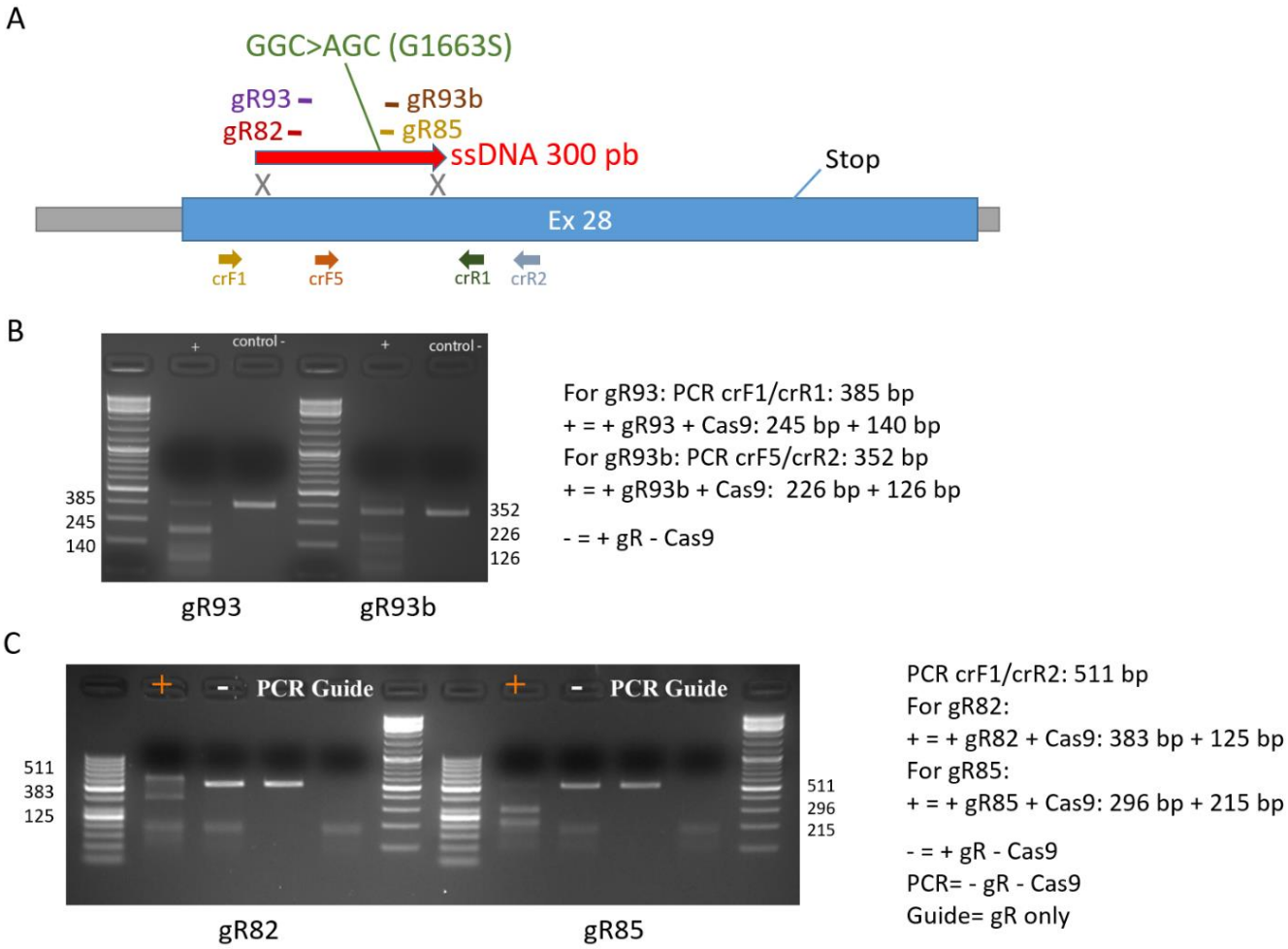

Supplementary Figure 3: Gel electrophoresis results for in vitro validation of gRNAs.

A. Scheme showing the location of the 4 sgRNAs: gR93, gR93b, gR82 and gR85 and the primers used for these gRNAs validation: crF1, crF5, crR1 and crR2. **B.** In vitro validation of gR93 and gR93b used in strategy 1. **C** In vitro validation of gR93 and gR93b used in strategy 2.

1.1.5 Preparation of the ssODN sequence to be injected

We need to prepare the ssODN identical to the deleted region and harbouring the targeted PM. The ssODN was prepared by digestion of X501 plasmid by ECORV enzyme.

2µl of plasmid DNA were transformed in 50µl bacterial cells. The sample was kept 15 min over ice, then heated for 45s at 42°C to produce a thermal shock for the plasmid DNA to incorporate the bacterial cells. 400 µl of Lysogeny Broth (LB) were added to the bacterial cells and then agitated at 37°C at 600 rpm for 45 min. Then the broth was spread over Petri dish containing ampicillin and kept overnight at 37°C. One isolated colony was cultured in 4 ml LB growth medium with ampicillin and kept overnight with agitation at 37°C.

The plasmid DNA was purified using the Plasmid DNA purification (NucleoBond® Xtra Midi/Maxi) (Macherey Nagel) kit. After purification, the DNA concentration was adjusted to 1µg/µl.
X501 plasmid was digested with ECORV enzyme mix. After long migration, the digested fragments (350 bp size) were recuperated from the gel. We proceeded to gel extraction using Nucleospin® Gel and PCR clean up (Macherey Nagel). The purified fragment was loaded on agarose gel and quantified. The digested purified fragment is the ssODN that was injected in mouse eggs.

1.1.6 Injection into one-cell embryos

All mice were housed at 21 °C on a 14/12 h light-dark cycle (5:00am-07:00 pm) in the specific-pathogen-free facility. Female C57BL/6NCr mice (4-5 weeks old) were superovulated by intraperitoneal injection of 5 IU equine Chorionic Gonadotropin followed by 2.5 IU human chorionic gonadotropin at an interval of 48 h and mated overnight with C57BL/6NCrl male mice that were > 10 weeks old. Zygotes were collected after 20 h of hCG injection by oviductal flashing, and pronuclei-formed zygotes were put into the M2 medium (Sigma M-7167). Microinjection was performed using a microinjector (Eppendorf Femtojet 4i) equipped microscope. Cas9 protein or RNA, gRNAs and ssDNA were injected into the cytoplasm and the pronucleus of each zygote using continuous pneumatic pressure. After injection, embryos were *in vitro* cultured in the M16 medium (Sigma M-7292) at 37 °C in a 5% CO2 incubator. The survivors of the injected embryos were implanted into the oviducts of pseudo-pregnant CD1 mice. The progeny was subsequently genotyped to detect potential deletions or mutations.

1.1.7 Mouse genotyping to detect deletions or mutations

Genomic DNA was isolated from ear of the mice. The genotype was then determined using Genomic Red PCR with specific primers (Figure 12- Supplementary Table S1) to identify deletions and mutations in the region of interest.

After PCR amplification, the samples are digested by 2 different enzymes: NheI enzyme to detect the presence of the mutation in the DNA sample, since by inserting the ssODN carrying the G1663S mutation we created a NheI restriction site; T7EI endonuclease in order to detect small or big deletions caused by gRNA cutting. Both enzyme genotyping tests can serve to know if the gRNA in 5' and 3' sides are cutting simultaneously. Two size markers were used (GeneRuler 50 bp DNA ladder SM0372 and Generuler DNA ladder Mix SM0333). Potential PCR products were sent for Sanger sequencing by GATC-Biotech sequencing services.

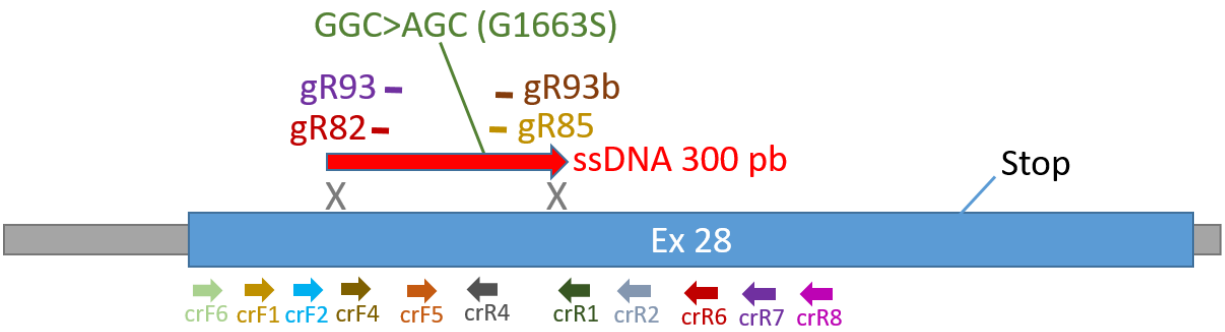

Figure 12: Scheme showing the location of the 4 gRNAs and PCR primers used for genotyping.

1.2 3rd targeting strategy using homologous recombination in ES cells

HR is a type of genetic recombination in which specific DNA sequences are exchanged between two similar or identical molecules of DNA. Briefly, gene targeting is done as follows: the PM of interest is introduced into a cloned copy of the chosen gene by recombinant DNA technology. The PM is transferred by HR to genomic locus in ES cells and only those bearing the PM are selected and then injected into mouse blastocysts, which are brought to term by implantation into foster mothers. Chimeric mice bearing the recombinant allele are generated and are capable of efficiently transmitting the PM to their offspring [145].

A targeted allele was engineered bearing two homology arms of the original *Scn10a* endogenous gene and an auto-selection cassette. The 3' arm of homology (1.2 kb) consisted of a part of intron 27 that doesn't have any similarity with other *Scn* genes and of a part of exon 28 bearing the mutation locus. The 3' arm was cloned into C5206 targeting vector containing the auto-selection cassette using SbfI and SfiI enzymes. The 5' arm of homology (1.1 kb) consisted of part of intron 27 and was cloned into the vector containing the auto-selection cassette and the 3' arm, using AscI and SgrAI enzymes (Figure 13).

Sequence and Ligase Independent Cloning (SLIC) is a type of cloning that does not utilize restriction enzymes or ligase. The cloning efficiency of SLIC in the absence of RecA is rather low. One-step SLIC utilizes only T4 DNA polymerase but shows cloning efficiencies similar to those of the original SLIC method in the presence of RecA. First, the vector needs to be linearized by restriction enzyme digestion. DNA sequence fragments to be cloned into the destination vector

were PCR amplified with oligos whose 5' termini contain about 25 bp of sequence homology to the ends of the linearized destination vector. Second, the destination vector and the fragments to be inserted are mixed with T4 DNA polymerase in the absence of dNTPs to generate 5′ overhangs. In the absence of dNTPs, T4 DNA polymerase has a 3' exonuclease activity, chewing-back the linearized destination vector and PCR products from 3' to 5'. Once the termini of the linearized destination vector and PCR products have sufficient complementary single-stranded 5' overhangs exposed, the reaction mixture is placed on ice to arrest the chew-back reaction and favor the single-strand annealing. Since there is no ligase in the reaction, this results in a plasmid with four single stranded gaps or nicks. Once transformed into competent *Escherichia coli* cells, the gaps are repaired. The annealed complex turns into seamless recombinant DNA through HR *in vivo* with high efficiency (Supplementary Figure 4) [170, 171].

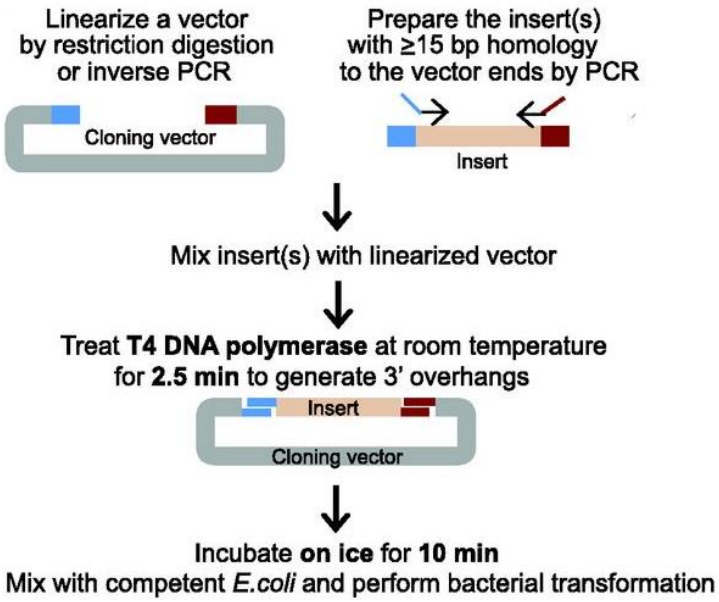

Supplementary Figure 4: Scheme of the one-step SLIC cloning. One-step SLIC utilizes only T4 DNA polymerase. The cloning vector needs to be linearized by restriction enzyme digestion or inverse PCR. The insert with more than 15 bp homology to the vector ends are PCR amplified. Then, the cloning vector and the insert are mixed with T4 DNA polymerase in the absence of dNTPs for 2.5 min at room temperature to generate 3′ overhangs. The reaction mixture is then incubated on ice for 10 min to arrest the chew-back reaction and favor the single-strand annealing. Once transformed into competent Escherichia coli cells, the gaps are repaired. A copied figure from Jeong J. Y. 2012 [170]

The auto-selection cassette, positioned outside the homology region of the targeted allele was constituted of the auto-excision Cre recombinase encoding sequence and of a neomycin resistance gene cassette flanked with two LoxP sites (floxed neo) (Figure 13). LoxP is a site on

the bacteriophage P1 consisting of 34 bp. The site includes an asymmetric 8 bp sequence, variable except for the middle two bases (variable bases are indicated by 'N'), in between two sets of symmetric 13 bp sequences. The 13 bp sequences are palindromic but the 8 bp spacer is not, thus giving the LoxP sequence a certain direction.

13bp	8bp	13bp
ATAACTTCGTATA -	NNNTANNN	-TATACGAAGTTAT

The Cre protein, encoded by the locus originally named as "**C**auses **re**combination", with "**C**yclization **re**combinase", consists of 4 subunits and two domains: the larger carboxyl C-terminal domain, and smaller amino N-terminal domain. The total protein size is 38 kDa and has 343 aa.

The auto-selection cassette become integrated into the genome via HR, serving to select ES cells harboring the PM (Figure 13). In case of random integration of the targeted allele, the Cre sequence is expected to be incorporated into the genome. The resulting expression of Cre recombinase excises the floxed neo and thus such ES cells die in response to antibiotic treatment. However, in case of HR, the Cre sequence is expected to be lost, and the intact incorporated neo sequence is expected to render ES cells resistant to antibiotic.

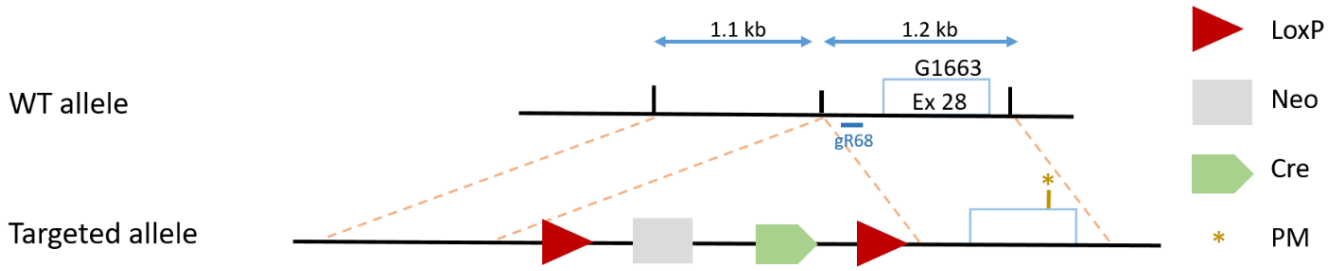

Figure 13: Scheme for *Scn10a* targeting strategy by homologous recombination. The targeted allele was engineered bearing two homology arms of the original *Scn10a* endogenous gene and an auto-selection cassette. The 3' arm of homology (1.2 kb) consisted of a part of intron 28 and of a part of exon 28 bearing the G1663S mutation. The 3' arm was cloned into a targeting vector containing the LoxP-flanked ('floxed') neo cassette. The 5' arm of homology (1.1 kb) consisted of part of intron 28 and was cloned into the vector containing the floxed neo cassette and the 3' arm. Light blue box: Exon 28 containing the locus G1663/S1663; the PM was indicated with a brown star; Blue double arrows lines: indicate size of the arms; Red triangles: LoxP sites; Light grey box: Neomycin selection cassette; Green pentagon: Cre site. Different colored lightning block arrows: primers used for genotyping.

1.2.1 SLIC cloning of 3' and 5' arms

The designed oligos (Supplementary Table S3) for amplifying 5' and 3' arms were tested using Genomic Phusion PCR with or without DMSO to choose the best pairs (Supplementary Figure 5).

Supplementary Table S3: Sequences of oligonucleotides and gRNA used in SLIC cloning

Oligos/gRNAs position	Oligos/gRNAs sequence
gR68	CTAATAAGATATTCTGGGTA
mutF	AGCTGGGATGGCCT
mutR	ATGGCCTCCTCAG
B1	AGAAGCTAACTAATAAGATATTCTG
B2	TGGACTAGACCACAGTCACTTCCAG
E1	GGTAGGGAGAAAGATAAGAATACAG
E2	CTGAACTTGGCTATGGAAGAGAGGG
F1	CAACGCTCCTTGATGCTCTCCAACC
F2	GGGCTGAGGAGGATGGCGTGTCACT
A1	TTATGGGACTTAACACAACAGGAGG
A2	CAAACGAGAGCCCTCCCTCTCAGAC

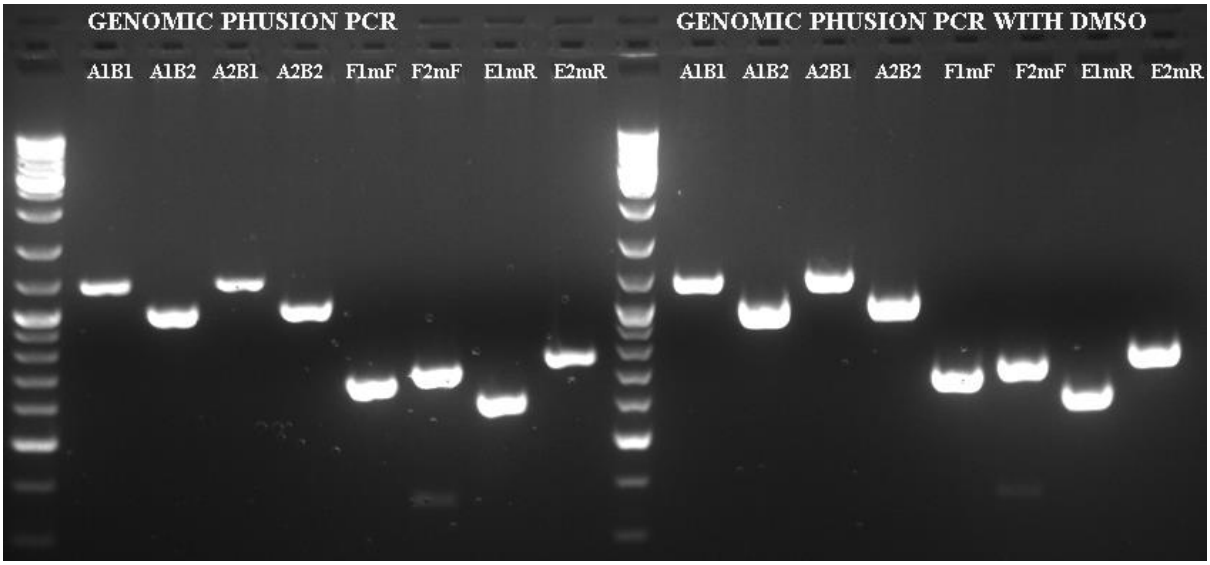

Supplementary Figure 5: Gel electrophoresis results of PCR amplification of 5' and 3' arms using Phusion PCR with DMSO (right part) and without DMSO (left part) and several designed primer pairs. See Supplementary Table S3 for primer sequences.

The SLIC cloning was done in two steps. Step 1 of the SLIC cloning consisted of cloning the 3' homology arm carrying the PM in C5206 vector (Supplementary Figure 6A). This vector was digested with SbfI and SfI enzymes prior to the cloning, so that the fragments can be inserted between these two restriction sites. The 3' side fragment was prepared in two separated fragments using oligos E1/mutR and F1/mutF (Supplementary table S3), and cellular DNA of

BL/6J wt mice. Amplification was done with Phusion HS PCR reaction. After checking PCR products on agarose gel, the fragments were purified using Nucleospin® Gel and PCR clean up (Macherey Nagel) and then quantified. Based on the concentration and size of the insert fragments E1mutR and F1mutF; and of the digested C5206 vector, the used volume of these fragments was determined. Two tubes were prepared: one containing the vector without the inserts (used as control) and the other one containing the vector and inserts. The 3' exonuclease activity of T4 polymerase was done at RT during 2.5 minutes. Directly after, the 3' exonuclease activity was stopped by putting samples over ice. Then both vectors were transformed in 50 µl of DH10 bacteria. Several isolated colonies were cultured in LB and kept overnight with agitation at 37°C. The colonies DNA were purified using Plasmid DNA purification (Nucleospin® Plasmid) (Macherey Nagel). Plasmid DNA was digested with HincII enzyme mix, at 37°C during one hour and a half. HincII enzyme cuts the DNA at two sites giving two bands: 4300 bp + 3000 bp, if the insert hadn't integrated the plasmid; and cuts at three sites giving three bands: 5000 bp + 3000 bp + 520 bp, if the insert had integrated the plasmid (Supplementary Figures 6A-7A). Therefore, fragments presenting three bands on the gel were chosen. The DNA of these chosen samples were sent to sequencing (to Eurofins GATC Biotech) to verify the DNA sequence. The sample that presented 100% similarity with the vector sequence + the 3' side sequence that we wanted to clone, was chosen as vector named X553. X553 was digested with AscI and SgrAI enzymes in order to introduce the 5' side fragment between these two restriction sites. The digested fragment was then purified using Nucleospin® Gel and PCR clean up (Macherey Nagel) and quantified.

Step 2 consisted of cloning the 5' homology arm in X553 plasmid obtained from step 1 (Supplementary Figure 6B). The 5' side fragment was prepared using oligos A1/B1 (Supplementary table S3) and the plasmid DNA BAC X558. Amplification was done with Phusion HS with DMSO PCR reaction. After checking the PCR product on agarose gel, the fragment was purified using Nucleospin® Gel and PCR clean up (Macherey Nagel) and then quantified. Based on the concentration and size of the insert fragment A1B1 and of the digested vector X553, the used volume of these fragments was determined. Then same steps were done as for the 3' homology arm. After purification, the plasmid DNA was digested with three different enzymes. AccI cuts at two sites giving two bands on the gel: 6330 bp + 3376 bp, if the 5' side fragment was incorporated in the plasmid; if not AccI cuts at one site giving one band of 8434 bp. ECONI cuts at two sites giving two bands: 5670 bp + 4036 bp, if the 5' side fragment was incorporated in the plasmid. PshAI cuts at two sites giving two bands: 6000 bp + 3706 bp, if the 5' side fragment was incorporated in the plasmid (Supplementary Figures 6B-7B). After choosing the sample that

presented two bands in these three digestions, and verifying its DNA sequence, the purified plasmid DNA was transformed in DH10 bacteria. One isolated colony was cultured in LB with ampicillin and kept overnight with agitation at 37°C. After purification and quantification of the DNA, five digestions with five different enzymes were done in order to confirm the total sequence of the vector. XmnI cuts at three sites giving three bands: 1447 bp + 3604 bp + 4496 bp, confirming the insertion of 5' and 3' sides fragments. ECORV: 1327 bp + 1998 bp + 6222 bp. BamHI: 1159 bp + 1661 bp + 6727 bp. ECONI + XbaI: 873 bp + 2210 bp + 2488 bp + 4037 bp. KpnI + SacI: 1117 bp + 2859 bp + 5571 bp (Supplementary Figures 6B-7C). Then the DNA sequence was confirmed by sequencing.

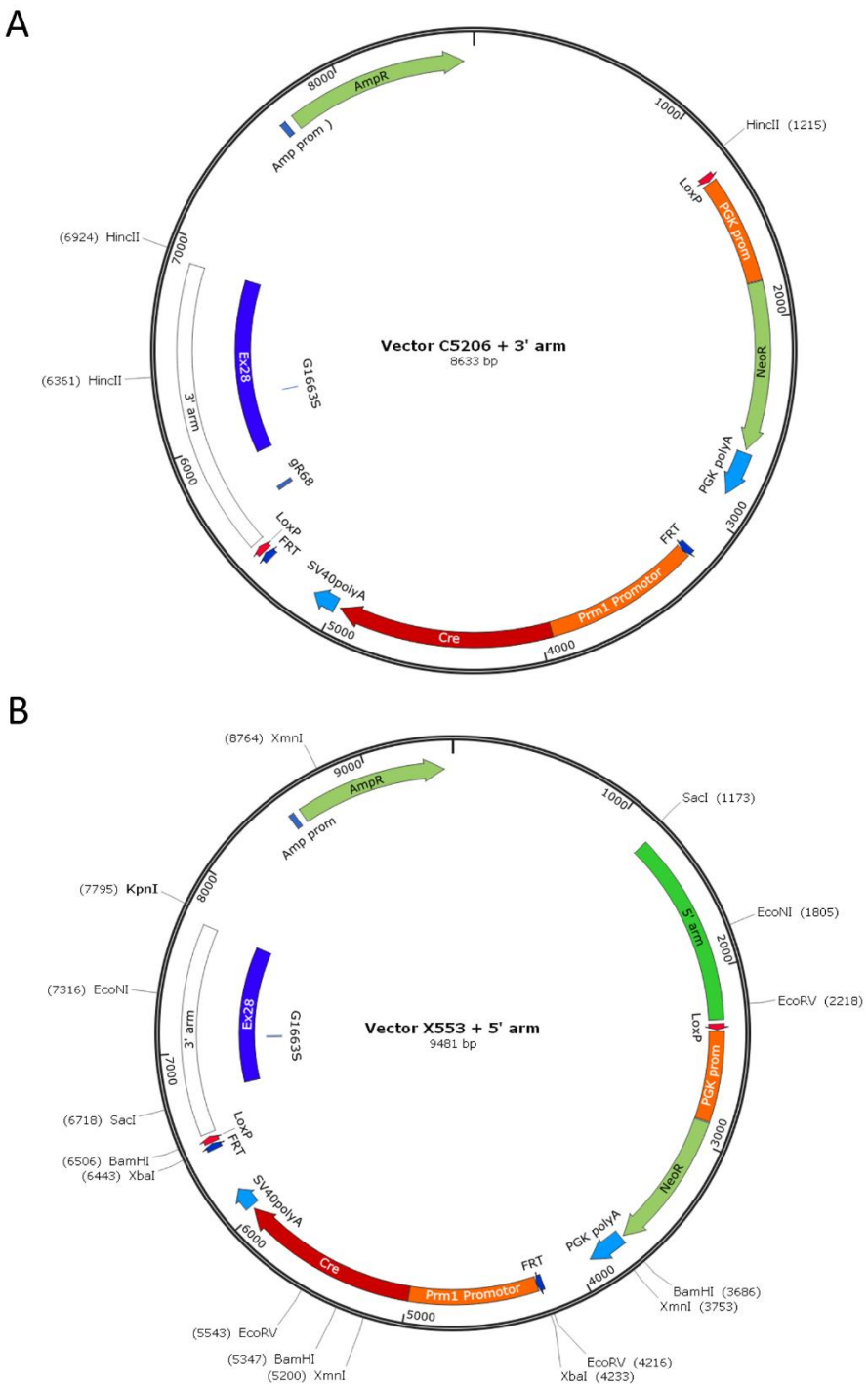

Supplementary Figure 6: Steps 1 and 2 and the restriction sites of the enzymes used to validate steps 1 and 2. A. Step 1 consisting of introducing the 3' arm in the C5206 targeting vector. The restriction sites of HincII used to validate the insertion of the 3' arm are showed. **B.** Step 2 consisting of introducing the 5' arm in the X553 vector. The restriction sites of ECONI used to validate the insertion of 5' arm; XmnI, ECORV, BamHI, XbaI, KpnI and SacI used to validate steps 1 and 2.

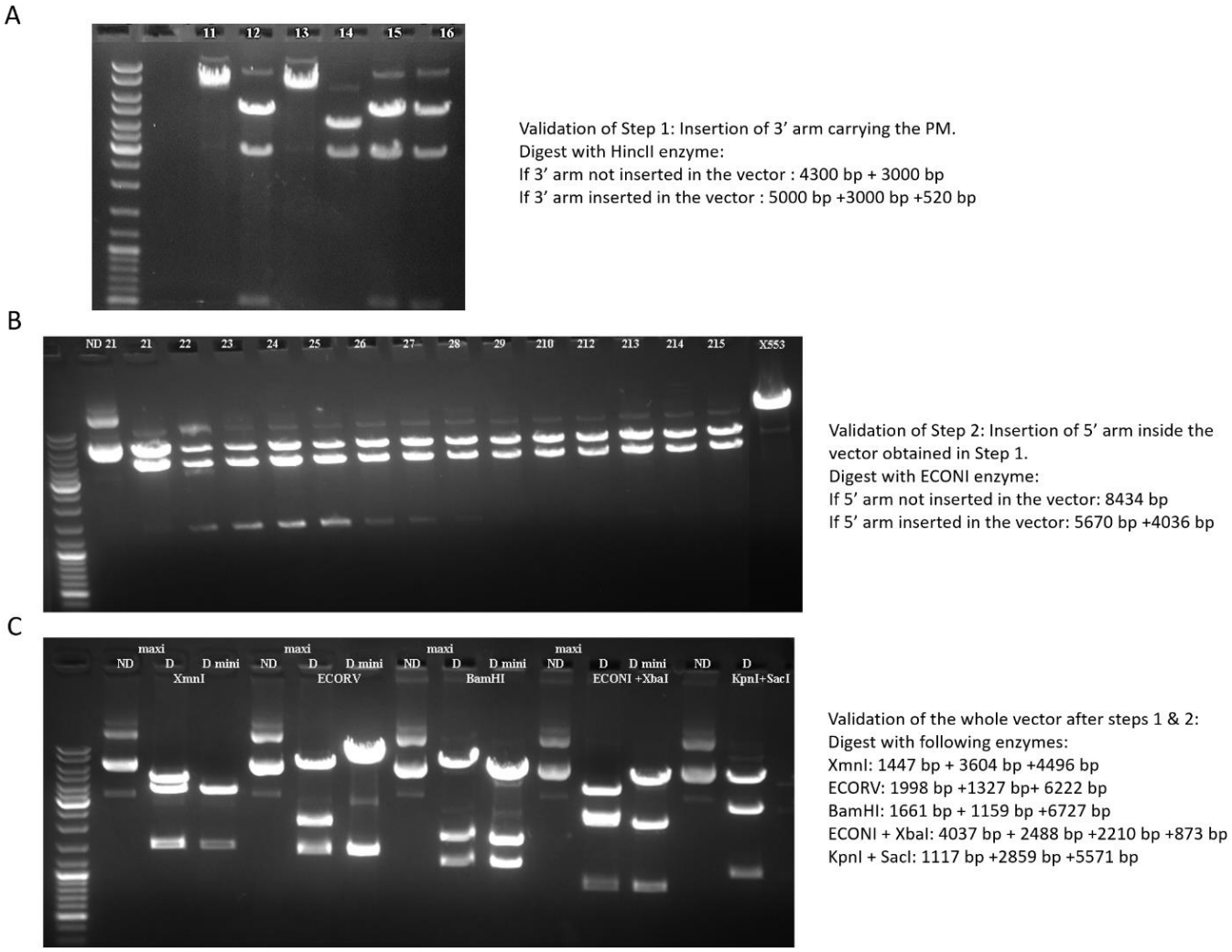

Supplementary Figure 7: Validation of Steps 1 and 2 and the whole vector obtained after steps 1 and 2. A. Validation of Step 1 of 3' arm insertion by digestion with HincII enzyme. **B.** Step 2 of 5' arm insertion was validated by three different enzymatic digestions: AccI, ECONI and PshAI enzymes. Only digestion with ECONI enzyme is shown here. **C.** Validation of the whole vector containing 5' and 3' arms. Five different enzymatic digestions were done on samples purified by miniprep and maxiprep.

The recombinant vector contains the 3' arm harboring the S1662 locus, the 5' arm and the selection cassette (LoxP-flanked neo cassette). The recombinant vector was linearized by digestion with AscI and SfI enzymes (so the vector loose the ampR segment coming from bacteria) and electroporated in the proprietary C57BL/6NCrl S3 cell line.

1.2.2 Classical cloning of sgRNA in plasmid vector

The use of CRISPR-Cas9 technology in combination to the classic HR allowed to force HR at the correct locus and to obtain many positive ES cell clones. A circular CRISPR vector bearing the

Cas9 and a sgRNA with a specificity score of 68 (gR68) was designed to be co-electroporated in the proprietary C57BL/6NCrl S3 cell line. The gR68 targets the intronic sequence of the ES cells of wt mice, where the Cas9 will generate a DSB, which will favour the HR to incorporate the insert.

Forward and reverse gR68 were heated at 95°C for 5 min in order to be dimerized; then the mix was put over ice to stop dimerization. Afterwards, we proceeded to a classical cloning using C5347 Vector, the dimerized gR68, DNA dilution buffer, DNA ligation buffer and DNA T4 DNA ligase (Rapid DNA Dephos and ligation kit). After transformation in DH10 bacterias, six colonies were chosen and purified using Plasmid DNA purification (Nucleospin® Plasmid) kit. After what, the purified DNA was digested with BbsI. The insertion of the gRNA into the vector will delete the BbsI restriction site, so the BbsI enzyme will not cut the DNA sequence in the vector where the gRNA was inserted. Based on the analysis of digested and not digested samples on agarose gel, we chose the positive sample; and verified the sequence by Sanger sequencing. The plasmid vector C5347 + gR68 is electroporated in 129-derived ES cells together with the recombinant vector.

1.2.3 Screening

After electroporation in C57BL/6NCrl S3 cell line, transfected ES clones were submitted to neomycin selection (G418) and 93 resistant ES clones were isolated. The clones were then submitted to the screening process allowing secured identification of those harbouring the expected HR events at both ends of targeting vector.

The screening process steps are:

1. Identification of candidate recombinant clones by initial 3’ Long-Range PCR
2. Detection by Amp PCR of possible concatemers presence due to the use of CRISPR-Cas9 strategy
3. Clones that are 3’ PCR positive and negative for Amp are confirmed for 5’ recombination event by 5’ Long-Range PCR
4. Selected positive clones from steps 1-3 are further validated by Southern blot analysis using internal and external probes
5. The karyotype of at least 2 validated clones is verified using ddPCR aneuploidy screening and Giemsa staining

Screening steps 1 and 3 by selective Long-Range PCRs (amplifying till 10 kb) enable to select clones of ES cells that integrated by HR the construction inside their genome after electroporation. It is important to confirm the HR events at both arms of the introduced donor DNA. In this context, in order to identify correctly targeted clones, both the upstream and downstream HR events as well as random integration of the template should be verified.

Long-Range PCRs are done using external and internal oligos. External oligos are those chosen after checking results of oligos test. Internal oligos are standard for this type of construction. Long-Range 3' PCR is first done using a forward oligo inside the Cre with a reverse external oligo Fcre/Rext giving a band of 2.8 kb; and Fint/Rext for H10, H11 and H12 controls giving a band of 1.2 kb (Supplementary Figures 8-9A). Screening results cannot be validated as positive or negative unless controls are positive. H10 is used as positive control to validate the screening, especially in case of negative screening, was done with supplementary sample cells (+) amplified by cell culture. H11 used as negative control to exclude a problem related to oligos degradation, was done with few sample cells (-) corresponds to the well containing a little amount of clones. H12 used to exclude a problem due to PCR mix, was done with S3 purified wt cells (Supplementary Table S4). Oligos used for controls are chosen after checking results of oligos test. 33 clones were positive for 3' side and were selected (Supplementary Figure 9A).

A

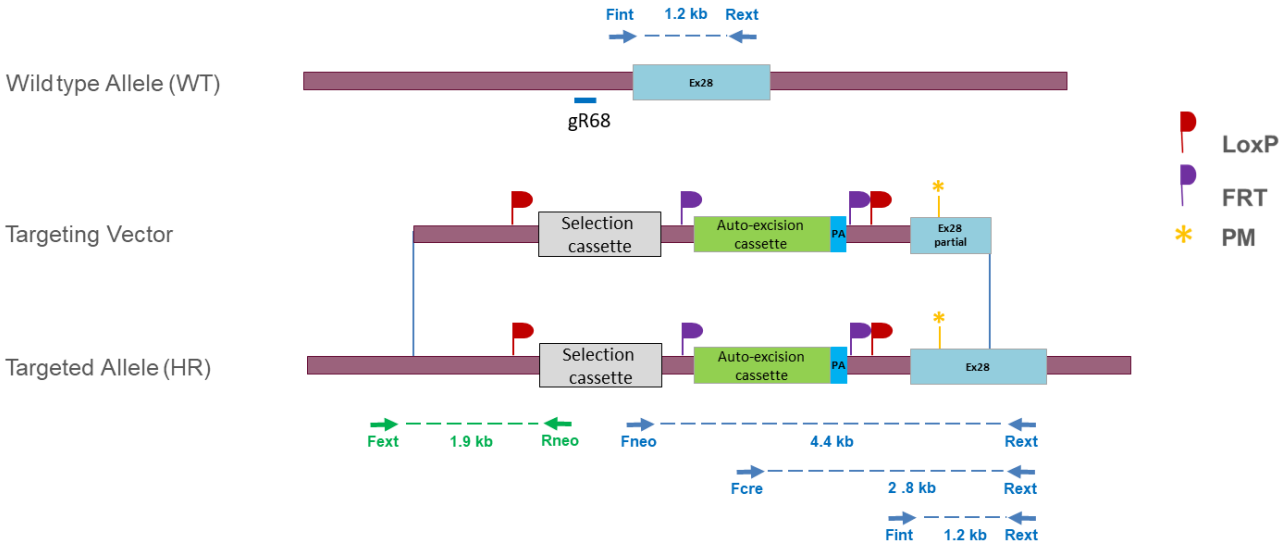

B

PCR	Primer Name	Primer sequences	PCR product size
5' PCR	Fext	TTAGTGCTGAGATTTACACTATTAG	1.9 kb
	Rneo	GCGGCCGGAGAACCTGCGTGCAATC	
3' PCR	Fneo	AGGGGCTCGCGCCAGCCGAACTGTTC	4.4 kb
	Rext	CATTTGCCATGAATGTAACATAGCC	
3' PCR	Fcre	GGCCAAGCCAGCACCATGTCCAATT	2.8 kb
	Rext	CATTTGCCATGAATGTAACATAGCC	
3' PCR	Fint	GGTAGGGAGAAAGATAAGAATACAG	1.2 kb
	Rext	CATTTGCCATGAATGTAACATAGCC	

Supplementary Figure 8: Long-Range 3' and 5' PCRs screening strategy.

A. Long-Range 3' and 5' PCRs screening strategy showing the location of the screening oligos within the construction. **B.** Primers name, sequences and PCR product size of Long-Range 5' and 3' PCRs.

Supplementary table S4: Table showing conditions and usage of H10, H11, H12 controls

Wells	H10	H11	H12
AND	Lysis +	Lysis -	Purified DNA
Oligos pair	Fint/Rext	Fint/Rext	Fint/Rext
Verification	Functional mix and oligos on the lysis	Functional Mix and oligos pair validated by oligos test	Functional Mix and PCR

Since we performed HR with CRISPR-Cas9, multiple copies at random sites can be present as concatemers. We performed screening step 2 where Long-Range PCRs are done using AmpR/SqF and AmpF/SqR to detect possible concatemers: bands that appear on the gel indicate that there are a lot of concatemers. We just selected samples which bands don't appear on the gel, or appear very faint compared with wt sample which band appears weak. These clones were considered positive clones in the screening process, because they are negative for Amp. 21 clones were positive in screening steps 1 and 2 and thus were selected for screening step 3 (Supplementary Figure 9A-B). Long-Range 5' PCR is done using a forward external oligo Fext and a reverse oligo inside the Neo RNeo giving a band of 1.9 kb (Supplementary Figure 8). 20 clones were positive for 5' side (Supplementary Figure 9C).

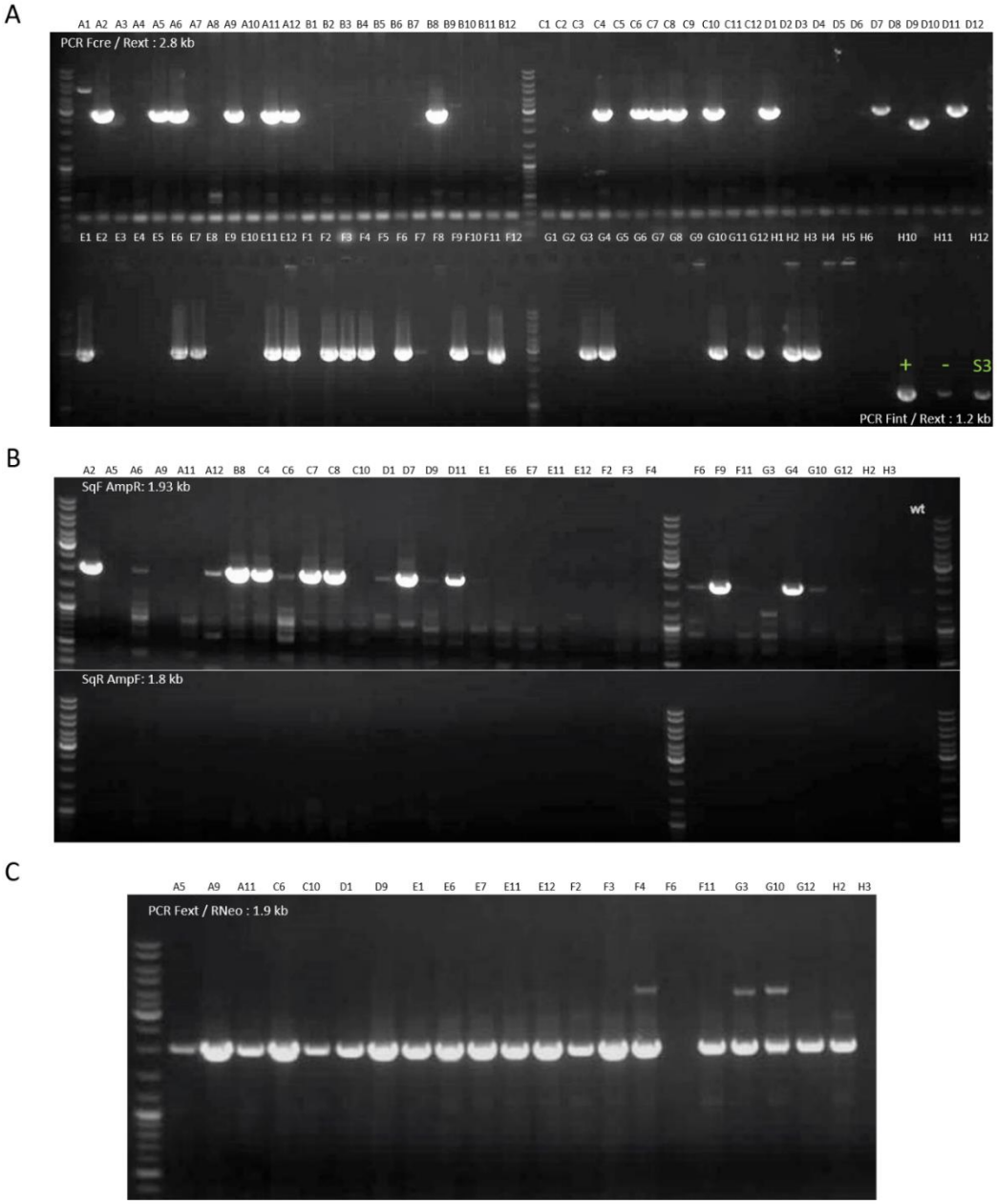

Supplementary Figure 9: Screening steps 1-3 of the 93 Neomycin resistant clones using Long-Range PCRs. Primers location and band sizes are illustrated in Supplementary Figure 8.

A. Screening step 1 identifying 3' recombinant clones by Long-Range PCR using Fcre and Rext oligos. 33 clones were positive in step 1 showing a band of 2.8 kb and were selected for step 2. **B.** Screening step 2 identifying concatemers presence using SqF/AmpR and AmpF/sqR oligos in the 33 positive clones. Samples which bands don't appear on the gel, or appear very faint compared with wt sample are selected. 21 clones were negative for Amp and so considered positive clones in the screening process. **C.** Screening step 3 identifying 5' recombinant clones by Long-Range PCR using Fext and RNeo oligos. 20 clones were positive for 5' side showing a band of 1.9 kb.

Fcre/Rext PCR products of the 20 positive clones were sent for Sanger sequencing by GATC-Biotech sequencing services to confirm the presence of the PM in the mutant allele, without amplifying the wt allele. Based on sequencing results, 9 clones were selected and then screened in a second round of Long-Range PCRs using same and additional internal and external screening oligos: Fcre/Rext and FNeo/Rext for the 3' side; Fext/RNeo for 5' side; AmpF/SqR and SqF/AmpR to detect concatemers (Supplementary Figure 10). These 9 samples were confirmed positive in 3' and 5' Long-Range PCRs, only sample #5 was positive for Amp (Supplementary Figure 10). Sequencing results revealed two different versions of the mutant allele at PM level in samples # 31, 39, 54 and 60 (Supplementary Figure 10). Samples # 5, 31, 39, 54 and 60 were not convenient to select, yet we included them in the screening step 4.

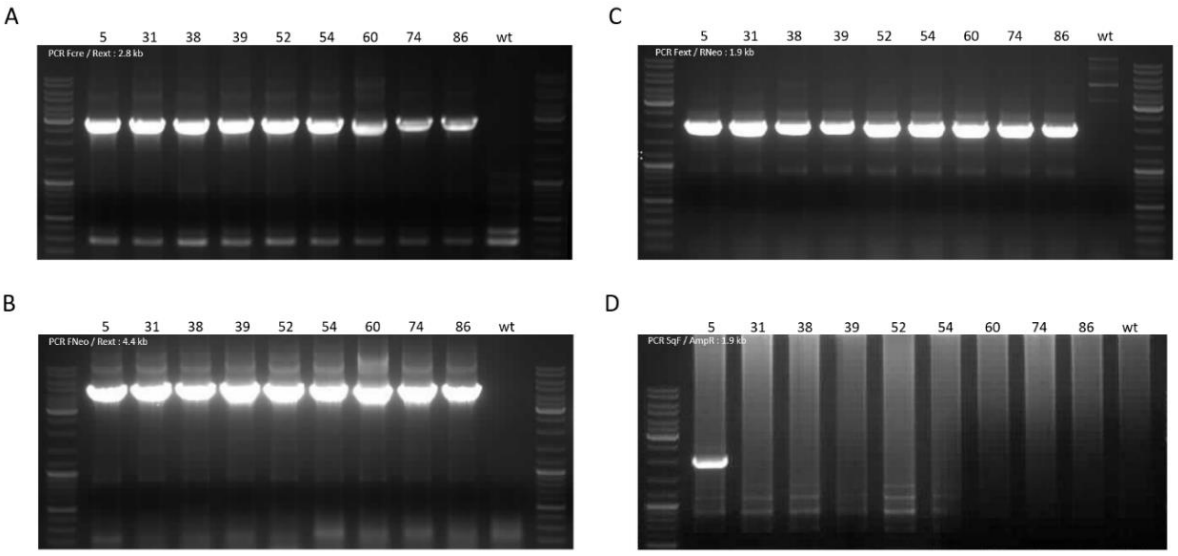

E

```
Mutant allele :  TCACCACGTCGGCTAGCTGGGAT
      #5      :  TCACCACGTCGGCTAGCTGGGAT
      #31     :  TCACCACGTCGGCTAGCTGGGAT
              :  --------------G--------
      #38     :  TCACCACGTCGGCTAGCTGGGAT
      #39     :  TCACCACGTCGGCTGGCTGGGAT
              :  --------------A--------
      #52     :  TCACCACGTCGGCTAGCTGGGAT
      #54     :  TCACCACGTCGGCTAGCTGGGAT
              :  --------------n--------
      #60     :  TCACCACGTCGGCTGGCTGGGAT
              :  --------------A--------
      #74     :  TCACCACGTCGGCTAGCTGGGAT
      #86     :  TCACCACGTCGGCTAGCTGGGAT
```

Supplementary Figure 10: Confirmation and validation of the 9 selected positive recombinants using Long-Range PCRs. Primers location and band sizes are illustrated in Supplementary Figure 8.

A. B. Long-Range 3' PCRs using Fcre/Rext and FNeo/Rext primers giving bands of 2.8 and 4.4 kb respectively. The 9 clones were confirmed positive for the 3' side. **C.** Long-Range 5' PCR using Fext/RNeo primers giving a band of 1.9 kb. The 9 clones were confirmed positive for the 5' side. **D.** Long-Range Amp PCR using SqF/ AmpR primers giving a band of 1.9 kb. Sample #5 was positive for Amp. **E.** Sanger sequencing results for the 9 recombinants showing two different versions of the mutant allele at PM level in samples #31; 39; 54 and 60.

Screening step 4: HR at the targeted locus is verified by two subsequent Southern blot analysis using a probe at the level of the Neo or an external probe and specific restriction enzymes. Southern blot analysis consisted of several steps described here briefly. DNA is digested with specific restriction enzymes overnight at 37°C. Then the total reaction volume is loaded on the gel. After migration, a picture is taken under UV and bands are marked with scalpel especially the bands at 10000 kb and 3000 kb. Then we proceed for an alkaline transfer: the gel is depurinated with diluted HCl, then denaturated with NaOH, afterwards gel is transferred to Hybond-XL membrane. After this step, we proceed for membrane hybridization using labelled probes. The labelled probes are prepared from a template dsDNA using Amersham Megaprime™ DNA Labelling Systems (Supplementary Figure 11). The probes are purified using Sephadex NICK columns and T10E1 (Tris 10 mM, EDTA 1 mM, pH 8) buffer.

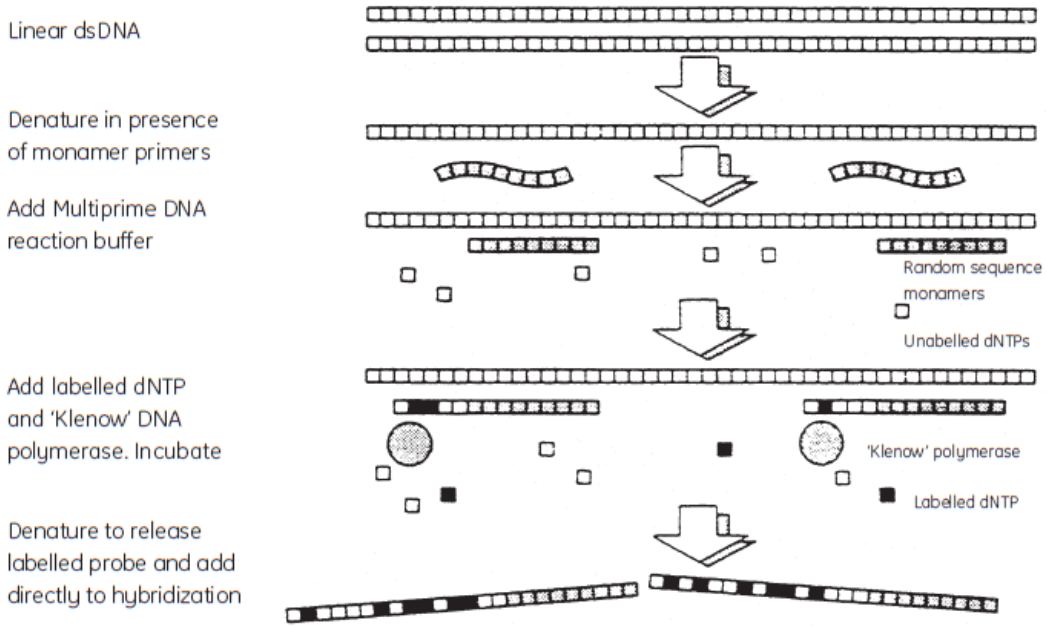

Supplementary Figure 11: Preparation of labelled probes using GE Healthcare's Megaprime DNA labelling systems.

Afterwards, the membrane is prehybridized with hybridization buffer in the hybrid furnace for 45 minutes. In parallel, the labelled probe is denatured for 5-10 min at 99°C in the heating block. The denatured probe is used to hybridize the membrane. Then we proceed for membrane exposition and revelation.

The first Southern blot was done using an internal probe at the level of Neo and specific restriction enzymes; to verify 5' arm: HincII and XcmI cutting outside 5' arm and inside 3' arm, giving bands

of 6.3 kb and 6 kb on the gel respectively; to verify 3' arm: DrdI cutting before the Neo probe and outside 3' arm giving a band of 6.8 kb; ApaLI cutting outside 3' and 5' arms, giving a band of 11.9 kb on the gel (Supplementary Figure 12). The 9 selected clones have the correct restriction map. A second Southern blot was done using 5' external probe and XbaI cutting before the external probe and inside the construction to distinguish wt allele (6.4 kb) from targeted allele (5.6 kb) (Supplementary Figure 13).

To select the final positive clones: we looked at Southern blot results (Supplementary Figure 12-13) together with clone's sequence (Supplementary Figure 10). Samples #31, #39, #54 and #60 presented double peaks in the mutant allele at PM level and were excluded from selection. Samples #5, #38 and #86 have a stronger wt band compared to the targeted band. Only clones #52 and #74 were selected for screening step 5. Clones #52 and #74 were karyotyped by ddPCR as described in Codner et al. [172] and by Giemsa metaphase staining. Both clones were validated.

A

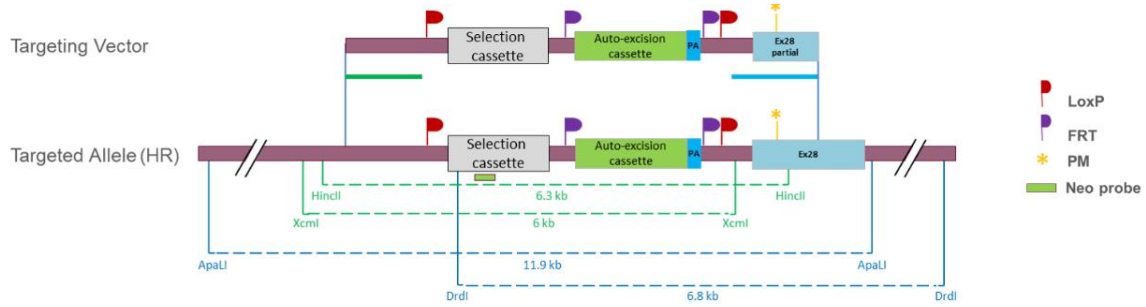

B

Probe	Name	Genomic DNA digest	Targeted Allele (kb)
Neo	5' digest	HincII	6.3
		XcmI	6
	3' digest	DrdI	6.8
		ApaLI	11.9

C

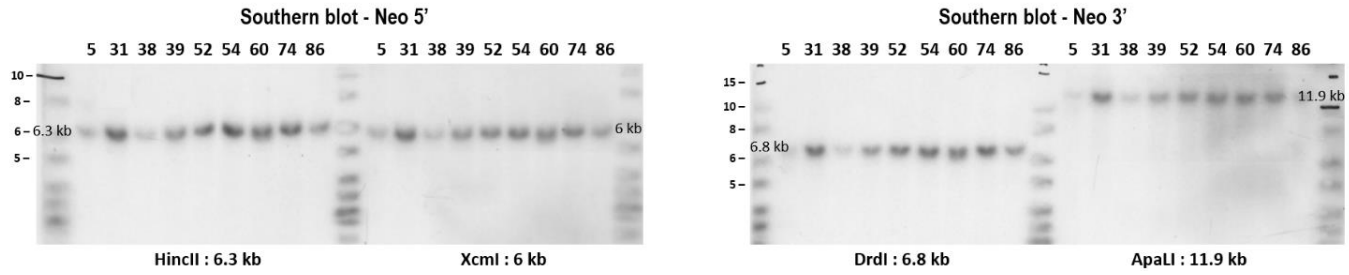

Supplementary Figure 12: Screening step 4 of the 9 selected positive recombinants using Southern blot with internal probe at the level of the Neo.

A. Screening strategy showing the Neo probe and the restriction enzymes. HincII and XcmI were used to verify 5' arm and DrdI and ApaLI to verify 3' arm. **B.** Table recapitulating the size of genomic digests. **C.** Southern blot results proving that the 9 selected clones have the correct restriction map.

A

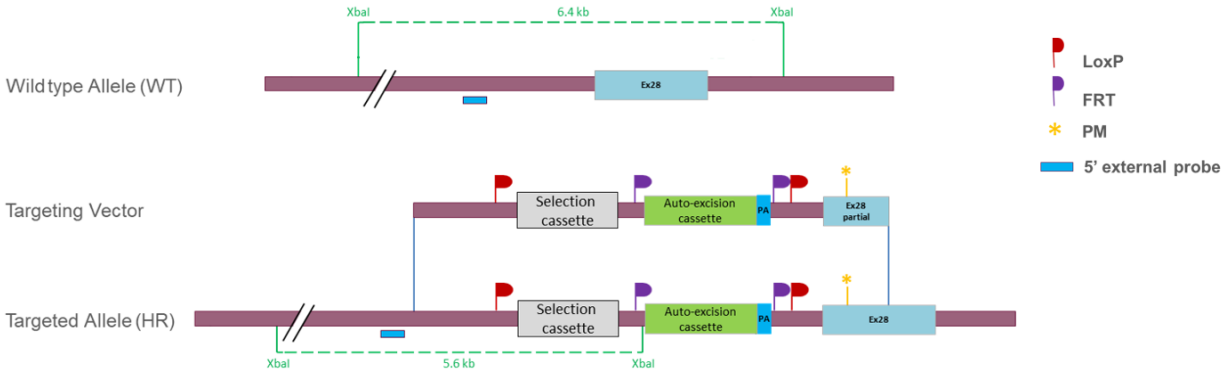

B

Probe	Name	Genomic DNA digest	WT allele (kb)	Targeted Allele (kb)
5' external probe	5' digest	XbaI	6.4	5.6

C

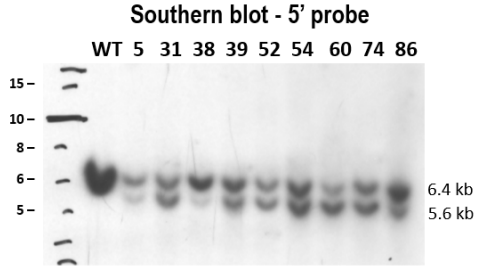

Supplementary Figure 13: Screening step 4 of the 9 selected positive recombinants using Southern blot with 5' external probe.

A. Screening strategy showing the probe and XbaI restriction enzyme. **B.** Table recapitulating the size of genomic digests of wt and targeted alleles. **C.** Southern blot results showing that samples #5, #38 and #86 have a stronger wt band compared to the targeted band.

1.2.4 Microinjection and breeding

The ES cells used in the injection experiment were originally derived from a C57BL/6N mouse strain, which have a black coat colour. The selected ES cells with the desired targeted mutation were injected into blastocysts isolated from mated BALB/CN females, which have a white coat colour. These blastocysts were subsequently implanted into CBA C57BL/6 F1 foster mothers to allow the embryos to come to term. To facilitate isolation of the desired progeny, the ES cells and recipient blastocysts are derived from mice with distinguishable coat-colour alleles (as already mentioned ES cells from black mice and blastocysts from white mice). The resulting offspring are thus chimeras of two different cell types: ES derived cells and host blastocyst-derived cells. The

extent of the contribution of ES cells to the formation of the chimeric mouse can be evaluated by visual assessment of coat-colour chimerism. ES cell contribution to the germline can be evaluated by observing the coat colour of the progeny that is derived by breeding the chimeric mouse with black mice. Recombinant ES clones #52 and #74 validated in the screening process were injected into BALB/CN female blastocysts. Resulting highly chimeric males with a color score >85% were mated with C57BL/6NCr wt females to investigate whether the recombined ES cells have contributed to the germ layer. The selection cassette is deleted by the mean of crossing the chimeras with wt females holding a Cre-deleter line. 80% germline transmission of ES cell coat color was obtained and heterozygous animals harboring *Scn10a*^{G1663S} mutation and one LoxP site were generated. Heterozygous mice were subsequently crossed to generate mice with homogeneous genotypes.

2. Molecular and cellular characterization of *Scn10a*^{G1663S} mutant mice

2.1 Quantification of transcripts by Real Time droplet digital PCR (RT-ddPCR)

This part was performed with the help of Loïc Lindner and Pauline Cayrou at the ICS.

Dorsal root ganglia, spinal cord and brain tissues were carefully collected from wt and mutant mice and flash frozen in liquid nitrogen. All tissues were disrupted using Precellys® CK14 Lysing kit in a convenient volume of TRIzol Reagent. Chloroform was added slowly to separate the different phases then samples were centrifuged. The supernatant containing RNA is taken from the Precellys tubes to new collection tubes and the remaining phases are discarded. 1 volume (=volume of supernatant) of 75% ethanol is added. Then total RNA is purified using RNeasy Mini Kit (Qiagen) according to manufacturer's instructions. Afterwards, RNA concentration is measured and RNA is diluted with treated pure water to have a 500ng/ul concentration before proceeding to RNA transcription. cDNA synthesis was performed using the SuperScript™VILO™ cDNA Synthesis Kit (Invitrogen). cDNA concentration is around 2000-2200ng/ul. mRNA quantification by RT-ddPCR was performed in 20 µL reactions containing 1× ddPCR Supermix for Probes (No dUTP), 125 nM of wt and KI probes, 250 nM forward and reverse primers, and 50 ng DNA according to manufacturer's recommendations. Hypoxanthine phosphoribosyl transferase (Hprt) gene was used as a reference gene. PCR conditions were 10 min at 95°C, 40 cycles of 20s at 95°C 30s at 59.2°C, 2min at 72°C; and 10min at 98°C. Droplet generation and

absolute droplet quantification were performed in a QX200 ddPCR System (Bio-Rad) and analyzed by QuantaSoft Software (Bio-Rad). In addition to determining *Scn10a* transcripts expression in *Scn10a*^{G1663S} mice, we also investigated the effect of *Scn10a*^{G1663S} mutation on *Scn9a* and preproenkephalin (*Penk*) transcript expression levels (Supplementary Table S5).

Supplementary Table S5: Sequence of *Scn9a* and *Penk* probes and primers used for RT-ddPCR. *Scn10a* primer sequences are indicated in the manuscript for publication.

mRNA expression	
Scn9a-Forward primer sequence (5'-3')	CATGAGCAACCCTCCAGATT
Scn9a-Reverse primer sequence (5'-3')	AAACAATGACAACAAAGTCCAG
Scn9a-Probe	/56HEX/AATTCACCT/ZEN/TCCTCCGTGACCCTT/3IABkFQ/
PENK-Forward primer sequence (5'-3')	AGCAGCAAACAGGATGAGAG
PENK-Reverse primer sequence (5'-3')	CTTCTGGCTCCATGGGATATAG
PENK-Probe	/56-FAM/AGCCAAGAA/ZEN/GTACGGAGGCTTCAT/3IABkFQ/
Hprt-Forward primer sequence (5'-3')	CCCCAAAATGGTTAAGGTTGC
Hprt -Reverse primer sequence (5'-3')	AACAAAGTCTGGCCTGTATCC
Hprt –Probe	5HEX/CTTGCTGGT/ZEN/GAAAAGGACCTCTCGAA/3IABkFQ/

2.2 Histological analysis

Conditions of IHC on skin samples were determined based on previous studies that looked for PGP9.5-positive intra-epidermal sensory nerve fibers and determined IENFD in skin of mutant and diabetes-induced mouse models. These studies are summarized in Supplementary Table S6. We can see that IENFs were clearly visible in all of these studies and IENFD was quantified.

Supplementary Table S6: Table summarizing studies on PGP9.5 expression and IENFD quantification in skin of various mutant and diabetes-induced mouse models.

Reference	Animal model	Part of skin	Thickness/sections/ nb animals	Measured parameter	Results	Image
Yang et al., 2018 [173]	NGF^{R100W} mouse model of hereditary sensory autonomic neuropathy	Hind paw footpad skin	45 µm. 10-15 sections. entire length (200 um)	IENFD; identify all of the fibers and the intensity of PGP9.5-labeled fibers in the epidermis region (%) was quantified.	Loss of PGP9.5-positive intra-epidermal sensory fibers (IENF) in the footpad skin in homozygous	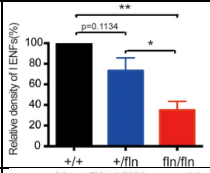
Pham et al., 2018 [174]	Type-2 diabetic mouse model	Skin	20 µm. 27-30 images were captured per group.	IENFD; The nerves crossing the basement membrane of the epidermis were counted. The nerves that appeared as branches below or within the basement membrane were counted as 2, while the nerves that branched in the epidermis were counted as 1. Quantification of the nb of IENF per mm and length of IENF (um/100 um2) in the epidermis.	As compared to that in the Non-Db 10W group, nb of IENF was significantly reduced in the Non-Db 25W group and it further decreased in the Type 2-Db 25W group	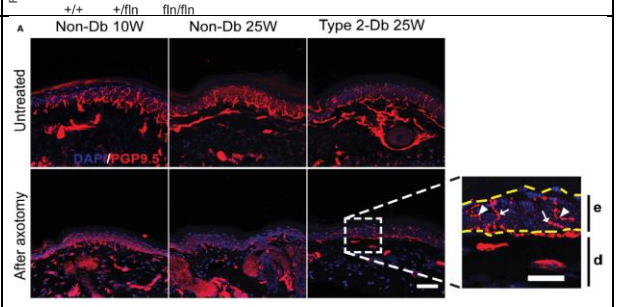
Gregorio et al., 2018 [175]	Spontaneous type-2 diabetic transgenic mice line	Hind limb plantar skin	20 µm. A stack of eight images per foot pad.	IENFD; the number of fibers crossing from the dermis to epidermis per linear mm of skin were quantified.	Diabetic mice displayed a significant decrease in IENFD from 18 weeks of age compared to its littermates.	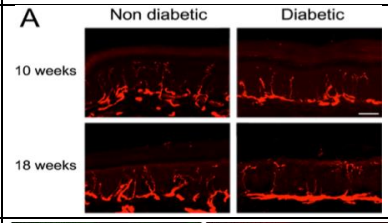
Zhang et al., 2018 [176]	Induced diabetes high fat diet	Hind footpads	30 µm. 12 sections/animal. 6 sections/footpad. Forty images per stack. The optical section thickness was 0.5 µm.	IENFD; cell density data were presented as the mean number of cells per linear mm of epidermis.	The PGP-positive IENFs included Trk A-positive (arrows) and Trk A-negative fibers (arrowheads). No in PGP-positive IENFD in HF mice in comparison with CF mice.	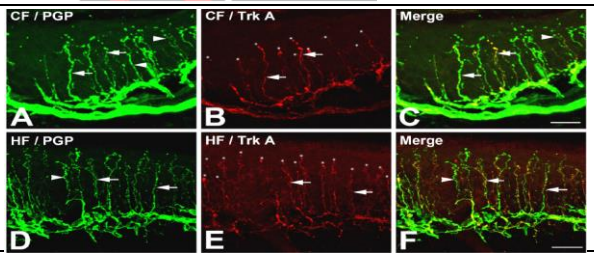
Ceredig et al., 2018 [177]	DOPcKO mice, cuffing of the main branch of sciatic nerve	Plantar skin of both hindpaws (footpad and glabrous skin)	50 µm thickness Longitudinal cross-sections	IENFD; Density was obtained by dividing the number of afferents crossing the dermal-epidermal junction excluding secondary branching, by the total length of the section	The density of PGP 9.5+ free nerve endings in the glabrous skin of the right hind paw was similar in sham and cuff animals.	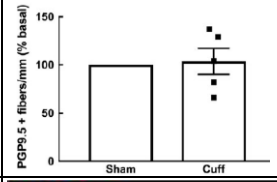
Arcourt et al., 2017 [178]	$Npy2r^{ChR2}$, $MafA^{ChR2}$ models for crosstalk of nociceptors and low-threshold mechanoreceptors in acute pain signaling		50 µm	IENFD not determined. Anti-PGP9.5 to visualize free nerve endings, both myelinated and unmyelinated.	Anti-PGP9.5, which labels all sensory afferents, was used to visualize free nerve endings, both myelinated and unmyelinated. EYFP fluorescence was observed in free nerve endings (marked by arrows) in both glabrous (F) and hairy (G) hindpaw skin	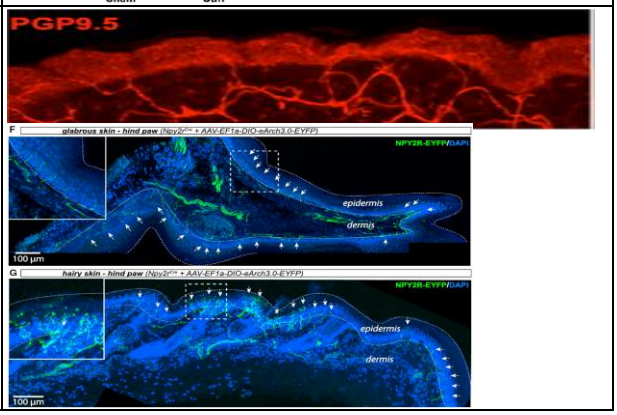

Yeo et al., 2016 [179]	Treatment with oxaliplatin, diluted bee venom	Footpad of the right and left hind paws	20 µm. 2.5 mm biopsy from the footpad of the right and left hind paws. Five slices/paw	IENFD. Nerve fibers that crossed dermal-epidermal junction counted. Nb of IENF per mm of epidermis. Fibers branching after crossing basement membrane counted as a single fiber. The volume (area x section thickness) and IENFD per volume (um/mm3) determined.	On D14 after OXA injection (B), IENFD and nb in hind paws significantly reduced compared to SHAM animals (A). Animals that received saline in OXA-injected mice (D) had significantly fewer IENFs	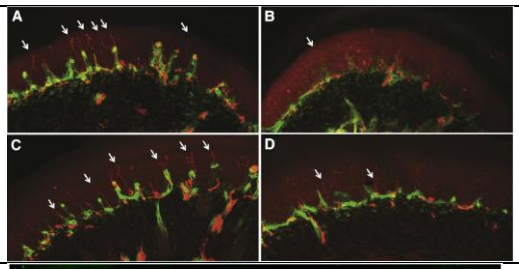
Leckelt et al., 2016 [180]	Thy1-YFP mice, diabetes was induced by multiple low-dose injection of streptozotocin	Plantar surface of the right hind paw	Ten serial 10 µm thick slices per animal. 3 sections per animal were randomly analyzed. 15-20 overlapping images.	IENFD. Intraepidermal nerve fibers crossing the dermal-epidermal border were counted along the length of the epidermis. IENFD was expressed as the nb of nerve fibers per millimeter epidermis.	(A) IENFD did not change after 4 weeks of diabetes in thy1-YFP mice. An example of IENF is shown in a control mouse. The merged image (C) demonstrates the good correlation between YFP (A) and PGP9.5 staining (B).	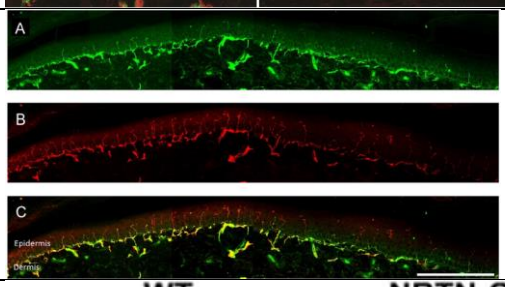
Wang et al., 2013 [181]	Neurturin-overexpresser (NRTN-OE), glial cell line-derived neurotrophic factor family of ligands	Glabrous hindpaw skin	20 µm. 3 animals. 3 sections/animal.	IENFD. Nb of PGP9.5-positive nerve fibers in epidermis area counted. Data are presented as the nb of immunopositive fibers per 100 µm.	NRTN overexpression increases the density of PGP9.5-positive nerve endings in the epidermis of footpad skin	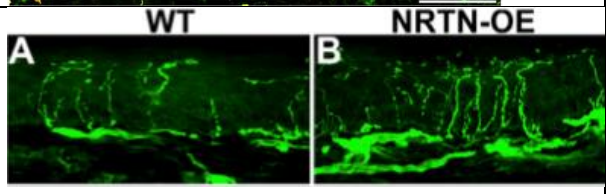
Jin et al., 2013 [182]	Vitis vinifera grape seed extract (VVE) given to a prediabetic neuropathy mouse model induced by a high-fat diet	Skin	3 mm punch skin biopsy on the dorsum of the foot. 40 µm thick.	IENFD. The mean value of IENF density (number/mm)	Nerve fibers increased in the VVE administration group. Arrows indicate the epidermal nerve fiber with branching points inside the epidermis.	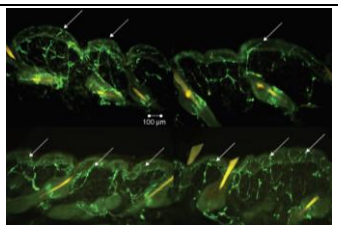
Unezaki et al., 2012 [183]	Y1472F-KI: NMDA receptor NR2B subunit	Hindlimb skin on lumbar dermatome	10 µm. n=6 and 8 for PGP9.5. 34-48 images.	IENFD. The lengths of PGP9.5-positive IENF were measured, the total length of all nerve fibers in each image and the mean nb of nerve fibers per mm epidermis were calculated.	Nerve fibers were observed in both epidermis and dermis. No difference in PGP9.5 expression between wt and Y1472F-KI mice	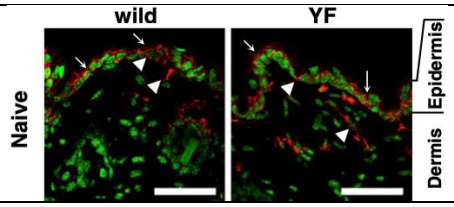
Maklad et al., 2009 [184]	EGFR null, family of receptor tyrosine kinases	Dorsal skin	40 um thick. 10 skin sections for each of 3 animals per group. In each section, 3 randomly selected microscopic fields.	Total area of the PGP9.5-positive fibers was quantified for each of 3 mice, and the mean for each mouse was calculated. Fiber counting was restricted to the fibers of the deep dermal and subepidermal plexuses	Normal organization of sensory nerves into deep dermal plexus, radial fibers (large arrows), subepidermal plexus (small arrows), and epidermal free nerve endings (arrowheads). PGP9.5 fibers were not different between genotypes.	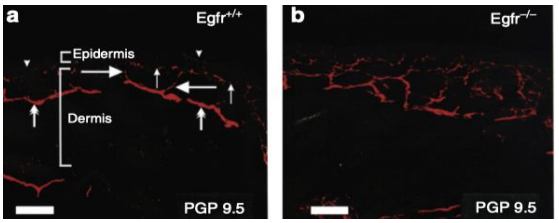
Sullivan et al., 2007 [185]	Male and female BKS-db+ and BKS-db/db mice; diabetes induced by injection of streptozotocin	Foot pads from the plantar surface of the hind paw	30 µm. 3 images per sample were collected. 40 images per stack were flattened.	IENFD. Quantitation of IENF is presented as the number of fibers/linear mm of epidermis.	A) Normal pattern of innervation. B) Decrease in the nb of fibers within a diabetic BKS-db/db foot pad. d = dermis, e = epidermis, dots = IENF, arrowhead = dermal fiber bundles	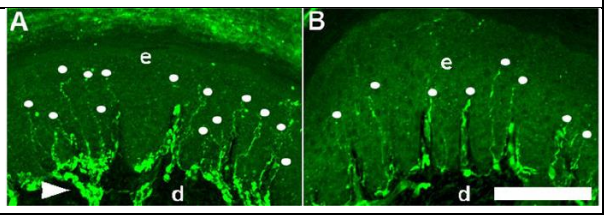

2.2.1 Tissue preparation

Mice were anesthetized with ketamine/xylazine and perfuse intracardially with 40 ml of phosphate buffer saline 0.1 M pH 7.4 (PBS) following 4% paraformaldehyde (PFA) in 0.1 M pH 7.4 PBS. Glabrous hindpaws skin samples (5mm long) were carefully dissected out and post-fixed for overnight at 4°C in 4% PFA in PBS, then tissues are removed from PFA and cryoprotected at 4°C in 30% sucrose in phosphate buffer (PB) for 3 days, embedded in Optimal Cutting Temperature medium, frozen and kept at -80°C. Glabrous skin (30 µm thick) longitudinal sections were cut with a cryostat and kept at -20°C.

2.2.2 Immunohistochemistry (IHC)

IHC of skin sections was performed with free floating sections following the steps below:

1) Rinse sections in 0.02 M PBS, 2 x 5 minutes.
2) For light antigen retrieval, treat sections in 0.2 % hydrogen peroxide in 0.1 M PB pH 7.3 containing 0.05% Triton X-100 for 25 minutes at RT.
3) Rinse sections in 0.02 M PBS, 2x 5 minutes.
4) Block with a TBS with 0.05% Tween 20, 2% BSA and 2% normal donkey serum.
5) Incubate sections with 1:500 diluted rabbit anti-PGP9.5 (ab108986, Abcam) in blocking solution, overnight at 4°C, then leave sections 1h at RT.
6) Rinse sections in 0.02M PBS, 2 x 5 minutes.
7) Incubate sections with 1:500 of donkey anti-rabbit Alexa-647 (Molecular Probes) and 1:2000 of DAPI (Molecular Probes) in blocking solution, 1h at RT.
8) Rinse sections in 0.02M PBS, 2 x 5 minutes.
9) Mount sections on superfrost glass slides
10) Allow to dry in a fume hood for 1h in the dark.
11) Add glue ImmuMount and coverslip.
12) Leave slides to dry overnight in the dark.
13) Store at 4 ºC until microscopy.

2.2.3 Image acquisition and analysis

N= 4 mice per genotype and sex were used for IENFD determination. Both hind paws skin and five randomly selected sections per paw were analyzed. Images were visualized with Leica SP8 UV/Visible Laser Confocal Microscope using a 20× dry objective. The 20× resolution was achieved with a digital zoom factor of 3. Image acquisitions in the sequential mode (excitation intervals: 415 nm – 550 nm and 643 nm – 750 nm) were used for marker co-localization to avoid potential crosstalk between the different fluorescence emissions. Images were acquired with the LCS (Leica) software. The whole length of the skin sections was acquired as a tilescan and an overview of the epidermis-dermis was reconstructed by acquisition of z-stacks with a total depth of 1 µm in 30 overlapping images.

IENF are counted and the length of the epidermal surface is measured using ImageJ software on digitized confocal images. Counting on blinded samples was performed manually on five randomly chosen sections per paw per animal. IENFD was determined by dividing the number of afferents crossing the dermal-epidermal junction excluding secondary branching, by the total length of the section.

3. Behavioral characterization of *Scn10a*^{G1663S} mutant mice

A pipeline for behavioral assessment was defined and conducted on mutants and control littermates in order to investigate nociception and proprioception. The tests were carried on from the least noxious to the most noxious test in the following order: string test, crenellated bar, von Frey, Hargreaves plantar, acetone test, tail flick, tail pressure, cold plate and hot plate. At least 2 days were kept between two consecutive nociceptive tests. The pipeline is presented in Figure 14. All the behavioral tests were already described in the publication manuscript. In addition to these behavioral tests, scratching and wiping behaviors were recorded. Habituation to the room and to the plastic boxes is done one day before recording mice behavior. Mice are placed in small plastic boxes and are left there to acclimatize for 30 minutes. One day before performing string test and crenelated bar test, mice movement was recorded for 20 minutes using a camera. Care was taken to avoid visual contact between two mice during the recording time. Wiping of the cheek is done with the forelimb, this type of behavior is an indicator of pain. Scratching of the cheek is done with the hind limb, this type of behavior is an indicator of itch (Figure 20) [186]. Number and duration of wiping and scratching were measured.

For the hot and cold plate tests, extra parameters and conditions that were not noted and shown in the publication part, were recorded and described here. The hot plate test is not just a reflexive

test as Hargreaves and tail flick, but rather requires decision-making behavior and involves supraspinal pathways. Latency to display first hind paws reaction and the number of total coping reactions per one minute at 47°C, 50°C and 54°C were shown in the publication manuscript part. In addition to these parameters, here we show the number of flicking and licking per one minute that contributed the most to the total number of reactions. For the cold plate test, the mean number of hind paw lifts and total jumps at 5°C was shown in the publication manuscript. In addition, cold plate was performed at 0°C in a separate day and latency to the first reaction (jumping or paw lifting) was measured at 5°C and 0°C in addition to the mean number of hind paw lifts and total jumps.

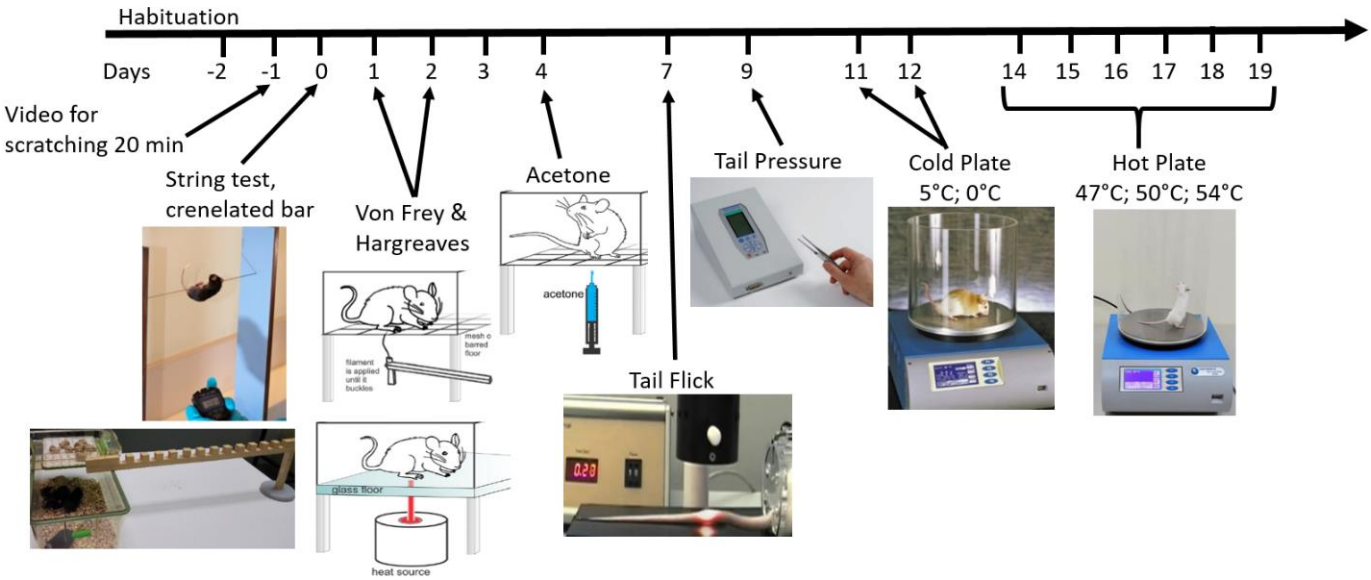

Figure 14: The pipeline of behavioral tests conducted in order to investigate nociception and proprioception. Habituation to the room and to the plastic boxes (day -2) is done one day before recording mice behavior (day -1). The tests were carried on from the least noxious to the most noxious test in the following order: string test (day 0), crenellated bar (day 0), von Frey (days 1-2), Hargreaves plantar (days 1-2), acetone test (day 4), tail flick (day 7), tail pressure (day 9), cold plate (days 11-12), and hot plate (days 14-19).

III Results

In this part, I will show the most important results in the publication manuscript. Supplementary results and undergoing analyses are presented in parts 2 to 5 following the publication manuscript.

1. Publication Manuscript in Preparation

The human *SCN10A*^{G1662S} point mutation established in mice have a small impact on mechanical, heat and cool sensitivity

Celeste Chidiac[1], Yaping Xue[1], Ameer Abu Bakr Rasheed[1], Romain Lorentz[2], Marie-Christine Birling[2], Claire Gaveriaux-Ruff[1$] and Yann Herault[1,2$,#]

1. Université de Strasbourg, CNRS, INSERM Institut de Génétique et de Biologie Moléculaire et Cellulaire (IGBMC), 1 rue Laurent Fries, 67400 Illkirch, France
2. Université de Strasbourg, CNRS, INSERM, PHENOMIN-Institut Clinique de la Souris, (PHENOMIN-ICS), 1 rue Laurent Fries, 6740, Illkirch, France

$ equal last authors

#Corresponding author:

Name Yann Herault

Mail herault@igbmc.fr

Keywords: SCN10A, sodium channel, Small Fiber Neuropathy, nociception, neuropathic pain

ABSTRACT

The voltage-gated sodium channel NAV1.8 is expressed in primary nociceptive neurons and is involved in pain transmission. Mutations in *SCN10A* gene (encoding NAV1.8 channel) have been identified in patients with idiopathic painful Small Fiber Neuropathy (SFN) including the *SCN10A*^{G1662S} gain-of-function mutation. However, the role of this mutation in pain sensation remains unknown. We have generated the first model for the G1662S mutation by using the homologous recombination technique in the mouse. The corresponding *Scn10a*^{G1663S} mouse model had been analysed for *Scn10a* expression and nociception using behavioral tests for thermal and mechanical sensitivity. The *Scn10a*^{G1663S} mutants had a similar *Scn10a* expression level in dorsal root ganglia (DRG) as their wild-type littermates. Mutant mice were more sensitive to touch than their wildtype littermates in the von Frey test. Female homozygous mutants tended to be more sensitive to cooling stimuli in the acetone test. For heat sensitivity, male homozygous mutants showed shorter latencies to radiant heat in the Hargreaves test while homozygous females had longer latencies in the tail flick test. Also, mutant males displayed a shorter reaction latency on the 54°C hot plate. Collectively, *Scn10a*^{G1663S} mutant mice show a moderate but consistent increased sensitivity in behavioral tests of nociception. This altered nociception found in *Scn10a*^{G1663S} mice demonstrates that the corresponding G1662 mutation of *SCN10A* found in painful SFN patients contributes to their pain symptoms.

INTRODUCTION

Neuropathic pain “arises as a direct consequence of a lesion or diseases affecting the somatosensory system” as defined by IASP [1-3]. It is a pathological pain related to

functional changes in primary afferents and sensitization within the central nervous system (CNS) [1, 4]. Neuropathic pain affects 5% of the general population and 40% of patients with neurological diseases [5]. It is generally characterized by abnormal sensations such as hyperalgesia (increased response to painful stimuli) and allodynia (pain in response to a stimulus that does not normally provoke pain) [6]. Primary sensory neurons express unique repertoires of voltage-gated sodium channels. These channels are critical in initiating and propagating the all-or-none action potential of action potentials to the CNS [4]. Tissue damage or injury can lead to changes in expression of sodium channels subunits in the sensory neurons, leading to imbalance between excitatory and inhibitory signaling. These modifications will affect pain thresholds and activity resulting in hyper or hyposensitivity to pain [7, 8].

Inherited disorders of ion channels are known to account for a wide spectrum of human diseases called channelopathies. More than 1000 disease-related mutations have been identified in the family of NAV channels (NAV1.1-NAV1.9) [9]. Pathogenic variants in *SCN10A* gene encoding NAV1.8 channel have been found in 3.7% of patients with small fiber neuropathy (SFN) [10]. The missense point mutation c.4984G>A (p.Gly1662Ser) was identified in three patients with SFN [10, 11]. One of them was 24 years-old with 2 years of pain history. She suffered from continuous tingling and cramps and reported more pain when exposed to cold temperature or exercising. The second patient was 62 years-old with 16 years of pain history. She experienced continuous burning and stabbing pain and was very sensitive and intolerant to sheet. The first patient had abnormal sensitivity thresholds for warmth and cold stimuli as assessed by quantitative sensory testing (QST), while the second one showed hypoesthesia and reduced vibration sense

in physical examination and abnormal warmth sensation levels revealed by QST [11]. The third patient was recently reported. She was 28 years-old with 3 years of pain history. Her temperature sensitivity thresholds were abnormal, and intraepidermal nerve fiber density was normal [10]. The *SCN10A*^{G1662S} mutation was shown to be the first human disease-causing mutation that enhanced generation of tetrodotoxin-resistant (TTX-R) resurgent currents [12], impaired inactivation and accelerated recovery from inactivation, which result in hyperexcitability of DRG neurons [11, 13].

With the aim to study the causality of the G1662S mutation in *SNC10A* we decided to generate the corresponding mouse model. The comparison of human and mouse SCN10A protein sequences showed 82% homology with a resultant of one additional amino acid found in the mouse vs human sequence before the G1662 residue, leading to a change in the position of the human G1662 to G1663 in mice (see Supplementary Fig. 1). To investigate the p.G1662S genotype-phenotype link and better relate this mutation with SFN symptoms, we have created the *Scn10a*^{G1663S} mouse model corresponding to the G1662S mutation in the human gene. After several assays using CRISPR/cas9, the mouse line was successfully generated by homologous recombination in Embryonic Stem (ES) cells and characterized *in vivo*. The *Scn10a* transcripts are well expressed in the DRG of mutant mice as compared to wild-type controls. The mutant animals showed no alteration of growth, survival and health state. The *Scn10a*^{G1663S} mutant mice of both sexes were evaluated for pain behavioral responses to noxious cold, heat and mechanical stimuli. We found that the *Scn10a*^{G1663S} mutant mice displayed a moderate pain phenotype. This suggests that the *SCN10A*^{G1662S} mutation identified in painful SFN patients favors their pain symptoms.

MATERIALS AND METHODS

Animals

Experimental subjects and ethical approval

Animal experiments were performed after approval from the local ethical committee (Com'Eth, Comité d'Ethique pour l'Expérimentation Animale IGBMC-ICS) with the agreement number 14691. The number of mice used for the experiments was adapted according to the 3R principles. Mouse breeding and behavioral experiments were conducted at ICS animal facility. Animals were housed under a 12-h/12-h light/dark cycle (lights on at 7 AM) and 21 ± 1°C, 55 ± 10% humidity condition. Standard Chow (D04 for maintenance and D03 for breeding, SAFE, les Oncins, France) and autoclaved tap water were provided ad libitum with 2-5 mice were housed per cage. Prior to beginning behavioral experiments, all mice were habituated to the environmental conditions and to handling.

Establishment of the genetic animal model

The mouse line creation was done on the C57BL/6NCrl genetic background. Mutant mice carrying the G1663S mutation in *Scn10a* gene corresponding to the G1662S mutation in the human gene (Supplementary Fig. 1) were created by homologous recombination in ES cells. A targeted allele was engineered bearing two homology arms of the original *Scn10a* endogenous gene and a floxed Neo resistance auto-selection cassette. A 1.2 kb fragment encompassing *Scn10a* exon 28 (ENSMUSE00000582971) and 5' intronic sequence was amplified by PCR on ES cell C57BL/6N genomic DNA in two steps to allow the introduction of the GGC>AGC point mutation (leading to the G1663S mutation) and subcloned in an ICS proprietary vector. The 5' arm of homology (1.1 kb) consisted of part of intron 27 was amplified by PCR and subcloned in step1 plasmid to generate the final targeting construct. A RNA guide, gR68 (guide RNA sequence CTAATAAGATATTCTGGGTA) targeting the intronic sequence at the site of insertion of the NeoR selection cassette was cloned in pX330 from Addgene (CRISPR/Cas9 plasmid). This vector was used to increase the efficiency of homologous recombination

at the *Scn10a* locus. Before performing homologous recombination, the whole construct was verified by DNA sequencing.

Homologous recombination strategy is shown in Fig. 1A. Both plasmids (targeting plasmid and CRISPR/Cas9 plasmid were electroporated circular in C57BL/6N mouse ES cells (ICS proprietary line). After G418 selection, targeted clones were identified by long-range PCR and further confirmed by Southern blot with an internal (Neo) probe and a 5' external probe.

We confirmed Neo cassette insertion by long-range PCR and verified that the construct was not integrated randomly in the genome. Clones with the correct genotype were injected into BALB/CN blastocysts, and resulting chimeric males having the correct targeted genotype and a color score >85% were bred with C57BL/6NCrl wt females for germline transmission. Heterozygous *Scn10a*$^{+/G1663S}$ male and female mice were crossed to generate the homozygous *Scn10a*$^{G1663S/G1663S}$ mouse line.

Determination of genotype

For genotype determination, 0.5 cm of mouse tails were harvested. Genomic DNA was extracted by DirectPCR Lysis Reagent-Tail (Viagen Biotech, Cat # 101-T) according to the manufacturer's instructions. 500 ng genomic DNA extracted from wt or mutant mouse were PCR-amplified by 0.2 µl Taq DNA polymerase (Roche), 1.5 µl 10X PCR Buffer with $MgCl_2$, 0.3 µl dNTP PCR Grade nucleotide (dATP, dCTP, dGTP, dTTP at 10 mM, Thermo Scientific), 0.5 µl each primer at 10 µM and H2O in a total volume of 20 ml. Using a T100 thermocycler (Bio-Rad), PCRs were subject to the following thermal conditions: a denaturation step at 94°C for 2 min followed by 40 cycles of 94°C for 30s, a gradient of annealing temperatures between 55-65°C for 45s and 72°C for 1 min/kb and a final elongation step for 5min at 72°C. PCR outcome was analyzed on a 1.5% agarose gel. To confirm the G1663S mutation, genomic DNA from mutated mice was PCR-amplified and confirmed by DNA sequencing. Genotyping of G1663S mutant mice consisted of 5 PCR reactions: PCR1 and PCR2 to confirm the excision of the selection marker using Ef/Er2 and Ef2/Er3 primers and giving bands of 4484 bp and 4357 bp for the recombinant allele, 363 bp and 236 bp for the PM allele and 250 bp and 123 bp for the wt allele, respectively. PCR3 and PCR4 targeting the 5' and 3' sides of the selection marker respectively, using

Ef/Mq1r and Mq1f/Er primers giving respectively bands of 286 bp and 461 bp for the targeted allele and no bands for PM and wt alleles. PCR5 specific for the LoxP site using Ef/Lxr primers giving a band of 194 bp for the targeted and PM alleles. Primer sequences and PCR reactions information are shown in Supplementary Tables 1A and 1B, and primers cutting sites are shown in the homologous recombination strategy in Fig. 1A.

Determination of gene/transcript expression by Real Time droplet digital PCR (RT ddPCR)

Dorsal root ganglia were collected from wt and mutant mice and flash frozen in liquid nitrogen. All tissues were disrupted using Precellys® CK14 Lysing kit in TRIzol Reagent, and total RNA purified using RNeasy Mini Kit (Qiagen) according to manufacturer's instructions. cDNA synthesis was performed using the SuperScript™VILO™ cDNA Synthesis Kit (Invitrogen). mRNA amplification by ddPCR was performed in 20 µL reactions containing 1× ddPCR Supermix for Probes (No dUTP), 125 nM of each probe, 250 nM specific primers, and 50 ng DNA according to manufacturer's recommendations (PCR conditions: 10 min at 95°C, 40 cycles of 20s at 95°C 30s at 59.2°C, 2min at 72°C; and 10min at 98°C). Droplet generation and absolute droplet quantification were performed in a QX200 Droplet Digital PCR System (Bio-Rad) and analyzed by QuantaSoft Software (Bio-Rad). Probe and primer sequences are shown in Supplementary Table 2.

Behavioural assessment of the *Scn10a*^{G1663S} mouse model

A pipeline for behavioral assessment was defined and conducted on mutants and control littermates to investigate nociception and proprioception. All behavioral tests were conducted between 9:00 AM and 5:00 PM. Animals were transferred to the experimental room 30 min before each experimental test. Body weight of wt and mutant mice were measured at the age of 7-11 weeks. The behavioral tests were carried on from the least noxious to the most noxious test in the following order: string test, crenellated bar, von Frey, Hargreaves plantar, acetone test, tail flick, tail pressure, cold plate and hot plate. At least 2 days were kept between two consecutive tests. Females and males of the different genotypes were tested at 2-months-age. The experimenter was blind to mouse genotype.

The grip string test (in-house) was used to measure muscle strength. The tool is about a horizontal wire placed at 40 cm above a table. The mouse was hanged by the forelimb to the wire and the latency to gain hindlimb traction was measured. Three consecutive trials were done by 5 min intervals.

The notched/crenellated bar test was used to evaluate motor coordination and balance. The method described by Carter et al. was used [14]. Briefly, mice were put on an elevated crenellated bar and had to traverse the distance from the beginning of the bar till the end where the home cage is placed. The time required to traverse the whole bar distance was recorded. In addition, the number of mistakes was defined as the times when mice were touching the gaps of the crenelated bar by their hind paws while passing over the bar.

One day prior to the Von Frey test, mice were placed in small transparent plastic boxes over a mesh floor and are let there to acclimatize for 45 min. On the test day, mice could habituate for 30 min before starting the test. Mechanical sensitivity was determined using 8 different von Frey filaments of specific forces from 0.008g to 2g ('Touch-Test', North Coast Medical, Inc., San Jose, CA). Filaments are applied to the mid-planter hind paws starting with the filament of 0.4g. The "up-down" von Frey method was used. The 50% threshold was calculated by the Excel program generously provided by A. Basbaum (University of California, San Francisco). Each trial was done by applying the filaments onto one hind paw of the mice placed consecutively, and then applying them onto the second hind paw of each mouse. The test was done on two consecutive days with 2 trials per day.

Two days prior to the Rodent pincher test, mice were habituated to be restrained in a 50 ml tube, with the whole tail exposed. The "Rodent pincher" test (Bioseb, France) was used to determine sensitivity to noxious mechanical stimuli, by applying a gradually increasing pressure to mice tail. This test allows calibrated forceps to induce quantifiable mechanical stimulation on a linear scale. Three measures were performed for each mouse, recording on three different locations of the tail. The tail withdrawal threshold was recorded, with a cutoff of 500 g.

The acetone test was used to measure sensitivity to cool stimuli. Mice were placed and habituated in the same manner as for the von Frey test. 10 µL of acetone was applied to the center of the plantar surface of each hind paw, using 50µL Hamilton Gastight Syringe (Model 1705 TLL). Acetone was applied in three successive testing sessions for each paw. The interval between each application was at least 5 min. The duration of hind paw withdrawal and flicking was measured during 30s following acetone application. The values of hind paw withdrawal and flicking duration displayed in the six trials were added.

The cold plate assay (Bioseb, France) was used to assess sensitivity to noxious cold temperatures. One day prior to the test, mice were acclimatized to the plate at room temperature, then on the test day, mice were tested on 5°C cold plate. To avoid tissue damage, a cutoff of 5 min was used. The mean number of hind paw lifts and total jumps were measured.

The Hargreaves test consisted of applying a radiant infrared heat stimulus to the hind paws of mice to determine heat thresholds. One day prior to the test, mice were habituated to the apparatus by placing them in small transparent plastic boxes over a glass plate. Withdrawal latency was recorded on two consecutive days, with two trials per day. A trial was done by applying the heat stimulus on one hind paw for all the mice, then applying it to the second hind paw for all the mice, in a manner to leave at least 5 min between each hind paw recording of the same mice. The mean of all measurements of both hind paws were calculated. The radiant heat was applied using a temperature ramp speed allowing to get a paw withdrawal latency of 7s in wt mice.

Tail flick consisted in applying a focused beam of light to the mouse tail, to determine heat thresholds. Two days prior to the test, mice are habituated to be restrained in a 50 ml tube, with the whole tail exposed. The heat stimuli were applied at three different places of the tail tip and the mean of the three withdrawal latencies was calculated.

Hot plate test was used as an integrated test to determine heat sensitivity. One day before the test, mice were habituated to the plate at room temperature. In our study, the mice were tested at 3 different temperatures on 3 separate days with specific cutoffs to avoid tissue damage: 47°C for 3 min, 50°C for 1 min and 54°C for 30s. At each temperature, the latency to display first hind paws reaction was recorded. In addition, we also measured

the number of coping reactions as reported by Huang et al. [15]. Recently, Huang et al. introduced the scoring of the number and duration of licking and jumping as coping behaviors. The mutant mice in which spinal preprotachykinin-positive neurons had been ablated showed withdrawal latencies to their wt littermates on the 47°C, 50°C and 56°C hot plate while they showed reduced number of licking episodes compared to wt [15], revealing the importance of scoring coping behaviors as an additional information of heat pain sensitivity in this test. In our study, the coping behaviors included lifting, flicking, licking of the hind paws and jumping. The number of total reactions was calculated per one minute at each temperature.

Statistical Analysis

Results are expressed as mean ± SEM. Statistical analyses were performed by using GraphPad Prism 9 software. All data sets were tested for normality using the D'Agostino & Pearson normality test. One-way ANOVA analysis was done when data were found normally distributed, and Kruskal-Wallis analysis was used when data were not normally distributed. For transcript expression level analysis, genotype effect in each sex was analyzed using one-way ANOVA analysis followed by Šídák's multiple comparisons test when appropriate. The analysis of behavioral tests results was performed by one-way ANOVA or Kruskal-Wallis analyses to test for genotype difference on grouped sexes and separated sexes, followed by post-hoc analysis when appropriate. A p-value < 0.05 was considered statistically significant.

Results

Generation and characterization of the *Scn10a*^{G1663S} mouse model

Initially we tried to create the *Scn10a*^{G1663S} mouse model the CRISPR-Cas9 innovative technology. We tried two different strategies that were unsuccessful due to the high similarity between *Scn10a* and other *Scn* genes, especially *Scn5a* gene that shares the most similarity with *Scn10a* and is expressed on the same chromosome. We moved then to homologous recombination in ES cells to generate *Scn10a*^{G1663S} mouse line Fig. 1A. Briefly, the G1663S targeting vector was electroporated into C57BL/6N ES cells, together with the plasmid vector containing gR68. The guide RNA gR68 in association with the

Cas9 protein specifically generates a double strand break in the intronic region close to the mutation to introduce. The intronic sequence, in contrary to the exonic sequence, does not show any similarity to intronic sequences of any other *Scn* genes. The CRISPR/Cas9 double strand break drive by the guide RNA gR68 has forced the ES cells to repair and the presence of the targeting construct with the selection pressure (NeoR) has increased the homologous recombination rate (even if the size of the homology arms is much less important than with classical ES cell targeting). Among positive ES clones, one clone was selected. Genomic DNA from the mutant allele of this clone was PCR-amplified with a forward primer located in the Cre cassette (Fcre) (Fig. 1A) and a 3' external reverse primer and was then sequenced. Sequencing results demonstrated the presence of the mutation in this positive ES clone (Fig. 1B). Heterozygous *Scn10a*$^{+/G1663S}$ mice were crossed to generate the *Scn10a*$^{G1663S/G1663S}$ mice and their control wt mice. An example of genotyping results is shown in Fig. 1C. The *Scn10a* transcript expression level was evaluated in DRG of G1663S and control mice by RT-ddPCR. One-way ANOVA revealed a genotype effect for each alleles-derived (wt or mutant G1663S) transcripts expression in grouped or separate sexes. When ratios of *Scn10a*$^{+}$ and *Scn10a*^{G1663S} transcripts were summed, no effect on genotype or sex was detected by the two-Way ANOVA. Both transcripts were equally expressed in DRG of wt or *G1663S/G1663S* mutant mice, respectively and in both sexes, indicating that the mutation did not alter *Scn10a* expression. Heterozygous *+/G1663S* mice expressed about 50% of each allelic transcripts in DRG (Fig. 1D and Supplementary Table 3).

The *Scn10a*^{G1663S} mutation did not affect the body weight of the mutant mice. Heterozygous *+/G1663S* and homozygous *G1663S/G1663S* mice showed a normal body weight compared to wt littermates (Fig. 2). To evaluate whether the mutation alter proprioception of mutant mice, string test and crenelated bar were performed. String test latency analysis revealed a sex effect (two-way ANOVA $F_{1, 105}$=10.76, p=0.0014) but no genotype effect. Similarly, no genotype or sex effect was detected in the crenelated bar test. Heterozygous and homozygous mutant mice behaved in the same manner than control mice in these two tests (Fig. 2 B-D and Supplementary Table 4). We concluded that the presence of one or two alleles with the G1663S mutation did not change the proprioception in the mutant mice.

Enhanced pain sensitivity to mechanical stimuli in the *Scn10a*^{G1663S} mice

The oldest SFN patients with heterozygous c.4984G>A, p.G1662S mutation developed sensitive skin and intolerance to sheets over her feet with continuous pain [11]. We used the von Frey test to assess touch allodynia and the rodent pincher test to evaluate sensitivity to noxious mechanical stimuli in the *Scn10a*^{G1663S} mutant mice. In the von Frey test, a genotype effect was present (two-way ANOVA $F_{2, 93}$=3.461, p=0.0355). The one-way ANOVA showed a genotype effect on grouped sexes where heterozygote and homozygote mice showed a higher sensitivity to mechanical stimuli compared to their wt littermates (Fig. 3A and Supplementary Table 5). This did not reach significance when males and females were analyzed separately. In the rodent pincher test, two-way analysis resulted in a sex effect (two-way ANOVA $F_{1, 106}$=4.186, p=0.043). There was a tendency for higher sensitivity in the mutants that was above the significance threshold (Fig. 3B and Supplementary Table 5). Therefore, *Scn10a*^{G1663S} mutant mice developed mechanical allodynia.

Sensitivity to cooling and cold stimuli in the *Scn10a*^{G1663S} mice

One of the SFN patients with G1662S mutation reported that cold temperature aggravated her complaints and QST revealed abnormal thresholds for cold sensation [11]. We performed the acetone test to investigate sensitivity of the *Scn10a*^{G1663S} mice to cooling stimuli (12°C-15°C) and cold plate at 5°C for cold stimuli. In the acetone test, the duration of withdrawal and flicking reactions revealed an interaction between genotype and sex (two-way ANOVA $F_{2, 107}$=4.336, p=0.015). The Kruskal-Wallis analysis showed quite higher behavioural response to the acetone stimulus in mutant females while males did similar duration of withdrawal and flicking reactions as compared to wt males (Fig. 3C and Supplementary Table 5). In the cold plate test, the number of hind paw lifts and jumps showed a sex effect (two-way ANOVA $F_{1, 107}$=21.61, p<0.0001) with less reactions in males. Mutant and control mice of both sexes had comparable reactions on the cold plate (Fig. 3D and Supplementary Table 5). Therefore, *Scn10a*^{G1663S} mutant mice showed a higher sensitivity to cool, but not cold temperatures.

Enhanced heat pain sensitivity in the *Scn10a*^{G1663S} mice

An abnormal threshold for warmth sensation was also an important clinical feature of SFN patients with the G1662S mutation [10, 11]. *Scn10a*^{G1663S} mutant mice were tested for their sensitivity to radiant heat stimuli in the Hargreaves and tail flick tests (Fig. 4). Latencies in each of the Hargreaves and tail flick tests resulted in an interaction between sex and genotype (two-way ANOVA $F_{2, 113}$=3.808, p=0.025 and $F_{2, 108}$=3.345, p=0.039 respectively). In the Hargreaves test, the mutation did significantly lower latency to response, with homozygous males withdrawing their hind-paw earlier than wt males (Fig. 4A and Supplementary Table 6). In the Tail Flick assay, female mutant mice showed a general genotype effect (Fig. 4B and Supplementary Table 6).

The hot plate test is classically used to determine heat thresholds and involves supraspinal pathways. According to previous study by Huang and colleagues [15], latency to first hind paw reaction and latency to first jump reaction are important variables in this assay. Huang et al. introduced the scoring of the number and duration of licking and jumping as coping behaviors. Accordingly, we scored both the latency to first hindpaw reaction at 47°C, 50°C and 54°C, and the number of coping reactions (Fig. 4C-E). The latency to first hindpaw reaction in the hot plate showed a sex effect at 54°C (two-way ANOVA $F_{1, 108}$=5.703, p=0.0187), and a genotype effect was detected at 54°C for the homozygous males (Fig. 4E and Supplementary Table 6). For the coping reactions, a tendency for genotype effect was recorded at 47°C although it did not reach significance (Fig. 4C and Supplementary Table 6). Therefore, *Scn10a*^{G1663S} mutant male mice showed an increased sensitivity to heat.

DISCUSSION

The *SCN10A*^{G1662S} mutation was described in three patients with SFN. In this study, we generated a similar mutation in a mouse model using homologous recombination in ES cells in order to investigate the association between genotype and phenotype, and better understand Scn10a-mediated pain mechanism underlying pain symptoms of SFN patients. The *Scn10a* mRNA is known to be expressed in DRG that contain cell bodies of sensory neurons. The *Scn10a*^{G1663S} mutation did not alter *Scn10a* transcript expression

level in DRG in mutant mice of both sexes. Sensitivity to mechanical, heat and cold stimuli was investigated in the mutants in both sexes. Our results collectively indicate that the *Scn10a*^{G1663S} mutant mice have moderately enhanced pain sensitivity towards mechanical, heat and cold stimuli in some behavioural tests that correlate with the pain symptoms of the SFN patients carrying the same mutation.

Enhanced pain sensitivity to mechanical stimuli in the *Scn10a*^{G1663S} mice

The enhanced sensitivity to mechanical stimuli in the *Scn10a*^{G1663S} mice can be compared to other genetic mouse models for *Scn10a.* The *Possum* mice harboring a *Scn10a*^{T790A} gain-of-function mutation were identified in an N-ethyl-N-nitrosourea-induced mutagenesis screen. Amanda Blasius and colleagues reported abnormal behaviors in the heterozygous and homozygous *Possum* mice [16]. Homozygous *Possum* mice showed no alteration in the sensitivity to touch stimuli in the von Frey test [16, 17] while they showed increased sensitivity when a needle prick was applied to the hindpaw plantar side [17]. The homozygous *Scn10a* KO mouse model, generated by Akopian and colleagues [18], was studied for pain behaviors in many studies. The *Scn10a* gene KO did not impact on touch stimuli as assessed by the von Frey test [8, 18-23], while it reduced pain sensitivity towards noxious mechanical stimuli as assessed by the tail pressure test [8, 18, 24]. These findings suggest that the *Scn10a* is important for sensitivity to noxious mechanical stimuli, but not for light touch. A third mouse model was developed where the Cre gene was knocked-in into *Scn10a* exon 1, the *Scn10a*$^{Cre/+}$ hemizygous mice. These mice were analyzed for pain behavior. They had no alteration in response to von Frey filaments [8, 25] which is like the result obtained with the *Scn10a* KO mice. In addition, the *Scn10a*$^{Cre/+}$ hemizygous mice behaved similarly to their wt littermates in the tail pressure test [25, 26], showing that inactivation of one *Scn10a* allele does impair mechanical sensitivity.

Our results show a reduced mechanical threshold of the *Scn10a*^{G1663S} mice in the von Frey test. This phenotype has not been previously reported in the other *Scn10a* mutant lines [8, 16-23, 25, 27] which displayed altered sensitivities to noxious mechanical stimuli

[8, 18, 24]. Our results on touch sensitivity in our mutant mice concur with the *SCN10A*$^{+/G1662S}$ SFN patient reports on sheet intolerance.

Sensitivity to cooling and cold stimuli in the *Scn10a*^{G1663S} mice

Previous works reported on response to extreme cold as assayed by cold plate behaviors in *Scn10a* mutant mice. The *Possum Scn10a*^{T790A} mice showed increased reactions on the cold plate at -1°C [16]. Collectively, previous studies with Cold Plate and acetone tests on *Scn10a* KO mice showed that *Scn10a* loss of function induces a loss of sensitivity to extreme cold but not to cool and mild cold [23, 28-30]. More precisely, *Scn10a* KO mice were less sensitive than wt when nocifensive responses were measured on the cold plate at 0°C [29]. *Scn10a*$^{Cre/Cre}$ mice presented a reduced pain phenotype by jumping later than wt mice on the -5°C cold plate and no phenotype when forepaw lifting in the cold plate was assessed at 10°C and 5°C [28]. Our study shows no difference in the mean number of hind paw lifts and total jumps in the cold plate at 5°C. In the future, further investigations using colder temperatures on the plate, like at 0°C or -1°C, may reveal an influence of the *Scn10a*^{G1663S} mutation on sensitivity to extreme cold as already shown in previous studies on *Scn10a* mouse models [16, 28, 29].

Following acetone application, *G1663S/G1663S* males did similar reactions as wt males while *G1663S/G1663S* females showed a tendency for longer duration of reactions. Previously, both*, Scn10a*$^{Cre/Cre}$ and *Scn10a* KO mice revealed no phenotype for the responding time of hind paw following acetone application [23, 28, 30]. The phenotype of increased sensitivity to cooling was more important in G1663S mutant females than males. Similarly, a sex difference was found for sensitivity to cooling in *Trpa1* KO mice [31]. Thus, the sex influences the phenotypes to cooling sensitivity. Our findings on the G1663S mutants in the acetone test suggest that an increase in *Scn10a* excitability as induced by the G1663S mutation [11, 13] alters the sensitivity to cooling while the loss of function of *Scn10a* as investigated with the *Scn10a* KO mice did not impact this sensitivity [23, 28, 30]. Our results on increased sensitivity to cooling in the mutant females is in agreement with the aggravated complaints of G1662S SFN patients when exposed to cold and with abnormal thresholds for cold sensation in the QST.

Sensitivity to heat pain in the *Scn10a*^{G1663S} mice

In the Hargreaves test, the *Scn10a* KO animals displayed analgesia when a slow ramp for radiant heat was used (13-15 s latency in wt mice) [18, 24] while no phenotype was found when using a faster heat ramp (7-8 s latency in wt mice) [8, 21, 22], indicating that the use of a slow temperature ramp allowed to detect analgesia in the *Scn10a* KO mice. In our study, the G1663S male animals were more sensitive in the Hargreaves test when using a heating ramp that led to a withdrawal latency of 7s for wt mice similar to the latency described in the fast ramps papers [8, 21, 22]. Therefore, in a fast ramp condition previously reported to lead to no phenotype in the KO mice, we could evidence the increased sensitivity of G1663S male animals to radiant heat.

In the tail flick assay, sex-grouped mice showed no phenotype, while mutant females had an overall higher latency time compared to control mice. Akopian et al. [18] showed increased latency of the *Scn10a* KO mice to light beam in the tail flick test while the data on the *Scn10a*^{G1663S} line did not show increased sensitivity under our condition. Also, the *Scn10a* KO mice showed no phenotype in the tail immersion test [8, 18, 21].

In the Hot plate assay, a shorter latency to the first hind paw reaction was found for G1663S male mice at 54°C, while no phenotype was found at the lower 47°C and 50°C temperatures. The *Possum* mice showed no alteration on the hot plate at 52°C [16] and their sensitivity at other temperatures or for other heat tests was not reported. The *Scn10a* KO mice showed no phenotype in the hot plate assay when the latency to first hind paw withdrawal reaction was recorded at 45°C, 50°C, 55°C and 60°C [8, 18, 21]. Also, *Scn10a*$^{Cre/+}$ mice had normal responses in hot plate test at 50°C and 55°C [8, 25, 26].

Altogether, our findings on *Scn10a*^{G1663S} mice in the three tests for heat sensitivity indicate that the *Scn10a*^{G1663S} mutation leads to increased sensitivity of the paw to strong heating. This appears in agreement with some data from previous publications on *Scn10a* KO mice in which *Scn10a* has been inactivated [8, 18, 21, 24].

Sex effect on the *Scn10a*^{G1663S} mouse behaviors

In our study, we studied pain behaviors of *Scn10a*^{G1663S} mice on both sexes and analyzed the data of each sex separately and sex-grouped. The results suggest that there are specific sex differences in *Scn10a*^{G1663S} mutants. Mutant females showed increased

reactions in the acetone test, while mutant males had an increased sensitivity in the Hargreaves test and in the hot plate at 54°C. The sex-grouped analysis allowed to detect an increased sensitivity to mechanical stimuli. This suggests an influence of sex on the effect of the mutation. The three SFN patients carrying *SCN10A*^{G1662S} mutation were women [10, 11], whose symptoms globally correlate with the pain phenotype found in *Scn10a*^{G1663S} mutant animals. Nevertheless, no male SFN patient with the *SCN10A*^{G1662S} mutation has been reported until now.

There are multifactorial and complex influences underlying the sex differences in pain in the clinical setting. Pain is reported more frequently by women than men. Healthy women have significantly lower pain thresholds for electrical, pressure and thermal stimuli [32]. Sex hormones and sociocultural factors are known to impact men and women pain experience [32]. Women manifest their pain with stronger emotion and evoke pain distress, while men seem to withstand pain and less eager to report pain [32]. In addition, pain thresholds of both males and females are affected by the sex of the examiner [33, 34]. Also, sex differences in opioid-induced analgesia were reported. Interestingly, the review by Marieke Niesters and colleagues reported that females display stronger morphine efficacy than men in both experimental and clinical studies [35], while the review by Jeff Mogil showed that male rodents were more sensitive to (mostly opioid) analgesics [36]. In recent years, more and more studies used animals of both sexes and reported sex-dependent differences or no differences in nociceptive behaviors in rodent models [36]. In addition, the genetic background may impact on sex differences or no differences in pain. In the last decade, a neuroimmune mediation of pain has also been discovered, with the preferential involvement of microglia in the spinal cord for pain hypersensitivity in male rodents [36-38]. The sex differences found for behavioral responses in *Scn10a*^{G1663S} mutants contribute to complete the list of genes or mutations for which a sex effect has been detected.

Conclusion and perspectives for *Scn10a*^{G1663S} mice

Globally the studies on *Scn10a* genetic rodent models have highlighted the important role of the NAV1.8 channel including the SCN10A protein in nociception. Also, the Navb4 subunit has been shown to contribute to sensory neuron excitability *in vitro* [12]. Still,

creating rodent models of the human *SCN10A* mutations that were identified in SFN patients was needed to study *in vivo* these mutations found in the patients. In our study, we successfully created the mouse model for *SCN10A*^{G1662S} mutation identified in SFN patients, by using homologous recombination in ES cells. *Scn10a*^{G1663S} mutant mice revealed a pain phenotype towards non-noxious and noxious mechanical stimuli, cooling stimuli, and some forms of heat stimuli. Hereafter, other devices could also be used to assess thermal preference as complementary tests for heat sensitivity, such as the two-plate choice test [39], the thermal gradient test [40] or the operant plantar thermal assay [41]. The results *Scn10a*^{G1663S} mutant animals concurs with pain features in the painful SFN patients with *SCN10A*^{G1662S} mutation, such as sensitive skin and abnormal thresholds for warm and cold stimuli as revealed by QST. However, pain remains a multifactorial experience of sensory, emotional, cognitive, and social components. Care should be taken to the fact that human only can report pain verbally. In this study, mostly evoked pain was assessed. In the future, spontaneous pain may also be assessed in the mutant mice. Different paradigms could be used to evaluate spontaneous pain, including weight bearing with the CatWalk or other methods, conditioned place preference for the chamber associated with analgesic administration [42-44].

The development of genetic rodent models recapitulating the *SCN* mutations found in SFN patients is a key step to explore pain mechanism involving sodium channels and be able to develop convenient novel analgesics. The *Scn10a*^{G1663S} mouse model opens the door for further investigations in the aim of complementing the knowledge about the role of NAV1.8 channel in painful SFN.

Acknowledgments

We thank Marie-Christine Birling, Laurence Schaeffer and Valerie Erbs from the genetic engineering team, Sylvie Jacquot and Amelie Jeanblanc from the genotyping team, and Marie Wattenhofer-Donze from the ES cells team at ICS for their help to create and genotype the mutant mouse model. We also thank Loïc Lindner and Pauline Cayrou for their help in ddPCR design and training. We thank the animal caretakers Sophie Brignon,

Charley Pinault and Dalila Ali-Hadji at PHENOMIN-ICS and IGBMC animal facility for their services.

Funding

This work has been funded by the Molecule-to-Man Pain Network, a European Commission Multi-Center Collaborative Project through the European Union's Horizon 2020 research and innovation program under the Marie Skłodowska-Curie grant agreement No. 721841-Pain-Net. This work has been supported by the National Centre for Scientific Research (CNRS), the French National Institute of health and medical research (INSERM) and the University of Strasbourg (Unistra). The French state funds through the "Agence nationale de la recherche" under the frame of Programme Investissements d'Avenir labelled ANR-10-IDEX-0002-02, ANR-10-LABX-0030-INRT, ANR-10-INBS-07 PHENOMIN. The funders had no role in study design, data collection and analysis, decision to publish, or preparation of the manuscript.

References

1. Brouwer, B.A., et al., *Neuropathic Pain due to Small Fiber Neuropathy in Aging: Current Management and Future Prospects.* Drugs Aging, 2015. **32**(8): p. 611-21.
2. Treede, R.-D., et al., *Neuropathic pain.* Redefinition and a grading system for clinical and research purposes, 2008. **70**(18): p. 1630-1635.
3. Woolf, C.J., *What is this thing called pain?* J Clin Invest, 2010. **120**(11): p. 3742-4.
4. Bennett, D.L., et al., *The Role of Voltage-Gated Sodium Channels in Pain Signaling.* Physiol Rev, 2019. **99**(2): p. 1079-1151.
5. Bouhassira, D., et al., *Prevalence of chronic pain with neuropathic characteristics in the general population.* Pain, 2008. **136**(3): p. 380-7.
6. Farrar, J.T. and R.K. Portenoy, *Neuropathic cancer pain: the role of adjuvant analgesics.* Oncology (Williston Park, N.Y.), 2001. **15**(11): p. 1435-42, 1445; discussion 1445, 1450-3.
7. Colloca, L., et al., *Neuropathic pain.* Nat Rev Dis Primers, 2017. **3**: p. 17002.
8. Nassar, M.A., et al., *Neuropathic pain develops normally in mice lacking both Na(v)1.7 and Na(v)1.8.* Mol Pain, 2005. **1**: p. 24.
9. Huang, W., et al., *Structure-based assessment of disease-related mutations in human voltage-gated sodium channels.* Protein Cell, 2017. **8**(6): p. 401-438.
10. Eijkenboom, I., et al., *Yield of peripheral sodium channels gene screening in pure small fibre neuropathy.* J Neurol Neurosurg Psychiatry, 2019. **90**(3): p. 342-352.
11. Han, C., et al., *The G1662S NaV1.8 mutation in small fibre neuropathy: impaired inactivation underlying DRG neuron hyperexcitability.* J Neurol Neurosurg Psychiatry, 2014. **85**(5): p. 499-505.
12. Xiao, Y., et al., *Increased Resurgent Sodium Currents in Nav1.8 Contribute to Nociceptive Sensory Neuron Hyperexcitability Associated with Peripheral Neuropathies.* J Neurosci, 2019. **39**(8): p. 1539-1550.
13. Huang, J., et al., *Small-fiber neuropathy Nav1.8 mutation shifts activation to hyperpolarized potentials and increases excitability of dorsal root ganglion neurons.* J Neurosci, 2013. **33**(35): p. 14087-97.
14. Carter, R., A. Morton, and S. Dunnett, *Motor Coordination and Balance in Rodents.* Current protocols in neuroscience / editorial board, Jacqueline N. Crawley ... [et al.], 2001. **Chapter 8**: p. Unit 8.12.
15. Huang, T., et al., *Identifying the pathways required for coping behaviours associated with sustained pain.* Nature, 2019. **565**(7737): p. 86-90.
16. Blasius, A.L., et al., *Hypermorphic mutation of the voltage-gated sodium channel encoding gene Scn10a causes a dramatic stimulus-dependent neurobehavioral phenotype.* Proc Natl Acad Sci U S A, 2011. **108**(48): p. 19413-8.
17. Garrison, S.R., et al., *A gain-of-function voltage-gated sodium channel 1.8 mutation drives intense hyperexcitability of A- and C-fiber neurons.* Pain, 2014. **155**(5): p. 896-905.
18. Akopian, A.N., Souslova, V., England, S., Okuse, K., Ogata, N., Ure, J., ... & Hill, R., *The tetrodotoxin-resistant sodium channel SNS has a specialized function in pain pathways.* Nature neuroscience, 1999. **2**(6): p. 541-548.

19. Kerr, B.J., Souslova, V., McMahon, S. B., & Wood, J. N., *A role for the TTX-resistant sodium channel Nav 1.8 in NGF-induced hyperalgesia, but not neuropathic pain.* Neuroreport, 2001. **12**(14): p. 3077-3080.
20. Laird, J.M., et al., *Deficits in visceral pain and referred hyperalgesia in Nav1.8 (SNS/PN3)-null mice.* J Neurosci, 2002. **22**(19): p. 8352-6.
21. Leo, S., R. D'Hooge, and T. Meert, *Exploring the role of nociceptor-specific sodium channels in pain transmission using Nav1.8 and Nav1.9 knockout mice.* Behav Brain Res, 2010. **208**(1): p. 149-57.
22. Shields, S.D., et al., *Sodium channel Na(v)1.7 is essential for lowering heat pain threshold after burn injury.* J Neurosci, 2012. **32**(32): p. 10819-32.
23. Minett, M.S., et al., *Pain without nociceptors? Nav1.7-independent pain mechanisms.* Cell Rep, 2014. **6**(2): p. 301-12.
24. Minett, M.S., N. Eijkelkamp, and J.N. Wood, *Significant determinants of mouse pain behaviour.* PLoS One, 2014. **9**(8): p. e104458.
25. Stirling, L.C., et al., *Nociceptor-specific gene deletion using heterozygous NaV1.8-Cre recombinase mice.* Pain, 2005. **113**(1-2): p. 27-36.
26. Agarwal, N., S. Offermanns, and R. Kuner, *Conditional gene deletion in primary nociceptive neurons of trigeminal ganglia and dorsal root ganglia.* Genesis, 2004. **38**(3): p. 122-9.
27. Nassar, M.A., et al., *Nociceptor-specific gene deletion reveals a major role for Nav1.7 (PN1) in acute and inflammatory pain.* Proc Natl Acad Sci U S A, 2004. **101**(34): p. 12706-11.
28. Luiz, A.P., et al., *Cold sensing by NaV1.8-positive and NaV1.8-negative sensory neurons.* Proc Natl Acad Sci U S A, 2019.
29. Zimmermann, K., et al., *Sensory neuron sodium channel Nav1.8 is essential for pain at low temperatures.* Nature, 2007. **447**(7146): p. 855-8.
30. Minett, M.S., et al., *Distinct Nav1.7-dependent pain sensations require different sets of sensory and sympathetic neurons.* Nat Commun, 2012. **3**: p. 791.
31. Kwan, K.Y., et al., *TRPA1 contributes to cold, mechanical, and chemical nociception but is not essential for hair-cell transduction.* Neuron, 2006. **50**(2): p. 277-89.
32. Nasser, S.A. and E.A. Afify, *Sex differences in pain and opioid mediated antinociception: Modulatory role of gonadal hormones.* Life Sci, 2019. **237**: p. 116926.
33. Gijsbers, K. and F. Nicholson, *Experimental pain thresholds influenced by sex of experimenter.* Percept Mot Skills, 2005. **101**(3): p. 803-7.
34. Kallai, I., A. Barke, and U. Voss, *The effects of experimenter characteristics on pain reports in women and men.* Pain, 2004. **112**(1-2): p. 142-7.
35. Niesters, M., et al., *Do sex differences exist in opioid analgesia? A systematic review and meta-analysis of human experimental and clinical studies.* Pain, 2010. **151**(1): p. 61-8.
36. Mogil, J.S., *Qualitative sex differences in pain processing: emerging evidence of a biased literature.* Nat Rev Neurosci, 2020. **21**(7): p. 353-365.
37. Rosen, S., B. Ham, and J.S. Mogil, *Sex differences in neuroimmunity and pain.* Journal of Neuroscience Research, 2017. **95**(1-2): p. 500-508.

38. Sorge, R.E. and S.K. Totsch, *Sex Differences in Pain.* Journal of Neuroscience Research, 2017. **95**(6): p. 1271-1281.
39. Bautista, D.M., et al., *The menthol receptor TRPM8 is the principal detector of environmental cold.* Nature, 2007. **448**(7150): p. 204-8.
40. Bohic, M., et al., *Loss of bhlha9 Impairs Thermotaxis and Formalin-Evoked Pain in a Sexually Dimorphic Manner.* Cell Rep, 2020. **30**(3): p. 602-610 e6.
41. Reker, A.N., et al., *The Operant Plantar Thermal Assay: A Novel Device for Assessing Thermal Pain Tolerance in Mice.* eNeuro, 2020. **7**(2).
42. Gregory, N.S., et al., *An overview of animal models of pain: disease models and outcome measures.* J Pain, 2013. **14**(11): p. 1255-69.
43. Barrot, M., *Tests and models of nociception and pain in rodents.* Neuroscience, 2012. **211**: p. 39-50.
44. Tappe-Theodor, A., T. King, and M.M. Morgan, *Pros and Cons of Clinically Relevant Methods to Assess Pain in Rodents.* Neurosci Biobehav Rev, 2019. **100**: p. 335-343.

Figures Legends

Fig. 1 Generation and validation of the *Scn10a*^{G1663S} mouse model. A) Targeting strategy by homologous recombination. The scheme shows the *Scn10a* WT allele, the targeted allele and the G1663S knock-in allele. The targeted allele was engineered bearing two homology arms of the original *Scn10a* endogenous gene and an auto-selection cassette. The 3' arm of homology (1.2 kb) consisted of a part of intron 28 and of a part of exon 28 bearing the S1663 mutation. The 3' arm was cloned into a targeting vector containing the LoxP-flanked ('floxed') neo cassette. The 5' arm of homology (1.1 kb) consisted of part of intron 28 and was cloned into the vector containing the auto-selection cassette and the 3' arm. The final mutant allele was obtained after excision of the selection cassette. Light blue box: Exon 28 containing the locus G1663/S1663; the PM was indicated with a brown star; Blue double arrows lines: indicate size of the arms; Red triangles: LoxP sites; Light grey box: Neomycin selection cassette; Green pentagon: Cre cassette. Different colored lightning block arrows show the primers used for genotyping. The green rectangle indicates the primer located in the Cre cassette (Fcre) used for DNA sequencing. **B)** Mutant allele sequence characterized through Sanger sequencing on a positive ES clone using a specific primer located in the Cre cassette (Fcre) amplifying only the mutant allele. The mutated nucleotide is indicated in red. **C)** Example of genotyping results on electrophoresis gel showing 3 different genotypes. For all samples, PCR3 and 4 gave no bands indicating that the selection marker was excised. For sample #7106: PCR1 and 2 gave one band each at 363 bp and 236 bp respectively. PCR5 gave one band of 194 bp. These reactions confirm that one LoxP site is still there and the *Scn10a*$^{G1663S/G1663S}$ genotype. For sample #7107: PCR1 and 2 gave two bands each at 363 bp and 250 bp; 236 bp and 123 bp respectively. One band at 194 bp for PCR5. These PCR reactions confirm that one LoxP site is still there and the *Scn10a*$^{+/G1663S}$ genotype. For sample #7108: PCR1 and 2 gave one band each at 250 bp and 123 bp respectively. No band for PCR5, confirming the wild type genotype. **D)** Upper panels. The wt and G1663S allele mRNA expression in DRG of *Scn10a*^{G1663S} heterozygous and homozygous mutant mice. *Scn10a* mRNA expression was normalized to *Hprt* expression. Homozygous mutant mice expressed *Scn10a*^{G1663S} transcript at levels comparable to wt transcript expression, and heterozygous mice express half levels of

each transcript type. Females, n=7-9/group; males, n=7-9/group. Data are presented as means ± SEM. One-way ANOVA analysis was followed by post-hoc analysis when appropriate. P values are indicated when significant (*P*<0.05) or close to significance. (See Supplementary Table 3 for detailed statistical analysis).

Fig. 2 *Scn10a*^{G1663S} mice show normal healthy conditions and proprioception capacities. A) Body weight of *Scn10a*^{G1663S} mice measured at the age of 7-11 weeks. Females, n=13-15/group; males, n=9-16/group. **B)** Muscle strength was evaluated by string test. Females, n=18-20/group; males, n=15-21/group. **C-D)** Motor coordination and balance were evaluated by the latency and the number of mistakes in the crenellated bar test. Females, n=17-21/group; males, n=16-21/group. A sex effect was detected in the string test. No sex and genotype effects were detected for the crenellated bar test. Data are expressed as means ± *SEM*. One-way ANOVA or Kruskal-Wallis analysis were followed by post-hoc analysis when appropriate. P values are indicated when significant (*P*<0.05) or close to significance. (See Supplementary Table 4 for detailed statistical analysis).

Fig. 3 *Scn10a*^{G1663S} mice show enhanced pain sensitivity to mechanical and cool stimuli. A) Sensitivity to touch analyzed by von Frey filaments. Females, n=17-18/group; males n=14-17/group. **B)** Noxious mechanical sensitivity analyzed by the tail pressure test. Females n=18-20/group; males n=16-20/group. **C)** Sensitivity to cool temperature analyzed by the acetone test. Females n=19-21/group; males n=16-20/group. **D)** Sensitivity to cold analyzed on the cold plate at 5°C. Females n=18-21/group; males n=17-20/group. G1663S mutant mice displayed hypersensitivity to von Frey filaments, and a tendency to increased sensitivity in the tail pressure test. Heterozygote female mice tended to display longer duration of withdrawal and flicking reactions following acetone application. No phenotype was identified in the cold plate at 5°C. Data are expressed as means ± SEM. One-way ANOVA or Kruskal-Wallis analyses were followed by post-hoc analysis when appropriate. P values are indicated when significant (*P*<0.05) or close to significance. (See Supplementary Table 5 for detailed statistical analysis).

Fig. 4 *Scn10a*^{G1663S} mice show enhanced pain sensitivity to heat stimuli. A) Hargreaves test. Females n=18-21/group; males n=18-22/group. **B)** Tail flick test.

Females n=19-20/group; males n=16-20/group. **C-E)** Hot plate test. The latency to the first hindpaw reaction is shown in left panels and the number of coping reactions in right panels. **C)** 47°C. n=17-22/group; males n=14-19/group. **D)** 50°C. Females n=19-21/group; males n=16-20/group**. E)** 54°C. Females n=17-22/group; males n=16-20/group. Homozygous *G1663S/G1663S* males showed increased sensitivity in the Hargreaves test. Mutant females had increased latency in the tail flick test. The male mutants were more sensitive than their wt counterparts on the 54°C hot plate. Data are expressed as means ± SEM. One-way ANOVA or Kruskal-Wallis analysis were followed by post-hoc analysis when appropriate. P values are indicated when significant (P<0.05) or close to significance. (See Supplementary Table 6 for detailed statistical analysis).

Supplementary Fig. 1 Alignment of SCN10A protein sequence in human and mouse species. The alignment shows that the residues deletion and insertions in mouse sequence as compared to human sequence. The site for 1662/1663 residue is highlighted.

Figures

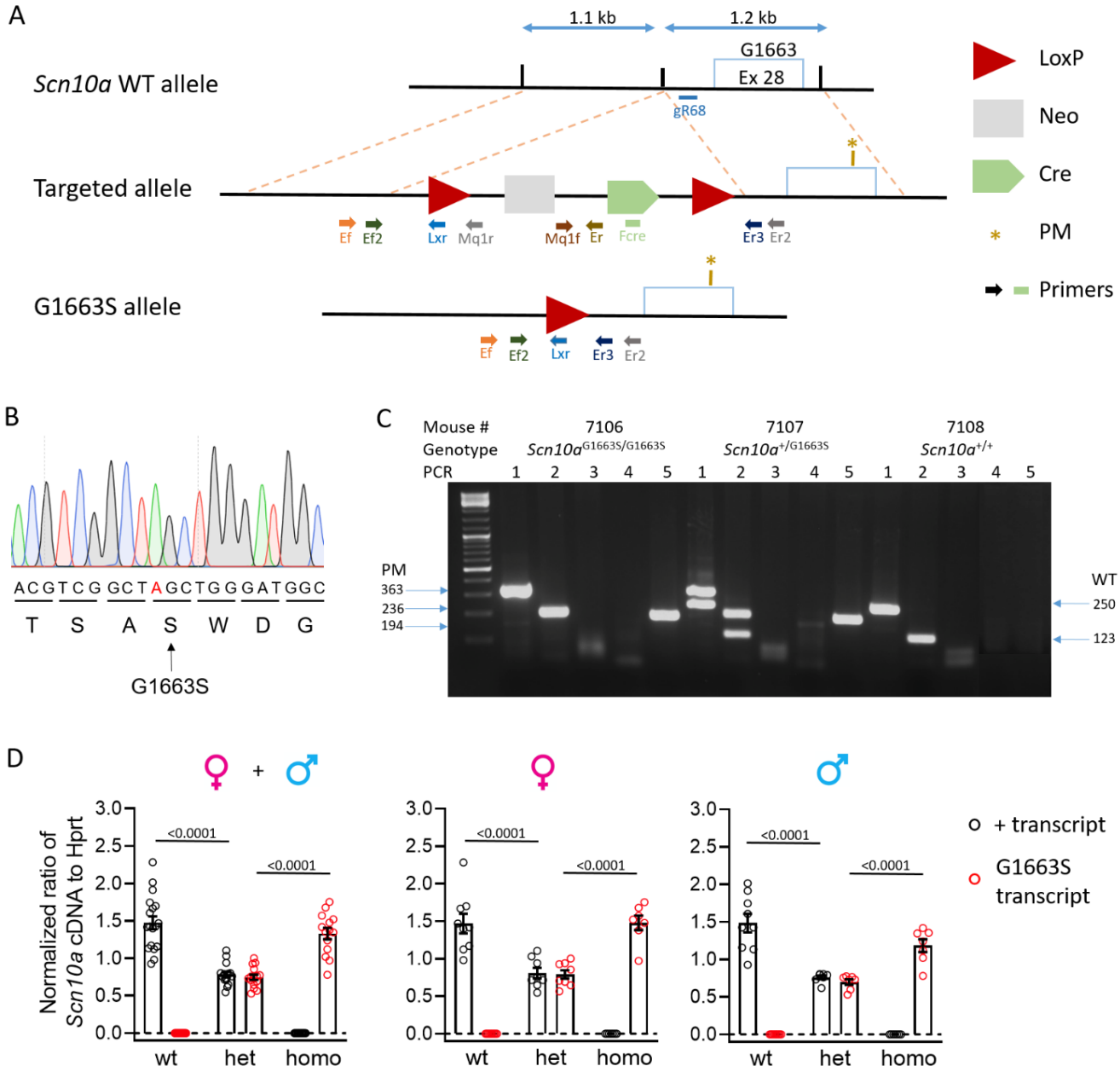

Figure 1

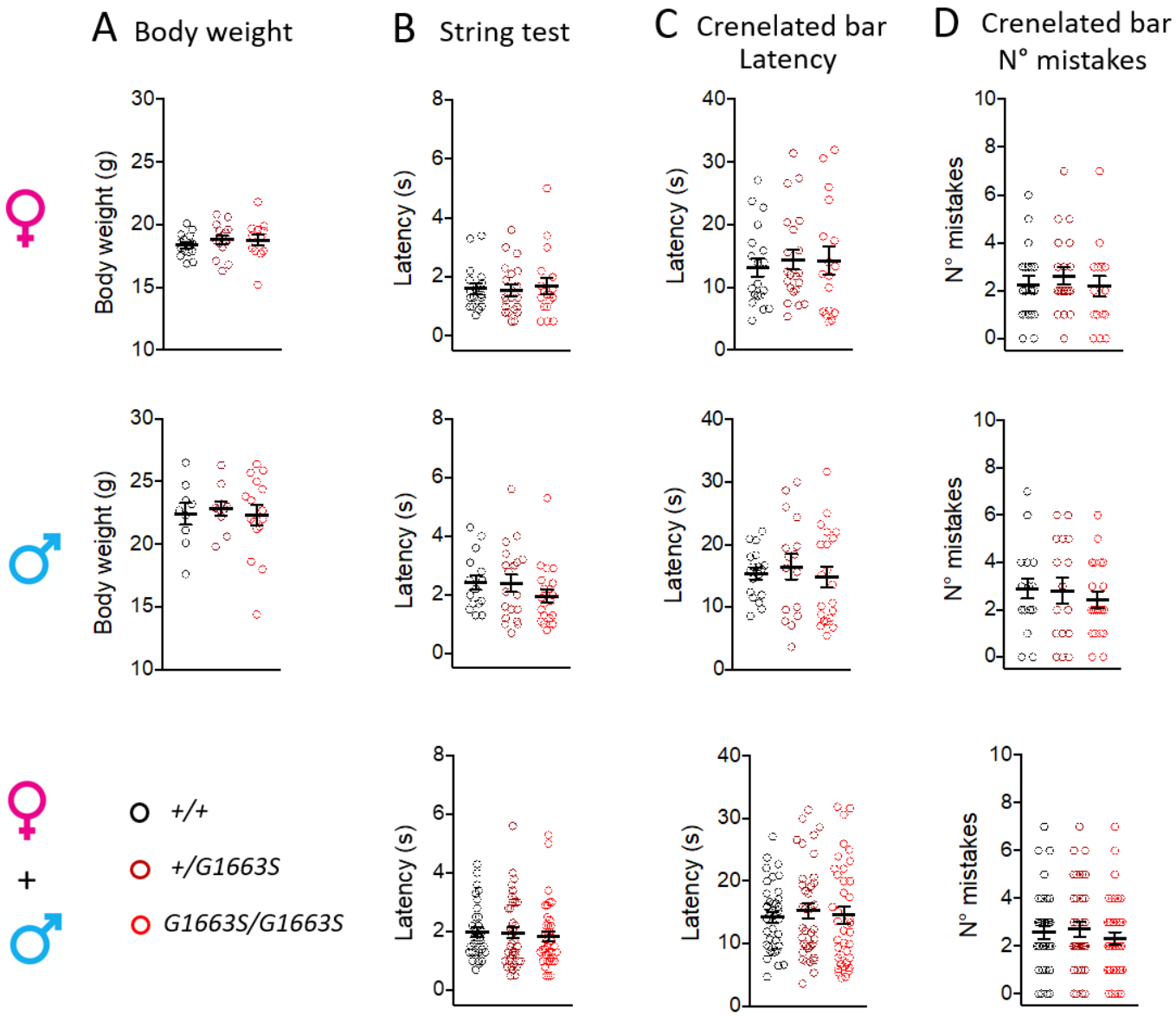
A Body weight
B String test
C Crenelated bar Latency
D Crenelated bar N° mistakes
Body weight (g)
Latency (s)
N° mistakes
+/+
+/G1663S
G1663S/G1663S

Figure 2

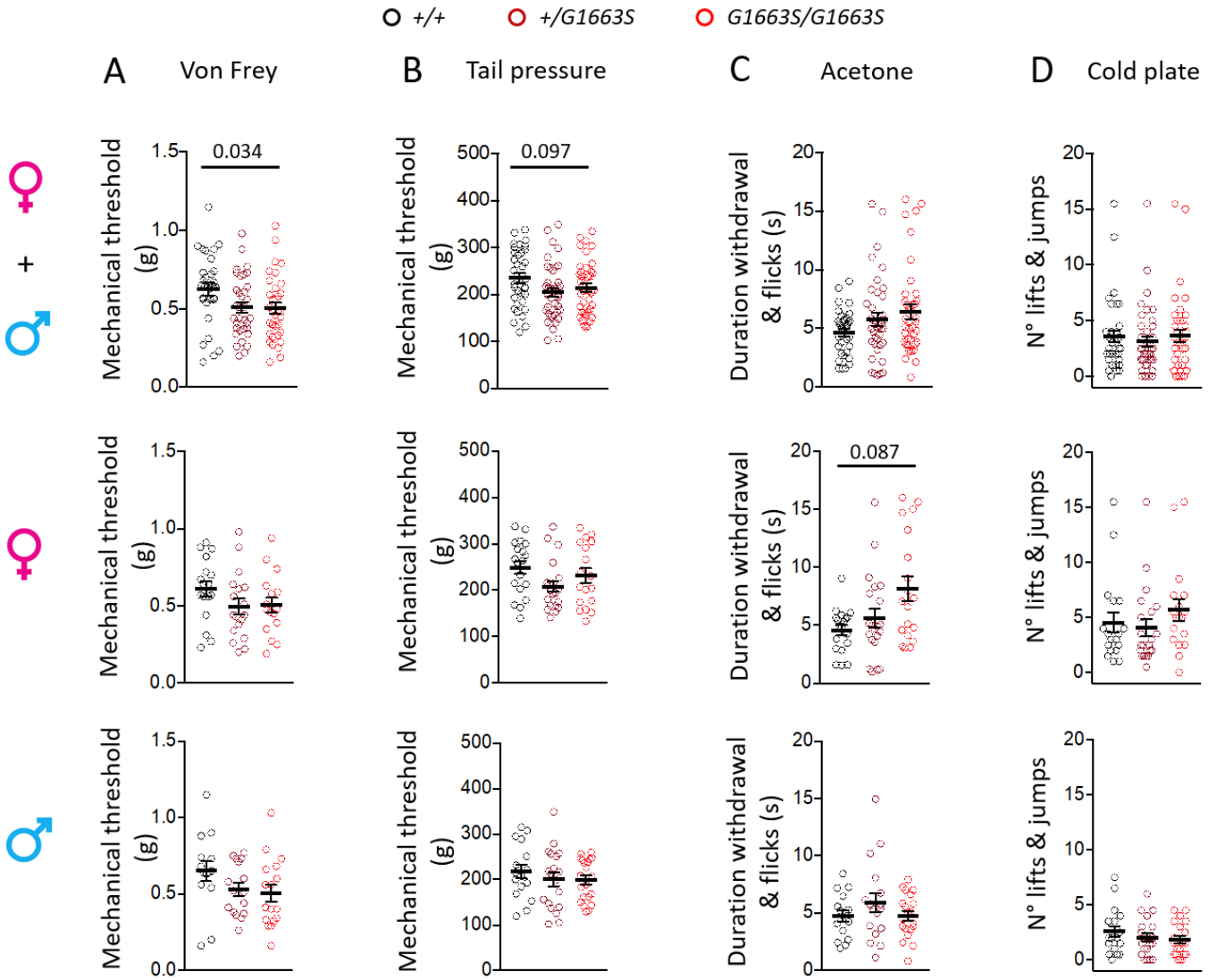
+/+
+/G1663S
G1663S/G1663S
A Von Frey
B Tail pressure
C Acetone
D Cold plate
♀ + ♂
♀
♂
Mechanical threshold (g)
Duration withdrawal & flicks (s)
N° lifts & jumps
0.034
0.097
0.087

Figure 3

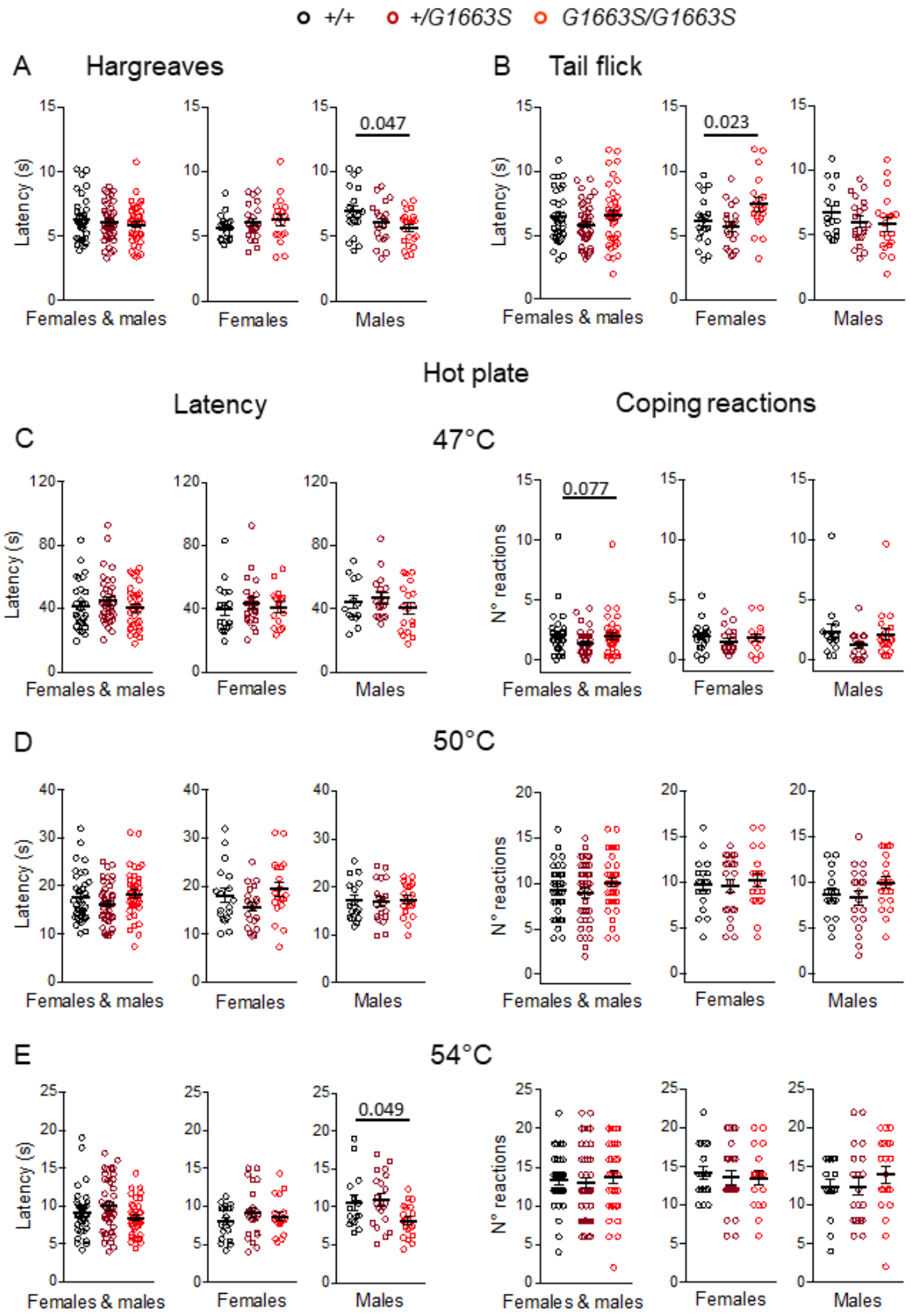
+/+
+/G1663S
G1663S/G1663S
A
Hargreaves
B
Tail flick
Latency (s)
0.047
0.023
Females & males
Females
Males
Hot plate
Latency
Coping reactions
C
47°C
N° reactions
0.077
D
50°C
E
54°C
0.049

Figure 4

Supplementary Materials

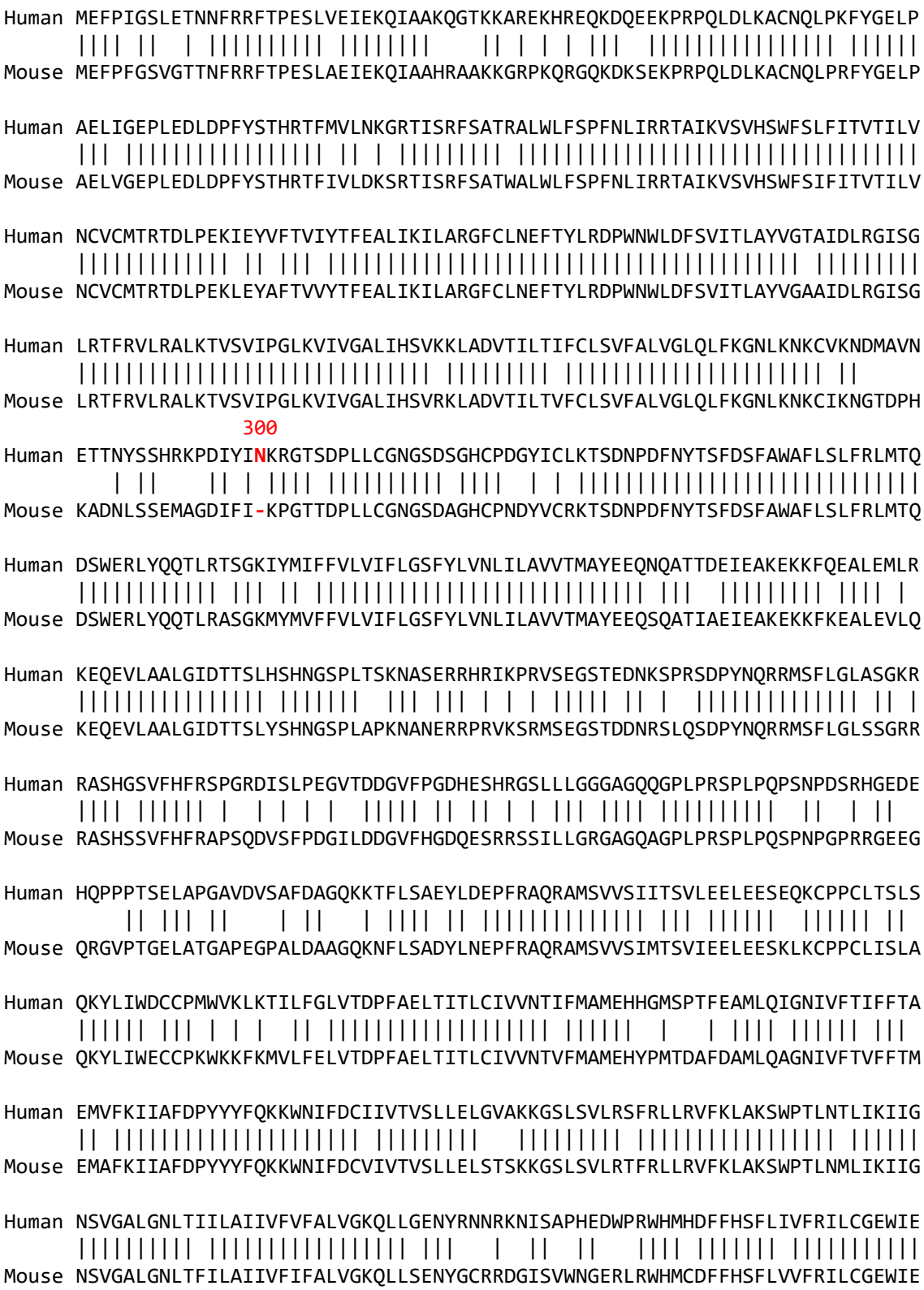

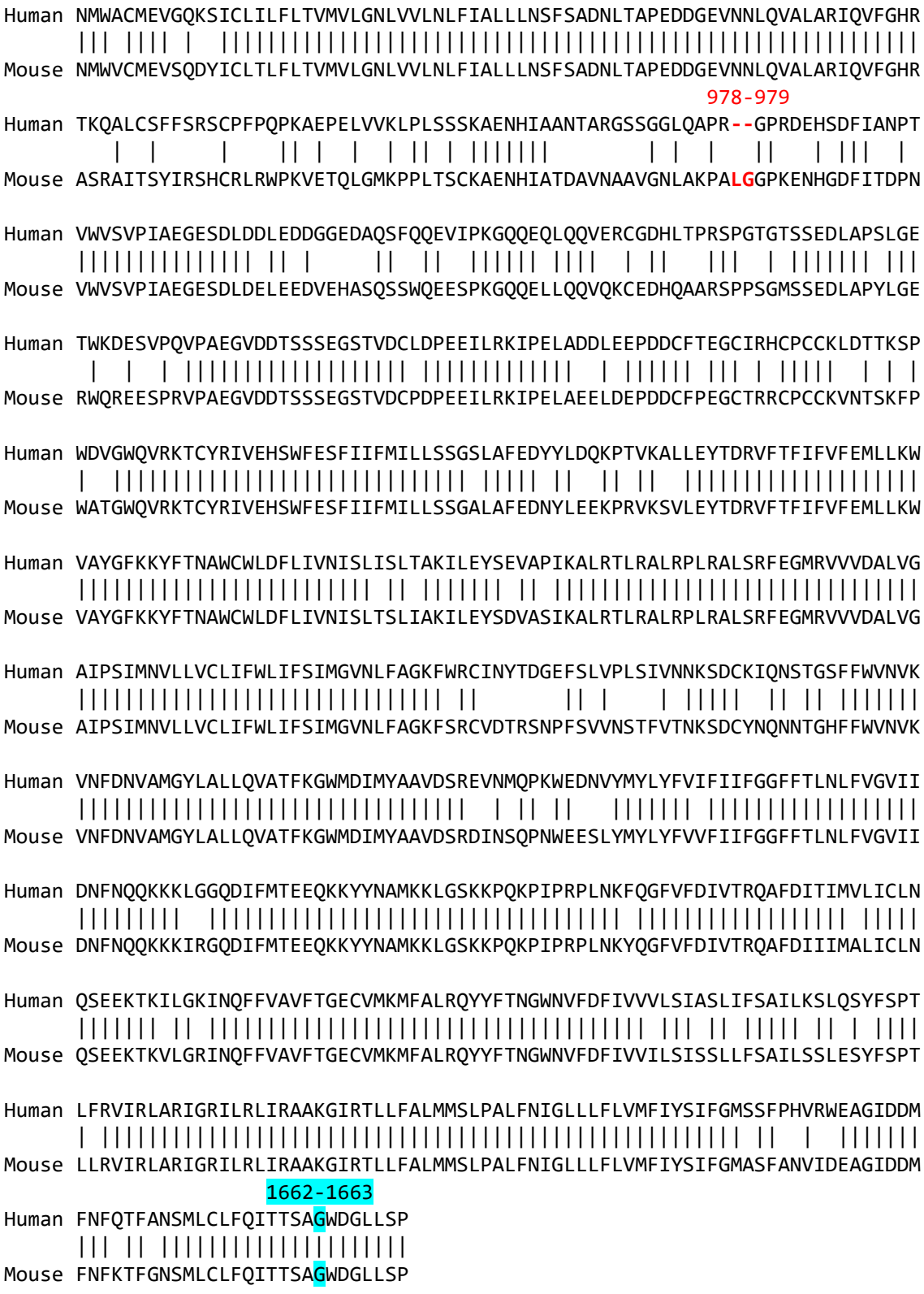

Supplementary figure 1

Supplementary Table 1A: PCR Primers sequence used for genotyping

Primers position	Primers sequence
Ef	CCAGCTGAACTTGGCTATGGAAGAG
Ef^2	GCTTGTAGATGAAGAAGGCAGGG
Er	GTGGGTGAAACAGCCACATGG
Er^2	CCGTTCAGTAGCTGTCCACTGC
Er^3	CCATCCCTTCCTTGGGTGGTG
Lxr	GAAGTTATACTAGAGCGGCCGTTCAC
Mf	CGGCCTCCTCCTCTTCCTCG
Mr	GGATGCCCACCGCTGGG
Mq1f	CCGCCCATTCTCCGCCC
Mq1r	TGCTAAAGCGCATGCTCCAGACTGC

Supplementary Table 1B: PCR reactions used for genotyping with the corresponding bands size

PCR	Region analyzed	Primer	Recombinant allele	PM allele	wt allele
PCR 1	Excision of selection marker	Ef / Er2	4484*	363	250
PCR 2	Excision of selection marker 2	Ef2 / Er3	4357*	236	123
PCR 3	5’ part of selection marker	Ef / Mq1r	286	-	-
PCR 4	3’ part of selection marker	Mq1f / Er	461	-	-
PCR 5	LoxP specific PCR	Ef / Lxr	194	194	-

Supplementary Table 2: Sequence of *Scn10a* probes and primers used for ddPCR

mRNA expression	
Scn10a^{G1663S}-Forward Primer sequence (5'-3')	TCGACTTCATTGTGGTGATTCT
Scn10a^{G1663S}-Reverse Primer sequence (5'-3')	GGTCCTGTGTTGAGGATGG
Scn10a^{+} Probe	/5HEX/ACGTCGGCT/ZEN/GGCTGGGATGG/3IABkFQ/
Scn10a^{G1663S} Probe	/56-FAM/ACGTCGGCT/ZEN/AGCTGGGATGG/3IABkFQ/

Supplementary Table 3: *Scn10a* transcript expression in wt and *Scn10a*^{G1663S} mutant mice

Gene	Tissue	Alleles	Analysis	Groups	Statistics
Scn10a	DRG	wt	One-way ANOVA for mouse genotype	F & M	***p*<0.0001** F (2, 44) = 144.6
				F	***p*<0.0001** F (2, 21) = 60.3
				M	***p*<0.0001** F (2, 20) = 77.28
			Šídák's multiple comparisons test	F & M +/+ vs +/*G1663S*	***p*<0.0001**
				F & M +/+ vs *G1663S/G1663S*	***p*<0.0001**
				F & M +/*G1663S* vs *G1663S/G1663S*	***p*<0.0001**
				F +/+ vs F +/*G1663S*	***p*=0.0001**
				F +/+ vs F *G1663S/G1663S*	***p*<0.0001**
				F +/*G1663S* vs F *G1663S/G1663S*	***p*<0.0001**
				M +/+ vs M +/*G1663S*	***p*<0.0001**
				M +/+ vs M *G1663S/G1663S*	***p*<0.0001**
				M +/*G1663S* vs M *G1663S/G1663S*	***p*<0.0001**
		PM*	One-way ANOVA for mouse genotype	F & M	***p*<0.0001** F (2, 44) = 245.5
				F	***p*<0.0001** F (2, 21) = 159.7
				M	***p*<0.0001** F (2, 20) = 157.0
			Šídák's multiple comparisons test	F & M +/+ vs +/*G1663S*	***p*<0.0001**
				F & M +/+ vs *G1663S/G1663S*	***p*<0.0001**
				F & M +/*G1663S* vs *G1663S/G1663S*	***p*<0.0001**
				F +/+ vs F +/*G1663S*	***p*=0.0001**
				F +/+ vs F *G1663S/G1663S*	***p*<0.0001**
				F +/*G1663S* vs F *G1663S/G1663S*	***p*<0.0001**
				M +/+ vs M +/*G1663S*	***p*<0.0001**
				M +/+ vs M *G1663S/G1663S*	***p*<0.0001**
				M +/*G1663S* vs M *G1663S/G1663S*	***p*<0.0001**
		wt + PM	One-way ANOVA for mouse genotype	F & M	*p*=0.221 F (2, 44) = 1.56
				F	*p*=0.700 F (2, 21) = 0.362
				M	*p*=0.094 F (2, 20) = 2.664

* PM, point mutation

Supplementary Table 4: Normal health conditions and proprioception capacities in wt and *Scn10a*^{G1663S} mutant mice

Test	Parameter	Analysis	Groups	Statistics
	Body weight	One-way ANOVA	F	*p*=0.596 F (2, 39) = 0.523
			M	*p*=0.883 F (2, 32) = 0.124
String test	Latency	Kruskal-Wallis test	F	*p*=0.855
			M	*p*=0.233
Crenelated bar	Latency	Kruskal-Wallis test	F & M	*p*=0.822
			F	*p*=0.820
			M	*p*=0.763
	Number of mistakes	Kruskal-Wallis test	F & M	*p*=0.682
			F	*p*=0.699
			M	*p*=0.710

Supplementary Table 5: Pain sensitivity to mechanical and cold stimuli in wt and *Scn10a*^{G1663S} mutant mice

Test	Parameter	Analysis	Groups	Statistics
Von Frey	Threshold	One-way ANOVA	F & M	***p*=0.034** F (2, 96) = 3.490
			F	*p*=0.216 F (2, 49) = 1.58
			M	*p*=0.157 F (2, 44) = 1.930
		Šídák's multiple comparisons test	F & M +/+ vs *+/G1663S*	*p*=0.082
			F & M +/+ vs *G1663S/G1663S*	*p*=0.058
		Unpaired t-test two-tailed	F & M +/+ vs *+/G1663S*	***p*=0.03**
			F & M +/+ vs *G1663S/G1663S*	***p*=0.025**
Tail pressure	Threshold	Kruskal-Wallis test	F & M	*p*=0.097
			F	*p*=0.123
			M	*p*=0.748
Acetone	Duration withdrawal and flicking	Kruskal-Wallis test	F & M	*p*=0.274
			F	*p*=0.087
			M	*p*=0.603
Cold Plate	Number of paw lifts and jumps	Kruskal-Wallis test	F & M	*p*=0.738
			F	*p*=0.206
			M	*p*=0.551

Supplementary Table 6: Pain sensitivity to heat stimuli in wt and *Scn10a*^{G1663S} mutant mice

Test	Parameter	T°	Analysis	Groups	Statistics
Hargreaves	Latency		One-way ANOVA	F & M	*p*=0.577 F (2, 115) = 0.553
				F	*p*=0.442 F (2, 55) = 0.827
				M	***p*=0.047** F (2, 57) = 3.237
			Šídák's multiple comparisons test	M +/+ vs M *+/G1663S*	*p*=0.273
				M +/+ vs M *G1663S/G1663S*	***p*=0.043**
			Unpaired t-test two-tailed	M +/+ vs M *+/G1663S*	*p*=0.139
				M +/+ vs M *G1663S/G1663S*	***p*=0.018**
Tail flick	Latency		One-way ANOVA	F & M	*p*=0.246 F (2, 111) = 1.422
				F	***p*=0.023** F (2, 55) = 4.049
				M	*p*=0.401 F (2, 53) = 0.930
			Šídák's multiple comparisons test	F +/+ vs F *+/G1663S*	*p*=0.729
				F +/+ vs F *G1663S/G1663S*	*p*=0.127
			Unpaired t-test two-tailed	F +/+ vs F *+/G1663S*	*p*=0.412
				F +/+ vs F *G1663S/G1663S*	*p*=0.073
Hot Plate	Latency 1st reaction	47°C	Kruskal-Wallis test	F & M	*p*=0.293
				F	*p*=0.587
				M	*p*=0.308
		50°C	One-way ANOVA	F & M	*p*=0.148 F (2, 111) = 1.943
				F	*p*=0.109 F (2, 56) = 2.309
				M	*p*=0.918 F (2, 52) = 0.086
		54°C	Kruskal-Wallis test	F & M	*p*=0.141
				F	*p*=0.643
				M	***p*=0.049**
			Dunn's multiple comparisons test	M +/+ vs M *+/G1663S*	*p*>0.999
				M +/+ vs M *G1663S/G1663S*	*p*=0.266
			Mann Whitney test two-tailed	M +/+ vs M *+/G1663S*	*p*=0.604
				M +/+ vs M *G1663S/G1663S*	*p*=0.087
Hot plate	Number of coping reactions	47°C	Kruskal-Wallis test	F & M	*p*=0.077
				F	*p*=0.429
				M	*p*=0.130
		50°C	One-way ANOVA	F & M	*p*=0.277 F (2, 111) = 1.3
				F	*p*=0.824 F (2, 56) = 0.194
				M	*p*=0.221 F (2, 52) = 1.55
		54°C	Kruskal-Wallis test	F & M	*p*=0.626
				F	*p*=0.883
				M	*p*=0.376

2. Creation of the knock-in mouse model for sodium channel *Scn10a*^{G1663S} mutation

The first part of my PhD project focused on creating the KI mouse model carrying the *Scn10a*^{G1663S} gain-of-function mutation in *Scn10a* gene. At the beginning of the project, we wanted to use the innovative CRISPR- Cas9 technology. As already detailed in the Materials and Methods section, we designed two strategies, the first one using gR93 and gR93b guide RNAs; the second one using gR93, gR93b, gR82 and gR85 guide RNAs. Both of these strategies failed as we could not obtain the mutant carrying the targeted PM. In addition, a high number of off-targets was recorded due to the high degree of conservation among the *Scn* genes of the region encompassing the G1663 amino-acid coding sequence. Results of these two strategies will be detailed below. We then defined a more classical strategy to engineer the mutation using HR in ES cells. The strategy was already described in the Materials and Methods section. We therefore describe the results below.

2.1 First and second targeting strategies using CRISPR-Cas9 technology

First strategy (Figure 11A): After checking gRNAs validity in vitro and preparing the ssODN to be injected, different quantities of gRNAs, Cas9 and ssODN were microinjected into eggs. First, two microinjections were performed and three weeks later 14 F0 mice were born. Details about these two microinjections are shown in Supplementary Table S7.

Supplementary table S7: 1st strategy - steps and details of one-cell embryo microinjection.

Concentration DNA/RNA (ng/ml)	Oocytes lineage	Nb of donor females	Nb of fertilized oocysts	Nb of injected oocysts	Nb of reimplanted oocysts	Nb of reimplanted females	Nb of born pups
Tube 1: Cas9 protein 20ng/µl +10ng/µl gR93 +10ng/µl gR93b +10ng/µl X501 ssDNA	C57BL/6N	13	142	142	68	3	2
		12	133	133	98	4	0
		13	46	46	39	2	3
Tube 2: Cas9 RNA 50ng/µl +25ng/µl gR93 +25ng/µl gR93b +10ng/µl X501 ssDNA		10	110	110	58	2	0
		10	104	104	104	3	9

The first 5 pups were genotyped. None of them held the PM. Genotyping was done using NheI enzyme and F1/R2 oligos. If the sample bears the PM, NheI enzyme will cut at the mutation locus; resulting in 2 bands of 236 bp and 275 bp on the gel. In addition, if the Cas9 is cutting simultaneously at the level of both guides, it results in a deletion of a 145 bp sequence which will be revealed by a 300-400 bp band in digested and not digested samples. This DNA analysis showed that there is no insertion of the mutation and that Cas9 is not cutting simultaneously at the level of gR93 and gR93b (Supplementary Figure 14A). Another genotype analysis was done using T7EI endonuclease. The sequence amplified with F2/R4 primers around gR93 has a size of 250 bp. If the Cas9 cuts at the level of gR93, one double band should appear on the gel (110 bp and 140 bp). The sequence amplified with F5/R2 oligos around gR93b has a size of 352 bp. If the Cas9 cuts at the level of gR93b, two bands of 126 bp and 226 bp should appear on the gel. Results showed that Cas9 was not cutting in any of these samples (Supplementary Figure 14B).

A

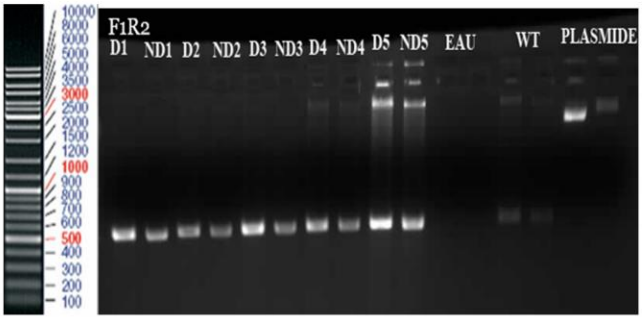

B

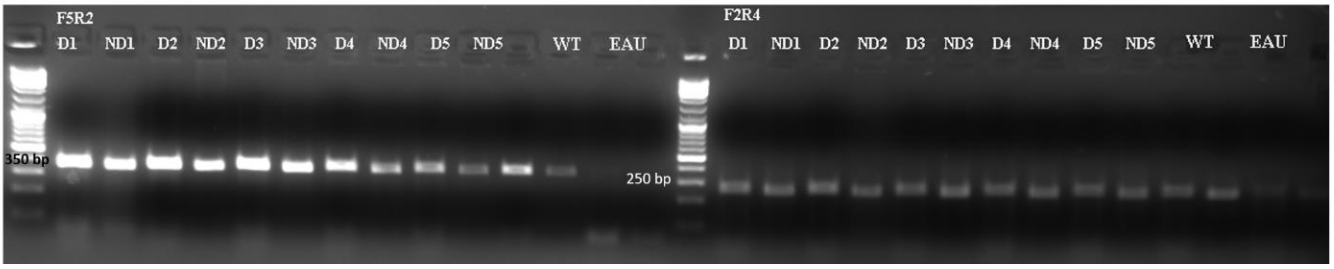

Supplementary Figure 14: Gel electrophoresis analysis of PCR amplification of *Scn10a* target in samples #1- #5.

A. Genotyping with NheI enzyme and F1/R2 primers. In all samples, a band of 500 bp was obtained. No mutant sample was detected. **B.** Genotyping with T7EI endonuclease and F5/R2 primers (left part) or F2/R4 primers (right part) around gR93 and F5/R2 oligos around gR93b. Cas9 enzyme was not cutting in any of the 5 samples.

The PCR products were sent for Sanger sequencing by GATC-Biotech sequencing services. As I was analyzing sequencing results, I noticed a lot of double peaks in samples sequence and at the same locus than in wt DNA. As I was searching for the reason, I blasted the sequence of

Scn10a gene in Ensembl and found that it shares high similarity with other *Scn* genes. In particular, *Scn10a* gene shares 94.15% similarity with *Scn5a* gene located in the same chromosome. After that, *Scn10a* gene and protein were aligned respectively with other *Scn* genes (Figure 15A-B) and proteins (Figure 15C). *Scn10a* gene sequence at the level of F1, F2 primers and gR93, gR93b guides shows a lot of similarities with other *Scn* genes, especially with *Scn5a* gene. This can explain the presence of double peaks in sample and wt DNA. The region at and around the mutation locus is highly similar between *Scn10a* and other *Scn* genes (Figure 15A). Based on this alignment and in order to regenotype the animals, we designed new primers that are specific for *Scn10a* (crF6; crR6; crR7; crR8) and others that are specific for *Scn5a* (crF11; crR9; crR10; crR11), having several mismatches between both genes (Figure 15B, Supplementary Table S1). Primers that are specific for *Scn5a* were used to detect off-targets in this gene. We focused on *Scn5a* which presented the highest similarity with *Scn10a*.

After primer validation and confirmation that there are no more double peaks in DNA sequence amplified by these new primers, I repeated the genotyping of samples #1 to #14, using F6/R6 for *Scn10a* gene and F11/R9 for *Scn5a* gene. None of the samples had the PM. Sample #11 sequencing analysis showed deletion of 3 nt at the level of gR93b cutting site, which leads to the deletion of Tyrosine at the level of the protein but does not induce a frameshift.

Second strategy: After failure of the first strategy, we designed a second strategy using the guides gR93, gR93b, gR82 and gR85 (Figure 11B). After checking gRNAs validity in vitro and preparing the ssODN to be injected, different quantities of gRNAs, Cas9 and ssODN were microinjected to eggs. Three microinjections were performed, and three weeks later 20 F0 mice were born. Details about these three microinjections are shown in Supplementary Table S8.

Figure 15: Alignment between *Scn10a* and other *Scn* genes and proteins.

A. *Scn10a* gene sequence at the level of F1, F2 oligos and gR93, gR93b guides shows a lot of similarities with other *Scn* genes, especially with *Scn5a* gene. The region at and around the mutation locus is highly similar between *Scn10a* and other *Scn* genes. **B.** New primers were designed. crF6; crR6; crR7; crR8 are specific for *Scn10a* and crF11; crR9; crR10; crR11 are specific for *Scn5a*. **C.** Alignment between Scn10a and other Scn proteins.

Nt and aa in black are the ones that are identical to *Scn10a* sequence among *Scn* family. Nt and aa in red are the ones that are different than *Scn10a*.

Supplementary Table S8: 2nd strategy - steps and details of the one-cell embryo microinjection.

Concentration DNA/RNA (ng/ml)	Oocytes lineage	Nb of donor females	Nb of fertilized oocysts	Nb of injected oocysts	Nb of reimplanted oocysts	Nb of reimplanted females	Nb of born pups
Tube 3: Cas9 H1 10ng/µl +10ng/µl gR82 +10ng/µl gR85 +10ng/µl gR93 +10ng/µl gR93b +10ng/µl X531 ssDNA2	C57BL/6N	13	109	109	95	3	5
Tube 4: Cas9 H1 10ng/µl +10ng/µl gR82 +10ng/µl gR85 +10ng/µl gR93 +10ng/µl gR93b +10ng/µl X531 ssDNA2		13	125	125	115	4	5
Tube 5: Cas9 H1 10ng/µl +10ng/µl gR82 +10ng/µl gR85 +10ng/µl gR93 +10ng/µl gR93b +10ng/µl X531 ssDNA2 +Rad51 10ng/µl		13	180	138	108	4	10

Among the twenty samples, none of them had the PM, but we got some mutants bearing deletions in *Scn10a* gene, as revealed by the T7EI endonuclease genotyping assay. In sample #28, the Cas9 endonuclease did cut at the level of gR85 and there was a deletion of approximately 12 bp, as shown by sequencing results. The gel electrophoresis results confirm this small deletion, by the presence of two bands at 400 bp and 300 bp when sample was digested by T7EI endonuclease, in contrast with the not digested sample. T7EI endonuclease forms a nick when there is a deletion of few nt; but when there is a big deletion (big whole), bands appear in digested and not digested sample (Supplementary Figure 15A). In sample #31, the Cas9 endonuclease did cut at the level of gR85 resulting in a deletion of a 72 bp sequence, as shown by sequencing

results. The presence of the 572 bp band on the gel confirms this deletion, and the 270 bp band corresponds to the size of the sequence from gR85 cutting site till R6 (Supplementary Figure 15B). In sample #33, the Cas9 endonuclease did cut at the level of gR93 and gR93b resulting in a deletion of a 150 bp sequence; which was also shown by the 494 bp band on the gel for digested and not digested samples. In the same time, the Cas9 endonuclease did cut at the level of gR93b in *Scn5*a gene leading to a deletion of 3 bp (Supplementary Figure 15C). Other off-targets on *Scn5a* gene were recorded among the twenty samples. In total, there were 13% off-targets compared to 18% on-targets.

A Analysis of F0-28 genotype for *Scn10a*

gR85

```
WT       CTACTGCGACCCCAACCGGCCCAACAGCAATGGCTCCAAGGGGAATTGTGGAAGCCCAGCGGTGGGCATCCTCTT
Del 12bp CTACTGCCACCCC............GGCAATGGCTCCAAGGCTAATTGGGGAATTGCGGAAGCGCACCTCCGCTT
```

ND D ND D ND D ND D
27 28 29 30

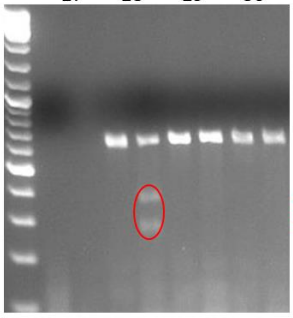

B Analysis of F0-31 genotype for *Scn10a*

gR85

```
WT       TTGGGCCGGTTGGGGTCGCAGTAGGGGGGTCCTGTGTTGAGGATGGGGCTGAGGAGGCCATCCCAGCCAGCCGACGTGGTGATCTG
Del 72bp TTG..........................................................................GTGGTGATCTG

WT       GAAAAGGCACAGCATGCTGTTGCCAAAGGTCTTGAAGTTGAACATGTCGTCGA
Del 72bp GAAAAGGCAACACATGCTGGTGGCAAAGGTC.......GGGGCTGAGGAGGCC
```

ND D ND D ND D ND D ND D
27 28 29 30 31

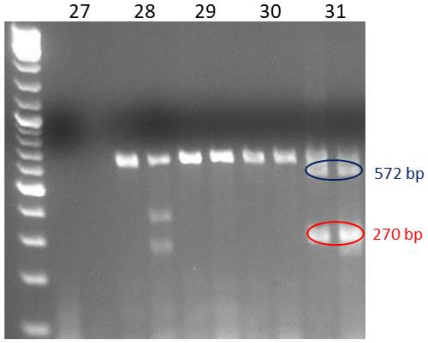

C Analysis of F0-33 genotype for *Scn10a*

gR93

gR93b

```
WT       AGCTTCGCTAATGTCATAGATGAGGCTGGCATCGACGACATGTTCAACTTCAAGACCTTTGGCAACAGCATGCTGTGCCTTTTCCA
Del 150bp AGCTT.....................................................................................

WT       GATCACCACGTCGGCTGGCTGGGATGGCCTCCTCAGCCCCATCCTCAACACAGGACCCCCCTACTGCGACCCCAACCGGCC
Del 150bp ..........................................................................ACCCCAACCGGCC
```

ND D ND D ND D ND D ND D ND D ND D
27 28 29 30 31 32 33

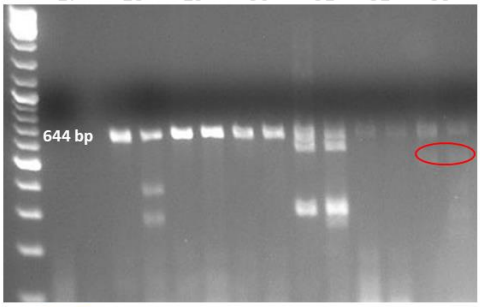

Analysis of off-target on *Scn5a*

gR93b

```
WT       CCCCTACTGCGACCCCAACCGGCCCAACAGCAATGGCTCCAAGGGGAATTGTGGA
Del 3bp  CCCCT...GTGACCCCAACCTGCCCAACAGCAATGGCTCCAGGGGGAACTGTGGG
```

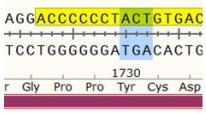

Supplementary Figure 15: Mutants bearing deletions in *Scn10a* gene as shown by sequencing results and gel electrophoresis.

A. In sample #28, the Cas9 endonuclease did cut at the level of gR85 and there was a deletion of approximately 12 bp, as shown by sequencing results. The gel electrophoresis results confirm this small deletion, by the presence of two bands at 400 bp and 300 bp when sample was digested by T7EI endonuclease, in contrast with the not digested sample. T7EI endonuclease forms a nick when there is a deletion of few nt; but when there is a big deletion (big whole), bands appear in digested and not digested sample. **B.** In sample #31, the Cas9 endonuclease did cut at the level of gR85 resulting in a deletion of a 72 bp sequence, as shown by sequencing results. The presence of the 540 bp band on the gel confirms this deletion, and the 270 bp band corresponds to the size of the sequence from gR85 cutting site till R6. **C.** In sample #33, the Cas9 endonuclease did cut at the level of gR93 and gR93b resulting in a deletion of a 150 bp sequence; which was also prouved by the 474 bp band on the gel. In the same time, the Cas9 endonuclease did cut at the level of gR93b in *Scn5*a gene leading to a deletion of 3 bp.

Nt in black are the ones that are similar between the different alleles. Nt in red are the ones that are different than the wt allele. Dots in purple indicate the sequences that were deleted. Arrows indicate the cutting sites of gRNAs. ND: Not digested. D: Digested.

2.2 Third targeting strategy using homologous recombination in ES cells

After the unsuccessful trials with CRISPR-Cas9 1st and 2nd strategies and the high percentage of off-targets, we moved to the HR in ES cells. The strategy and method used are described in the Materials and Methods section.

The recombinant ES clones #52 and #74 that were validated in the screening process were injected into BALB/CN female blastocysts. The first injection of clone #52 was realized in 14 blastocysts, but did not result in any chimera. A second injection of the same clone was done in 27 blastocysts and resulted in 7 chimeric males. Clone #74 injection in blastocysts resulted in 13 chimeric males. Only highly chimeric males with a color score > 70% were mated with C57BL/6NCrl wt females. 4 chimeric males with a score > 80% coming from clone #52 were mated with wt females and it resulted in only a few F1 black mice. 3 chimeric males with a score > 70% coming from clone #74 were mated with wt females and resulted in many F1 black mice. 14 of them (# 31, 32, 34, 36, 37, 38, 39, 41, 43, 44, 47, 51, 52, 59) carried the targeted allele and were confirmed *Scn10a*$^{+/G1663S}$ (Figure 16). Three confirmed *Scn10a*$^{+/G1663S}$ male mice # 36, 37 and 38 were used for in vitro fertilization with wt females. Heterozygous mice were subsequently crossed to generate mice with homogeneous genotype. Several breedings were done in order to generate enough mice needed for the different cohorts. Genotype ratios obtained by *+/G1663S* X *+/G1663S* breedings are presented in Table 3. The obtained ratio correlate well with Mendelian ratio.

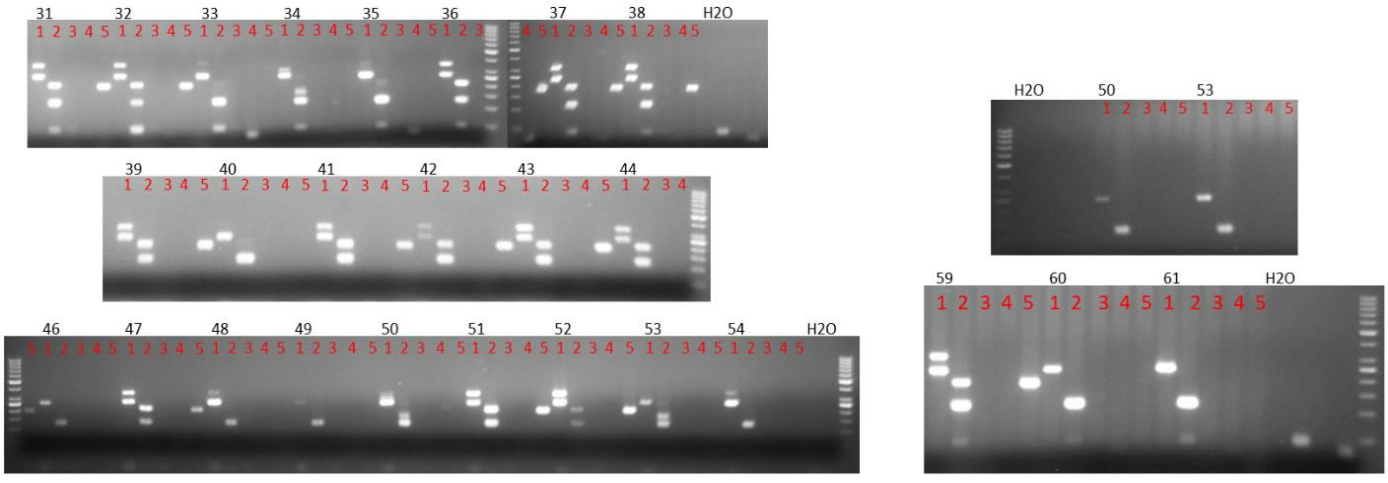

Figure 16: Genotyping results of F1 black mice coming from clone #74. The PCR reactions 1-5 were performed as described in the manuscript part. Heterozygous mice were confirmed by the presence

of two bands of 363 bp and 250 bp in PCR1; two bands of 236 bp and 123 bp in PCR2; no band in PCR3 and 4; and one band at 194 bp in PCR5. 14 mice were heterozygous for the mutation: # 31, 32, 34, 36, 37, 38, 39, 41, 43, 44, 47, 51, 52, 59.

Table 3: Genotype ratios of *Scn10a*^{G1663S} mouse line

Type of breeding	*+/G1663S* X *+/G1663S*		
Genotype	wt	*+/G1663S*	*G1663S/G1663S*
Females	57	106	34
Males	47	86	50
% in total	27.4%	50.5%	22.1%

3. Molecular and cellular characterization of *Scn10a*^{G1663S} mice

3.1 *Scn10a* transcript expression in *Scn10a*^{G1663S} mice

The *Scn10a* transcript expression level in DRG of *Scn10a*^{G1663S} mice was reported in the publication manuscript and again here (Figure 17A). *Scn10a*$^{+}$ and *Scn10a*^{G1663S} transcripts were equally expressed in DRG of +/+ or *G1663S/G1663S* mutant mice, respectively, and in both sexes, indicating that the mutation did not alter *Scn10a* expression. Heterozygous *+/G1663S* mice expressed about 50% of each *Scn10a*$^{+}$ and *Scn10a*^{G1663S} transcripts in DRG (Figure 17A).

Here we report *Scn10a* transcript expression in spinal cord of wt and *Scn10a*^{G1663S} mutant mice and we compare *Scn10a*$^{+}$ transcript expression in spinal cord to its expression in DRG. *Scn10a* transcript expression in spinal cord was very low and even not detectable in a significant part of samples from the three genotypes. The Kruskal-Wallis test revealed a genotype effect for *Scn10a*$^{+}$ transcript expression in grouped sexes and for *Scn10a*^{G1663S} transcript expression in grouped and separated sexes (Figure 17B, and Supplementary Table S9).

When ratios of *Scn10a*$^{+}$ and *Scn10a*^{G1663S} transcripts were summed, no effect on genotype or sex was detected by two-way ANOVA. *Scn10a* transcript expression in spinal cord was not altered by the G1663S mutation (Supplementary Table S9). *Scn10a*$^{+}$ transcript expression was highly different between DRG and spinal cord. *Scn10a*$^{+}$ transcript mean expression level in spinal cord was 300 times lower than in DRG (Figure 17C, and Supplementary Table S9).

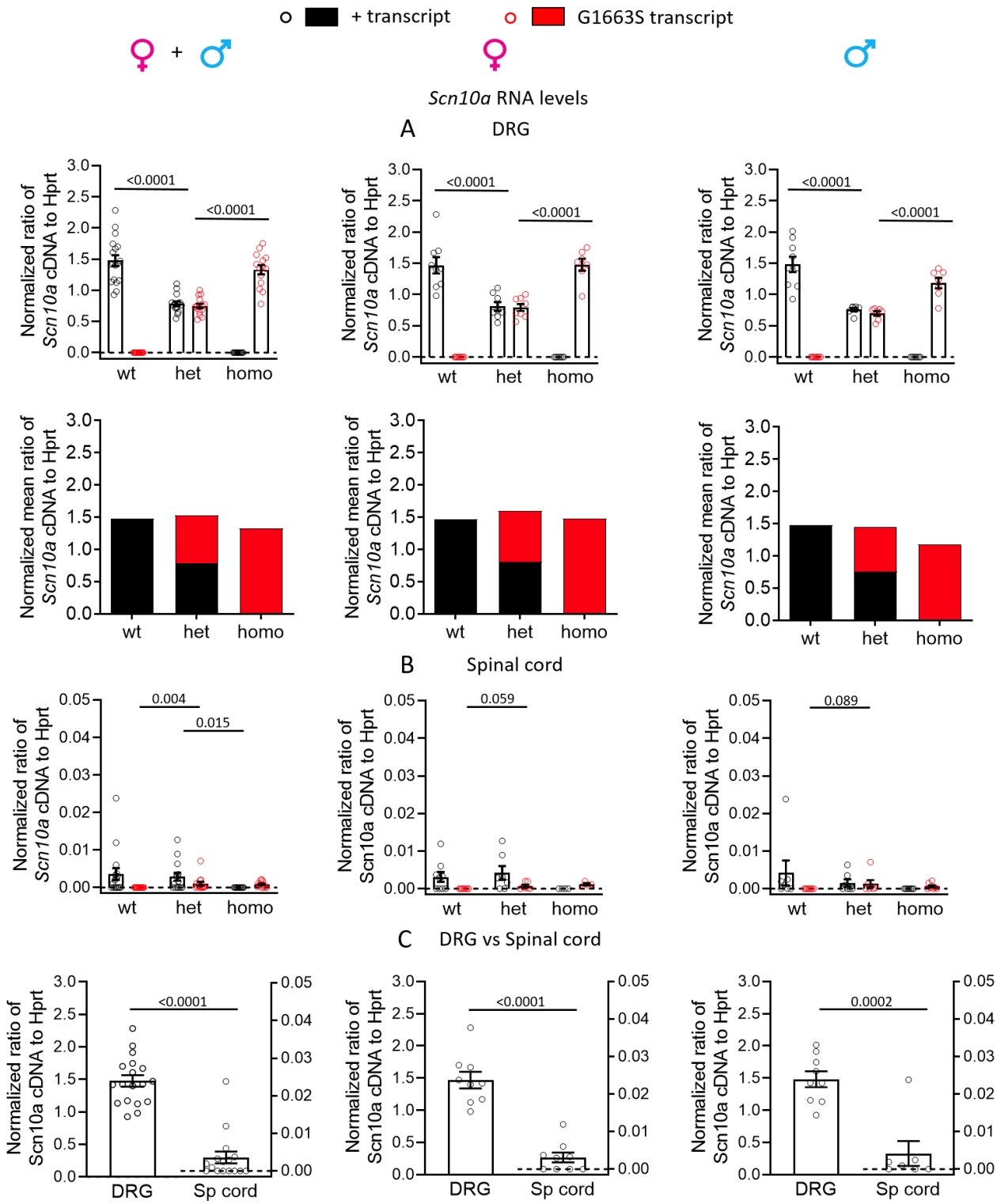

Figure 17: *Scn10a* mRNA expression in DRG and spinal cord of *Scn10a*^{G1663S} mutant mice.

A. *Scn10a* + and G1663S mRNA expression in DRG of *Scn10a*^{G1663S} heterozygous and homozygous mutant mice. *Scn10a* mRNA expression was normalized to *Hprt* expression. Upper panels. Homozygous mutant mice expressed G1663S transcript at levels comparable to + transcript expression by wt mice, and

heterozygous mice express half levels of each transcript type. Lower panels. The *Scn10a*^{G1663S} mutation did not alter global *Scn10a* transcript expression in heterozygous and homozygous mutant mice. Data are presented as means ± SEM. Females, n=7-9/group; males, n=7-9/group. **B.** *Scn10a* + and G1663S mRNA expression in spinal cord of *Scn10a*^{G1663S} heterozygous and homozygous mutant mice. The *Scn10a*^{G1663S} mutation did not alter global *Scn10a* transcript expression in heterozygous and homozygous mutant mice. Females, n=4-9/group; males, n=7-8/group. **C.** *Scn10a*$^{+}$ transcript expression is highly different between DRG and spinal cord, with expression 300 times higher in DRG. Females, n=7-9/group; males, n=7-9/group. mRNA expression was normalized to *Hprt* expression. Data are expressed as means ± *SEM*. One-way ANOVA or Kruskal-Wallis analysis were followed by post-hoc analysis when appropriate. P values are indicated when significant (P<0.05) or close to significance. For comparison of *Scn10a*$^{+}$ transcript expression in DRG and spinal cord, we did Mann-Whitney test. (See Supplementary Table S9 for detailed statistical analysis).

Supplementary Table S9: Statistical analysis of *Scn10a* transcript expression in wt and *Scn10a*^{G1663S} mutant mice

Gene	Tissue	Alleles	Analysis	Groups	Statistics
Scn10a	Spinal cord	wt	Kruskal-Wallis test	F & M	***p*=0.006**
				F	*p*=0.126
				M	*p*=0.055
			Dunn's multiple comparisons test	F & M +/+ vs *+/G1663S*	*p*>0.999
				F & M +/+ vs *G1663S/G1663S*	***p*=0.014**
				F & M *+/G1663S* vs *G1663S/G1663S*	***p*=0.015**
				M +/+ vs M *+/G1663S*	*p*>0.999
				M +/+ vs M *G1663S/G1663S*	*p*=0.081
				M *+/G1663S* vs *G1663S/G1663S*	*p*=0.241
		PM	Kruskal-Wallis test	F & M	***p*=0.0001**
				F	***p*=0.0004**
				M	***p*=0.030**
			Dunn's multiple comparisons test	F & M +/+ vs *+/G1663S*	***p*=0.004**
				F & M +/+ vs *G1663S/G1663S*	***p*=0.0004**
				F & M *+/G1663S* vs *G1663S/G1663S*	*p*>0.999
				F +/+ vs *+/G1663S*	*p*=0.059
				F +/+ vs *G1663S/G1663S*	***p*=0.003**
				F *+/G1663S* vs *G1663S/G1663S*	*p*=0.629
				M +/+ vs M *+/G1663S*	*p*=0.089
				M +/+ vs M *G1663S/G1663S*	*p*=0.054
				M *+/G1663S* vs *G1663S/G1663S*	*p*>0.999
		wt + PM	Kruskal-Wallis test	F & M	*p*=0.377
				F	*p*=0.667
				M	*p*=0.696
	DRG vs Spinal cord	wt	Mann Whitney test two-tailed	F & M	***p*<0.0001**
				F	***p*<0.0001**
				M	***p*=0.0002**

3.2 *Scn9a* and *Penk* transcripts expression in *Scn10a*^{G1663S} mice

Some previous publications had shown a regulation of *Penk* transcripts in *Scn9a* mutant mice but not *Scn10a* mutant mice [187, 188]. Also the *Scn10a*^{G1663S} mutation may have led to an alteration of *Scn9a* expression. Therefore, in addition to evaluating *Scn10a* transcript expression in *Scn10a*^{G1663S} mice, we have also analyzed *Scn9a* and *Penk* transcripts expression in these mice.

Scn9a transcript expression level was determined in DRG of wt and *Scn10a*^{G1663S} mice. A sex effect was detected (two-way ANOVA $F_{1, 41}$=4.716, *p*=0.036) and no genotype effect. *Scn9a* transcript was similarly expressed in DRG of +/+ or *G1663S/G1663S* mutant mice and in both sexes, indicating that the mutation did not alter *Scn9a* expression (Figure 18 and Supplementary Table S10).

Penk transcript expression level was determined in DRG and spinal cord tissues of wt and *Scn10a*^{G1663S} mice. No genotype or sex effect was detected for *Penk* transcript expression in DRG, however a sex effect was revealed for *Penk* transcript expression in spinal cord (two-way ANOVA $F_{1, 40}$=32.94, p<0.0001) and a genotype effect close to be significant was detected for females (one-way ANOVA $F_{2, 19}$=2.763, p=0.088). The *Scn10a*^{G1663S} mutation did not alter *Penk* expression in DRG and spinal cord. *Penk* transcript expression level in DRG was 15 times lower than *Scn10a* transcript expression in DRG. In the spinal cord, *Penk* transcript expression level was 10 times higher than in DRG and 200 times higher than *Scn10a* transcript expression in spinal cord. (Figure 18 and Supplementary Table S10).

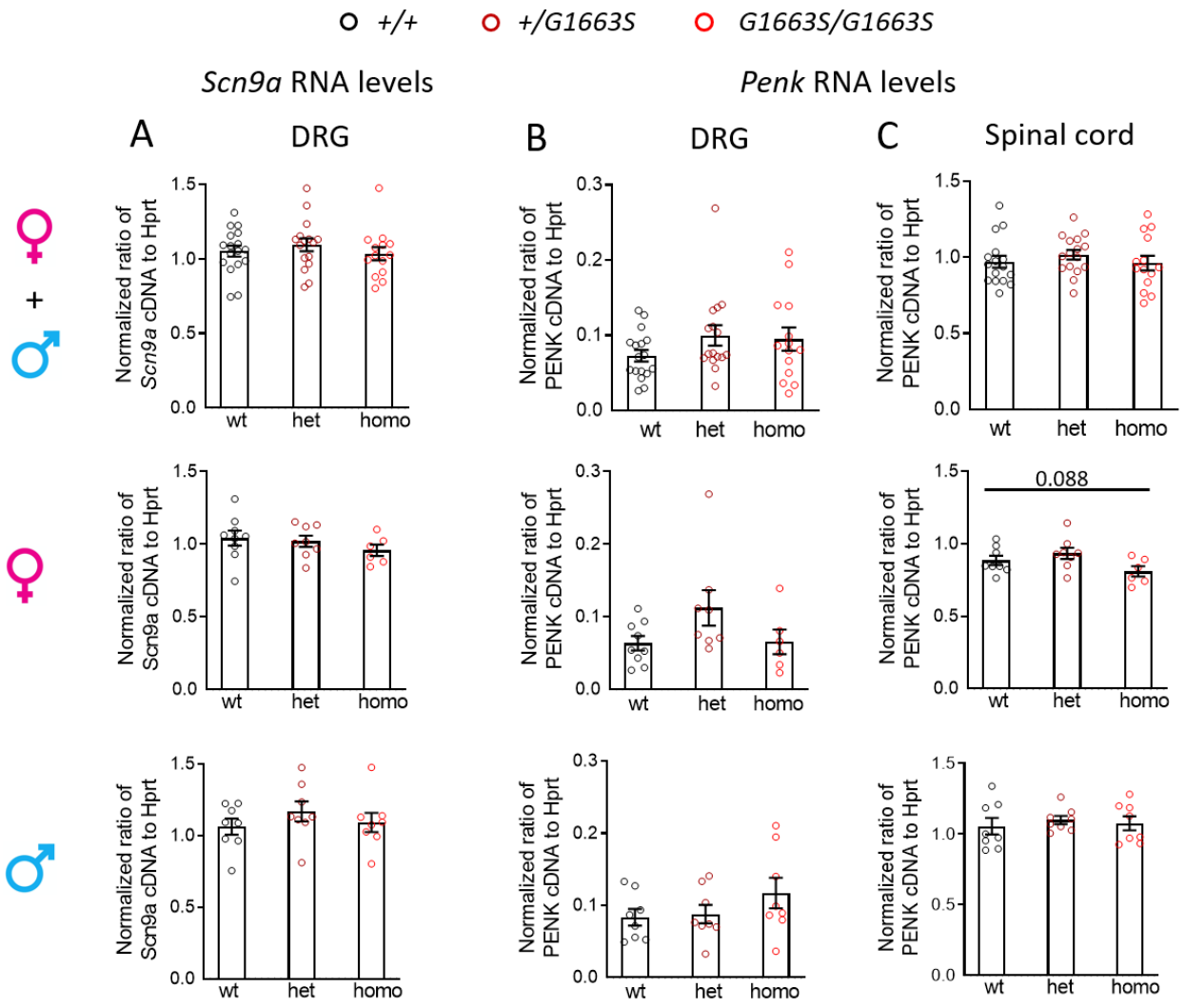

Figure 18: *Scn9a* and *Penk* mRNA expression in *Scn10a*^{G1663S} mutant mice. A. *Scn9a* mRNA expression in DRG of *Scn10a*^{G1663S} heterozygous and homozygous mutant mice. *Scn10a*^{G1663S} mutation didn't alter *Scn9a* transcript expression in DRG. Females, n=6-9/group; males, n=8/group. **B.C.** *Penk* mRNA expression in **B.** DRG of *Scn10a*^{G1663S} heterozygous and homozygous mutant mice, females, n=6-9/group; males, n=8/group; and in **C.** spinal cord of *Scn10a*^{G1663S} heterozygous and homozygous mutant mice, females, n=6-8/group; males, n=8/group. *Scn10a*^{G1663S} mutation didn't alter *Penk* transcript expression in DRG and spinal cord. mRNA expression was normalized to Hprt expression. Data are expressed as means ± SEM. One-way ANOVA or Kruskal-Wallis analysis were followed by post-hoc analysis when appropriate. P values are indicated when significant (P<0.05) or close to significance (See Supplementary Table S10 for detailed statistical analysis).

Supplementary Table S10: Statistical analysis of *Scn9a* and *Penk* transcripts expression in wt and *Scn10a*^{G1663S} mutant mice

Gene	Tissue	Analysis	Groups	Statistics
Scn9a	DRG	One-way ANOVA	F & M	p=0.588; F (2, 44) = 0.537
			F	p=0.462; F (2, 20) = 0.802
			M	p=0.501; F (2, 21) = 0.713
Penk	DRG	Kruskal-Wallis test	F & M	p=0.287
			F	p=0.118
			M	p=0.353
	Spinal cord	One-way ANOVA	F & M	p=0.572; F (2, 43) = 0.566
			F	p=0.088; F (2, 19) = 2.763
			M	p=0.807; F (2, 21) = 0.217

3.3 IENFD of *Scn10a*^{G1663S} mice

IENF density and morphology correlate well with small nerve fiber dysfunction and are important criterias in assessing SFN patients. In order to investigate if the *Scn10a*^{G1663S} mutation in mice induce an alteration in IENFD, we measured the IENFD in hindpaw plantar skin samples of WT and *Scn10a*^{G1663S} mutant mice. The analysis is undergoing.

Here we show the IENF that are well visible in a WT mouse hindpaw skin sample (Figure 19).

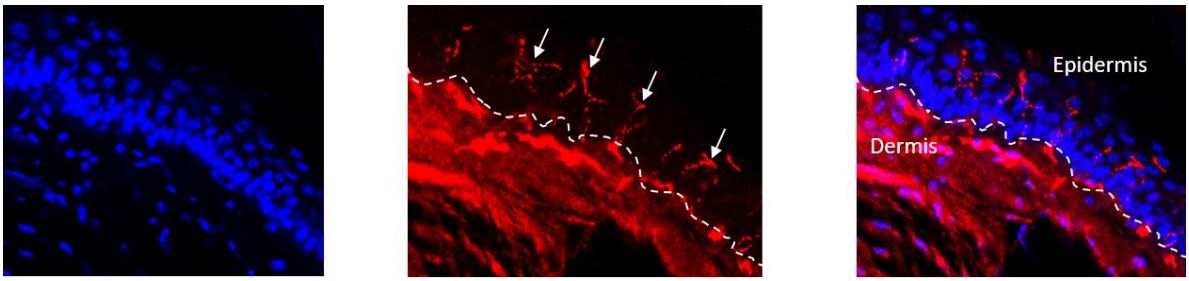

Figure 19: Intraepidermal nerve fibers in skin of a wt mouse. A representative picture showing the plantar side of a hindpaw skin sample of a wt mouse. DAPI staining in blue for cell nuclei. PGP9.5 staining in red for nerve fibers. The epidermis and dermis layers are indicated in the figure. The dermo-epidermal junction was drawn with the scribble dashed line. The intraepidermal nerve fibers are well seen and are indicated with white arrows.

4. Behavioral assessment of *Scn10a*^{G1663S} mutant mice for pain sensitivity

The thesis part with the manuscript to be submitted for publication contains the main findings for a pain phenotype in *Scn10a*^{G1663S} mice. These are summarized below.

For sensitivity for mechanical stimuli, *+/G1663S* and *G1663S/G1663S* mice showed an enhanced sensitivity to nonnoxious stimuli compared to their wt littermates, as measured in the von Frey test (Figure 3A), but not to noxious stimuli, as assessed by tail pressure (Figure 3B).

With regard to sensitivity to cooling, following acetone application on the hind paw, female mutants showed quite higher behavioural response (Figure 3C). In the cold plate test at 5°C, mutant and WT mice of both sexes had comparable reactions (Figure 3D).

For heat sensitivity, in the Hargreaves test, male *G1663S/G1663S* mice withdrew their hind paws earlier than male +/+ mice (Figure 4A), however female mutant had an overall higher latency time in the tail flick test (Figure 4B). In the Hot plate assay, a shorter latency to the first hind paw reaction was found for G1663S male mice at 54°C (Figure 4C-E).

In the following part, additional results are shown: scratching and wiping behaviors (part 4.1), the latency to the first withdrawal reaction and the mean number of hind paw lifts and total jumps in the cold plate at 5°C and 0°C (part 4.2) and the number of flicking and licking reactions in the hot plate at 47°C, 50°C and 54°C (part 4.3).

4.1 Scratching behavior of *Scn10a*^{G1663S} mice

The number and duration of spontaneous wiping and scratching were measured during camera recording of mice movement for 20 minutes. A part of the mice did not perform any scratching or wiping behaviors during the 20 minutes recording.

No genotype or sex effect was detected for the number and duration of wiping bouts, number and duration of scratching bouts (Figure 20 and Supplementary Table S10). Mutant and wt mice of both sexes had comparable reactions for these four parameters.

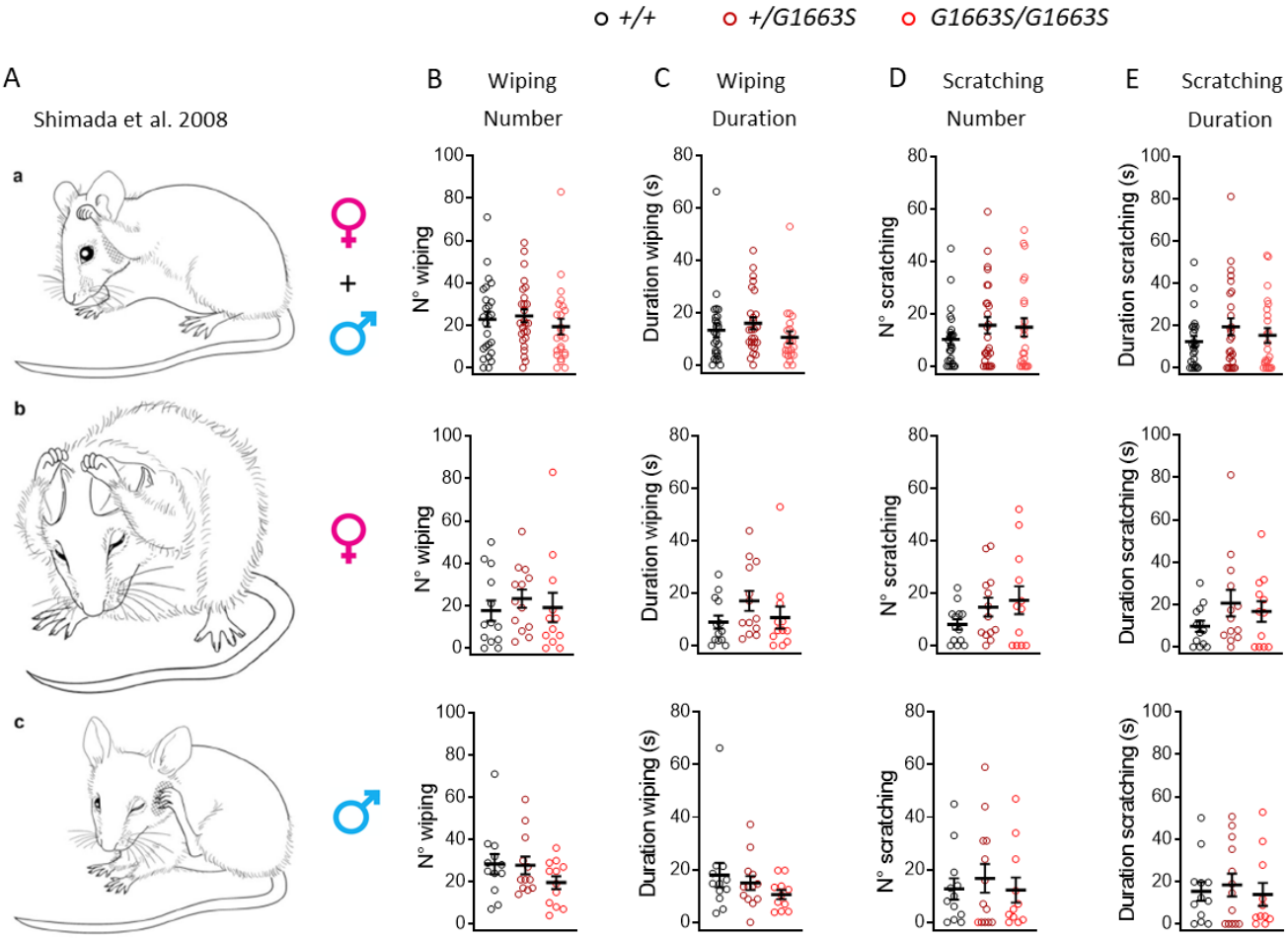

Figure 20: Scratching and wiping behaviors of *Scn10a*^{G1663S} mice. A. a) Wiping of the cheek with the forelimb, which is an indicator of pain. b) Grooming with forelimbs. c) Scratching of the cheek with the hind limb, which is an indicator of itch. Adapted from Shimada, S. G. et al., 2008 [186]. **B-C.** Wiping bouts number **B.** and duration **C. D-E.** Scratching bouts number **D.** and duration **E.** Females, n=12-13/group; males, n=12-13/group. No abnormal phenotype was recorded in the number and duration of wiping and scratching bouts. Data are expressed as means ± SEM. One-way ANOVA or Kruskal-Wallis analysis were followed by post-hoc analysis when appropriate. P values are indicated when significant (P<0.05) or close to significance. (See Supplementary Table S11 for detailed statistical analysis).

Supplementary Table S11: Statistical analysis of wiping and scratching behaviours in wt and *Scn10a*^{G1663S} mutant mice

Parameter	Analysis	Groups	Statistics
Wiping Number	Kruskal-Wallis test	F & M	p=0.338
		F	p=0.459
		M	p=0.358
Wiping Duration		F & M	p=0.166
		F	p=0.127
		M	p=0.265
Scratching Number		F & M	p=0.722
		F	p=0.426
		M	p=0.956
Scratching duration		F & M	p=0.676
		F	p=0.408
		M	p=0.910

4.2 Sensitivity to cold in *Scn10a*^{G1663S} mice

The mean number of hind paw lifts and total jumps at 5°C was shown in the publication manuscript and again here in Figure 21 in order to complete this part. The latency to the first withdrawal reaction and the mean number of hind paw lifts and total jumps were measured at 5°C and 0°C.

The latency to the first withdrawal reaction in the cold plate at 5°C and 0°C revealed a sex effect (two-way ANOVA $F_{1, 107}$=12.10, p=0.0007 and $F_{1, 88}$=9.019, p=0.0035, respectively). A genotype effect was detected for the number of hind paw lifts and total jumps in the 0°C cold plate, where males *+/G1663S* were doing less number of reactions than males wt (Figure 21 and Supplementary Table S12).

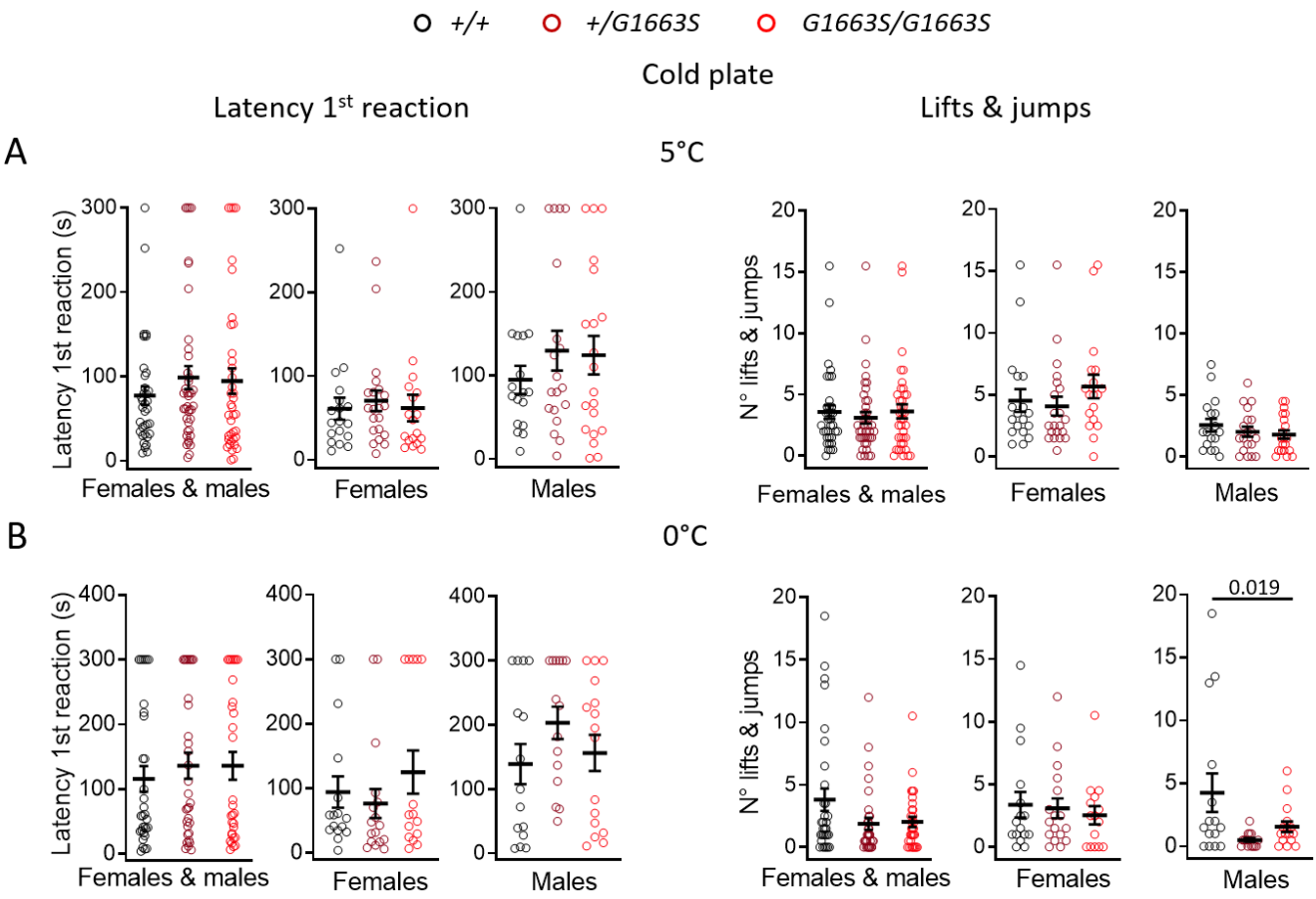

Figure 21: *Scn10a*^{G1663S} mice show normal pain sensitivity in the cold plate at 5°C and 0°C.

A-B) Latency to the first withdrawal reaction and number of lifts and jumps in the cold plate at **A)** 5°C, females, n=18-21/group; males, n=17-20/group; and **B)** 0°C, females, n=15-17/group; males, n=15-16/group. Male *+/G1663S* mice displayed a lower number of lifts and jumps in the cold plate at 0°C. Data are expressed as means ± SEM. One-way ANOVA or Kruskal-Wallis analysis were followed by post-hoc analysis when appropriate. P values are indicated when significant (P<0.05) or close to significance. (See Supplementary Table S12 for detailed statistical analysis).

Supplementary Table S12: Statistical analysis of pain sensitivity to cold of wt and *Scn10a*^{G1663S} mutant mice

Parameter	T°	Analysis	Groups	Statistics
Number of paw lifts + jumps	0°C	Kruskal-Wallis test	F & M	p=0.208
			F	p=0.897
			M	***p*=0.019**
		Dunn's multiple comparisons test	M +/+ vs M *+/G1663S*	***p*=0.021**
			M +/+ vs M *G1663S/G1663S*	p>0.999
		Mann Whitney test two-tailed	M +/+ vs M *+/G1663S*	***p*=0.015**
			M +/+ vs M *G1663S/G1663S*	p=0.347
Latency to 1st reaction	5°C	Kruskal-Wallis test	F & M	p=0.651
			F	p=0.796
			M	p=0.550
	0°C		F & M	p=0.647
			F	p=0.518
			M	p=0.186

4.3 Sensitivity to heat in *Scn10a*^{G1663S} mice

For the Hot plate test at 47°C, 50°C and 54°C, latency to display first hind paws reaction and the number of total coping reactions per one minute were shown in the publication manuscript part. A genotype effect was detected for latency to first hindpaw reaction in the hot plate at 54°C in males. A tendency for genotype effect was recorded for the number of coping reactions at 47°C, although it did not reach significance.

In addition to these results, here we show the number of flicking and licking reactions per one minute. A sex effect was revealed for the number of licks in the hot plate at 47°C (two-way ANOVA $F_{1, 101}$=6.032, p=0.016). No overall genotype effect was identified for the number of licks and the number of flicks at 47°C, 50°C and 54°C. No relevant phenotype was identified in the licks and flicks number at the three temperatures (Figure 22 and Supplementary Table S13).

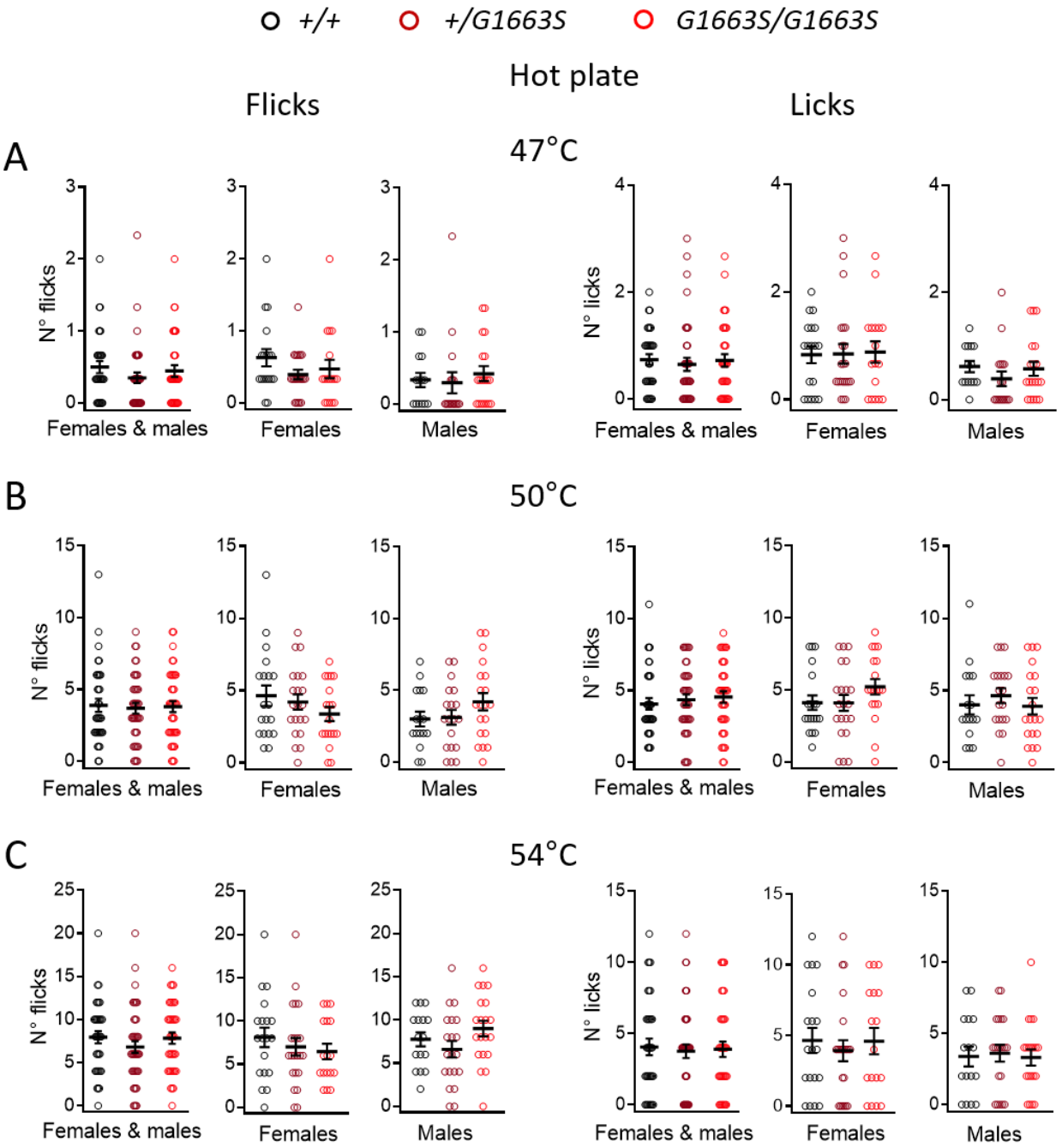

Figure 22: *Scn10a*^{G1663S} mice show normal pain sensitivity in the number of flicks and licks in the hot plate at 47°C, 50°C and 54°C. A-C) Number of flicks and licks in the hot plate at **A)** 47°C, females, n=17-22/group; males, n=14-19/group, **B)** 50°C, females, n=19-21/group; males, n=16-20/group and **C)** 54°C, females, n=17-22/group; males, n=16-20/group. No abnormal phenotype was identified in the number of flicks and licks in the hot plate at 47°C, 50°C and 54°C. Data are expressed as means ± SEM. One-way ANOVA or Kruskal-Wallis analysis were followed by post-hoc analysis when appropriate. P values are indicated when significant (P<0.05) or close to significance. (See Supplementary Table S13 for detailed statistical analysis).

Supplementary Table S13: Statistical analysis of pain sensitivity to heat of wt and *Scn10a*^{G1663S} mutant mice

Parameter	T°	Analysis	Groups	Statistics
Number of licks	47°C	Kruskal-Wallis test	F & M	p=0.586
			F	p=0.999
			M	p=0.147
	50°C		F & M	p=0.510
			F	p=0.134
			M	p=0.481
	54°C		F & M	p=0.967
			F	p=0.831
			M	p=0.887
Number of flicks	47°C	Kruskal-Wallis test	F & M	p=0.414
			F	p=0.411
			M	p=0.298
	50°C		F & M	p=0.989
			F	p=0.451
			M	p=0.330
	54°C	One-way ANOVA	F & M	p=0.426; F (2, 111) = 0.859
			F	p=0.543; F (2, 55) = 0.618
			M	p=0.162; F (2, 53) = 1.881

5. Supplementary statistical analysis on behavioral results

The behavioral data were analyzed in a novel way, consisting in identifying which variables contributed to the genotype and sex discrimination. I would like to acknowledge Maria del Mar MUNIZ MORENO for developing the gdaphen R package and performing the following Gdaphen statistical analysis.

5.1 Material and methods

Gdaphen analysis for the identification of the variables contributing the most to the genotype or sex discrimination

Gdaphen is a R pipeline that allows the identification of the most important predictor qualitative and quantitative variables for genotype discrimination in animal models of different diseases.

We used gdaphen an unpublished R package developed by Maria del Mar MUNIZ MORENO in our team (Muniz et al soon to be submitted to CRAN/ available on github https://github.com/munizmom) to identify the explanatory variables from experimental data. The variables included genotype and sex as well as all behavioral data I have obtained during my project. The aim was to identity the most relevant variables that contributed to the discrimination between the three mouse genotypes: wt, *Scn10a*$^{+/G1663S}$, *Scn10a*$^{G1663S/G1663S}$.

Moreover, in order to more deeply understand the differences and similarities in the relevance of the alterations in the phenotypic characterization performed in mouse line, we also identified, in two independent analyses, which variables were more relevant to discriminate between *Scn10a*$^{+/G1663S}$ and wt on one side, or *Scn10a*$^{G1663S/G1663S}$ and wt on the other side

Gdaphen principle:

Gdaphen takes as input data an excel table containing on the rows the info per animal and on each column all the variables recorded. As for some tests several variables were recorded, we grouped those variables with the same group label and identified the importance for the discrimination of i) each variable alone, ii) the overall contribution of the group. Then, some pre-processing steps are necessary to get the data into shape for the analysis:

1) **Pre-processsing steps:**

- **Imputation of NAs if they exist:**

  If one missing value exist per genotype/sex/variable and the number of animals is >10 then the imputed value is the calculated mean of the values for that genotype/sex/variable.

  Instead if more than one missing value exist per genotype/sex/variable and the total number of missing values are one per 10 animals then we implemented a method for imputation using Additive Regression, Bootstrapping, and Predictive Mean Matching based in closest random sampling implemented over the aregImpute function from the Hmisc R package.

- **Removal of quantitative variables with less than 3 different unique values** as no error or standard deviation can be calculated with so little different numbers.
- **Removal of qualitative variables** with an unique categorical value as we don't have any possible discrimination
- **Standardization of the data** by scaling: this step is really necessary as each independent variable has a different range of values that are observed and is necessary to calculate the contribution of each variable in a comparable way by re-scaling each variable so all have the same range of values observed and/or the same variance.

2) **Identification of the variables contributing more to the discrimination of genotype or sex by using classifiers.**

These classifiers are algorithms that will assign our data into one of the possible set of "classes" or categories previously defined. We decided to use two different classifiers to give answer to two different questions:

- A supervised algorithm that will allow us to identify which phenotypic variables or "predicting variables", if they have an exponential family distribution, are able to discriminate due to the fact that their linear combination is influencing the value of the dependent variable response.

  1) If the dependent variable to be discriminated have two factors, (for example the variable sex, has two possible categories "male" or "female"), then we use a Generalized Linear Model, noted as glm, from the caret R package. Instead, if the dependent variable have more than two possible categories then we use

i) multinomial log-linear models via neural networks algorithm, noted as multiGlm, from the caret R package, that identifies which phenotypic variables are able to discriminate between the categories of your dependent variable without identifying how well each variable discriminate specifically over each category.

ii) The Lasso and Elastic-Net Regularized Generalized Linear Model, noted as ElasticNet, from the nnet R package, that can identify the contribution of each phenotypic variable on the discrimination of each specific category of the dependent variable.

2) An unsupervised algorithm that will be able to identify relevant phenotypic variables for the discrimination even though there may not be coming from a linear distribution or exponential distribution family. We decided to implement the Random Forest algorithm, noted as RF, from the caret R package. This classifier builds a forest of 100000 individual decision trees per observation and predict in ensemble the class of the outcome (or the category of the dependent variable). Is based on the ***wisdom of the crowds*** principle, as a large number of relatively uncorrelated models (trees) as a team will outperform any individual tree decision.

3) Identify the weight of each variable to the prediction and visualization using the Multiple Factor Analysis (MFA).

This method is able to deal with groups of variables both qualitative and quantitative recorded from the same individuals. The MFA performs a normalization or "weighting" on each group by dividing all the variables belonging to the group by the first eigenvalue coming from the principal component analysis (PCA) of the group. Then a PCA on all the weighted variables is applied and we can identify the correlation between the qualitative or quantitative variables grouped or ungrouped, and the principal component dimensions or identify the individual coordinates of each observation on the PCA dimensions. The method is implemented using the MFAmix function from the PCAmixdata R package.

a. Pre-selection of phenotypic variables for the analysis to increase the variance explained of the data using those selected variables.

We analysed three different number of phenotypic predictor variables.

i) All phenotypic variables

ii) The phenotypic variables left after removing the highly correlated ones (correlation higher than 75%).

iii) The phenotypic variables contributing in the discrimination more than a 30% after running the MFA analysis using all variables and observing the correlation between the quantitative ungrouped phenotypic variables with the main three dimensions of the PCA. Our reasoning is to try to decrease the noise added by variables that are not strongly contributing to the discrimination, decrease the complexity of the model and the calculations and increase the power on the discrimination as lower number of variables are considered. To assure we are not performing worse with this model than with the model created using all the variables, we calculated the variance of the data we are able to explain using the first 10 dimensions and the accuracy of the models to answer to how well they can predict correctly each individual observation to the class of the dependent variable.

4) We run gdaphen pipeline to perform the genotype and sex discrimination analyses on:

i) All genotypes: *Scn10a*$^{+/G1663S}$, *Scn10a*$^{G1663S/G1663S}$ and control littermates phenotypic data

ii) *Scn10a*$^{+/G1663S}$ and wt

iii) *Scn10a*$^{G1663S/G1663S}$ and wt

In all those analyses, the model built using the phenotypic predictor variables known to contribute more than a 30% to the discriminations always was able to explain a higher percentage of the variance in the data and showed. Thus, we will present the results focusing on those selected variables alone but all have been analyzed. We will present the results for all genotypes and for *Scn10a*$^{G1663S/G1663S}$ and wt.

5.2 Variables selection

In our study, we considered 23 variables in total, genotype, sex as well as 21 behavioral variables. Among these 23, 13 variables were detected as the most relevant (>30%) to discriminate between the three genotypes of mice, 15 to discriminate *Scn10a*$^{+/G1663S}$ and wt and 11 to distinguish *Scn10a*$^{G1663S/G1663S}$ and wt (Table 4).

In the three analyzes, i) all genotypes together, ii) Het vs wt and iii) Homo vs wt, 9 variables were detected as contributing more than a 30% for the genotype discrimination: sex; coping reactions

in 47°C hot plate; latency, coping reactions and licks in 50°C hot plate; coping reactions and licks in 54°C hot plate; paw lifts and jumps in 5°C and 0°C cold plate. However, von Frey, tail pressure and latency in 54°C hot plate were selected for all genotypes and when considering wt vs het, but not wt vs homo. Withdrawal and flicks in the acetone test was selected for all groups except for wt vs het.

Table 4: Contribution of each variable to genotype discrimination in *Scn10a*^{G1663S} mice considering i) all genotypes together, ii) Het vs wt and iii) Homo vs wt.

Variables	All genotypes	Het vs wt	Homo vs wt
Genotype	★	★	★
Sex	★	★	★
Hot Plate 47: Latency			
Hot Plate 47: Coping reactions	★	★	★
Hot Plate 47: Coping reactions:: Licks			
Hot Plate 47: Coping reactions:: Flicks			
Hot Plate 50: Latency	★	★	★
Hot Plate 50: Coping reactions	★	★	★
Hot Plate 50: Coping reactions:: Licks	★	★	★
Hot Plate 50: Coping reactions:: Flicks			
Hot Plate 54: Latency	★	★	
Hot Plate 54: Coping reactions	★	★	★
Hot Plate 54: Coping reactions:: Licks	★	★	★
Hot Plate 54: Coping reactions:: Flicks		★	
Tail Flick:: Latency		★	
Hargreaves:: Latency			
Acetone:: Withdrawal and Flicks	★		★
Cold Plate 5: Paw lifts and jumps	★	★	★
Cold Plate 5: Latency			
Cold Plate 0: Paw lifts and jumps	★	★	★
Cold Plate 0: Latency		★	★
Von Frey:: Threshold	★	★	
Tail Pressure:: Threshold	★	★	

5.3 All genotypes

We were interested in identifying which variables were contributing more to genotype and sex discrimination, by assessing how well each variable could discriminate between the three genotypes and between the two sexes. The glmNET (Figure 23.1A- 24A) and RF (Figure 23.1C- 24A) classifiers identified von Frey, coping reactions in 47°C hot plate and paw lifts and jumps in 0°C cold plate, as the main variables discriminating between the three genotypes. RF was also able to identify coping reactions and latency in 54°C hot plate as major explanatory variables. Von Frey was the most relevant based on glmNet classifier and paw lifts and jumps in 0°C cold plate was the most relevant based on RF classifier. Von Frey was also ranked first based on multiGLM classifier (Figure 23.1B- 24A). Moreover, the three classifiers identify a strong sex effect conditioning the genotype response to each variable (Figure 23.1- 24A).

Most variables show a strong difference between sexes based on the GLM classifier analysis. These variables ordered by importance are tail pressure, licks and latency in the 54°C hot plate, paw lifts and jumps in 5°C cold plate, acetone, then 50°C hot plate (Figure 23.2A- 24E). Tail pressure and licks in the 54°C hot plate were also ranked as relevant for sex discrimination based on RF classifier, in addition to paw lifts and jumps in 0°C cold plate that was the most relevant variable (Figure 23.2B- 24E).

Heterozygous and homozygous animals seem to be similar in dim 2, but very different in dim 1 and 3, that are the most relevant dimensions for genotype discrimination. Looking deeply into the pairwise comparison of mouse groups, wt are highly distinct from homo in dim 1 and 3. Instead, wt and het seem to be very close in dim 1 and 3 and only discernable in dim 2. Moreover, males and females are highly separated in dim 1, but not in the other dimensions (Figure 24D).

Since wt and Homo seem to be more different than wt and Het, we showed in the next part 5.4 the analysis for wt and *Scn10a*$^{G1663S/G1663S}$.

1 Genotype discrimination

A glmNet

Sel model >30%: 13 Variables
Accuracy: glmNet: 0.37

wt	het	homo	Variable
0.37	32.06	61.64	Sex:: Sex_male
45.85	26.28	0.00	Hot Plate 47: Coping reactions:: Total (nb/min)
0.00	12.42	14.45	Hot Plate 50: Latency:: First response (s)
0.00	12.92	35.11	Hot Plate 50: Coping reactions:: Total (nb/min)
17.23	15.49	0.00	Hot Plate 50: Coping reactions:: Licks (nb/min)
4.77	8.49	0.00	Hot Plate 54: Latency:: First response (s)
0.01	0.00	3.57	Hot Plate 54: Coping reactions:: Total (nb/min)
13.35	4.96	0.00	Hot Plate 54: Coping reactions:: Licks (nb/min)
23.70	0.00	11.30	Acetone:: Withdrawal and Flicks (duration)
8.23	0.00	10.96	Cold Plate 5: Paw lifts and jumps:: Frequency (nb)
37.05	0.00	9.62	Cold Plate 0: Paw lifts and jumps:: Frequency (nb)
100.00	49.33	21.31	Von Frey:: Threshold (g)
0.00	0.70	1.00	Tail Pressure:: Threshold (g)

B multiGLM

Sel model >30%: 13 Variables
Accuracy multiGLM: Residual Deviance: 209.65 , AIC: 265.65

Overall	Variable
0.63	Sex:: Sex_male
0.42	Hot Plate 47: Coping reactions:: Total (nb/min)
0.11	Hot Plate 50: Latency:: First response (s)
0.20	Hot Plate 50: Coping reactions:: Total (nb/min)
0.22	Hot Plate 50: Coping reactions:: Licks (nb/min)
0.05	Hot Plate 54: Latency:: First response (s)
0.01	Hot Plate 54: Coping reactions:: Total (nb/min)
0.13	Hot Plate 54: Coping reactions:: Licks (nb/min)
0.23	Acetone:: Withdrawal and Flicks (duration)
0.12	Cold Plate 5: Paw lifts and jumps:: Frequency (nb)
0.35	Cold Plate 0: Paw lifts and jumps:: Frequency (nb)
3.23	Von Frey:: Threshold (g)
0.01	Tail Pressure:: Threshold (g)

C RF

Sel model >30%: 13 Variables
Accuracy: RF: 0.39

wt	het	homo	Variable
35.4	20.3	19.8	Sex:: Sex_male
41.8	51.1	5.4	Hot Plate 47: Coping reactions:: Total (nb/min)
12.9	74.2	49.1	Hot Plate 50: Latency:: First response (s)
2.3	60.8	87.1	Hot Plate 50: Coping reactions:: Total (nb/min)
29.2	37.7	30.6	Hot Plate 50: Coping reactions:: Licks (nb/min)
22.4	47.9	23.0	Hot Plate 54: Latency:: First response (s)
13.7	50.8	0.8	Hot Plate 54: Coping reactions:: Total (nb/min)
13.7	52.2	9.7	Hot Plate 54: Coping reactions:: Licks (nb/min)
39.8	44.8	27.1	Acetone:: Withdrawal and Flicks (duration)
22.6	35.7	6.7	Cold Plate 5: Paw lifts and jumps:: Frequency (nb)
100.0	90.4	53.2	Cold Plate 0: Paw lifts and jumps:: Frequency (nb)
76.6	61.2	27.3	Von Frey:: Threshold (g)
34.2	24.0	0.0	Tail Pressure:: Threshold (g)

2 Sex discrimination

A GLM

Sel model >30%: 13 Variables
Accuracy: GLM: 0.537

Overall	Variable
0.00	Genotype:: Genotype_b.het
28.72	Genotype:: Genotype_c.homo
37.33	Hot Plate 47: Coping reactions:: Total (nb/min)
36.28	Hot Plate 50: Latency:: First response (s)
48.13	Hot Plate 50: Coping reactions:: Total (nb/min)
56.22	Hot Plate 50: Coping reactions:: Licks (nb/min)
92.91	Hot Plate 54: Latency:: First response (s)
27.48	Hot Plate 54: Coping reactions:: Total (nb/min)
95.25	Hot Plate 54: Coping reactions:: Licks (nb/min)
73.28	Acetone:: Withdrawal and Flicks (duration)
87.48	Cold Plate 5: Paw lifts and jumps:: Frequency (nb)
3.25	Cold Plate 0: Paw lifts and jumps:: Frequency (nb)
19.35	Von Frey:: Threshold (g)
100.00	Tail Pressure:: Threshold (g)

B RF

Sel model >30%: 13 Variables
Accuracy: RF: 0.666

Overall	Variable
10.35	Genotype:: Genotype_b.het
5.82	Genotype:: Genotype_c.homo
14.56	Hot Plate 47: Coping reactions:: Total (nb/min)
19.07	Hot Plate 50: Latency:: First response (s)
9.52	Hot Plate 50: Coping reactions:: Total (nb/min)
15.57	Hot Plate 50: Coping reactions:: Licks (nb/min)
16.70	Hot Plate 54: Latency:: First response (s)
27.09	Hot Plate 54: Coping reactions:: Total (nb/min)
35.88	Hot Plate 54: Coping reactions:: Licks (nb/min)
0.00	Acetone:: Withdrawal and Flicks (duration)
100.00	Cold Plate 5: Paw lifts and jumps:: Frequency (nb)
21.60	Cold Plate 0: Paw lifts and jumps:: Frequency (nb)
4.71	Von Frey:: Threshold (g)
40.97	Tail Pressure:: Threshold (g)

Figure 23: Measuring the explanatory variables importance for genotype and sex discrimination considering the three genotypes together, using different statistical classifiers. **1.** Genotype discrimination: The relevance of the selected 13 variables to the genotype discrimination was analyzed using three different statistical classifiers: **A)** Multinomial log-linear models via neural networks, from the nnet R package, noted as MultiGLM, **B)** Lasso and Elastic-Net Regularized Generalized Linear Models, noted as GLM-Net taken from the caret R package and **C)** Random forest, noted RF taken from the caret R package. **2.** Sex discrimination: The relevance of the selected 13 variables to the sex discrimination was analyzed using three different statistical classifiers: **A)** Generalized linear model noted as GLM and **B)** Random forest, noted RF taken both from the caret R package.

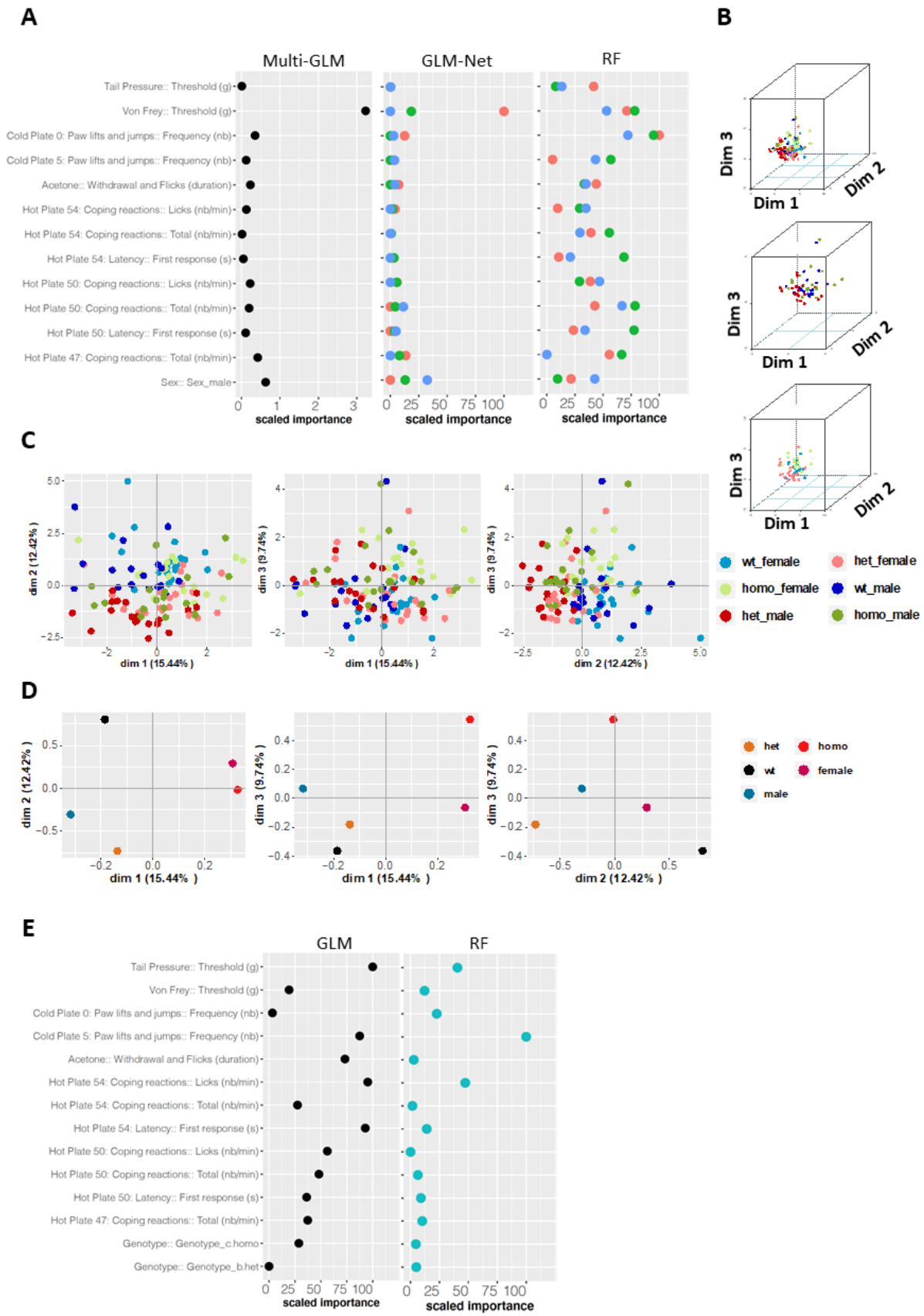
A
Multi-GLM
GLM-Net
RF
Tail Pressure:: Threshold (g)
Von Frey:: Threshold (g)
Cold Plate 0: Paw lifts and jumps:: Frequency (nb)
Cold Plate 5: Paw lifts and jumps:: Frequency (nb)
Acetone:: Withdrawal and Flicks (duration)
Hot Plate 54: Coping reactions:: Licks (nb/min)
Hot Plate 54: Coping reactions:: Total (nb/min)
Hot Plate 54: Latency:: First response (s)
Hot Plate 50: Coping reactions:: Licks (nb/min)
Hot Plate 50: Coping reactions:: Total (nb/min)
Hot Plate 50: Latency:: First response (s)
Hot Plate 47: Coping reactions:: Total (nb/min)
Sex:: Sex_male
scaled importance
B
Dim 3
Dim 1
Dim 2
C
dim 2 (12.42%)
dim 1 (15.44%)
dim 3 (9.74%)
wt_female
het_female
homo_female
wt_male
het_male
homo_male
D
dim 2 (12.42%)
dim 1 (15.44%)
dim 3 (9.74%)
het
homo
wt
female
male
E
GLM
RF
Tail Pressure:: Threshold (g)
Von Frey:: Threshold (g)
Cold Plate 0: Paw lifts and jumps:: Frequency (nb)
Cold Plate 5: Paw lifts and jumps:: Frequency (nb)
Acetone:: Withdrawal and Flicks (duration)
Hot Plate 54: Coping reactions:: Licks (nb/min)
Hot Plate 54: Coping reactions:: Total (nb/min)
Hot Plate 54: Latency:: First response (s)
Hot Plate 50: Coping reactions:: Licks (nb/min)
Hot Plate 50: Coping reactions:: Total (nb/min)
Hot Plate 50: Latency:: First response (s)
Hot Plate 47: Coping reactions:: Total (nb/min)
Genotype:: Genotype_c.homo
Genotype:: Genotype_b.het
scaled importance

Figure 24: Gdaphen analyses to identify the variables contributing more to the genotype and sex discrimination considering the three genotypes together, based on phenotypic data. A. Identification of the power of each explanatory phenotypic variable to the genotype discrimination. The explanatory variables selected were the ones known to contribute more than a 30% to the genotype discrimination. Those variables were identified using a principal component analysis (PCA) after applying a muti factor analysis of mixed data (MFA) implemented using MFAmix function from the PCAmixdata R package. The relevance of those variables to the genotype discrimination was analyzed using three different statistical classifiers: multinomial log-linear models via neural networks, from the nnet R package, noted as MultiGLM, Lasso and Elastic-Net Regularized Generalized Linear Models, noted as GLM-Net taken from the caret R package, and Random forest, noted RF taken from the caret R package. All measures of importance are scaled to have a maximum value of 100 in the variable contributing the most to the discrimination. With GLM-Net and RF we can identify the importance of each variable to discriminate each genotype. **B.** 3D-PCA plots showing the individual animals clustering on the 3D space based on the PCA analyses performed with all the phenotypic variables and colored based on genotype and sex. On the upper panel showing the three genotypes and two sexes individuals, on the middle plot showing only the females and on the bottom plot only the male data. **C.** Individual component map. The distribution in 2D space of the individual observations coordinates calculated based on the PCA analysis performed after the MFA implemented using MFAmix function from the PCAmixdata R package. **D.** Qualitative variable discrimination component map. Showing the distribution in 2D space of the qualitative variables coordinates calculated based on the PCA analysis performed after the MFA implemented using MFAmix function from the PCAmixdata R package. **E.** Identification of the power of each explanatory phenotypic variable known to contribute more than a 30% to the genotype discrimination, were analyzed to see the existence of different responses based on the sex using the three different statistical classifiers. All measures of importance are scaled to have a maximum value of 100 in the variable contributing the most to the discrimination.

5.4 Homo vs wt

After identifying the variables contributing the most to genotype and sex discrimination in the three genotypes, *Scn10a*$^{+/G1663S}$, *Scn10a*$^{G1663S/G1663S}$ and wt, and noticing that the Homo genotype is the most different from wt, we did the same Gdaphen analysis on wt and *Scn10a*$^{G1663S/G1663S}$. Among the 11 previously selected variables with more than 30% contribution to the genotype discrimination, acetone was the most relevant explanatory variable, identified by both GLM and RF classifiers. These classifiers also identified paw lifts and jumps in 0°C cold plate and 50°C hot plate as relevant variables. GLM and RF also detected a strong sex effect (25%) conditioning the genotype response to several behavioral variables (Figure 25.1- 26A).

The variables acetone, latency in 0°C cold plate and licks in 54°C hot plate are more contributing to sex discrimination, based on GLM classification (Figure 25.2A- 26E), while only paw lifts and jumps in 5°C cold plate is the most important variable as identified by RF classification (Figure 25.2B- 26E). Females and males are completely separated in dim 2 and 3 (Figure 26D).

1 Genotype discrimination

A GLM

Sel model >30%: 11 Variables
Accuracy: GLM:0.539

Overall	Variable
56.32	Sex:: Sex_male
50.63	Hot Plate 47: Coping reactions:: Total (nb/min)
57.85	Hot Plate 50: Latency:: First response (s)
51.05	Hot Plate 50: Coping reactions:: Total (nb/min)
14.68	Hot Plate 50: Coping reactions:: Licks (nb/min)
21.43	Hot Plate 54: Coping reactions:: Total (nb/min)
0.00	Hot Plate 54: Coping reactions:: Licks (nb/min)
100.00	Acetone:: Withdrawal and Flicks (duration)
29.32	Cold Plate 5: Paw lifts and jumps:: Frequency (nb)
80.89	Cold Plate 0: Paw lifts and jumps:: Frequency (nb)
1.31	Cold Plate 0: First response:: Latency (s)

B RF

Sel model >30%: 11 Variables
Accuracy: RF:0.497

Overall	Variable
39.74	Sex:: Sex_male
0.00	Hot Plate 47: Coping reactions:: Total (nb/min)
82.10	Hot Plate 50: Latency:: First response (s)
27.53	Hot Plate 50: Coping reactions:: Total (nb/min)
65.52	Hot Plate 50: Coping reactions:: Licks (nb/min)
50.91	Hot Plate 54: Coping reactions:: Total (nb/min)
38.03	Hot Plate 54: Coping reactions:: Licks (nb/min)
100.00	Acetone:: Withdrawal and Flicks (duration)
30.09	Cold Plate 5: Paw lifts and jumps:: Frequency (nb)
63.91	Cold Plate 0: Paw lifts and jumps:: Frequency (nb)
26.73	Cold Plate 0: First response:: Latency (s)

2 Sex discrimination

A GLM

Sel model >30%: 11 Variables
Accuracy: GLM:0.597

Overall	Variable
46.56	Genotype:: Genotype_c.homo
58.95	Hot Plate 47: Coping reactions:: Total (nb/min)
35.63	Hot Plate 50: Latency:: First response (s)
1.11	Hot Plate 50: Coping reactions:: Total (nb/min)
0.00	Hot Plate 50: Coping reactions:: Licks (nb/min)
4.17	Hot Plate 54: Coping reactions:: Total (nb/min)
75.34	Hot Plate 54: Coping reactions:: Licks (nb/min)
100.00	Acetone:: Withdrawal and Flicks (duration)
61.04	Cold Plate 5: Paw lifts and jumps:: Frequency (nb)
52.96	Cold Plate 0: Paw lifts and jumps:: Frequency (nb)
97.54	Cold Plate 0: First response:: Latency (s)

B RF

Sel model >30%: 11 Variables
Accuracy: RF:0.696

Overall	Variable
14.95	Genotype:: Genotype_b.het
0.00	Genotype:: Genotype_c.homo
22.72	Hot Plate 47: Coping reactions:: Total (nb/min)
8.08	Hot Plate 50: Latency:: First response (s)
8.20	Hot Plate 50: Coping reactions:: Total (nb/min)
16.38	Hot Plate 50: Coping reactions:: Licks (nb/min)
11.11	Hot Plate 54: Coping reactions:: Total (nb/min)
37.80	Hot Plate 54: Coping reactions:: Licks (nb/min)
15.55	Acetone:: Withdrawal and Flicks (duration)
100.00	Cold Plate 5: Paw lifts and jumps:: Frequency (nb)
1.48	Cold Plate 0: Paw lifts and jumps:: Frequency (nb)
1.00	Cold Plate 0: First response:: Latency (s)

Figure 25: Measuring the explanatory variable importance for genotype and sex discrimination using different statistical classifiers in WT vs Homo. The relevance of the selected 11 variables to **1.** genotype and **2.** sex discrimination was analyzed using **A.** GLM-Net and **B.** RF statistical classifiers.

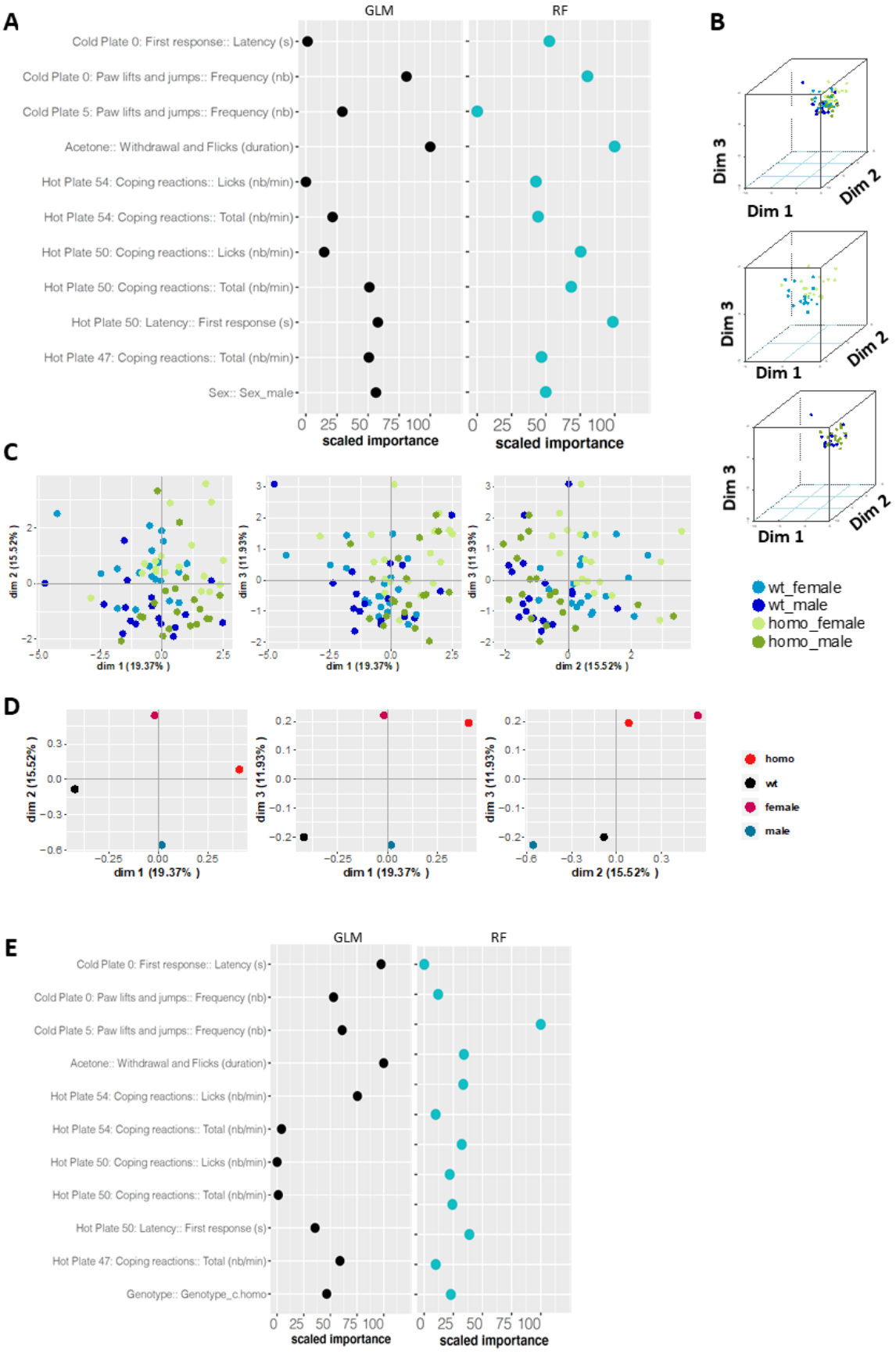
A
GLM
RF
Cold Plate 0: First response:: Latency (s)
Cold Plate 0: Paw lifts and jumps:: Frequency (nb)
Cold Plate 5: Paw lifts and jumps:: Frequency (nb)
Acetone:: Withdrawal and Flicks (duration)
Hot Plate 54: Coping reactions:: Licks (nb/min)
Hot Plate 54: Coping reactions:: Total (nb/min)
Hot Plate 50: Coping reactions:: Licks (nb/min)
Hot Plate 50: Coping reactions:: Total (nb/min)
Hot Plate 50: Latency:: First response (s)
Hot Plate 47: Coping reactions:: Total (nb/min)
Sex:: Sex_male
0 25 50 75 100
scaled importance
B
Dim 3
Dim 1
Dim 2
C
dim 2 (15.52%)
dim 1 (19.37%)
dim 3 (11.93%)
wt_female
wt_male
homo_female
homo_male
D
homo
wt
female
male
E
Genotype:: Genotype_c.homo

Figure 26: Gdaphen analyses to identify the variables contributing more to the discrimination between WT and Homo genotypes and sexes based on phenotypic data. A. Identification of the power of each explanatory phenotypic variable to the genotype discrimination. The explanatory variables selected were the ones known to contribute more than a 30% to the genotype discrimination. Those variables were identified using PCA performed after the MFA implemented using MFAmix function from the PCAmixdata R package. The relevance of those variables to the genotype discrimination was analyzed using GLM-Net and RF statistical classifiers. All measures of importance are scaled to have a maximum value of 100 in the variable contributing the most to the discrimination. With GLM-Net and RF we can identify the importance of each variable to discriminate between WT and Homo. **B.** 3D-PCA plots showing the individual animals clustering on the 3D space based on the PCA analyses performed with all the phenotypic variables and colored based on genotype and sex. On the upper panel showing the two genotypes and two sexes individuals, on the middle plot showing only the females and on the bottom plot only the male data. **C.** Individual component map. The distribution in 2D space of the individual observations coordinates calculated based on the PCA analysis performed after the MFA implemented using MFAmix function from the PCAmixdata R package. **D.** Qualitative variable discrimination component map. Showing the distribution in 2D space of the qualitative variables coordinates calculated based on the PCA analysis performed after the MFA implemented using MFAmix function from the PCAmixdata R package. **E.** Identification of the power of each explanatory phenotypic variable known to contribute more than a 30% to the genotype discrimination, were analyzed to see the existence of different responses based on the sex using GLM-Net and RF statistical classifiers. All measures of importance are scaled to have a maximum value of 100 in the variable contributing the most to the discrimination.

Following this first Gdaphen development and analysis done by Maria del Mar MUNIZ MORENO, we will complete with a deeper analysis that will compare the present results with the basic statistics performed with the Prism software and shown in the rest of the thesis.

IV General Discussion

1. Aims of the thesis

My PhD thesis project focused on three main objectives:

1. To establish the pain-related mouse model bearing G1663S mutation in *Scn10a*.
2. To characterize the effects of this mutation at the cellular and molecular levels.
3. To characterize the mutant mouse model for pain sensitivity using behavioral testing.

2. Creation of the knock-in mouse model for sodium channel *Scn10a*^{G1663S} mutation

We failed to establish the pain-related sodium channel *Scn10a*^{G1663S} mouse model using the CRISPR-Cas9 technology. The two designed strategies for CRISPR-Cas9 failed as we could not obtain the mutant sample carrying the targeted PM and a high number of off-targets was recorded due to the high degree of conservation among the *Scn* genes of the region encompassing the G1663 aa coding sequence. However we could generate the mutant line using HR in ES cells.

Scn10a KO mouse model was created using HR in 1999 [189] and used later on in many studies [128, 139, 190-195]. The first aim of our study was to create *Scn10a*^{G1663S} mouse model. As CRISPR-Cas9 gained a lot of popularity over last years and was proved as highly efficient genome engineering tool, we first wanted to create the *Scn10a*^{G1663S} mouse model using this innovative technology. We designed gRNAs with high specificity score and low number of possible off targets, using the CRISPOR software. As shown in the results part, we could not obtain the mutant sample carrying the targeted PM with the CRISPR-Cas9 technique. The failure of the two CRISPR-Cas9 strategies was in part due to the fact that gRNAs were not cutting the DNA sequence at the same time, so the ssODN bearing the PM was not incorporated between the two cutting sites. Deletions of some nucleotides (up to 150 bp) occurred when one gRNA did cut or when two gRNAs did cut. But as one gRNA was cutting previously to the second, deletion of the inward sequence was not corrected by the insertion of the similar ssODN sequence bearing the PM. In addition, we discovered high similarity between *Scn10a* and other *Scn* genes at and around the region of interest. We were not aware of this similarity at the beginning of the project. We obtained high percentage of off-targets on the *Scn5a* gene which is the most similar to *Scn10a*

gene. Even though, CRISPR-Cas9 technique is quite effective and specific, the fear of possible off-targets was raised. Off-targets occur when the specific Cas9-gRNA complex is able to recognize and cut non-target sites with up to five mismatches. Frequency of mutants with off-targets was published to be similar or even higher than on the expected target site [196, 197]. This indicated that CRISPR-Cas9 is not the easiest tool to be used when targeting a gene from a family of highly similar genes.
Using HR in ES cells enabled to create our *Scn10a*^{G1663S} mouse model. Combining HR to CRISPR-Cas9 technique appeared even more efficient as Cas9-gRNA triggered the DSB and thus forced the HR as a repair machinery.

3. Molecular and cellular characterization of *Scn10a*^{G1663S} mice

Scn9a gene is implicated in neuropathic pain and PMs in this gene were discovered in SFN patients previously to those reported in *Scn10a* gene. The *Scn10a*^{G1663S} mouse model is the first genetic in vivo model of the G1663S mutation reported in SFN patients. As the effect of this mutation on *Scn10a* transcript expression was not previously reported, we wanted to investigate whether this mutation altered *Scn10a* transcript expression in DRG and spinal cord tissues. In addition, we looked into *Scn9a* transcript expression in DRG and *Penk* expression in DRG and spinal cord of wt and *Scn10a*^{G1663S} mutant mice.
Scn10a mRNA is mainly expressed in DRG that contain cell bodies of sensory neurons. The *Scn10a*^{G1663S} mutation did not alter *Scn10a* transcript expression in DRG of mutant mice of both sexes. *Scn10a* transcript expression is normal in *+/G1663S* and *G1663S/G1663S* mice. *Scn10a* mRNA is expressed to a much lesser extent in central terminals of primary afferents in spinal dorsal horn [120]. It was shown that *Scn10a* transcript expression in spinal cord of wt mice is 300 times less than its expression in DRG [198]. We found that *Scn10a* transcript expression in spinal cord of wt and G1663S mutant mice is 300 times less than its expression in DRG. *Scn10a*^{G1663S} mutation had no impact on *Scn10a* transcript expression in spinal cord, which is expected since *Scn10a* expression was not altered in DRG where *Scn10a* mRNA is mainly expressed.

SCN9A and SCN10A share more than 75% sequence similarity and it was reported that they have strong physiological interactions. SCN9A and SCN10A work in tandem in the generation of repetitive firing within DRG neurons. SCN9A amplify small stimuli to bring membrane potential to the threshold for SCN10A activation, which will in turn provide the majority of the inward current

of AP upstroke during repetitive firing [199-201]. These reasons drove us to determine whether the G1663S mutation would impact on *Scn9a* transcript expression. Our results on *Scn9a* transcript expression in DRG of wt and G1663S mutant mice, indicate that the G1663S mutation did not alter *Scn9a* transcript expression and that also this expression was similar between wt, *+/G1663S* and *G1663S/G1663S* mice.

Enkephalin is a peptide of the endogenous opioid system relased by neurons and immune cells in the case of intense pain. It acts as an analgesic by inhibiting the propagation of nociceptive messages to the brain. The *PENK* gene encodes for the PENK polypeptide, a precursor of the Leu- and Met-enkephalin small peptides. Regulation of enkephalin peptides has been described in response to long-lasting nociceptive conditions [202, 203]. A study by Minett et al. showed an upregulation of *Penk* transcript expression in DRG of mutant mice where *Scn9a* was conditionally deleted from sensory neurons, contributing to CIP [187]. Another study by Pereira et al. strengthened the result by Minett et al. by showing that *Penk* expression was increased in cKO mice where *Scn9a* is conditionally deleted in sensory and sympathetic neurons [188]. However, one recent study using sensory neurons derived from induced pluripotent stem cells (iPSCs) could not show this upregulation in these neurons derived from SCN9A CIP human iPSCs and even could not detect *PENK* expression in iPSC-derived neurons from healthy controls [110]. Their findings are in contrast with a number of studies including transcriptomic studies that showed a solid *Penk* expression in DRG. The paper by Sapio et al 2020 showed *Penk* expression in rat DRG [204], and compared their results with five other RNA-seq studies that all showed *Penk* expression in DRG [204]. The recent work by Mecklenburg J et al 2020 also showed *Penk* transcripts in both DRG and TG as well as in neurons purified from DRG [205].

PENK is highly expressed in the dorsal horn of spinal cord throughout laminae I to III, 37% of all neurons in laminae I-III express PENK [206, 207]. *Penk* transcript expression levels are lower in DRG of female wt and *Scn10a* KO mice compared to those in male mice [187] and 1.4 fold higher in wt male spinal cord compared to female [207]. *Penk* transcript level was 30-45 times higher in rat and human dorsal spinal cord compared to rat and human DRG respectively [204]. In a model of sciatic nerve transaction, *Penk* was significantly decreased in DRG of operated rats, as assessed by RNA-Seq analysis; whereas *Penk* was increased in spinal cord in a model of carrageenan-induced inflammation, as revealed by *in situ* hybridization [204]. As we can see, *Penk* regulation was evaluated in different pain models and using various molecular and cellular methods giving a multifaceted picture with conflicting results of the whole literature with the paper by McDermott on iPSCs-derived sensory neurons.

Besides verifying that the G1663S mutation did not affect *Scn10a* and *Scn9a* transcripts expression, we wanted to check whether *Penk* expression levels are altered by the G1663S mutation. Contrary to the study of McDermott et al. [110], and in accordance to all other papers on DRG transcriptomics, we were able to detect *Penk* expression in DRG, but its expression in spinal cord is 10 times higher, which is in accordance with high *Penk* distribution in spinal cord [206, 207]. *Penk* expression did not differ among the three genotypes and was comparable between male and female DRG, in opposition to what was previously shown [187]. *P*enk expression was not altered in spinal cord of G1663S mutant mice. Only a genotype effect close to be significant was detected in females, but we failed to prove its significance. *Penk* expression level was 1.4 times higher in male spinal cord than in female, which is in accordance with previous findings [207]. In conclusion, *Penk* expression was not altered by *Scn10a*^{G1663S} mutation.

4. Behavioral characterization of *Scn10a*^{G1663S} mice

4.1 Scratching behavior of *Scn10a*^{G1663S} mice

Concerning the scratching and wiping behaviors, as I was doing experiments with the first cohort of mice, I noticed that some mice were doing wiping and scratching behaviors. Therefore, I decided to take video recording of mouse movement for the other cohorts before starting the pipeline of behavioral nociception tests. I measured the number and duration of wiping as an indicator of pain as well as the number and duration of scratching as indicator of itch [186].

Scratching behaviors can be induced by many factors. It can be acutely induced by histamine, chloroquine, serotonin and other pruritogens, or chronically caused by calcipotriol and other treatments and atopic dermatitis. In addition, many mutant mice were reported to display spontaneous scratching behaviors. Patients with L811P mutation in *SCN11A* encoding for SCN11A sodium channel reported unbearable itch and distorted pain sensation. Heterozygous mutant mice bearing L799P mutation recapitulating L811P mutation in *SCN11A* displayed increased spontaneous scratching behaviors. However, *Scn11a* KO mice exhibited reduced scratching behavior upon application of histamine, chloroquine or BAM8-22 another pruritic compound [208].

SCN10A is highly expressed in sensory neurons activated by itch and pain. Itching behaviors were not noticed in SFN patients with G1663S mutation, however one patient with L554P mutation in *SCN10A* gene suffered from intense paroxysmal itch in the feet [52]. A recent study

demonstrated that SCN10A regulate scratching behavior induced by the strong pruritic compounds 5-hydroxytryptamine and histamine. The application of these two compounds resulted in an important decrease in scratching activity of *Scn10a* KO mice. Application of other pruritogens did not result in a uniform variation. However, the grand sum of scratching bouts among the various pruritogens suggests that scratching responses declined from an initial maximum 10 min after injection. Pharmacological inhibition of SCN10A failed to decrease scratch activity. Deletion of the *Scn10a* gene made the channel loose its capacity of high-frequency repetitive firing, reducing scratching periods following strong pruritogen application [209].
We were not able to show the importance of SCN10A channel in spontaneous scratching and wiping behaviors in our mutant model. This can be explained by the low number of mice since the cohort 1 was not included in this experiment as I started the video recording from cohort 2. Adding more animals in this experiment can help to find a phenotype. This experiment needs to be more developed by applying some pruritic compounds to induce scratching and then look for the difference in wt and mutant mice behaviors.

4.2 Sensitivity to cold in *Scn10a*^{G1663S} mice

Concerning the cold plate test, I measured the latency to the first reaction (jumping or paw lifting) and the number of lifts and jumps in the cold plate at 5°C and 0°C. Previous studies on *Scn10a* mutant mice showed the importance of *Scn10a* in cold sensitivity. *Possum* mice bearing *Scn10a*^{T790A} mutation were doing more hind paw liftings or body jumps than wt on the cold plate at -1°C during 2 min [210]. K. Zimmermann et al. showed that *Scn10a* KO mice were less sensitive than wt measuring the nocifensive responses as the mean number of hind paw lifts and body jumps from two trials during 5 min on the cold plate at 0°C [139] (Table 5). In the same study, inactivation properties of SCN10A were proved to be entirely cold-resistant which confers to SCN10A a special role for the perception of noxious cold [139]. When measuring the latency to the first jump on the cold plate at -5°C, the *Scn10a* KO mice were jumping later (at 300s) than wt mice [194]. Similarly to the paper of K. Zimmermann et al. [139] we measured the number of hind paw lifts and body jumps during 5 min on the cold plate at 0°C, but we only performed one trial. Zimmermann et al. were able to find a pain phenotype [139], whereas in our study we failed to find a pain phenotype in the *Scn10a*^{G1663S} mutant mice (Table 5). Furthermore, female mice overall reaction at 0°C was reduced compared to 5°C and male *+/G1663S* mice were displaying fewer numbers of paw lifts and jumps than their wt littermates. These results can be explained by the fact that the mice were more and more habituated to the cold plate so they were performing

less at 0°C than at 5°C. To solve the problem of habituation, further investigations should be done using cold plate at 0°C without previous testing at 5°C. Nevertheless, as shown in the publication manuscript part, our results for the acetone test suggest an increase in duration of withdrawal and flicking reactions for female *G1663S/G1663S* mice (Table 5). Thus, we were able to prove that the *Scn10a*^{G1663S} mutant mice have an enhanced sensitivity to cool stimuli but we were not able to prove the role of SCN10A in noxious cold. Our findings on the G1663S mutants suggest that an increase in *Scn10a* excitability as induced by the G1663S mutation [94, 142] alters the sensitivity to cooling while the loss of function of *Scn10a* as investigated with the *Scn10a* KO mice did not impact this sensitivity [193, 194, 211] (Table 5).

4.3 Sensitivity to heat in *Scn10a*^{G1663S} mice

Concerning the hot plate, we measured the number of flicks and licks in addition to the latency to first hind paw reaction and the number of total behaviors at 47°C, 50°C and 54°C. Previous studies on *Scn10a* mutant mice were not able to show a phenotype of the mutant mice on the hot plate test. The *Possum* mice did not reveal a phenotype for the latency to first response (jumping or paw lifting) on the hot plate at 52°C [210]. In the same manner, *Scn10a* KO mice showed a normal phenotype on hot plate at 45°C, 50°C, 55°C and 60°C [189, 195, 212]. However, a recent study done by T. Huang et al. could not detect a phenotype for the withdrawal latency in the hot plate at 47°C, 50°C and 56°C for the mutant mice where the spinal preprotachykinin-positive neurons were ablated. However, a phenotype was detectable only when measuring the number of licking episodes [213]. In our study, we were able to show that male *G1663S/G1663S* mice had reduced hindpaw withdrawal latency in the 54°C hot plate. We were not able to detect a clear phenotype for total coping reactions, number of licks and flicks at 47°C, 50°C and 54°C. In addition, male *G1663S/G1663S* mice displayed shorter latencies than wt in the Hargreaves test, while in the tail flick assay, female mutant mice showed a general genotype effect. The Hargreaves and tail flick tests are based on spinal reflex to heat, whereas the hot plate test is not just a reflexive test but requires decision-making from the mice and involves supraspinal pathways. Thus, this test is more complex to evaluate and more difficult to interpret. In our study, we were able to prove that the *Scn10a*^{G1663S} mutant mice, especially homozygous males, have an enhanced sensitivity to heat stimuli involving supraspinal pathways only at high temperatures and spinal reflex. Altogether, our findings on *Scn10a*^{G1663S} mice in the three tests for heat sensitivity indicate that the *Scn10a*^{G1663S} mutation leads to increased sensitivity of the paw to

strong heating. This appears in agreement with some data from previous publications on *Scn10a* KO mice in which *Scn10a* has been inactivated [128, 189, 195, 212] (Table 5).

4.4 Overall pain sensitivity of *Scn10a*^{G1663S} mice

In addition to cold and heat sensitivity that we recapitulated in parts 4.2 and 4.3, mechanical sensitivity was described in the manuscript part. Our results show a reduced mechanical threshold of the *Scn10a*^{G1663S} mice in the von Frey test. This phenotype has not been previously reported in the other *Scn10a* mutant lines [84, 124, 189-193, 195, 210, 212, 214] which displayed altered sensitivities to noxious mechanical stimuli [128, 189, 195] (Table 5).

Overall, *Scn10a*^{G1663S} mutant mice revealed an enhanced sensitivity towards non noxious mechanical stimuli as shown by von Frey test. The mutant mice showed a tendency to increased reaction to cool stimuli as revealed by acetone application and an increased sensitivity to heat stimuli in Hargreaves test and 54°C hot plate. No phenotype was identified in the cold plate test. Therefore, we were able to show the importance of SCN10A channel in sensitivity towards non-noxious mechanical stimuli, cool stimuli and its implication in supraspinal pathways and spinal reflex to heat. However, we were not able to prove SCN10A channel importance for sensitivity to cold. These results translate pain symptoms reported in SFN patients with *SCN10A*^{G1662S} mutation, such as burning pain, aggravated pain when exposed to cold temperature, and sensitive skin, in addition to the abnormal thresholds for warmth and cold stimuli as revealed by QST. Diagnosing more SFN patients with G1662S mutation in *SCN10A* and reporting more clinical data are needed for better understanding of pain mechanism underlying this mutation. However, we cannot really translate results found in our mutant model to patient's symptoms. A study done by C. Han et al. showed distinct biophysical properties of human SCN10A transfected in rodent DRG neurons compared with native human DRG neurons. Larger persistent current and ramp current as well as slower inactivation were found for human SCN10A channels and longer-lasting AP were demonstrated in rodent DRG neurons carrying human SCN10A. These differences should be taken into consideration when extrapolating from rodent studies of pain to humans and testing novel blockers for treatment of pain [137]. Another study done by C. Rostock et al. pointed out to the molecular differences between human and rodents that can lead to physiological and pathological differences between human and rodent pain pathways. They found larger expression of SCN10A and SCN11A in human tropomyosin receptor kinase A-positive sensory neuron populations than in mice [215]. Moreover, pain remains a multifactorial experience of sensory, emotional, cognitive and social components. Care should be taken to the fact that humans can

report pain verbally while animals cannot do it. Each human being reports pain differently based on his own perception and feeling of pain. This report can also be influenced by life history, psychological and cultural factors. Pain terminology can be used as metaphors describing a psychological issue without the presence of a real tissue damage [4, 9, 14]. In addition, in some countries and cultures, men are seen as powerful human beings and do not show that they are in pain or do not express their pain feeling as much as women. Furthermore, newborns, young children, some patients, verbally handicapped individuals, cognitively or developmentally disabled individuals and even primate and non-primate animals can experience pain without being able to clearly think about it and verbalize it [3, 14-16].

Table 5: A summary of overall pain sensitivity of *Scn10a*^{G1663S} mice in comparison with *Scn10a*^{T790A} and *Scn10a* global KO mouse models.

Model	Mechanical		Cold		Heat		
	Von Frey	Tail pressure/ needle prick	Acetone	Cold plate	Hargreaves	Tail flick	Hot plate
Scn10a^{G1663S}	↗	—	↗	—	↗	↘	↗
Scn10a^{T790A} [210, 214]	—	↗	NA	↗	NA	NA	—
Scn10a global KO [128, 139, 189-195, 211, 212]	—	↘	—	↘	— ↘	↘	—
Scn10a^{Cre} [84, 113, 124]	—	—	NA	NA	—	NA	—

NA: Not available, — : no change, ↗: more sensitive than control, ↘: less sensitive than control

V Conclusions and perspectives

Conclusion

Chronic pain can be distressing and even torturing for the patients. However, pain sensation is essential for protecting us from danger and allowing for tissue repair. Patients with CIP do not benefit from these particularities, since they do not feel pain from any noxious stimuli, including inflammation and heat [34]. SFN comprises a heterogeneous group of neuropathies selectively or predominantly affecting the small-diameter myelinated Aδ-fibers and unmyelinated C-fibers and sparing the large diameter fibers [47, 48]. SFN is accompanied with positive sensory symptoms, mainly spontaneous pain with burning, shooting, electric-like, prickling or itching sensations. Some patients can develop a sensitive skin, intolerance to wear sheet, socks or shoes over the feet and restless leg syndrome. Cramps and tingling are also noticeable in the lower legs and feet. Negative sensory symptoms are also prominent such as loss of thermal, pinprick and other nociceptive sensations and numbness or tight feeling [38, 48-50]. Mutations in *SCN9A* and *SCN10A* genes were found in a proportion of patients with SFN [49, 52]. Studies on *Scn10a* rodent models have highlighted the important role of SCN10A channel in nociception. To have a better understanding of the mechanism of chronic pain in patients and explore novel analgesics, novel relevant pre-clinical models are required. Two teams have developed sensory neurons differentiated from patient-derived iPSCs that model inherited erythromelalgia in vitro [216-218]. These cells can provide a platform which enables assessment of sodium channel blocker effects in vitro. It will then be necessary to analyze their effects and safety in the available *Scn* genetic models and additional preclinical animal models.

Creating animal models carrying human *SCN10A* mutations that were identified in neuropathic patients is needed and pharmacological studies are lacking. The heterozygous $SCN10A^{G1662S}$ mutation was initially reported in two female patients with SFN. Both patients reported continuous pain especially in the feet or legs and other autonomic symptoms. One of them showed abnormal thresholds for warmth and cold sensations in both hands as revealed by QST. The second one developed sensitive skin, intolerance to sheets over her feet, and showed hypoesthesia and reduced vibration sense of the legs revealed by physical examination and abnormal warmth sensation levels for both feet revealed by QST [142]. A third patient with G1662S mutation in *SCN10A* gene was recently reported. She showed abnormal temperature thresholds in QST [141]. The aim of our study was to first create the $Scn10a^{G1663S}$ mouse model and then to proceed

for the molecular, cellular and behavioral characterization of the mutant mice. To our knowledge, we are the first group that has created this mouse model bearing a human pain-related mutation in *Scn10a* gene. We could generate this *Scn10a*^{G1663S} mouse line using HR in ES cells. We increased the efficiency of the HR by using a vector containing the Cas9-gR68. A 80% germline transmission of ES cell coat color was obtained and heterozygous animals harboring *Scn10a*^{G1663S} mutation were generated. We used in vitro fertilization to increase the number of heterozygous mice and then heterozygous mice were subsequently crossed to generate mice with homogeneous genotypes. G1663S mutation did not alter *Scn10a* transcript expression in DRG and spinal cord tissues of mutant mice. *Scn10a*^{G1663S} mutant mice revealed an enhanced sensitivity towards non noxious and noxious mechanical stimuli as shown by von Frey and tail pressure tests respectively. The mutant mice had also an increased reaction to cool stimuli as revealed by acetone application and an increased sensitivity to heat stimuli in Hargreaves test. Therefore, we were able to prove the importance of SCN10A channel in sensitivity towards noxious and innocuous mechanical stimuli, cool stimuli and its implication in spinal reflex.

IENF density in mutant mice

IENF density and morphology correlate well with small nerve fiber dysfunction and are important criterias in assessing SFN patients. IENFD is compared to normative reference values adjusted for decade of life and sex [50, 55]. In three CIP patients, there was a complete loss of IENF and only dermal fibers were present [110]. The three patients with *SCN10A*^{G1662S} mutation had normal IENFD values compared to age-matched and gender-matched normative values [142]. However, patients carrying other mutations in *SCN10A* showed loss of IENFs. In a father-son pair, harboring L554P mutation in *SCN10A* gene, the father showed almost complete loss of IENFs and the son showed complete depletion of IENFs and severe reduction in density of dermal nerve bundles, which appeared fragmented due to axonal degeneration [52]. Other SFN patients with I1706V and D1639N mutations in *SCN10A* gene also showed remarkably decreased IENFD [47, 94]. However, the study by de Greef et al 2018 indicated that, out of 921 patients with SFN, 239 + 68 had abnormal IENF while 614 had normal IENFD (Figure 27) [219].

We have begun the experiments on IENF in *Scn10a*^{G1663S} mutants. We will pursue and complete these experiments for characterizing IENF in the mutants, in order to determine whether the *Scn10a*^{G1663S} mutation has a deleterious effect of skin sensory innervation.

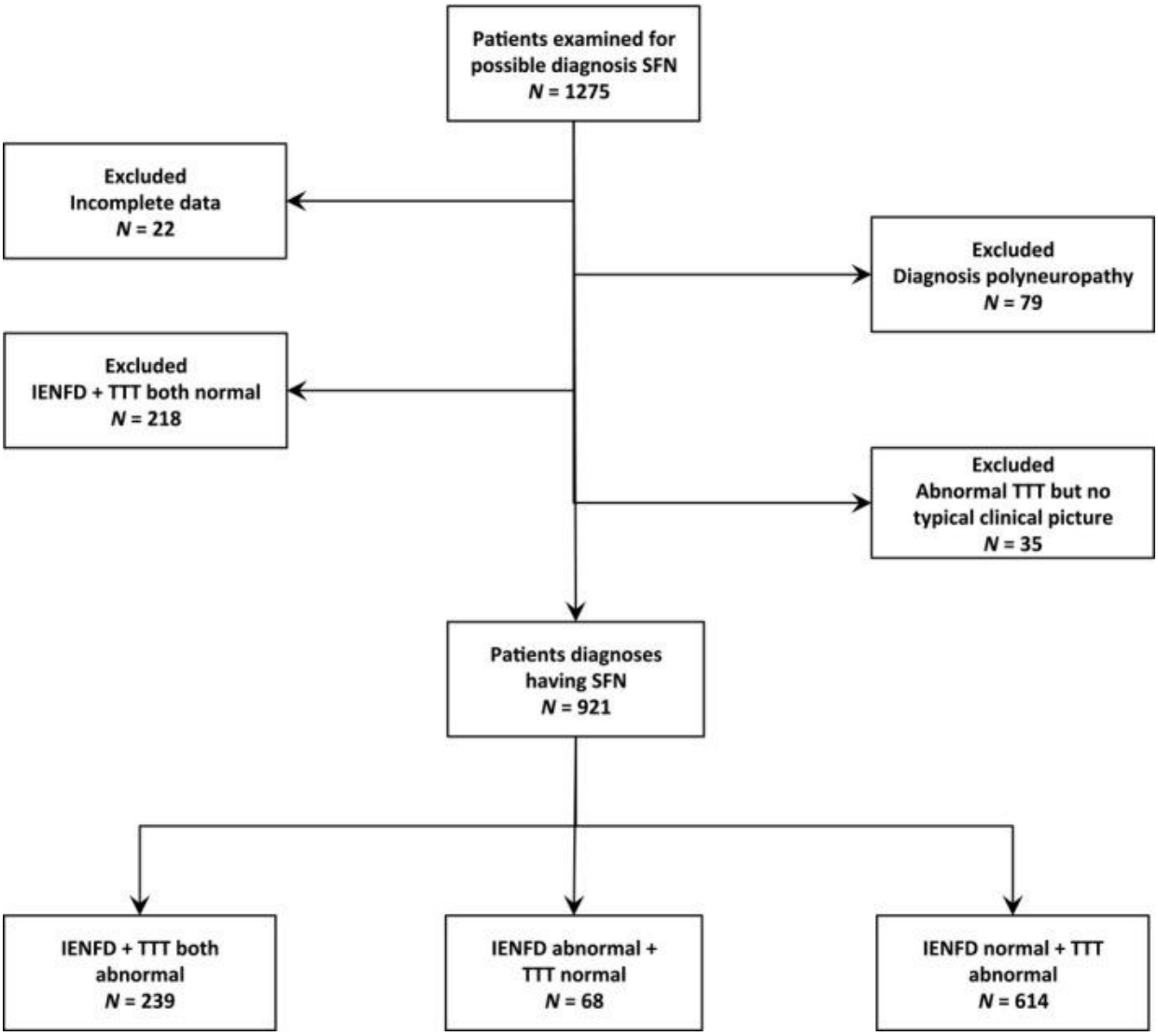

Figure 27: Flowchart of inclusion and exclusion criterias for SFN diagnosis in B. T. A. de Greef et al. 2018. To confirm the diagnosis of SFN, patients needed to have the typical complaints of SFN combined with a reduced intraepidermal nerve fiber density (IENFD) in skin biopsy and/or abnormal temperature threshold testing (TTT) without large nerve fiber involvement based on neurological examination and nerve conduction studies. Adapted from de Greef B. T. A. et al. 2018 [219].
IENFD: intraepidermal nerve fiber density; SFN: small fiber neuropathy; TTT: temperature threshold testing.

Non-evoked spontaneous pain

Reflexive pain behaviors were assessed for several years in animal models. Nevertheless, neuropathic pain is generally characterized by evoked pain, but also non-evoked spontaneous pain. As the behavioral tests that we performed were mostly reflexive tests, it would be important

to conduct non-reflexive and non-evoked pain tests on our mutant model in future studies. Many tests and parameters evaluating spontaneous pain are available and have been used in previous studies. In a rat model of induced-bone cancer where the tumor cells were injected in the right hindlimb, spontaneous pain was evaluated by placing the animal in a transparent plastic cylinder and measuring the duration of different spontaneous behaviors including spontaneous flinching or guarding of the affected hindlimb and intermittent jumping without using the affected limb [220]. The Catwalk is an automated gait analysis system based on the voluntary movement of rodents in an enclosed walkway and used to assess motor function and coordination in rodent models. This method has proved to be reliable for measuring pain-associated behaviors in rodents, when also assessed with other evoked-pain tests [221]. The rodent is first placed in the open end of the illuminated glass platform and is allowed to freely walk voluntarily through the walkway, while a high-speed camera positioned below the apparatus captures images of the illuminated area of each paw. Limb guarding, which is a common clinical manifestation in people with joint, neuropathic and postoperative pain, can be measured in rodents by checking weight bearing on the limbs during a short walk [222]. In the same study on the rat model of induced-bone cancer, different parameters were measured, maximum print area and intensity reflecting pressure exerted by one hind paw maximum contact; duration of ground contact of one hind paw while the other hind paw did not touch the plate and duration in which no hind paw touched the glass plate [220]. The conditioned place preference can be used to inspect preference to analgesics. During a preconditioning phase, animals are placed in a box consisting of a neutral middle chamber and two chambers differing by visual, textural, and olfactory cues. Then conditioning trials are performed with the analgesic being administrated in one of the two chambers, associating the analgesic to a certain chamber. On the test day, the time spent in the chamber associated with the drug indicates a preference in the absence of an analgesic, linking pain relief with a distinct context. The conditioned place avoidance test reflects clinical outcomes in that patients with pain avoid painful stimuli. This test is similar to the conditioned place preference test, but during conditioning, animals are injected with a noxious substance. On the test day, in the absence of a pain-producing injection, quantifying chamber preference is measured as an indication of the abstention of a noxious condition [222].

Additional thermal tests

In addition to the hot and cold plate standard thermal testing, other devices can be used to assess thermal preferences as complementary tests. The two-plate choice test measures the time the animal spends on a 30°C plate compared to an adjacent plate with various temperatures. TRP

melastatin 8 KO mice made full transitions to the colder side whereas wt mice preferred the 30°C plate. Nonetheless, the KO mice displayed same preference for 30°C and noxious 49°C plates, not exhibiting a general deficiency in thermosensation. Mutant mice displayed similar latencies to first reaction than the wt mice when placed on a plate set to 52°C, 10°C, 0°C or -5 °C [223]. The thermal gradient test consists of a continuous temperature gradient going from cold to high temperatures along a metallic plate on which the animal walks freely while being video-recorded from above. The arena is virtually divided in 15 zones of equal size with a specific and stable temperature. The animal shows a preference for a comfortable temperature range during a defined measuring time. Basic Helix-Loop-Helix Family Member A9 KO male mice showed a preference for colder temperatures compared to wt during the second 30 min of recording. This behavior was highly enhanced during the last 30 min where the wt strongly preferred 33°C and KO mice were unable to distinguish temperatures between 24°C and 37°C [224]. TRPV1 KO mice showed a slight preference for hotter temperatures 25°C-36°C whereas TRPV3 KO mice tend to the cooler temperatures 22°C-26°C. This phenotype is reduced in TRPV1/ TRPV3 double KO mice [225]. The operant plantar thermal assay is a recently developed tool consisting of two chamber floors fixed to a thermoregulator plate. One bottle of water was introduced in each chamber. One bottle was empty and the second contained sucrose solution which is rewarding for the animals. Animals were video-recorded and placed in the neutral side at the beginning of each training and testing sessions. The test is based on that the animal learns and decides to get a reward by going through an aversive temperature or abstain from it. Mice model with chronic constriction injury and sham mice both avoided high and low temperatures, despite the fact that injured mice spent more time in the reward zone across even aversive temperatures. However, mice receiving an administration of complete Freund's adjuvant spent similar time in the rewarding zone than control mice [226].

In our study, in addition to the standard hot plate procedure, I have measured different coping reactions. This approach is kind of new in the pain domain, and was firstly introduced by Huang et al. [213]. As a future perspective for our study, performing additional thermal tests will be beneficial to deeply investigate sensitivity and preference to hot and cold temperatures.

Microneurography

Repetitive firing in axons can outlast the period of excitatory input and lead to reduced conduction velocity and prolonged hyperpolarization of the axons [227]. Microneurography is used to record the electrical currents flowing through a nerve, analyzing this signal by characterizing the spikes, to detect activity-dependent changes in AP. Studying chronic conditions or genetic alterations

doesn't depend only on the observation of a change in the signal during recording, but rather aims to evaluate differences in the baseline recordings by absolute quantification of nerve activity. Single spikes have to be distinguished, by excluding artefactual elements by selecting spikes with certain duration and intensities values. This method provides absolute value of spikes per time frame of the baseline activity, that can be compared between distinct animals and experimental groups [228]. Single C-units can be recorded and identified into discrete groups following repetitive electrical stimulation, according to changes in the displayed latency. These changes allowed functional classification of fibers in humans and rodents [227, 229]. Based on C fibers distinct profiles of activity-dependent slowing, or the effect on spontaneous efferent activity of a proximal anesthetic block, these fibers were classified in subpopulations. Type 1A units are mechano-heat-sensitive. Type 1B are mechano-heat-insensitive or silent fibers, they become sensitive to noxious mechanical or heat stimuli after being sensitized by inflammatory mediators (capsaicin, heat sensitization). Type 2 are non-nociceptive fibers, including thermoreceptor fibers and low threshold cutaneous mechanoreceptor fibers as pleasure fibers. Type 3 are cold units and type 4 are sympathetic [20-22]. C fibers do not generally fire AP unless challenged with adequate noxious stimuli. Though, these nociceptors can become hyperexcitable and can generate spontaneous ectopic discharges in pathological cases. Spontaneous activity was recorded in a proportion of C-nociceptors in neuropathic pain states in patients and rat models [230]. Moreover, in diabetic patients with SFN, the ratio of mechano-sensitive to mechano-insensitive nociceptors was 2:1 in healthy controls, compared to 1:2 in patients. 12.5% of characterized C-fibers in nonpainful and 18.9% in painful neuropathy resembling mechano-responsive nociceptors had lost their mechanical and heat responsiveness. This condition implicate polymodal nociceptors function loss and can be helpful in exploring mechanisms responsible for small fiber dysfunction [231]. In three CIP patients, a total of 38 C-fibers were detected and recorded by microneurography. None of the recordings identified fibers with properties consistent with C-nociceptors. Type 1 C-fibers were absent, 26.3 % of type 2, 13.2% of type 3 and 60.5% of type 4 C-fibers were identified. These values were significantly different than those of healthy individuals [110]. Interestingly, an EM patient with M650K mutation in *Scn10a* gene revealed enhanced activity dependent slowing in mechano-insensitive nociceptors and reduced spontaneous firing compared to EM patients without mutations in *Scn* [57]. The $SCN10A^{G1662S}$ mutation was shown to be the first human disease-causing mutation that enhanced generation of TTX-R resurgent currents [199], impaired inactivation and accelerated recovery from inactivation, which result in hyperexcitability of DRG neurons [94, 142]. However, electrophysiological data of microneurography applied on the $Scn10a^{G1663S}$ mouse model is still

lacking. During my PhD, I had the opportunity to follow microneurography experiment on the *Scn9a*^{R185H} mouse model performed by our partners in Neuroscience Technology company in Barcelona. However, I did not get the opportunity to test my mouse model using this technique, which will be an interesting future project.

The development of genetic rodent models recapitulating *SCN* mutations of SFN patients is a key step to explore the mechanism of sodium channels in pain and be able to conceive convenient novel analgesics. Our mutant mouse model opens the door for further behavioral and electrophysiological investigations in the aim of complementing the understanding on the role of SCN10A in painful SFN.

References

1. Hill, R.Z. and D.M. Bautista, *Getting in Touch with Mechanical Pain Mechanisms.* Trends Neurosci, 2020. **43**(5): p. 311-325.
2. Loeser, J.D. and R.D. Treede, *The Kyoto protocol of IASP Basic Pain Terminology.* Pain, 2008. **137**(3): p. 473-7.
3. Aydede, M., *Defending the IASP Definition of Pain.* The Monist, 2017. **100**(4): p. 439-464.
4. Wilson, P.R., *Narrative, Pain, and Suffering.* Pain Medicine, 2006. **7**(3): p. 276-281.
5. Treede, R.D., *The International Association for the Study of Pain definition of pain: as valid in 2018 as in 1979, but in need of regularly updated footnotes.* Pain Rep, 2018. **3**(2): p. e643.
6. Brouwer, B.A., et al., *Neuropathic Pain due to Small Fiber Neuropathy in Aging: Current Management and Future Prospects.* Drugs Aging, 2015. **32**(8): p. 611-21.
7. Woolf, C.J., *What is this thing called pain?* J Clin Invest, 2010. **120**(11): p. 3742-4.
8. Lewis, T., *Pain.* 1942.
9. Cohen, M., J. Quintner, and S. van Rysewyk, *Reconsidering the International Association for the Study of Pain definition of pain.* Pain Rep, 2018. **3**(2): p. e634.
10. Merskey, H., *History and Definition of Pain*, in *Chronic Pain*. 2008. p. 19-28.
11. Raja, S.N., et al., *The revised International Association for the Study of Pain definition of pain: concepts, challenges, and compromises.* Pain, 2020.
12. Williams, A.C. and K.D. Craig, *Updating the definition of pain.* Pain, 2016. **157**(11): p. 2420-2423.
13. Cunningham, N., *Primary requirements for an ethical definition of pain.* Pain Forum, 1999. **8**(2): p. 93-99.
14. Wright, A., *A Criticism of the IASPs Definition of Pain.* 2011.
15. Anand, K.J.S., B.J. Stevens and P.J. McGrath, *Pain in Neonates and Infants.* BJA: British Journal of Anaesthesia, 2007. **99**(3): p. 450-450.
16. Anand, K.J.S. and K.D. Craig, *New perspectives on the definition of pain.* 1996.
17. Craig, A.D., *How do you feel Interoception the sense of the physiological condition of the body.* 2002.
18. Woo, C.W., et al., *Quantifying cerebral contributions to pain beyond nociception.* Nat Commun, 2017. **8**: p. 14211.
19. Colloca, L., et al., *Neuropathic pain.* Nat Rev Dis Primers, 2017. **3**: p. 17002.
20. George, A., et al., *Velocity recovery cycles of single C fibres innervating rat skin.* J Physiol, 2007. **578**(Pt 1): p. 213-32.
21. Armstrong, S.A. and M.J. Herr, *Physiology, Nociception*, in *StatPearls*. 2020: Treasure Island (FL).
22. Sneddon, L.U., *Comparative Physiology of Nociception and Pain.* Physiology (Bethesda), 2018. **33**(1): p. 63-73.
23. Stahl, S.M., *Chronic pain and its treatment*, in *Stahl's Essential Psychopharmacology: neuroscientific basis and practical applications*. 2013, Cambridge university press. p. chap 10.
24. Treede, R.-D., et al., *Neuropathic pain.* Redefinition and a grading system for clinical and research purposes, 2008. **70**(18): p. 1630-1635.
25. Farrar, J.T. and R.K. Portenoy, *Neuropathic cancer pain: the role of adjuvant analgesics.* Oncology (Williston Park, N.Y.), 2001. **15**(11): p. 1435-42, 1445; discussion 1445, 1450-3.
26. Bennett, D.L., et al., *The Role of Voltage-Gated Sodium Channels in Pain Signaling.* Physiol Rev, 2019. **99**(2): p. 1079-1151.
27. Dydyk, A.M. and S. Munakomi, *Thalamic Pain Syndrome*, in *StatPearls*. 2020, StatPearls Publishing: Treasure Island (FL).

28. Falk, S. and A.H. Dickenson, *Pain and nociception: mechanisms of cancer-induced bone pain.* J Clin Oncol, 2014. **32**(16): p. 1647-54.
29. Kaur, G., A.S. Jaggi, and N. Singh, *Exploring the potential effect of Ocimum sanctum in vincristine-induced neuropathic pain in rats.* J Brachial Plex Peripher Nerve Inj, 2010. **5**: p. 3.
30. Smith, Y., *What-is-the-Difference-Between-Nociceptive-and-Neuropathic-Pain.* News Medical life science, 2018.
31. Bouhassira, D., et al., *Prevalence of chronic pain with neuropathic characteristics in the general population.* Pain, 2008. **136**(3): p. 380-7.
32. Kaur, A. and Y. Guan, *Phantom limb pain: A literature review.* Chin J Traumatol, 2018. **21**(6): p. 366-368.
33. *Propane study: Probing the role of sodium channels in painful neuropathies* 2017, Fondazione IRCCS Istituto Neurologico Carlo Besta
34. Schon, K.R., A.P.J. Parker, and C.G. Woods, *Congenital Insensitivity to Pain Overview*, A.H. Adam MP, Pagon RA, et al., Editor. 2018, GeneReviews®.
35. Cox, J.J., et al., *An SCN9A channelopathy causes congenital inability to experience pain.* Nature, 2006. **444**(7121): p. 894-8.
36. Tang, Z., et al., *Primary erythromelalgia: a review.* Orphanet J Rare Dis, 2015. **10**: p. 127.
37. Mann, N., T. King, and R. Murphy, *Review of primary and secondary erythromelalgia.* Clin Exp Dermatol, 2019. **44**(5): p. 477-482.
38. Bennett, D.L.H. and C.G. Woods, *Painful and painless channelopathies.* The Lancet Neurology, 2014. **13**(6): p. 587-599.
39. Yang, Y., et al., *Mutations in SCN9A, encoding a sodium channel alpha subunit, in patients with primary erythermalgia.* J Med Genet, 2004. **41**(3): p. 171-4.
40. Lampert, A., M. Eberhardt, and S.G. Waxman, *Altered sodium channel gating as molecular basis for pain: contribution of activation, inactivation, and resurgent currents.* Handb Exp Pharmacol, 2014. **221**: p. 91-110.
41. Fertleman, C.R., et al., *SCN9A mutations in paroxysmal extreme pain disorder: allelic variants underlie distinct channel defects and phenotypes.* Neuron, 2006. **52**(5): p. 767-74.
42. Renthal, W., *Chapter 90 - Pain Genetics*, in *Rosenberg's Molecular and Genetic Basis of Neurological and Psychiatric Disease (Fifth Edition)*, R.N. Rosenberg and J.M. Pascual, Editors. 2015, Academic Press: Boston. p. 1089-1100.
43. Dib-Hajj, S.D., P. Geha, and S.G. Waxman, *Sodium channels in pain disorders: pathophysiology and prospects for treatment.* Pain, 2017. **158 Suppl 1**: p. S97-S107.
44. Gruver, C. and K.B. Guthmiller, *Postherpetic Neuralgia*, in *StatPearls*. 2020, StatPearls Publishing: Treasure Island (FL).
45. Feldman, E.L., et al., *New Horizons in Diabetic Neuropathy: Mechanisms, Bioenergetics, and Pain.* Neuron, 2017. **93**(6): p. 1296-1313.
46. Blesneac, I., et al., *Rare NaV1.7 variants associated with painful diabetic peripheral neuropathy.* Pain, 2018. **159**(3): p. 469-480.
47. Dabby, R., et al., *Painful small fiber neuropathy with gastroparesis: A new phenotype with a novel mutation in the SCN10A gene.* J Clin Neurosci, 2016. **26**: p. 84-8.
48. Devigili, G., D. Cazzato, and G. Lauria, *Clinical diagnosis and management of small fiber neuropathy: an update on best practice.* Expert Rev Neurother, 2020. **20**(9): p. 967-980.
49. Faber, C.G., et al., *Gain of function Nanu1.7 mutations in idiopathic small fiber neuropathy.* Ann Neurol, 2012. **71**(1): p. 26-39.
50. Hoeijmakers, J.G., et al., *Small-fibre neuropathies--advances in diagnosis, pathophysiology and management.* Nat Rev Neurol, 2012. **8**(7): p. 369-79.

51. Sene, D., *Small fiber neuropathy: Diagnosis, causes, and treatment.* Joint Bone Spine, 2018. **85**(5): p. 553-559.
52. Faber, C.G., et al., *Gain-of-function Nav1.8 mutations in painful neuropathy.* PNAS, 2012. **109**(47): p. 19444–19449.
53. Kremeyer, B., et al., *A gain-of-function mutation in TRPA1 causes familial episodic pain syndrome.* Neuron, 2010. **66**(5): p. 671-80.
54. Devigili, G., et al., *Diagnostic criteria for small fibre neuropathy in clinical practice and research.* Brain, 2019. **142**(12): p. 3728-3736.
55. Magrinelli, F., G. Zanette, and S. Tamburin, *Neuropathic pain: diagnosis and treatment.* Pract Neurol, 2013. **13**(5): p. 292-307.
56. Backonja, M.M., et al., *Value of quantitative sensory testing in neurological and pain disorders: NeuPSIG consensus.* Pain, 2013. **154**(9): p. 1807-19.
57. Kist, A.M., et al., *SCN10A Mutation in a Patient with Erythromelalgia Enhances C-Fiber Activity Dependent Slowing.* PLoS One, 2016. **11**(9): p. e0161789.
58. Siao, P. and M. Kaku, *A Clinician's Approach to Peripheral Neuropathy.* Semin Neurol, 2019. **39**(5): p. 519-530.
59. Lefaucheur, J.P., et al., *Diagnosis of small fiber neuropathy: A comparative study of five neurophysiological tests.* Neurophysiol Clin, 2015. **45**(6): p. 445-55.
60. Bucher, F., et al., *Small-Fiber Neuropathy Is Associated With Corneal Nerve and Dendritic Cell Alterations: An In Vivo Confocal Microscopy Study.* Cornea, 2015. **34**(9): p. 1114-9.
61. Tavakoli, M., et al., *Corneal confocal microscopy: a novel means to detect nerve fibre damage in idiopathic small fibre neuropathy.* Exp Neurol, 2010. **223**(1): p. 245-50.
62. Papanas, N. and D. Ziegler, *Corneal confocal microscopy: Recent progress in the evaluation of diabetic neuropathy.* J Diabetes Investig, 2015. **6**(4): p. 381-9.
63. Di Stefano, G., et al., *Diagnostic accuracy of laser-evoked potentials in diabetic neuropathy.* Pain, 2017. **158**(6): p. 1100-1107.
64. Ziemssen, T. and T. Siepmann, *The Investigation of the Cardiovascular and Sudomotor Autonomic Nervous System-A Review.* Front Neurol, 2019. **10**: p. 53.
65. Novak, P., *Electrochemical skin conductance: a systematic review.* Clinical Autonomic Research, 2019. **29**(1): p. 17-29.
66. Selvarajah, D., et al., *SUDOSCAN: A Simple, Rapid, and Objective Method with Potential for Screening for Diabetic Peripheral Neuropathy.* PLoS One, 2015. **10**(10): p. e0138224.
67. Fabry, V., et al., *Which Method for Diagnosing Small Fiber Neuropathy?* Front Neurol, 2020. **11**: p. 342.
68. Kremer, M., et al., *Antidepressants and gabapentinoids in neuropathic pain: Mechanistic insights.* Neuroscience, 2016. **338**: p. 183-206.
69. Finnerup, N.B., et al., *Pharmacotherapy for neuropathic pain in adults: a systematic review and meta-analysis.* The Lancet Neurology, 2015. **14**(2): p. 162-173.
70. Dworkin, R.H., et al., *Pharmacologic management of neuropathic pain: evidence-based recommendations.* Pain, 2007. **132**(3): p. 237-51.
71. Demant, D.T., et al., *The effect of oxcarbazepine in peripheral neuropathic pain depends on pain phenotype: A randomised, double-blind, placebo-controlled phenotype-stratified study.* PAIN, 2014. **155**(11).
72. O'Neill, J., et al., *Unravelling the mystery of capsaicin: a tool to understand and treat pain.* Pharmacol Rev, 2012. **64**(4): p. 939-71.
73. de Greef, B.T.A., et al., *Lacosamide in patients with Nav1.7 mutations-related small fibre neuropathy: a randomized controlled trial.* Brain, 2019. **142**(2): p. 263-275.

74. Wang, J., S.W. Ou, and Y.J. Wang, *Distribution and function of voltage-gated sodium channels in the nervous system.* Channels (Austin), 2017. **11**(6): p. 534-554.
75. Huang, W., et al., *Structure-based assessment of disease-related mutations in human voltage-gated sodium channels.* Protein Cell, 2017. **8**(6): p. 401-438.
76. Miceli, F., et al., *Molecular pathophysiology and pharmacology of the voltage-sensing module of neuronal ion channels.* Front Cell Neurosci, 2015. **9**: p. 259.
77. Whitaker, W.R.J., et al., *Comparative distribution of voltage-gated sodium channel proteins in human brain.* Molecular Brain Research, 2001. **88**(1): p. 37-53.
78. Caldwell, J.H., et al., *Sodium channel Na(v)1.6 is localized at nodes of ranvier, dendrites, and synapses.* Proc Natl Acad Sci U S A, 2000. **97**(10): p. 5616-20.
79. Vacher, H., D.P. Mohapatra, and J.S. Trimmer, *Localization and targeting of voltage-dependent ion channels in mammalian central neurons.* Physiol Rev, 2008. **88**(4): p. 1407-47.
80. Duflocq, A., et al., *Nav1.1 is predominantly expressed in nodes of Ranvier and axon initial segments.* Mol Cell Neurosci, 2008. **39**(2): p. 180-92.
81. Frenz, C.T., et al., *NaV1.5 sodium channel window currents contribute to spontaneous firing in olfactory sensory neurons.* J Neurophysiol, 2014. **112**(5): p. 1091-104.
82. Wu, L., et al., *Localization of Nav1.5 sodium channel protein in the mouse brain.* Neuroreport, 2002. **13**(18): p. 2547-51.
83. Verkerk, A.O., et al., *Functional Nav1.8 channels in intracardiac neurons: the link between SCN10A and cardiac electrophysiology.* Circ Res, 2012. **111**(3): p. 333-43.
84. Stirling, L.C., et al., *Nociceptor-specific gene deletion using heterozygous NaV1.8-Cre recombinase mice.* Pain, 2005. **113**(1-2): p. 27-36.
85. Catterall, W.A., *Voltage-gated sodium channels at 60: structure, function and pathophysiology.* J Physiol, 2012. **590**(11): p. 2577-89.
86. Jarecki, B.W., et al., *Paroxysmal extreme pain disorder mutations within the D3/S4-S5 linker of Nav1.7 cause moderate destabilization of fast inactivation.* J Physiol, 2008. **586**(17): p. 4137-53.
87. Savio-Galimberti, E., M.H. Gollob, and D. Darbar, *Voltage-gated sodium channels: biophysics, pharmacology, and related channelopathies.* Front Pharmacol, 2012. **3**: p. 124.
88. Ahern, C.A., *What activates inactivation?* J Gen Physiol, 2013. **142**(2): p. 97-100.
89. Raouf, R., K. Quick, and J.N. Wood, *Pain as a channelopathy.* J Clin Invest, 2010. **120**(11): p. 3745-52.
90. Yu, F.H., et al., *Reduced sodium current in GABAergic interneurons in a mouse model of severe myoclonic epilepsy in infancy.* Nat Neurosci, 2006. **9**(9): p. 1142-9.
91. Lossin, C., et al., *Molecular Basis of an Inherited Epilepsy.* Neuron, 2002. **34**(6): p. 877-884.
92. Rush, A.M. and T.R. Cummins, *Painful research: identification of a small-molecule inhibitor that selectively targets Nav1.8 sodium channels.* Mol Interv, 2007. **7**(4): p. 192-5, 180.
93. Han, C., et al., *The Novel Activity of Carbamazepine as an Activation Modulator Extends from NaV1.7 Mutations to the NaV1.8-S242T Mutant Channel from a Patient with Painful Diabetic Neuropathy.* Mol Pharmacol, 2018. **94**(5): p. 1256-1269.
94. Huang, J., et al., *Small-fiber neuropathy Nav1.8 mutation shifts activation to hyperpolarized potentials and increases excitability of dorsal root ganglion neurons.* J Neurosci, 2013. **33**(35): p. 14087-97.
95. Duan, G., et al., *A SCN10A SNP biases human pain sensitivity.* Mol Pain, 2016. **12**.
96. Rush, A.M., et al., *A single sodium channel mutation produces hyper- or hypoexcitability in different types of neurons.* Proc Natl Acad Sci U S A, 2006. **103**(21): p. 8245-50.
97. Zhang, Y., et al., *A novel SCN1A mutation identified in a Chinese family with familial hemiplegic migraine: A case report.* Cephalalgia, 2017. **37**(13): p. 1294-1298.

98. Cestele, S., et al., *Self-limited hyperexcitability: functional effect of a familial hemiplegic migraine mutation of the Nav1.1 (SCN1A) Na+ channel.* J Neurosci, 2008. **28**(29): p. 7273-83.
99. Liao, Y., et al., *Molecular correlates of age-dependent seizures in an inherited neonatal-infantile epilepsy.* Brain, 2010. **133**(Pt 5): p. 1403-14.
100. Guo, F., et al., *Voltage-gated sodium channel Nav1.1, Nav1.3 and beta1 subunit were up-regulated in the hippocampus of spontaneously epileptic rat.* Brain Res Bull, 2008. **75**(1): p. 179-87.
101. Veeramah, K.R., et al., *De novo pathogenic SCN8A mutation identified by whole-genome sequencing of a family quartet affected by infantile epileptic encephalopathy and SUDEP.* Am J Hum Genet, 2012. **90**(3): p. 502-10.
102. Blanchard, M.G., et al., *De novo gain-of-function and loss-of-function mutations of SCN8A in patients with intellectual disabilities and epilepsy.* J Med Genet, 2015. **52**(5): p. 330-7.
103. Trudeau, M.M., et al., *Heterozygosity for a protein truncation mutation of sodium channel SCN8A in a patient with cerebellar atrophy, ataxia, and mental retardation.* Journal of Medical Genetics, 2006. **43**(6): p. 527-530.
104. Aurlien, D., et al., *New SCN5A mutation in a SUDEP victim with idiopathic epilepsy.* Seizure, 2009. **18**(2): p. 158-60.
105. Michel, P., et al., *Comparative efficacy of repetitive nerve stimulation, exercise, and cold in differentiating myotonic disorders.* Muscle Nerve, 2007. **36**(5): p. 643-50.
106. Parisi, P., et al., *Coexistence of epilepsy and Brugada syndrome in a family with SCN5A mutation.* Epilepsy Res, 2013. **105**(3): p. 415-8.
107. Dib-Hajj, S.D., et al., *Gain-of-function mutation in Nav1.7 in familial erythromelalgia induces bursting of sensory neurons.* Brain, 2005. **128**(Pt 8): p. 1847-54.
108. Baker, M.D. and M.A. Nassar, *Painful and painless mutations of SCN9A and SCN11A voltage-gated sodium channels.* Pflugers Arch, 2020. **472**(7): p. 865-880.
109. Hoeijmakers, J.G., et al., *Painful peripheral neuropathy and sodium channel mutations.* Neurosci Lett, 2015. **596**: p. 51-9.
110. McDermott, L.A., et al., *Defining the Functional Role of NaV1.7 in Human Nociception.* Neuron, 2019.
111. Tanaka, B.S., et al., *A gain-of-function mutation in Nav1.6 in a case of trigeminal neuralgia.* Mol Med, 2016. **22**: p. 338-348.
112. Sangameswaran, L., et al., *Structure and function of a novel voltage-gated, tetrodotoxin-resistant sodium channel specific to sensory neurons.* The Journal of biological chemistry, 1996. **271**(11): p. 5953-5956.
113. Agarwal, N., S. Offermanns, and R. Kuner, *Conditional gene deletion in primary nociceptive neurons of trigeminal ganglia and dorsal root ganglia.* Genesis, 2004. **38**(3): p. 122-9.
114. Djouhri, L., et al., *The TTX-resistant sodium channel Nav1.8 (SNS/PN3): expression and correlation with membrane properties in rat nociceptive primary afferent neurons.* J Physiol, 2003. **550**(Pt 3): p. 739-52.
115. Novakovic, S.D., et al., *Distribution of the tetrodotoxin-resistant sodium channel PN3 in rat sensory neurons in normal and neuropathic conditions.* The Journal of neuroscience : the official journal of the Society for Neuroscience, 1998. **18**(6): p. 2174-2187.
116. Amaya, F., et al., *Diversity of expression of the sensory neuron-specific TTX-resistant voltage-gated sodium ion channels SNS and SNS2.* Mol Cell Neurosci, 2000. **15**(4): p. 331-42.
117. Hudmon, A., et al., *Phosphorylation of sodium channel Na(v)1.8 by p38 mitogen-activated protein kinase increases current density in dorsal root ganglion neurons.* J Neurosci, 2008. **28**(12): p. 3190-201.

118. Belkouch, M., et al., *The chemokine CCL2 increases Nav1.8 sodium channel activity in primary sensory neurons through a Gbetagamma-dependent mechanism.* J Neurosci, 2011. **31**(50): p. 18381-90.
119. Gautron, L., et al., *Genetic tracing of Nav1.8-expressing vagal afferents in the mouse.* J Comp Neurol, 2011. **519**(15): p. 3085-101.
120. Shields, S.D., et al., *Nav1.8 expression is not restricted to nociceptors in mouse peripheral nervous system.* Pain, 2012. **153**(10): p. 2017-30.
121. Lu, V.B., S.R. Ikeda, and H.L. Puhl, 3rd, *A 3.7 kb fragment of the mouse Scn10a gene promoter directs neural crest but not placodal lineage EGFP expression in a transgenic animal.* J Neurosci, 2015. **35**(20): p. 8021-34.
122. Coward, K., et al., *Immunolocalization of SNS/PN3 and NaN/SNS2 sodium channels in human pain states.* Pain, 2000. **85**(1): p. 41-50.
123. Soriano, P., *Generalized lacZ expression with the ROSA26 Cre reporter strain.* Nat Genet, 1999. **21**(1): p. 70-1.
124. Nassar, M.A., et al., *Nociceptor-specific gene deletion reveals a major role for Nav1.7 (PN1) in acute and inflammatory pain.* Proc Natl Acad Sci U S A, 2004. **101**(34): p. 12706-11.
125. Zhao, J., et al., *Tamoxifen-inducible NaV1.8-CreERT2 recombinase activity in nociceptive neurons of dorsal root ganglia.* Genesis, 2006. **44**(8): p. 364-71.
126. Madisen, L., et al., *A robust and high-throughput Cre reporting and characterization system for the whole mouse brain.* Nat Neurosci, 2010. **13**(1): p. 133-40.
127. Seal, R.P., et al., *Injury-induced mechanical hypersensitivity requires C-low threshold mechanoreceptors.* Nature, 2009. **462**(7273): p. 651-5.
128. Minett, M.S., N. Eijkelkamp, and J.N. Wood, *Significant determinants of mouse pain behaviour.* PLoS One, 2014. **9**(8): p. e104458.
129. Thun, J., A.K. Persson, and K. Fried, *Differential expression of neuronal voltage-gated sodium channel mRNAs during the development of the rat trigeminal ganglion.* Brain Res, 2009. **1269**: p. 11-22.
130. Klein, A.H., et al., *Sodium Channel Nav1.8 Underlies TTX-Resistant Axonal Action Potential Conduction in Somatosensory C-Fibers of Distal Cutaneous Nerves.* J Neurosci, 2017. **37**(20): p. 5204-5214.
131. Udit, S., et al., *Nav1.8 neurons are involved in limiting acute phase responses to dietary fat.* Mol Metab, 2017. **6**(10): p. 1081-1091.
132. Facer, P., et al., *Localisation of SCN10A gene product Na(v)1.8 and novel pain-related ion channels in human heart.* International heart journal, 2011. **52**(3): p. 146-152.
133. Hameed, S., *Nav1.7 and Nav1.8: Role in the pathophysiology of pain.* Mol Pain, 2019. **15**: p. 1744806919858801.
134. Dib-Hajj, S.D. and S.G. Waxman, *Diversity of composition and function of sodium channels in peripheral sensory neurons.* Pain, 2015. **156**(12): p. 2406-7.
135. Akopian, A.N., L. Sivilotti, and J.N. Wood, *A tetrodotoxin-resistant voltage-gated sodium channel expressed by sensory neurons.* 1996.
136. Dib-Hajj, S.D., et al., *Two tetrodotoxin-resistant sodium channels in human dorsal root ganglion neurons.* FEBS Lett, 1999. **462**(1-2): p. 117-20.
137. Han, C., et al., *Human Na(v)1.8: enhanced persistent and ramp currents contribute to distinct firing properties of human DRG neurons.* J Neurophysiol, 2015. **113**(9): p. 3172-85.
138. Cummins, T.R., S.G. Waxman, and J.N. Wood, *Sodium Channels and Pain.* 2019.
139. Zimmermann, K., et al., *Sensory neuron sodium channel Nav1.8 is essential for pain at low temperatures.* Nature, 2007. **447**(7146): p. 855-8.

140. Zhang, Z., et al., *Exonic mutations in SCN9A (NaV1.7) are found in a minority of patients with erythromelalgia.* Scand J Pain, 2014. **5**(4): p. 217-225.
141. Eijkenboom, I., et al., *Yield of peripheral sodium channels gene screening in pure small fibre neuropathy.* J Neurol Neurosurg Psychiatry, 2019. **90**(3): p. 342-352.
142. Han, C., et al., *The G1662S NaV1.8 mutation in small fibre neuropathy: impaired inactivation underlying DRG neuron hyperexcitability.* J Neurol Neurosurg Psychiatry, 2014. **85**(5): p. 499-505.
143. Capecchi, M.R., *Gene targeting in mice: functional analysis of the mammalian genome for the twenty-first century.* Nat Rev Genet, 2005. **6**(6): p. 507-12.
144. Capecchi, M.R., *High efficiency transformation by direct microinjection of DNA into cultured mammalian cells.* Cell, 1980. **22**(2, Part 2): p. 479-488.
145. Capecchi, M.R., *Generating mice with targeted mutations.* Nature Medicine, 2001. **7**(10): p. 1086-1090.
146. Smithies, O., et al., *Insertion of DNA sequences into the human chromosomal β -globin locus by homologous recombination.* Nature, 1985. **317**(6034): p. 230-234.
147. Mansour, S.L., K.R. Thomas, and M.R. Capecchi, *Disruption of the proto-oncogene int-2 in mouse embryo-derived stem cells: a general strategy for targeting mutations to non-selectable genes.* Nature, 1988. **336**(6197): p. 348-352.
148. Evans, M.J. and M.H. Kaufman, *Establishment in culture of pluripotential cells from mouse embryos.* Nature, 1981. **292**(5819): p. 154-6.
149. Thomas, K.R. and M.R. Capecchi, *Site-directed mutagenesis by gene targeting in mouse embryo-derived stem cells.* Cell, 1987. **51**(3): p. 503-12.
150. Cheah, S.S. and R.R. Behringer, *Gene-targeting strategies.* Methods Mol Biol, 2000. **136**: p. 455-63.
151. Gerlai, R., *Gene Targeting Using Homologous Recombination in Embryonic Stem Cells: The Future for Behavior Genetics?* Front Genet, 2016. **7**: p. 43.
152. Bouabe, H., M. Moser, and J. Heesemann, *Enhanced selection for homologous-recombinant embryonic stem cell clones by Cre recombinase-mediated deletion of the positive selection marker.* Transgenic Res, 2012. **21**(1): p. 227-9.
153. Zhang, Y., et al., *Inducible site-directed recombination in mouse embryonic stem cells.* Nucleic Acids Res, 1996. **24**(4): p. 543-8.
154. Feil, R., et al., *Ligand-activated site-specific recombination in mice.* Proceedings of the National Academy of Sciences, 1996. **93**(20): p. 10887-10890.
155. Theunissen, T.W. and R. Jaenisch, *Molecular control of induced pluripotency.* Cell Stem Cell, 2014. **14**(6): p. 720-34.
156. Kim, Y.G., J. Cha, and S. Chandrasegaran, *Hybrid restriction enzymes: zinc finger fusions to Fok I cleavage domain.* Proc Natl Acad Sci U S A, 1996. **93**(3): p. 1156-60.
157. Boch, J., et al., *Breaking the Code of DNA Binding Specificity of TAL-Type III Effectors.* Science, 2009. **326**(5959): p. 1509-1512.
158. Moscou, M.J. and A.J. Bogdanove, *A Simple Cipher Governs DNA Recognition by TAL Effectors.* Science, 2009. **326**(5959): p. 1501-1501.
159. Bedell, V.M., et al., *In vivo genome editing using a high-efficiency TALEN system.* Nature, 2012. **491**(7422): p. 114-118.
160. Bibikova, M., et al., *Enhancing gene targeting with designed zinc finger nucleases.* Science, 2003. **300**(5620): p. 764.
161. Kim, E., et al., *Precision genome engineering with programmable DNA-nicking enzymes.* Genome Res, 2012. **22**(7): p. 1327-33.
162. Lee, H.B., et al., *Genome Engineering with TALE and CRISPR Systems in Neuroscience.* Frontiers in genetics, 2016. **7**: p. 47-47.

163. Porteus, M.H. and D. Baltimore, *Chimeric nucleases stimulate gene targeting in human cells.* Science, 2003. **300**(5620): p. 763.
164. Urnov, F.D., et al., *Highly efficient endogenous human gene correction using designed zinc-finger nucleases.* Nature, 2005. **435**(7042): p. 646-51.
165. Ishino, Y., et al., *Nucleotide sequence of the iap gene, responsible for alkaline phosphatase isozyme conversion in Escherichia coli, and identification of the gene product.* J Bacteriol, 1987. **169**(12): p. 5429-33.
166. Barrangou, R., et al., *CRISPR provides acquired resistance against viruses in prokaryotes.* Science, 2007. **315**(5819): p. 1709-12.
167. Jinek, M., et al., *A Programmable Dual-RNA–Guided DNA Endonuclease in Adaptive Bacterial Immunity.* Science, 2012. **337**(6096): p. 816-821.
168. Fineran, P.C. and E. Charpentier, *Memory of viral infections by CRISPR-Cas adaptive immune systems: acquisition of new information.* Virology, 2012. **434**(2): p. 202-9.
169. Charpentier, E. and J.A. Doudna, *Rewriting a genome.* Nature, 2013. **495**(7439): p. 50-51.
170. Jeong, J.Y., et al., *One-step sequence- and ligation-independent cloning as a rapid and versatile cloning method for functional genomics studies.* Appl Environ Microbiol, 2012. **78**(15): p. 5440-3.
171. Li, M.Z. and S.J. Elledge, *Harnessing homologous recombination in vitro to generate recombinant DNA via SLIC.* Nat Methods, 2007. **4**(3): p. 251-6.
172. Codner, G.F., et al., *Aneuploidy screening of embryonic stem cell clones by metaphase karyotyping and droplet digital polymerase chain reaction.* BMC Cell Biol, 2016. **17**(1): p. 30.
173. Yang, W., et al., *Targeted Mutation (R100W) of the Gene Encoding NGF Leads to Deficits in the Peripheral Sensory Nervous System.* Front Aging Neurosci, 2018. **10**: p. 373.
174. Pham, V.M., et al., *Impaired peripheral nerve regeneration in type-2 diabetic mouse model.* Eur J Neurosci, 2018. **47**(2): p. 126-139.
175. De Gregorio, C., et al., *Characterization of diabetic neuropathy progression in a mouse model of type 2 diabetes mellitus.* Biol Open, 2018. **7**(9).
176. Zhang, C., et al., *Cytokine-mediated inflammation mediates painful neuropathy from metabolic syndrome.* PLoS One, 2018. **13**(2): p. e0192333.
177. Ceredig, R.A., et al., *Peripheral delta opioid receptors mediate duloxetine antiallodynic effect in a mouse model of neuropathic pain.* Eur J Neurosci, 2018. **48**(5): p. 2231-2246.
178. Arcourt, A., et al., *Touch Receptor-Derived Sensory Information Alleviates Acute Pain Signaling and Fine-Tunes Nociceptive Reflex Coordination.* Neuron, 2017. **93**(1): p. 179-193.
179. Yeo, J.H., et al., *Repetitive Acupuncture Point Treatment with Diluted Bee Venom Relieves Mechanical Allodynia and Restores Intraepidermal Nerve Fiber Loss in Oxaliplatin-Induced Neuropathic Mice.* J Pain, 2016. **17**(3): p. 298-309.
180. Janine, L., et al., *Early detection of diabetic neuropathy by investigating CNFL and IENFD in thy1-YFP mice.* Journal of Endocrinology, 2016. **231**(2): p. 147-157.
181. Wang, T., et al., *Neurturin overexpression in skin enhances expression of TRPM8 in cutaneous sensory neurons and leads to behavioral sensitivity to cool and menthol.* J Neurosci, 2013. **33**(5): p. 2060-70.
182. Jin, H.Y., et al., *Neuroprotective effects of Vitis vinifera extract on prediabetic mice induced by a high-fat diet.* Korean J Intern Med, 2013. **28**(5): p. 579-86.
183. Unezaki, S., et al., *Involvement of Tyr1472 phosphorylation of NMDA receptor NR2B subunit in postherpetic neuralgia in model mice.* Mol Pain, 2012. **8**: p. 59.
184. Maklad, A., et al., *The EGFR is required for proper innervation to the skin.* J Invest Dermatol, 2009. **129**(3): p. 690-8.
185. Sullivan, K.A., et al., *Mouse models of diabetic neuropathy.* Neurobiol Dis, 2007. **28**(3): p. 276-85.

186. Shimada, S.G. and R.H. LaMotte, *Behavioral differentiation between itch and pain in mouse.* Pain, 2008. **139**(3): p. 681-7.
187. Minett, M.S., et al., *Endogenous opioids contribute to insensitivity to pain in humans and mice lacking sodium channel Nav1.7.* Nat Commun, 2015. **6**: p. 8967.
188. Pereira, V., et al., *Analgesia linked to Nav1.7 loss of function requires micro- and delta-opioid receptors.* Wellcome Open Res, 2018. **3**: p. 101.
189. Akopian, A.N., Souslova, V., England, S., Okuse, K., Ogata, N., Ure, J., ... & Hill, R., *The tetrodotoxin-resistant sodium channel SNS has a specialized function in pain pathways.* Nature neuroscience, 1999. **2**(6): p. 541-548.
190. Kerr, B.J., Souslova, V., McMahon, S. B., & Wood, J. N., *A role for the TTX-resistant sodium channel Nav 1.8 in NGF-induced hyperalgesia, but not neuropathic pain.* Neuroreport, 2001. **12**(14): p. 3077-3080.
191. Laird, J.M., et al., *Deficits in visceral pain and referred hyperalgesia in Nav1.8 (SNS/PN3)-null mice.* J Neurosci, 2002. **22**(19): p. 8352-6.
192. Shields, S.D., et al., *Sodium channel Na(v)1.7 is essential for lowering heat pain threshold after burn injury.* J Neurosci, 2012. **32**(32): p. 10819-32.
193. Minett, M.S., et al., *Pain without nociceptors? Nav1.7-independent pain mechanisms.* Cell Rep, 2014. **6**(2): p. 301-12.
194. Luiz, A.P., et al., *Cold sensing by NaV1.8-positive and NaV1.8-negative sensory neurons.* Proc Natl Acad Sci U S A, 2019.
195. Nassar, M.A., et al., *Neuropathic pain develops normally in mice lacking both Na(v)1.7 and Na(v)1.8.* Mol Pain, 2005. **1**: p. 24.
196. Fu, Y., et al., *High-frequency off-target mutagenesis induced by CRISPR-Cas nucleases in human cells.* Nature Biotechnology, 2013. **31**(9): p. 822-826.
197. Mali, P., et al., *CAS9 transcriptional activators for target specificity screening and paired nickases for cooperative genome engineering.* Nat Biotechnol, 2013. **31**(9): p. 833-8.
198. Hillsley, K., et al., *Dissecting the role of sodium currents in visceral sensory neurons in a model of chronic hyperexcitability using Nav1.8 and Nav1.9 null mice.* J Physiol, 2006. **576**(Pt 1): p. 257-67.
199. Xiao, Y., et al., *Increased Resurgent Sodium Currents in Nav1.8 Contribute to Nociceptive Sensory Neuron Hyperexcitability Associated with Peripheral Neuropathies.* J Neurosci, 2019. **39**(8): p. 1539-1550.
200. Renganathan, M., T.R. Cummins, and S.G. Waxman, *Contribution of Na(v)1.8 sodium channels to action potential electrogenesis in DRG neurons.* J Neurophysiol, 2001. **86**(2): p. 629-40.
201. Yang, L., et al., *Roles of Voltage-Gated Tetrodotoxin-Sensitive Sodium Channels NaV1.3 and NaV1.7 in Diabetes and Painful Diabetic Neuropathy.* Int J Mol Sci, 2016. **17**(9).
202. Pohl, M., et al., *Enkephalinergic and dynorphinergic neurons in the spinal cord and dorsal root ganglia of the polyarthritic rat — in vivo release and cDNA hybridization studies.* Brain Research, 1997. **749**(1): p. 18-28.
203. Cesselin, F., et al., *Met-enkephalin levels and opiate receptors in the spinal cord of chronic suffering rats.* Brain Research, 1980. **191**(1): p. 289-293.
204. Sapio, M.R., et al., *Dynorphin and Enkephalin Opioid Peptides and Transcripts in Spinal Cord and Dorsal Root Ganglion During Peripheral Inflammatory Hyperalgesia and Allodynia.* J Pain, 2020. **21**(9-10): p. 988-1004.
205. Mecklenburg, J., et al., *Transcriptomic sex differences in sensory neuronal populations of mice.* Sci Rep, 2020. **10**(1): p. 15278.
206. Francois, A., et al., *A Brainstem-Spinal Cord Inhibitory Circuit for Mechanical Pain Modulation by GABA and Enkephalins.* Neuron, 2017. **93**(4): p. 822-839 e6.

207. McCallum-Loudeac, J., G. Anderson, and M.J. Wilson, *Age and Sex-Related Changes to Gene Expression in the Mouse Spinal Cord.* J Mol Neurosci, 2019. **69**(3): p. 419-432.
208. Salvatierra, J., et al., *A disease mutation reveals a role for NaV1.9 in acute itch.* J Clin Invest, 2018. **128**(12): p. 5434-5447.
209. Kuhn, H., et al., *Complementary roles of murine NaV1.7, NaV1.8 and NaV1.9 in acute itch signalling.* Sci Rep, 2020. **10**(1): p. 2326.
210. Blasius, A.L., et al., *Hypermorphic mutation of the voltage-gated sodium channel encoding gene Scn10a causes a dramatic stimulus-dependent neurobehavioral phenotype.* Proc Natl Acad Sci U S A, 2011. **108**(48): p. 19413-8.
211. Minett, M.S., et al., *Distinct Nav1.7-dependent pain sensations require different sets of sensory and sympathetic neurons.* Nat Commun, 2012. **3**: p. 791.
212. Leo, S., R. D'Hooge, and T. Meert, *Exploring the role of nociceptor-specific sodium channels in pain transmission using Nav1.8 and Nav1.9 knockout mice.* Behav Brain Res, 2010. **208**(1): p. 149-57.
213. Huang, T., et al., *Identifying the pathways required for coping behaviours associated with sustained pain.* Nature, 2019. **565**(7737): p. 86-90.
214. Garrison, S.R., et al., *A gain-of-function voltage-gated sodium channel 1.8 mutation drives intense hyperexcitability of A- and C-fiber neurons.* Pain, 2014. **155**(5): p. 896-905.
215. Rostock, C., et al., *Human vs. Mouse Nociceptors - Similarities and Differences.* Neuroscience, 2018. **387**: p. 13-27.
216. Cao, L., et al., *Pharmacological reversal of a pain phenotype in iPSC-derived sensory neurons and patients with inherited erythromelalgia.* Sci Transl Med, 2016. **8**(335): p. 335ra56.
217. Mis, M.A., et al., *Resilience to Pain: A Peripheral Component Identified Using Induced Pluripotent Stem Cells and Dynamic Clamp.* J Neurosci, 2019. **39**(3): p. 382-392.
218. Meents, J.E., et al., *The role of Nav1.7 in human nociceptors: insights from human iPS cell-derived sensory neurons of erythromelalgia patients.* Pain, 2019.
219. de Greef, B.T.A., et al., *Associated conditions in small fiber neuropathy - a large cohort study and review of the literature.* Eur J Neurol, 2018. **25**(2): p. 348-355.
220. Hu, X.M., et al., *Vascular Endothelial Growth Factor A Signaling Promotes Spinal Central Sensitization and Pain-related Behaviors in Female Rats with Bone Cancer.* Anesthesiology, 2019. **131**(5): p. 1125-1147.
221. Gabriel, A.F., et al., *The CatWalk method: assessment of mechanical allodynia in experimental chronic pain.* Behav Brain Res, 2009. **198**(2): p. 477-80.
222. Gregory, N.S., et al., *An overview of animal models of pain: disease models and outcome measures.* J Pain, 2013. **14**(11): p. 1255-69.
223. Bautista, D.M., et al., *The menthol receptor TRPM8 is the principal detector of environmental cold.* Nature, 2007. **448**(7150): p. 204-8.
224. Bohic, M., et al., *Loss of bhlha9 Impairs Thermotaxis and Formalin-Evoked Pain in a Sexually Dimorphic Manner.* Cell Rep, 2020. **30**(3): p. 602-610 e6.
225. Marics, I., et al., *Acute heat-evoked temperature sensation is impaired but not abolished in mice lacking TRPV1 and TRPV3 channels.* PLoS One, 2014. **9**(6): p. e99828.
226. Reker, A.N., et al., *The Operant Plantar Thermal Assay: A Novel Device for Assessing Thermal Pain Tolerance in Mice.* eNeuro, 2020. **7**(2).
227. Serra, J., et al., *Activity-dependent slowing of conduction differentiates functional subtypes of C fibres innervating human skin.* J Physiol, 1999. **515 (Pt 3)**(Pt 3): p. 799-811.
228. Carnevale, L., *Microneurography of Peripheral Nerves in Mice: An Old Approach Applied to the Novel Concept of Neural Modulation of Immune Organs in Cardiovascular Diseases.* Biomedical Journal of Scientific & Technical Research, 2018. **2**(5).

229. Serra, J., H. Bostock, and X. Navarro, *Microneurography in rats: a minimally invasive method to record single C-fiber action potentials from peripheral nerves in vivo.* Neurosci Lett, 2010. **470**(3): p. 168-74.
230. Serra, J., et al., *Microneurographic identification of spontaneous activity in C-nociceptors in neuropathic pain states in humans and rats.* Pain, 2012. **153**(1): p. 42-55.
231. Orstavik, K., et al., *Abnormal function of C-fibers in patients with diabetic neuropathy.* J Neurosci, 2006. **26**(44): p. 11287-94.